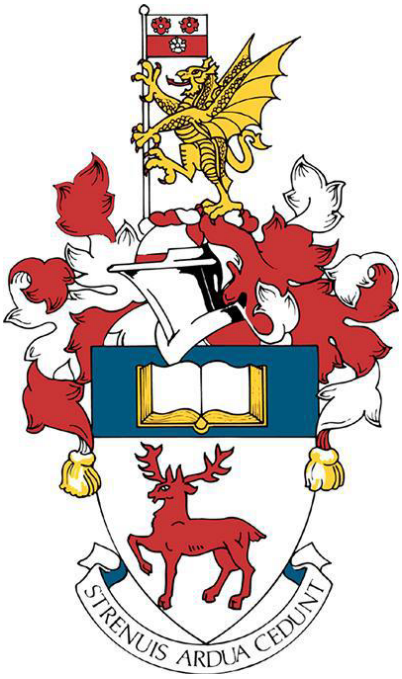

University of Southampton

Faculty of Environmental and Life Sciences

School of Biological Sciences

Microbiologically influenced corrosion: Development of a model system to investigate the role of biofilm communities within MIC and their control using industrial biocides

DOI https://doi.org/10.5258/SOTON/D3245

by

Liam Matthew Jones

ORCID ID 0000-0002-2695-0464 https://orcid.org/my-orcid?orcid=0000-0002-2695-0464

Thesis for the degree of Doctor of Philosophy

26 March 2025

University of Southampton

Abstract

Faculty of Environmental and Life Sciences

School of Biological Sciences

Doctor of Philosophy

Microbiologically influenced corrosion: Development of a model system to investigate the role of biofilm communities within MIC and their control using industrial biocides

by

Liam Matthew Jones

Microbiologically influenced corrosion (MIC) presents persistent challenges to the maritime, offshore renewable, and energy sectors, with biofilm formation playing a crucial role in corrosion mechanisms. However, understanding the complex interactions between biofilms and MIC is hindered by the lack of reproducible physical models that accurately reflect real-world conditions. This research employed a novel dual anaerobic biofilm reactor, using a complex microbial consortium derived from marine littoral sediment, and highlights the importance of a multidisciplinary approach, utilising multiple lines of evidence to understand the mechanistic interactions between biofilms and corrosion.

DNA extraction and 16S rRNA amplicon sequencing revealed that electroactive bacteria, particularly sulphate-reducing and iron-reducing bacteria, were the principal contributors to biofilm activity. *Desulfovibrio* and *Shewanella* spp., key electroactive and corrosive microorganisms, were identified as playing a critical role in extracellular electron transport, a process integral to MIC. The biotic condition exhibited significantly greater pit density, depth, and size compared to abiotic controls, highlighting the impact of continual biofilm growth on corrosion severity.

Biocide treatment was also investigated using the dual anaerobic biofilm reactor. Cyclic dosing led to an electronegative shift and reduced H_2S concentrations, indicating biofilm susceptibility. However, the biocide failed to fully eradicate the mixed-species biofilm, likely due to its structural properties acting as a diffusion barrier. These findings underscore the limitations of traditional biocide treatments and emphasize the need for improved biofilm management strategies. By bridging the gap between laboratory studies and real-world applications, this research enhances our understanding of MIC processes and contributes to the development of more effective corrosion mitigation techniques for industrial applications.

This research provides new insights into MIC mechanisms and highlights the need for evidence-based approaches to biofilm management and biocide application in industrial environments. The findings represent a step toward the development of standardised biofilm testing methods, improving MIC prediction and mitigation strategies.

Table of Contents

Research Thesis: Declaration of Authorship xiii

Acknowledgements xv

Definitions and Abbreviations 17

Units and Parameters 19

Chapter 1 Introduction 20

1.1 Statement of the Problem 20

1.2 Literature Review 23

1.2.1 MIC – Problematic Microorganisms 23

1.2.2 Corrosion Mechanisms 30

1.2.3 Mitigation Strategies 35

1.2.4 Threat Assessment – Current Standards 39

1.3 Methods for Assessing Biocorrosion 45

1.3.1 How to establish and test biofilms in the lab 45

1.3.2 Analytical methods and information to collect 47

1.3.3 Data interpretation for biocide efficacy 54

1.4 Aims and Objectives 54

1.5 Overview of Research Design 55

1.6 Significance of the Research and Contribution 56

Chapter 2 Materials and Methods 58

Test conditions. 58

Microbial consortia 60

Carbon steel coupon preparation. 60

Experimental setup. 60

Sulphide microsensor. 61

Surface profilometry and visual inspection. 61

Gravimetric analysis. 62

Corrosion product analysis. 62

Electrochemical analysis 63

Confocal laser scanning microscopy and post-image analysis. 64

Microbial community analysis. 65
ATP assay. 65

Chapter 3 Investigating the effects of surface roughness and nutrient-enriched artificial seawater on anaerobic marine biofilm formation and microbiologically influenced corrosion of UNS G10180 carbon steel..... 66

3.1 Introduction 66
3.2 Results 69
3.3 Discussion 80
3.4 Summary 87

Chapter 4 Investigating the effects of surface roughness and ATCC 1249 Modified Baar's media on anaerobic marine biofilm formation and microbiologically influenced corrosion of UNS G10180 carbon steel..... 89

4.1 Introduction 89
4.2 Results 92
4.3 Discussion 102
4.4 Summary 109

Chapter 5 Investigating the effects of produced water on anaerobic marine biofilm formation and microbiologically influenced corrosion of UNS G10180 carbon steel 111

5.1 Introduction 111
5.2 Results 113
5.3 Discussion 126
5.4 Summary 132

Chapter 6 Investigating the effects of glutaraldehyde on anaerobic marine biofilm formation and microbiologically influenced corrosion of UNS G10180 carbon steel 135

6.1 Introduction 135
6.2 Results 137
6.3 Discussion 151
6.4 Summary 156

Chapter 7 Conclusions, Limitations and Future Work.....158

7.1 Conclusions 158

7.2 Study Limitations 163

7.3 Future Work 164

Table of Tables

Table 1.1. Industry Standards for the energy sector. 40

Table 3.1. Fitted electrochemical parameters from polarisation curves; comparison between the abiotic and biotic AR and P UNS G10180 coupons after exposure to anaerobic nutrient-enriched artificial seawater media for 28 days. 76

Table 4.1. Fitted electrochemical parameters from polarisation curves; comparison between the abiotic and biotic AR and P UNS G10180 carbon steel coupons after exposure to anaerobic MB media for 28 days. 99

Table 5.1. Fitted electrochemical parameters from polarisation curves; comparison between the abiotic and biotic AR, UNS G10180 carbon steel coupons, after exposure to anaerobic produced water media for 28 days. 122

Table 6.1. Fitted electrochemical parameters from polarisation curves; comparison between the abiotic and biotic AR, UNS G10180 carbon steel coupons, after exposure anaerobic nutrient-enriched artificial seawater media dosed bi-weekly with glutaraldehyde for 28 days. 147

Table of Figures

Figure 1.1. A diagram illustrating biofilm formation cycle. Adapted from “Biofilm Formation Cycle”, by BioRender.com (2022). Retrieved from https://app.biorender.com/biorender-templates (accessed on 12 May 2022).21

Figure 1.2. A diagram illustrating sulphate reducing bacteria metabolic pathway. The process of iron dissolution occurs at the interface of the metal surface and biofilm by BioRender.com (2022). 24

Figure 1.3. A diagram illustrating nitrate reducing bacteria metabolic pathway. The process of iron dissolution occurs at the interface of the metal surface and biofilm by BioRender.com (2022). 26

Figure 1.4. Illustration of abiotic H_2S corrosion. The process of iron dissolution occurs at the interface of the metal surface and iron sulphide by BioRender.com (2022). .31

Figure 1.5. Illustration of oxygen corrosion. The process of iron dissolution occurs at the interface of the metal surface and bulk fluid by BioRender.com (2022). 32

Table of Figures

Figure 1.6. Illustration of pitting corrosion due to the creation of an oxygen concentration cell. The process of iron dissolution occurs at the interface of the metal surface and biofilm by BioRender.com (2022). Figure adapted from Jia *et al*., 2019. 33

Figure 1.7. Illustration of extracellular electron transfer in microbiologically influenced corrosion, through both direct and mediated electron transfer by BioRender.com (2022). Figure adapted from Jia *et al*., 2019. 34

Figure 1.8. CBR 90-3 Anaerobic CDC Biofilm Reactor® (key dimensions: 22 cm reactor height and 12 cm internal diameter; 21 cm coupon holder rod; 1.27 cm coupon diameter) Includes seals around each rod and between lid and vessel. The anaerobic CBR includes coupon holder rods, polycarbonate coupons, coupon removal tool, coupon manipulation tool, and glass flow breaks [181]. 46

Figure 1.9. Schematic view of a three-electrode setup. 52

Figure 2.1. (a) The dual anaerobic biofilm reactor system (abiotic and biotic reactors) comprising 10 L media containers, peristaltic pump, magnetic stirrer/hot plate, sulphide microsensor, and the three electrode cell setup. Each reactor has five rods, with three coupons in each rod (15 coupons in total). Each reactor has four inlets. ① The first inlet is connected to the peristaltic pump and then the media container. ② The outlet is connected to the waste containers. ③ Connection to the nitrogen gas source. ④ Air filter (Millex, 0.2 µm) that acts as the exit for excess gas in the reactors. ⑤ The 10 L media container is connected via the peristaltic pump and feeds the first inlet in the reactor. ⑥ Connection to the nitrogen gas source. ⑦ Air filter (Millex, 0.2 µm) that acts as the exit for excess gas in the media containers. **(b)** detailed three-electrode cell setup in an anaerobic CDC biofilm reactor: There are three separate carbon steel coupon working electrodes that can be measured per rod. Each reactor had two rods that were modified for electrochemical analysis, *n* = 3 for both as-received (AR) and polished (P) UNSG10180 carbon steel coupons. Created by BioRender.com. 59

Figure 2.2. Equivalent circuit models used to generate EIS parameters. The element '*R*' corresponds to a resistor and represents either the solution resistance, the resistance of the biofilm or the corrosion product film, and the charge transfer resistance, respectively. The element '*Q*' represents a constant phase element, which characterises the 'non-ideal' capacitance behaviour of either the biofilm or the corrosion product film layer, and the charge transfer capacitance. 64

Figure 3.1. Aqueous sulphide measurements (*SULF*, µmol L^{-1}) for the abiotic and biotic conditions over 28 days (nb. measured the anaerobic nutrient-enriched artificial seawater media *in situ* adjacent to corroding UNS G10180 carbon steel). 70

Figure 3.2. Three-dimensional optical surface profilometry of the cleaned UNS G10180 surfaces at day 28. AR coupons for: **(a)** abiotic and **(b)** biotic conditions; and P coupons for: **(c)** abiotic and **(d)** biotic conditions, after exposure to anaerobic nutrient-enriched artificial seawater media for 28 days. 71

Figure 3.3. Abiotic and biotic corrosion performance after exposure to anaerobic nutrient-enriched artificial seawater media for 28 days: **(a)** corrosion rate via gravimetric analysis and surface profilometry assessed **(b)** pit rate and **(c)** pit density ($P < 0.05$), for the AR and P coupons. 72

Figure 3.4. LPR data for UNS G10180 carbon steel: **(a)** open-circuit potentials and **(b)** polarisation resistance in anaerobic nutrient-enriched artificial seawater media (abiotic and biotic conditions), for the as-received (AR) and polished (P) coupons (data points represent mean ± standard deviation, *n* = 3). Reactor stirrer at 50 rpm. 72

Figure 3.5. EIS data for UNS G10180 carbon steel in anaerobic nutrient-enriched artificial seawater media at OCP: **(a, b)** Nyquist, **(c, d)** Bode phase angle (q vs. f), and **(e, f)** Bode impedance modulus (|Z| vs. f) over 28-days. (*n* = 3). Reactor stirrer at 50 rpm.....74

Figure 3.6. Potentiodynamic polarisation curves for the abiotic and biotic AR and P UNS G10180 carbon steel coupons at ambient temperature after exposure to anaerobic nutrient-enriched artificial seawater media for 28 days. Scan rate of 0.5 mV s^{-1} and reactor stirrer at 50 rpm. Dissolved oxygen levels were 2.6 ppm (abiotic) and 0.2 (biotic), at Day 28.....76

Figure 3.7. Principal Component Analysis biplot **(a)**; Microbial community. The results show the mean relative abundances of microbial communities classified at the genus level, for the top 25 genera, from 16S rRNA amplicon sequencing **(b)**; for environmental marine sediment, Day 0, and Day 28 planktonic samples, AR and P biofilm samples after exposure to anaerobic nutrient-enriched artificial seawater media for 28 days. 79

Figure 3.8. **(a)** Dissolved ATP (dATP) concentrations comparing the anaerobic nutrient-enriched artificial seawater media taken on Day 0 and Day 28 and **(b)** Total ATP (tATP)

concentration comparing the biofilm of the AR and P coupons, from the biotic condition, after exposure to anaerobic nutrient-enriched artificial seawater media for 28 days. 80

Figure 3.9. Schematic of the initial stages for UNS G10180 carbon steel in anaerobic abiotic and biotic nutrient-enriched artificial seawater media. corrosion mechanisms, **(a, b)** the formation of nascent inorganic corrosion film and the organic conditioning film with pioneering bacterial attachment; **(c, d)** maturing corrosion film under the abiotic condition and biofilm growth and colonisation under the biotic condition; **(e, f)** uniform and pitting corrosion under patchy corrosion deposits and bacteria clusters. BioRender.com (2023). 82

Figure 3.10. Schematic overview of key reactions and diversity of microorganisms within a biofilm involved in metal corrosion. It is important to note that the reactions illustrated may occur simultaneously. Numbers 1–6 refer to abiotic reactions associated with corrosion. Biotic reactions involved in corrosion of ferrous metals are also shown for electroactive corrosive bacteria, respiratory electroactive bacteria, and fermentative electroactive bacteria. BioRender.com (2023)..... 86

Figure 4.1. Aqueous sulphide measurements (*SULF*, µmol L^{-1}) for the abiotic and biotic conditions over 28 days (nb. measured the anaerobic MB media *in situ* adjacent to corroding UNS G10180 carbon steel). 93

Figure 4.2. Three-dimensional optical surface profilometry of the cleaned UNS G10180 surfaces at day 28. AR coupons for: **(a)** abiotic and **(b)** biotic conditions; and P coupons for: **(c)** abiotic and **(d)** biotic conditions, after exposure to anaerobic MB media for 28 days. 94

Figure 4.3. Abiotic and biotic corrosion performance after exposure to anaerobic MB media for 28 days: **(a)** corrosion rate via gravimetric analysis and surface profilometry assessed **(b)** pit rate and **(c)** pit density ($P < 0.05$ for the abiotic and biotic AR coupons, $P < 0.0001$ for the abiotic and biotic P coupons, $P < 0.0066$ for the biotic AR and biotic P coupons), for the AR and P coupons. 94

Figure 4.4. LPR data for UNS G10180 carbon steel: **(a)** open-circuit potentials and **(b)** polarisation resistance in anaerobic MB media (abiotic and biotic conditions), for AR and P coupons (data points represent mean ± standard deviation, $n = 3$). Reactor stirrer at 50 rpm. 96

Figure 4.5. EIS data for UNS G10180 carbon steel in anaerobic MB media at OCP: **(a, b)** Nyquist, **(c, d)** Bode phase angle (θ *vs.* f), and **(e, f)** Bode impedance modulus ($|Z|$ *vs.* f) over 28-days. (*n* = 3). Reactor stirrer at 50 rpm. 97

Figure 4.6. Potentiodynamic polarisation curves for the abiotic and biotic AR and P, UNS G10180 carbon steel coupons, at ambient temperature after exposure to anaerobic MB media for 28 days. Scan rate of 0.5 mV s^{-1} and reactor stirrer at 50 rpm. Dissolved oxygen levels were 0.5 ppm (abiotic) and 0.0 ppm (biotic), at Day 28. 98

Figure 4.7. Principal Component Analysis biplot **(a)**; Microbial community. The results show the mean relative abundances of microbial communities classified at the genus level, for the top 25 genera, from 16S rRNA amplicon sequencing **(b)**; for environmental marine sediment, Day 0, and Day 28 planktonic samples, AR and P biofilm samples after exposure to anaerobic MB media for 28 days.....101

Figure 4.8. **(a)** Dissolved ATP (dATP) concentrations comparing the anaerobic MB media taken on Day 0 and Day 28 ($P < 0.05$) and **(b)** Total ATP (tATP) concentration comparing the biofilm of the AR and P coupons ($P < 0.05$), from the biotic condition, after exposure to anaerobic MB media for 28 days.....102

Figure 4.9. Schematic of the initial stages for UNS G10180 carbon steel in anaerobic abiotic ATCC 1249 MB media. Corrosion mechanisms, **(a, b)** the formation of nascent inorganic corrosion film and the organic conditioning film with pioneering bacterial attachment; **(c, d)** general absence of a maturing corrosion film under the abiotic condition with a prolonged period of charge accumulation; whilst there was sustained biofilm growth and colonisation for the biotic condition **(e, f)** moderate uniform and pitting corrosion for both conditions; under patchy corrosion deposits and a thick slimy biofilm with black granular deposits for the biotic condition. BioRender.com (2024).....104

Figure 5.1. Three-dimensional optical surface profilometry of the cleaned UNS G10180 surfaces at day 28. AR coupons for: **(a,b)** abiotic and **(c,d)** biotic conditions, after exposure to anaerobic produced water media for 28 days. 114

Figure 5.2. Abiotic and biotic corrosion performance after exposure to anaerobic produced water media for 28 days: **(a)** corrosion rate via gravimetric analysis and surface profilometry assessed and **(b)** pit rate ($P < 0.05$), for the AR coupons. 115

Table of Figures

Figure 5.3. SEM-EDS elemental mapping of the UNS G10180 carbon steel, AR surfaces, after exposure to anaerobic produced water media, taken on day 28. **(a)** SEM image; **(b)** iron map; **(c)** sulphur map; **(d)** oxygen map. 117

Figure 5.4. Raman spectra of the UNS G10180 carbon steel surfaces after exposure to anaerobic produced water media, taken on day 28. For the AR **(a,b)** abiotic and; **(c, d)** biotic condition..... 118

Figure 5.5. LPR data for UNS G10180 carbon steel: **(a)** open-circuit potentials and **(b)** polarisation resistance in anaerobic produced water media (abiotic and biotic conditions), for AR and P coupons (data points represent mean ± standard deviation, *n* = 6). Reactor stirrer at 50 rpm..... 119

Figure 5.6. EIS data for UNS G10180 carbon steel in anaerobic produced water media at OCP: **(a, b)** Nyquist, **(c, d)** Bode phase angle (θ *vs.* f), and **(e, f)** Bode impedance modulus ($|Z|$ *vs.* f) over 28-days. (*n* = 6). Reactor stirrer at 50 rpm. 122

Figure 5.7. Potentiodynamic polarisation curves for the abiotic and biotic AR, UNS G10180 carbon steel coupons, at ambient temperature after exposure to anaerobic produced water media for 28 days. Scan rate of 0.5 mV s^{-1} and reactor stirrer at 50 rpm. 122

Figure 5.8. Principal Component Analysis biplot **(a)**; Microbial community. The results show the mean relative abundances of microbial communities classified at the genus level, for the top 25 genera, from 16S rRNA amplicon sequencing **(b)**; for environmental marine sediment, Day 0, and Day 28 planktonic samples, and AR biofilms, after exposure to anaerobic produced water media for 28 days. . 125

Figure 5.9. Dissolved ATP (dATP) concentrations comparing the anaerobic produced water media, taken on Day 0 and Day 28 ($P < 0.05$). 126

Figure 5.10. Schematic of the initial stages for UNS G10180 carbon steel in anaerobic abiotic and biotic PW media. corrosion mechanisms, **(a, b)** the formation of nascent inorganic corrosion film and the organic conditioning film with pioneering bacterial attachment during the initial batch phase; **(c, d)** maturing corrosion film under the abiotic condition with reduced biofilm growth and colonisation under the biotic condition due to the limited availability of organic carbon; **(e, f)** moderately low uniform and pitting corrosion under patchy corrosion deposits and thin biofilm with increasing granular deposits. BioRender.com (2024).128

Figure 5.11. Schematic overview of key reactions for UNS G10180 carbon steel in anaerobic abiotic and biotic PW media. It is important to note that the reactions illustrated may be complementary or antagonistic processes, particularly within the heterogeneous biofilm. 131

Figure 6.1. Aqueous sulphide measurements (*SULF*, µmol L^{-1}) for the biotic condition over 28 days (nb. measured the anaerobic nutrient-enriched artificial seawater media dosed bi-weekly with glutaraldehyde *in situ* adjacent to corroding UNS G10180 carbon steel). 138

Figure 6.2. Three-dimensional optical surface profilometry of the cleaned UNS G10180 surfaces at day 28. AR coupons for: **(a,b)** abiotic and **(c,d)** biotic conditions, after exposure to anaerobic nutrient-enriched artificial seawater media dosed bi-weekly with glutaraldehyde for 28 days.....139

Figure 6.3. Abiotic and biotic corrosion performance after exposure to anaerobic nutrient-enriched artificial seawater media dosed bi-weekly with glutaraldehyde for 28 days: **(a)** corrosion rate via gravimetric analysis and surface profilometry assessed ($P < 0.05$) and **(b)** pit rate, for the AR coupons.....139

Figure 6.4. SEM-EDS elemental mapping of the UNS G10180 carbon steel, AR surfaces, after exposure to anaerobic nutrient-enriched artificial seawater media dosed bi-weekly with glutaraldehyde, taken on day 28. **(a)** SEM image; **(b)** iron map; **(c)** sulphur map; **(d)** oxygen map. 142

Figure 6.5. Raman spectra of the UNS G10180 carbon steel surfaces after exposure to anaerobic nutrient-enriched artificial seawater media dosed bi-weekly with glutaraldehyde, taken on day 28. For the AR **(a,b)** abiotic and; **(c, d)** biotic condition. 143

Figure 6.6. LPR data for UNS G10180 carbon steel: **(a)** open-circuit potentials and **(b)** polarisation resistance in anaerobic nutrient-enriched artificial seawater media dosed bi-weekly with glutaraldehyde (abiotic and biotic conditions), for AR coupons (data points represent mean ± standard deviation, *n* = 6). Reactor stirrer at 50 rpm. 144

Figure 6.7. EIS data for UNS G10180 carbon steel in anaerobic nutrient-enriched artificial seawater media dosed bi-weekly with glutaraldehyde at OCP: **(a, b)** Nyquist, **(c,**

d) Bode phase angle (θ *vs.* f), and **(e, f)** Bode impedance modulus ($|Z|$ *vs.* f) over 28-days. (n = 6). Reactor stirrer at 50 rpm. 145

Figure 6.8. Potentiodynamic polarisation curves for the abiotic and biotic AR, UNS G10180 carbon steel coupons, at ambient temperature after exposure to anaerobic nutrient-enriched artificial seawater media dosed bi-weekly with glutaraldehyde for 28 days. Scan rate of 0.5 mV s^{-1} and reactor stirrer at 50 rpm. 147

Figure 6.9. Confocal microscopy of biofilm formed over UNS G10180 carbon steel surfaces for AR **(a, b)** biotic coupon sample 1; **(c, d)** biotic coupon sample 2, after exposure anaerobic nutrient-enriched artificial seawater media dosed bi-weekly with glutaraldehyde for 28 days..... 148

Figure 6.10. Principal Component Analysis biplot **(a)**; Microbial community. The results show the mean relative abundances of microbial communities classified at the genus level, for the top 25 genera, from 16S rRNA amplicon sequencing **(b)**; for environmental marine sediment, Day 0, and Day 28 planktonic samples, and AR biofilms, after exposure anaerobic nutrient-enriched artificial seawater media dosed bi-weekly with glutaraldehyde for 28 days. 149

Figure 6.11. Dissolved ATP (dATP) concentrations comparing the anaerobic nutrient-enriched artificial seawater media dosed bi-weekly with glutaraldehyde, taken on Day 0 and Day 28 ($P < 0.05$). 151

Figure 6.12. Schematic of the initial stages for UNS G10180 carbon steel in anaerobic abiotic and biotic artificial seawater media. corrosion mechanisms, **(a)** the formation of nascent inorganic corrosion film and the organic conditioning film; **(b)** maturing corrosion film under the abiotic condition; **(c)** moderate uniform and pitting corrosion under patchy corrosion deposits, with increasing granular deposits. BioRender.com (2024)..... 152

Figure 6.13. Schematic of the initial stages for UNS G10180 carbon steel in anaerobic abiotic and biotic artificial seawater media. Corrosion mechanisms, **(a)** the formation of nascent inorganic corrosion film and the organic conditioning film with pioneering bacterial attachment; **(b)** maturing corrosion film with inhibited biofilm growth and colonisation due to biocidal activity; **(c)** moderate uniform and pitting corrosion under patchy corrosion deposits, with increasing granular deposits, as well as patchy biofilm due to biocidal activity. BioRender.com (2024). 155

Research Thesis: Declaration of Authorship

Print name: Liam Matthew Jones

Title of thesis: Microbiologically-influenced corrosion (MIC): Development of a model system to investigate the role of biofilm communities within MIC and their control using industrial biocides

I declare that this thesis and the work presented in it are my own and has been generated by me as the result of my own original research.

I confirm that:

1. This work was done wholly or mainly while in candidature for a research degree at this University;
2. Where any part of this thesis has previously been submitted for a degree or any other qualification at this University or any other institution, this has been clearly stated;
3. Where I have consulted the published work of others, this is always clearly attributed;
4. Where I have quoted from the work of others, the source is always given. With the exception of such quotations, this thesis is entirely my own work;
5. I have acknowledged all main sources of help;
6. Where the thesis is based on work done by myself jointly with others, I have made clear exactly what was done by others and what I have contributed myself;
7. None of this work has been published before submission.

Signature:

Date: .....26 March 2025

Acknowledgements

Firstly, I would like to express my appreciation and gratitude to both Professor Julian Wharton and Professor Jeremy Webb in their capacity as primary supervisors. Julian has contributed significantly to the research detailed in this thesis through his wisdom, leadership, guidance, and council. Thanks, and acknowledgements extend to co-supervisors Dr Torben Lund Skovhus and Dr Maria Salta, who's detailed and knowledgeable feedback was instrumental throughout the course of the project. My sincere gratitude is also expressed to my industry co-supervisors Dr Kathryn Thomas and Dr Timothy Illson, for their guidance, industry experience and role in funding acquisition.

This work was supported by the South Coast Biosciences Doctoral Training Partnership (SoCoBio DTP), a Biotechnology and Biological Sciences Research Council (BBSRC) funded research training programme (reference number BB/T008768/1) in affiliation with DNV, and the National Biofilms Innovation Centre (NBIC). I acknowledge the University of Southampton, the SoCoBio DTP and DNV for providing the resources and facilities to execute research questions. Many thanks to Dr Joe Parker who generously provided his expertise and assistance when it came to bioinformatics analysis. I am also grateful to Dr Terence Harvey and Dr Mark Willet for their assistances with Infinite Focus Microscopy and Confocal Laser Scanning Microscopy. Also, thanks to Dr Niall Hanrahan for his knowledge and guidance with Raman spectroscopy. We are very grateful for the technical support from our colleagues in the Department at the University of Southampton

I would like to thank the team at DNV for their collaboration and involvement in the project: especially Dr Kathryn Thomas, Dr Timothy Illson as well as Dr Martin Brown and Dr Martin Maple during my 3-months internship at their offices in Loughborough. The team's motivation, knowledge and broad skill set were appreciated throughout my time there. I would also like to thank Dr Lilian Strand Ree, from Aker BP who contributed to research outlined here through providing produced water and provided valuable discussions about asset conditions and biocide dosage concentrations and frequency used in industry.

I am grateful to Professor Jeremy Webb for constructing the core team at the University of Southampton, and to and the wider NBIC community as well as Euro-MIC networks which have provided valuable insight into the broader research.

Finally, I would like to express my sincere appreciation to my family, especially my parents Suzanne and John Jones, and my brothers Sean, Joe and Eoin Jones for their patience, support, compassion, and love. I would not be where I am today without their support and encouragement.

Definitions and Abbreviations

AFM ..... Atomic Force Microscopy

AMPP ..... Association for Materials Protection and Performance

APB ..... Acid producing bacteria

AR ..... As Received

ASW ..... Artificial seawater

ATP ..... Adenosine triphosphate

BCNR ..... Biocatalytic cathodic nitrate reduction

BCSR ..... Biocatalytic cathodic sulphate reduction

CDC ..... Centre for disease control and prevention

CE ..... Counter electrode

CLSM ..... Confocal laser scanning microscopy

CMIC ..... Chemical microbial influenced corrosion

CPE ..... Constant phase element

CRA ..... Corrosion resistant alloys

CS ..... Carbon steel

DET ..... Direct electron transfer

DLVO ..... Derjaguin−Landau−Verwey−Overbeek theory

DNA ..... Deoxyribonucleic acid

ECM ..... Equivalent circuit model

EDS ..... Energy dispersive X-ray spectroscopy

EIS ..... Electrochemical impedance spectroscopy

EMIC ..... Electrical microbial influenced corrosion

EPS ..... Extracellular polymeric substance

GR ..... Green rust

HER ..... Hydrogen evolution reaction

IOB ..... Iron oxidising bacteria

IRB..... Iron reducing bacteria

LPR ..... Linear polarisation resistance

MB..... ATCC 1249 Modified Baar's media

MET..... Mediated electron transfer

MIC..... Microbiologically influenced corrosion

MLOE ..... Multiple lines of evidence

MMM..... Molecular microbiological methods

MPN ..... Most probable number

NACE ..... National Association of Corrosion Engineers

NGS ..... Next generation sequencing

NRB ..... Nitrate reducing bacteria

OCP ..... Open circuit potential

P ..... 25 micrometres polished

PCA..... Principal component analysis

PW ..... Produced water

qPCR..... Quantitative polymerase chain reaction

QAC..... Quaternary ammonium compounds

QS..... Quorum sensing

QSI..... Quorum sensing inhibitor

RE ..... Reference electrode

RPS..... Relative pitting severity

SEM..... Scanning electron microscopy

SRA..... Sulphate reducing archaea

SRB..... Sulphate reducing bacteria

SRM..... Sulphate reducing microorganisms

SS ..... Stainless steel

UDC..... Under deposit corrosion

WE.....Working electrode

XRD.....X-Ray Diffraction

Units and Parameters

Parameter		Unit
A	Sample area	cm^2
$dATP$	Dissolved Adenosine triphosphate	$pg\ ml^{-1}$
$tATP$	Total Adenosine triphosphate	$pg\ cm^{-2}$
β_a	Anodic Tafel slope	$mV\ dec^{-1}$
β_c	Cathodic Tafel slope	$mV\ dec^{-1}$
CR	Corrosion rate	$mm\ y^{-1}$
D	Density	$g\ cm^{-3}$
DO	Dissolved Oxygen	ppm
E_{corr}	Corrosion potential or Open Circuit Potential (OCP)	V
j_{corr}	Corrosion current density	$A\ cm^{-2}$
PD	Pit density	$pits\ mm^{-2}$
PR	Pit rate	$mm\ y^{-1}$
R_p	Polarisation resistance	$k\Omega\ cm^{-2}$
R_a	Average mean of roughness profile	µm
R_t	Maximum peak to valley height of roughness profile	µm
R_z	Mean peak to valley height of roughness profile	µm
R_{peak}	Maximum peak height of roughness profile	µm
R_v	Maximum valley height of roughness profile	µm
R_c	Mean height of profile irregularities of roughness profile	µm
R_{sm}	Mean spacing of profile irregularities of roughness profile	µm
R_t/R_z	Extreme Scratch/Peak value of roughness profile, (≥1), higher values represent larger scratches/peaks	µm
$SULF$	Aqueous sulphide measurements	$\mu mol\ L^{-1}$
Z	Impedance	$\Omega\ cm^{-2}$
Z'	Real impedance or resistance	$\Omega\ cm^{-2}$
Z''	Imaginary impedance or capacitance	$\Omega\ cm^{-2}$

Chapter 1 Introduction

1.1 Statement of the Problem

Microbiologically influenced corrosion (MIC) or biocorrosion is a major industrial concern, which is estimated globally to cost around $2.5 to $4 trillion annually [1]. It is a complex process that poses a major threat due to the interactions between biofilms and surfaces. The challenge in understanding and predicting MIC is the lack of robust and reproducible model biofilm systems that reflect real-world and operating environments. Furthermore, there are not nationally or internationally recognised standards or test methods with which to evaluate control strategies effective against biofilm-mediated corrosion.

Biofilms are surface-adherent sessile microbial communities that are more tolerant towards antimicrobials and biocides than planktonic microorganisms (Figure 1.1). This is due to the presence of extracellular polymeric substances (EPS), which consists of proteins, lipids, polysaccharides, and nucleic acids [2, 3]. Microorganisms that attach to surfaces and embed within biofilms are termed sessile, whilst those microorganisms that remain within bulk fluid are termed planktonic [3, 4]. EPS production by sessile microorganisms' initiates attachment and surface colonisation, which is subsequently followed by the formation of biofilm structures [3, 5].

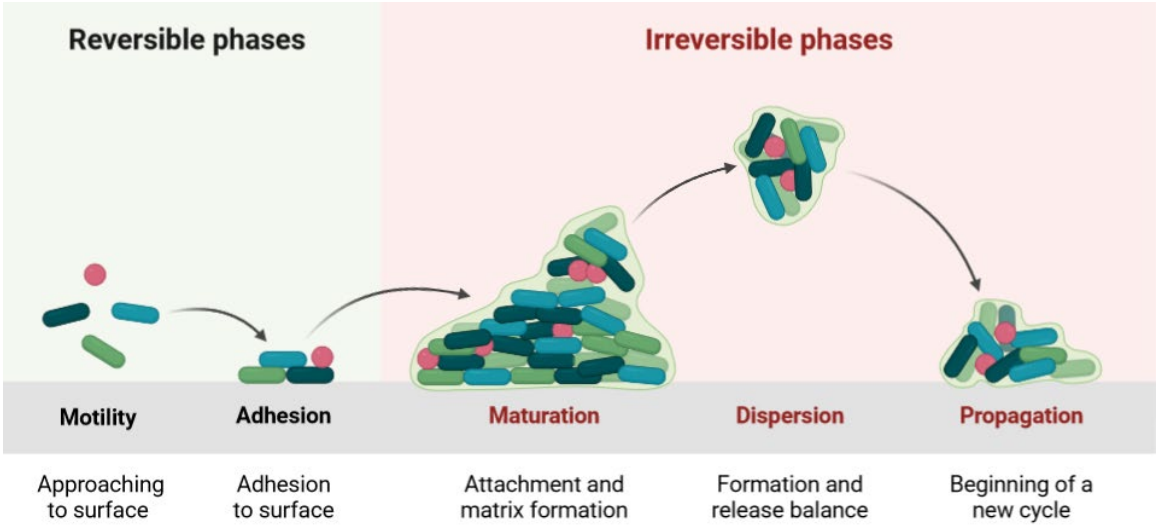

Figure 1.1. A diagram illustrating biofilm formation cycle. Adapted from "Biofilm Formation Cycle", by BioRender.com (2022). Retrieved from https://app.biorender.com/biorender-templates (accessed on 12 May 2022).

The interaction between a surface and a bacterial cell has been shown to follow the principle of colloidal physics described by the Derjaguin−Landau−Verwey−Overbeek (DLVO) theory [5]. There are several ecological advantages associated with the formation of biofilms. In nature, a biofilm will typically comprise of a mixed-species consortium that will form synergistic relationships enabling the mixed-species biofilm to be more recalcitrant, compared to single-species biofilms [6]. Sessile microorganisms are also able to detach from a biofilm to colonise a new surface which can exacerbate the threat of MIC [7]. These surfaces can be organic or inorganic, and in distinct environmental conditions. Consequently, biofilms have been found on a wide range of metals and alloys across industrial sectors. This includes carbon steel (CS) [8], stainless steel (SS) [9], aluminium [10], copper [11], as well as magnesium [12] and zinc alloys [13]. The distinct environmental conditions in combination with the surfaces physical and chemical metallurgical properties greatly influences the metabolic activities of biofilms attached, altering the physical and chemical properties of these materials, and changing their susceptibility to MIC [14]. It is this process, whereby biofilms modify the kinetics of corrosion reactions that is known as MIC [15]. Though, it is important to quantify corrosion rate (*CR*) appropriately, as abiotic conditions can also lead to corrosion without the influence of microorganisms. Biofilms can initiate, accelerate, or facilitate corrosion reactions via several mechanisms [16], causing significant damage to equipment and infrastructure in many industries including but not limited to the energy sector [17], as well as in water systems [18], marine environments [19], nuclear waste storage facilities [20], aviation fuel systems [21] and medical devices [22].

The exact mechanisms can be difficult to accurately identify within industry as corrosion can arise through a variety of different mechanisms, either abiotic or biotic. Nonetheless, corrosion depends on redox reactions which involve the oxidised and reduced forms of a species be it an ion, a molecule, or a biological entity at the metal/electrolyte interface [23]. Abiotic types of corrosion are those that are not influenced by microorganisms [23]. Whilst biotic MIC can contribute to corrosion either directly or indirectly through electrical microbial influenced corrosion (EMIC), and chemical microbial influenced corrosion (CMIC) in anaerobic conditions, as well as through a few mechanisms under aerobic conditions [6]. Currently, there is a general lack a critical understanding of how microorganisms behave in mixed biofilm communities [24]. Moreover, distinguishing the degree to which abiotic or biotic conditions lead to corrosion is a major challenge. In a case study from 2012, CS pipe spools from an oil production system on the Otter offshore platform in the North Sea were found during inspection to exhibit severe internal corrosion. At the time of commissioning, the major internal corrosion threat was believed to be the high partial pressure of carbon dioxide (CO_2) in the system that was to be mitigated using corrosion inhibitors. The investigation took into consideration data for microbiology, materials/corrosion products, as well as the chemical and physical environment. It was concluded that, although CO_2 was likely contributing to general corrosion under the deposits, MIC associated with the high numbers of methanogens and sulphate reducing bacteria (SRB) was driving or contributing to high localised CR. The integration of various types of data was essential for determining that MIC was the predominant corrosion mechanism [23]. The different mechanisms make it difficult to correctly assess the threat, identify the appropriate mitigation strategy and effectively manage MIC *in situ* [6, 25]. A fundamental understanding of the corrosion mechanisms is essential for selecting appropriate measures for mitigating or preventing corrosion.

Diverse microorganisms can all play a role in MIC. Therefore, it is essential to be able to identify various microorganisms within a mixed-species heterogeneous biofilm to be able to fully understand different MIC mechanisms. Current industrial standards, such as those from the Association for Materials Protection and Performance (AMPP) formerly known as the National Association of Corrosion Engineers (NACE), emphasize that sessile microorganisms are the most crucial biological factor. However, it is acknowledged that methods and procedures for studying sessile microorganisms are restricted and can produce inconsistent results [26, 27]. It has been reported recently in Alberta, Canada over a three year period, that only 70% of all risk-based inspections collected microbial samples for investigation. From these, <25% took sessile biofilm samples [28]. For the same risk-based inspection investigations, >90% analysed materials and corrosion products, as well as monitoring physical and chemical environmental conditions [28].

Consequently, it is no surprise that misdiagnosis of MIC and ineffective treatment with biocides is common.

This review highlights the different microorganisms that can lead to MIC in industry and examines the different corrosion mechanisms that have been described. Current standard methods for assessing the threat of MIC and common mitigation strategies that are used are discussed. It aims to explore recent advances in biofilm testing and MIC research to influence recommendations of new standards being drafted by AMPP.

1.2 Literature Review

1.2.1 MIC – Problematic Microorganisms

A wide diversity of microorganisms, including bacteria, archaea, and fungi, have been implicated in MIC. Typically, these grow as biofilms, and it is the interactions within these heterogeneous biofilm communities that induce corrosion. Specifically, it is the activity of electroactive microorganisms, within these 'electromicrobiomes', which is of particular ecological significance [29]. Electrogenic and electrotrophic bacteria, such as *Shewanella* and *Desulfovibrio* species, play crucial roles in extracellular electron transfer (EET) processes, which are central to microbiologically influenced corrosion (MIC). *Shewanella oneidensis* utilizes a well-characterised multiheme cytochrome system, including MtrA, MtrB, and MtrC, to shuttle electrons across the outer membrane to external electron acceptors, such as Fe(III) oxides, or conductive surfaces. Additionally, *Shewanella* produces conductive pili and outer membrane vesicles that facilitate electron flow over extended distances. *Desulfovibrio* spp., known for their sulphate-reducing capabilities, contribute to corrosion through the production of hydrogen sulphide (H_2S) and direct electron uptake mechanisms. These bacteria possess periplasmic hydrogenases, as well as c-type cytochromes such as OmcA, which are involved in both electron donation and uptake from metal surfaces. Some MIC-associated microorganisms, including *Geobacter* spp., utilize conductive protein filaments known as bacterial nanowires, enabling long-range electron transfer in biofilms. These adaptations allow electrotrophic bacteria to exploit external electron donors (e.g., metallic iron) and drive corrosion processes, while electrogenic species facilitate metal reduction and redox cycling in anaerobic environments [29]. Understanding these biochemical and physiological traits is crucial for mitigating MIC, as these biofilms play a key role in EET. These bacteria engage in EET strategies, such as direct electron transfer (DET) via outer membrane cytochromes like MtrC and OmcA; mediated electron transfer (MET), which involves soluble redox mediators such as flavins or

hydrogen; and direct interspecies electron transfer (DIET), where conductive pili or cytochrome-rich nanowires enable electron exchange between microbial partners, facilitating syntrophic interactions in biofilms and corrosion environments. Therefore, identifying the different microorganisms involved in corrosion is crucial for accurately determining the specific MIC mechanisms at play.

SRB and sulphate reducing archaea (SRA), collectively termed sulphate reducing microorganisms (SRM) are anaerobic microorganisms involved in MIC. SRB are found in the Deltaproteobacteria class, a subclass of Proteobacteria which contains exclusively Gram-negative microorganisms. This class of bacteria comprises a branch of anaerobic genera, which contains many known SRB such as *Desulfovibrio* sp., *Desulfobacter* sp., and *Desulfomonas* sp. SRB are bacteria that obtain energy by oxidising molecular hydrogen (H_2) or a range of organic compounds, such as lactate, acetate, pyruvate, and malate to reduce sulphate (SO_4^{2-}), the terminal electron acceptor, to biogenic H_2S (Figure 1.2).

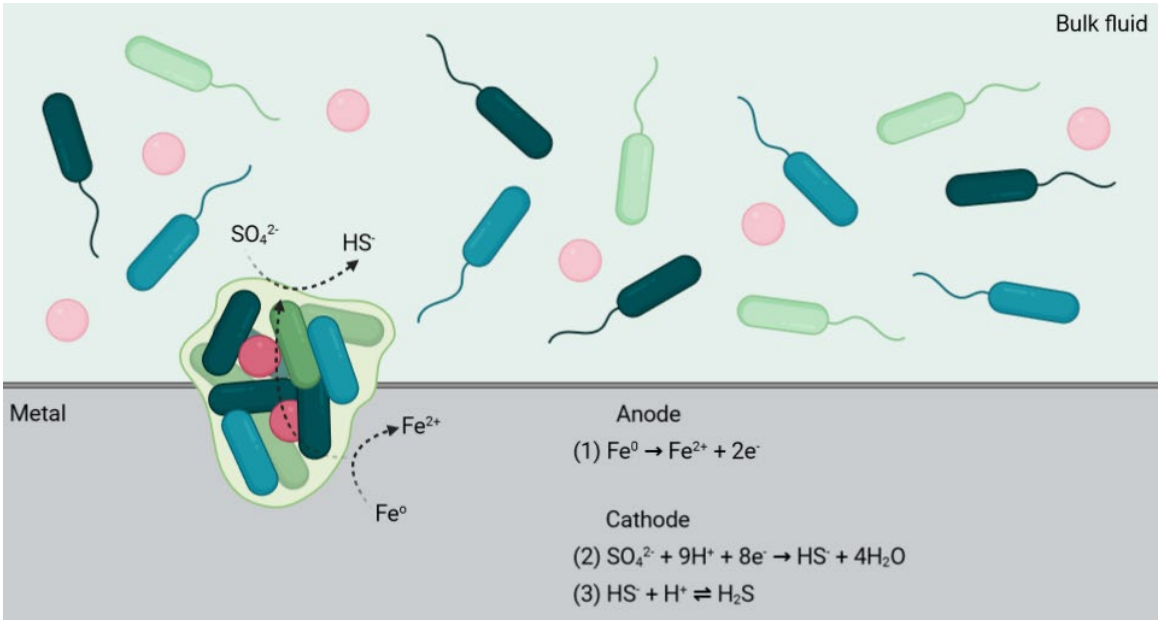

Figure 1.2. A diagram illustrating sulphate reducing bacteria metabolic pathway. The process of iron oxidation at the anode occurs at the interface of the metal surface and biofilm, whilst the process of sulphide reduction at the cathode occurs at surface of the biofilm EPS by BioRender.com (2022).

Most SRB can also reduce other oxidised inorganic sulphur compounds, such as sulphite (SO_3^{2-}), thiosulphate ($S_2O_3^{2-}$) and elemental sulphur amongst others [30]. SRB can also directly utilise elemental iron (Fe^0) as an electron donor. As such, SRB are widely studied in MIC literature and are generally considered to play an important role in the corrosion of metal surfaces. SRB are aerotolerant anaerobes that will typically grow under anoxic conditions at the bottom of a mixed-species biofilm, in contact with a metal surface. Facultative and/or aerobic microorganisms provide a locally anaerobic environment in a mixed-species biofilm that supports SRB growth [31, 32]. For example, some strains of *Desulfovibrio vulgaris* and *Desulfovibrio desulfuricans*, have been shown

to develop the ability of aerobic respiration. However, these strains seem only to get maintenance energy without growth when oxygen (O_2) is used as the terminal electron acceptor [31, 32, 33]. Corrosion studies have historically used single-species SRB biofilms to study corrosion mechanisms, with *Desulfovibrio vulgaris* often being used as a model organism. *Desulfovibrio* sp. are commonly found in aquatic environments and are typically mesophilic (grows best in moderate temperatures, optimum growth ranges from 20 - 45 °C) but can survive in extreme environments such as oligotrophic (very low levels of nutrients) as well as thermophilic (thrives at relatively high temperatures, between 41 and 122 °C) habitats. Yet, attributing the exact corrosion mechanisms can still be complicated due to the production of H_2S and iron sulphides such as mackinawite (FeS). MIC through the respiration of SRB produces biogenic H_2S. Instead of contributing protons (H^+) to the bulk fluid, H_2S generated by SRB consumes H^+ and this increases the pH [34]. Under a high concentration of dissolved H_2S, FeS can form which will influence the corrosion of the underlying metal [35], offering varied degrees of passivation [2, 36]. The biocathode theory, or more specifically the biocatalytic cathodic sulphate reduction (BCSR) theory, is the mechanism that leads to biocorrosion in the presence of SRB and biogenic H_2S [37, 38, 39]. In contrast, sulphate oxidising bacteria (SOB) are a group of microorganisms that oxidises diverse reduced sulphur species (e.g., H_2S and $S_2O_3^{2-}$) and elemental sulphur to sulphuric acid under more acidic conditions. A diverse range of SOB is involved in metal corrosion, including both aerobic and anaerobic microorganisms [40]. Among these, SOB, particularly those belonging to the *Sulfuricurvum* sp. and *Thiomicrospira* sp., have been extensively researched [41, 42].

Nitrate reducing bacteria (NRB) are a diverse group of bacteria that can be found across several classes including Gammaproteobacteria, Betaproteobacteria, Bacilli and Clostridia. Gammaproteobacteria are comprised of Gram-negative microorganisms and are a phylogenetically and physiologically diverse class of Proteobacteria. Moreover, they are widely distributed and abundant in various ecosystems such as soil, freshwater lakes and rivers, oceans, and salt lakes. Furthermore, they play a vital role in nutrient cycling in marine and coastal ecosystems. Similarly, Betaproteobacteria are a class of Gram-negative bacteria which are closely related to Gammaproteobacteria and represent a broad class of Proteobacteria. They play a vital role in maintaining soil pH and in nutrient cycling. Bacilli are comprised almost exclusively of Gram-positive microorganisms and are obligate or facultative aerobes. Whilst Clostridia are obligate anaerobes and O_2 is toxic to them. Clostridia are a highly polyphyletic class of bacteria comprised predominately of Gram-positive microorganisms. Both Bacilli and Clostridia are found in many places in the environment, most notably the soil. NRB are bacteria that metabolise nitrates (NO_3^-) or nitrites (NO_2^-) into nitrogen-containing gases through what is termed the biocatalytic cathodic

nitrate reduction (BCNR) theory (Figure 1.3). The BCNR theory is the mechanism whereby NO_3^- or NO_2^- intermediates are reduced, as the terminal electron acceptors, to oxidise Fe^0, the electron donor. These bacteria are grouped according to their use of organic or inorganic electron donors and their NO_3^- reduction process, whether via nitrogen (N_2) or ammonia (NH_4) production [43]. Examples include *Pseudomonas* sp., *Klebsiella* sp., and *Clostridioides* sp.

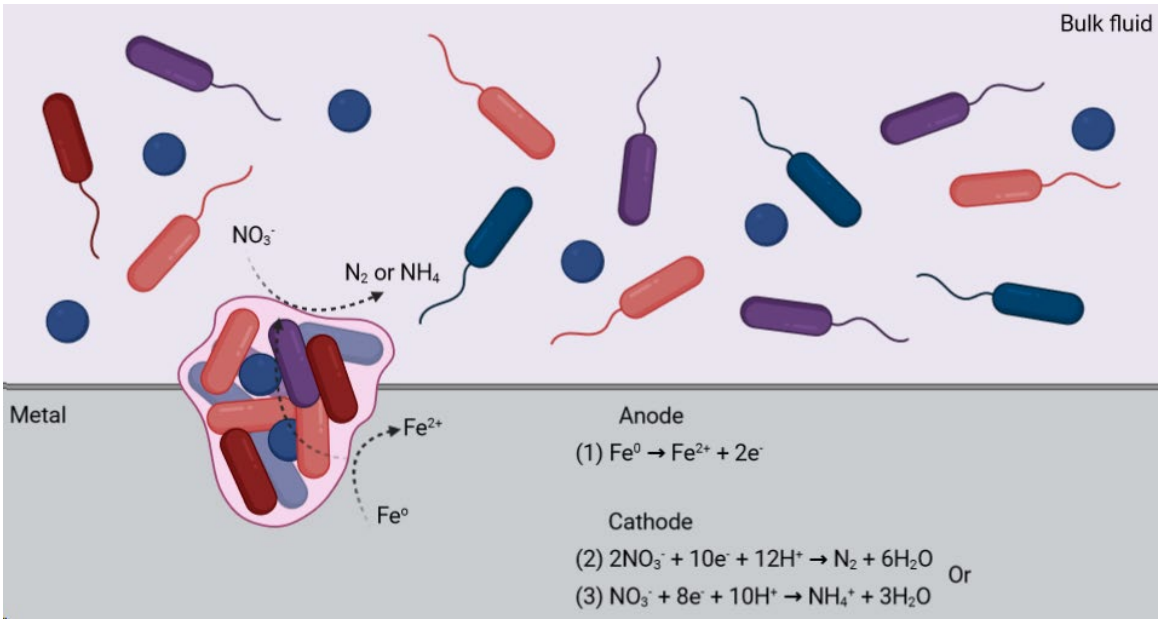

Figure 1.3. A diagram illustrating nitrate reducing bacteria metabolic pathway. The process of iron oxidation at the anode occurs at the interface of the metal surface and biofilm, whilst the process of nitrate reduction at the cathode occurs at surface of the biofilm EPS by BioRender.com (2022).

In the energy sector, NO_3^- has often been injected into oil reservoirs to suppress SRB growth with limited efficacy [44]. This mitigation strategy can prevent and remediate souring by stimulating the growth and activity of NRB [45, 46, 47, 48, 49]. However, the problem is that all subsurface microbiomes are different, and will respond differently to treatment [44]. Though, when successful, two different mechanisms for NRB-facilitated souring control have been proposed. Nitrate-sulphate competition is the mechanism whereby NO_3^-, a better more energetically favourable electron acceptor, is utilised over SO_4^{2-}, and therefore NRB outcompete SRB. Consequently, NO_3^- injection suppresses SO_4^{2-} reduction as it is thermodynamically more favourable. Alternatively, NO_3^- driven H_2S oxidation is the mechanism whereby the H_2S produced by SRB during souring is re-oxidised with NO_3^- as electron acceptor [50, 51]. Again, this mechanism has been shown to be thermodynamically more favourable. However, whilst NRB can mitigate souring, Fe^0 oxidation coupled with NRB is thermodynamically more favourable compared to Fe^0 oxidation coupled with SRB [52]. Under low organic carbon concentrations or localised accumulations of NO_2^-, EET between the metal surface and the NRB biofilm occurs. A localised cathodic site is developed due to the NRB activity, with an anodic site at an adjacent uncovered surface [53]. Miller *et al*. demonstrated that under nitrate-reducing conditions, uniform and pitting CS corrosion can occur due to NO_2^- accumulation. Moreover, conditions of sustained NO_2^-

accumulation can lead to more-aggressive corrosion [53]. Thus, NO_3^- injection should be managed carefully as NRB associated MIC is an equally important risk factor [54].

Acid producing bacteria (APB) are another group of microorganisms that are well characterised in MIC, which are phylogenetically diverse across the tree of life. APB are fermentative microorganisms prevalent across several classes. These include Bacilli, Clostridia, and Bacteroides. Examples include *Ligilactobacillus* sp., *Ruthenibacterium* sp., *Anaerotignum* sp. and *Parabacteroides* sp. Unlike Bacilli and Clostridia mentioned previously, Bacteroides are a genus of Gram-negative obligate anaerobic bacteria that can be found in the rhizosphere. They are also present in anaerobic environments such as sewage, wastewater treatment plants, marine and freshwater sediments, and deep subsurface ecosystems, where they contribute to organic matter degradation. Members of the Bacteroides genus are saccharolytic microorganisms which are capable of several metabolic processes. They can produce succinic, acetic, lactic, and propionic acids depending on available nutrients. Bacteroides species are known to be mutualistic in nature, where they play a fundamental role in processing of complex molecules to simpler ones. APB cause MIC due to the production of organic acids in the absence of O_2. For example, acetic acid bacteria are a group of Gram-negative bacteria which oxidise sugars or ethanol and produce acetic acid during fermentation [55]. Whilst lactic acid bacteria are a group of Gram-positive bacteria which produce lactic acid as the major metabolic end-product of carbohydrate fermentation [56]. These fermentative microorganisms use the metabolite as the electron acceptor to achieve redox balance [38, 57]. The different organic acids produced by these microorganisms, and others, generate an acidic environment underneath a biofilm, which in turn leads to the generation of separate anodic and cathodic sites. With a sufficiently low pH, H^+ attack is thermodynamically favourable when coupled with Fe^0 oxidation [58]. Corrosive metabolites accelerate the rate of cathodic reduction through the buffering effect theory, which is where undissociated weak acids dissociate near a metal surface to provide H^+. For APB associated MIC to be significant, the pH value needs to be much lower than 7, for the dissociation of H^+ [38]. Both sessile and planktonic cells can contribute to corrosion by producing H^+ to help maintain an acidic environment [6]. Though, the pH value underneath an APB biofilm will be lower than that in the bulk fluid, due to the sessile cell density [58]. As such, localised pitting corrosion underneath APB biofilms will be much more severe than any general uniform corrosion. Additionally, an acidic environment also inhibits the formation of protective corrosion products or passivation films which can further exacerbate corrosion [59].

Iron oxidising bacteria (IOB), are bacteria that derive their energy for growth by oxidising dissolved ferrous iron (Fe^{2+}) to ferric iron (Fe^{3+}) and subsequently forming insoluble ferric oxide

deposits [60]. Examples of IOB cited as causing MIC can be found in the Betaproteobacteria and Gammaproteobacteria classes, including *Gallionella* sp., *Leptothrix* sp., *Sphaerotilus* sp., and *Crenothrix* sp. [61]. These microorganisms are chemolithotrophic (generate energy by the oxidation of inorganic molecules for biosynthesis), microaerophilic (requires environments containing lower levels of O_2) species which can be found in many different types of habitats such as freshwater, brackish waters, marine hydrothermal water environments, as well as in soil environments. Conversely, iron reducing bacteria (IRB), including strict anaerobes such as *Geobacter* sp. and facultative anaerobes such as *Shewanella* sp., utilise Fe^{3+} as efficient electron acceptors that are capable of out-competing electron acceptors of lower potential, such as SO_4^{2-} [62, 63]. Again, these can be found in aquatic and soil environments. Both groups of microorganism's influence corrosion by either forming or dissolving minerals. Metal oxidising microorganisms cause biomineralization that results in mineral deposition on a metal surface which can shift the corrosion potential (E_{corr}) in either a positive or negative direction, depending on the nature of the mineral. For example, iron oxide formation can initiate a sequence of events that results in under deposit corrosion (UDC) of susceptible metals [63, 64]. UDC leads to a large increase in electrical potential difference between anodic and cathodic sites [64, 65, 66, 67, 68, 69], leading to localised pitting corrosion. Biomineral dissolution reactions by metal reducing microorganisms remove oxide layers or force mineral replacement reactions that lead to further dissolution of metals [63]. Metal dissolution is a localised preferential corrosion. The rate of dissolution depends on many aspects and parameters, such as chemical nature of the solvent and solute, temperature, and interfacial surface area.

In recent years, there has been an intensified research focus on the archaeal groups involved in microbial corrosion. Archaea are prokaryotic microorganisms, like bacteria, that do not have membrane-bound organelles or nucleus [70]. However, archaea possess several metabolic pathways that are more closely related to those of eukaryotes and distinct from bacteria. Furthermore, archaea use more energy sources ranging from organic compounds, such as sugars, to NH_4, metal ions or H_2. Many extremophiles are archaea that can tolerate extreme conditions such as very high temperatures, salinity, and pressures [71]. For example, *Methanobacterium* sp. are a group of methanogens which belong to the archaea domain, that produce methane as a metabolic by-product in hypoxic environments and have been found in environments such as hot springs and submarine hydrothermal vents. There has been increasing evidence that suggests methanogens also contribute to iron corrosion in O_2-free environments leading to pitting corrosion [72, 73, 74]. Methanogens use H_2 as an electron donor during their respiration coupled with CO_2 reduction [75]. Anaerobic respiration that utilises H_2 as an electron donor and CO_2 as an electron acceptor occurs through the acetyl coenzyme A pathway, also known as the Wood-Ljungdahl

pathway [76, 77]. H_2 utilisation can cause cathodic depolarisation, thus accelerating corrosion by CO_2. Cathodic depolarisation removes the H_2 gas surrounding the cathode and speeds up the corrosion process [78, 79]. In the context of corrosion, depolarisation through the removal of H_2 prevents polarisation on the metal surface. Cathodic polarisation is a potential shift in the negative direction, whilst anodic polarisation is a shift in the positive direction. For all metals, cathodic polarisation always reduces the *CR* as current will flow from metals with a lower E_{corr} to materials with a higher E_{corr}. Ultimately, if the E_{corr} is dropping because of cathodic depolarisation, then the surface is oxidising, accelerating the rate of corrosion. Moreover, when the H_2 supply is limited, methanogenic biofilms may switch to Fe^0 as an electron donor thus causing more severe corrosion [6]. Similarly, there are also some acetogenic archaea that utilise the Wood-Ljungdahl pathway. Examples include *Acetobacterium* sp. and *Sporomusa* sp. Though there is some taxonomic ambiguity here. Acetogens, whether bacteria or archaea have diverse metabolic roles, which help them thrive in different environments. These microorganisms generate acetate as an end-product of anaerobic respiration or fermentation. Again, cathodic depolarisation through the consumption of chemically generated H_2 is the corrosion mechanism, though acetogenic biofilms are also capable of using elemental Fe^0 as an electron donor [80, 78]. In both instances, cathodic depolarisation of the metal surface occurs, where CO_2 reacts by consuming electrons at the cathode. The cathodic reaction involves the formation water and methane in the presence of methanogens or acetate in the presence of acetogens. Some archaea are also SO_4^{2-} or NO_3^- reducers.

Fungi, such as yeasts and moulds, are another type of microorganism which are poorly studied in the literature. Recent evidence indicates that these fungi are vital in marine food webs and are associated with marine corrosion processes [40, 81, 82]. Most fungi are aerobic heterotrophs, that are ubiquitous in atmospheric and aquatic environments where they metabolise organic material and produce organic acids including oxalic, lactic, formic, acetic, and citric acid [83]. Although, fungi have only received limited attention in the MIC literature, they can be a dominant factor in warm and humid environments. Fungi are implicated in MIC of various metals including copper, CS, SS, and aluminium [84, 85]. In natural environments, fungal biofilms can consume O_2 that helps anaerobic microorganisms to thrive [2]. Fungi can also degrade hydrocarbons to produce organic acids [2]. These organic acids can either cause corrosion or serve as nutrients to some other corrosive microorganisms such as SRB [6]. Additionally, some marine fungi produce exogenous enzymes such as proteases and cellulases that exacerbate metal corrosion [86, 87]. These enzymes promote the breakdown of organic matter and proteins on the surface of

marine facilities, leading to the production of additional acidic substances and accelerating the progression of corrosion [40].

1.2.2 Corrosion Mechanisms

Once the threat has been correctly assessed, we can begin to hypothesise specific corrosion mechanisms that are likely occurring. However, distinguishing between abiotic and biotic corrosion mechanisms is vitally important to ensure an effective mitigation strategy.

Abiotic corrosion is caused by physical and non-biological factors. This includes acid gas, O_2, galvanic, flow assisted, and UDC [23]. In acid gas corrosion, dissolved gases such H_2S or CO_2 can be highly corrosive. The severity of corrosion by acid gases is dependent on various parameters such as type of materials, temperature, partial pressure, flow rate, chemical environment, and headspace volume. Depending on the microstructure of the metal, acid gas corrosion can lead to highly localised pitting or stress cracking in the presence of H_2S, which is also referred to as sour corrosion due to the presence of a highly acidic environment. Equally, sweet corrosion can occur in the presence of CO_2 without high levels of H_2S and lead to mesa corrosion [88]. Mesa corrosion is where exposure to wet CO_2 at elevated temperatures leads to the formation of iron carbonate or siderite ($FeCO_3$) on metal surfaces. Though, acid gases not only promote abiotic corrosion, but can also be associated with MIC. It is therefore important to distinguish between abiotic acid gas corrosion and biotic MIC. The mechanism for abiotic H_2S corrosion involves the dissociation and release of H^+ (Eqn. 1.1) which can contribute to an increase in the rate of cathodic reduction through increased H^+ reduction as illustrated in Figure 1.4 [89].

$$2H_2S + 2e^- \rightarrow H_2 + 2HS^- \quad \ldots\ldots (1.1)$$

$$Fe + H_2S \rightarrow FeS + H_2 \quad \ldots\ldots (1.2)$$

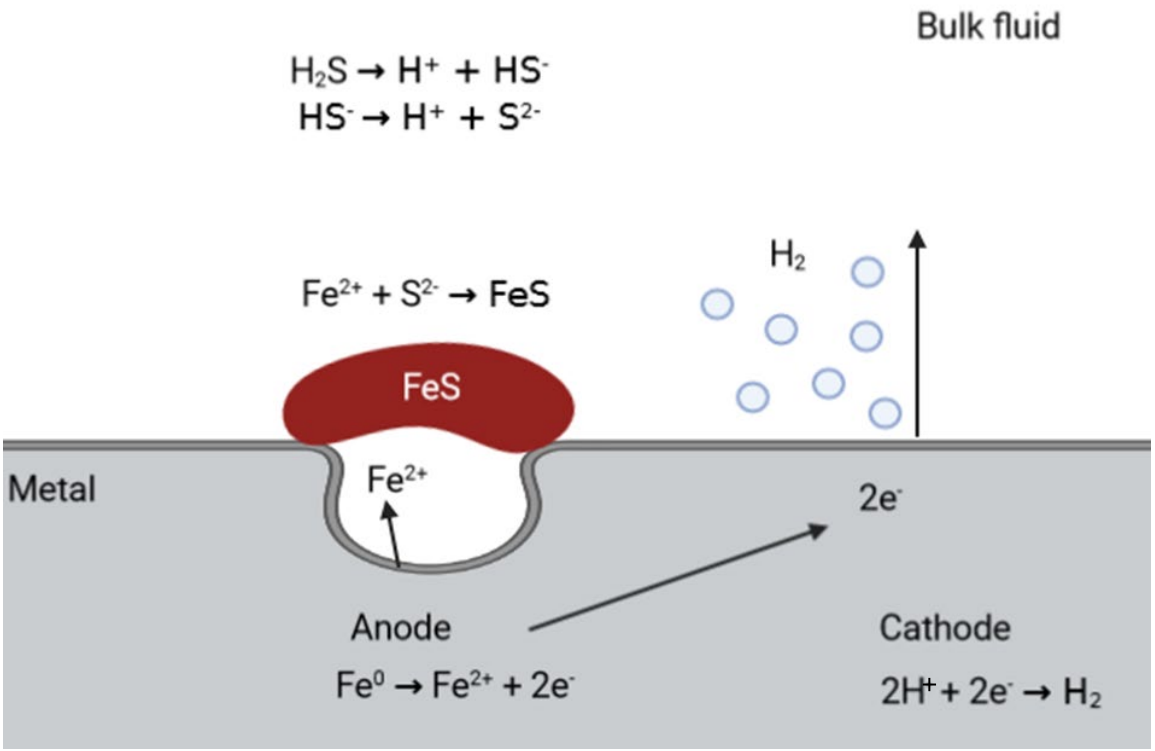

Figure 1.4. Illustration of abiotic H_2S corrosion. The process of iron dissolution occurs at the interface of the metal surface and iron sulphide by BioRender.com (2022).

The bulk fluid phase has a greater concentration of dissolved H_2S, the electron donor, compared to the metal surface, the electron acceptor, which corresponds to an acidic pH. Under a high concentration of dissolved H_2S, FeS can form (Eqn. 1.2). FeS act as a better catalyst of H_2 compared to bare steel. Thus, FeS facilitates electron transfer between steel and SRB cells.

In comparison, biotic MIC through the respiration of SRB produces biogenic H_2S. SO_4^{2-} reduction does not produce H_2S directly, it first produces HS^- (Eqn. 1.4) which can combine with a H^+ to form H_2S (Eqn. 1.5). The electron donor in this instance is Fe^0 (Eqn. 1.3) with SO_4^{2-} as the terminal electron acceptor [6]. The oxidation state of sulphur in microbial systems is highly pH-dependent, as demonstrated in the Schikorr reaction [91, 92, 93]. SO_4^{2-} can be reduced to H_2S under acidic conditions or remain as HS^- or S^{2-} at higher pH, influencing redox equilibria, microbial metabolic pathways, and corrosion mechanisms. Simply, the presence of microorganisms catalyses the cathodic reaction thereby accelerating cathodic reduction where electrons are consumed. Conversely, electrons are released by the anodic reaction where anodic oxidation occurs. The key distinction between abiotic H_2S corrosion and biotic MIC are the electron donor and electron acceptor. It is important to model acid gas *CR*s and compare against observed *CR*s to diagnose the cause of corrosion correctly. *CR*s within a system that are higher than probable abiotic *CR*s, along with the existence of a MIC threat, may reveal MIC as the corrosion mechanism and not acid gas corrosion [23].

$$\mathrm{Fe} \rightarrow \mathrm{Fe}^{2+} + 2\mathrm{e}^{-} \quad \ldots\ldots (1.3)$$

$$\mathrm{SO}_4^{2-} + 9\mathrm{H}^{+} + 8\mathrm{e}^{-} \rightarrow \mathrm{HS}^{-} + 4\mathrm{H}_2\mathrm{O} \quad \ldots\ldots (1.4)$$

$$\mathrm{HS}^{-} + \mathrm{H}^{+} \rightleftharpoons \mathrm{H}_2\mathrm{S} \quad \ldots\ldots (1.5)$$

O_2 corrosion is the degradation of metals caused by dissolved oxygen (*DO*) illustrated in Figure 1.5. The *DO* concentration that can be held by the bulk fluid depends on the temperature, salinity, and pressure. Gas solubility increases with decreasing temperature, and decreasing salinity, and decreases as pressure decreases.

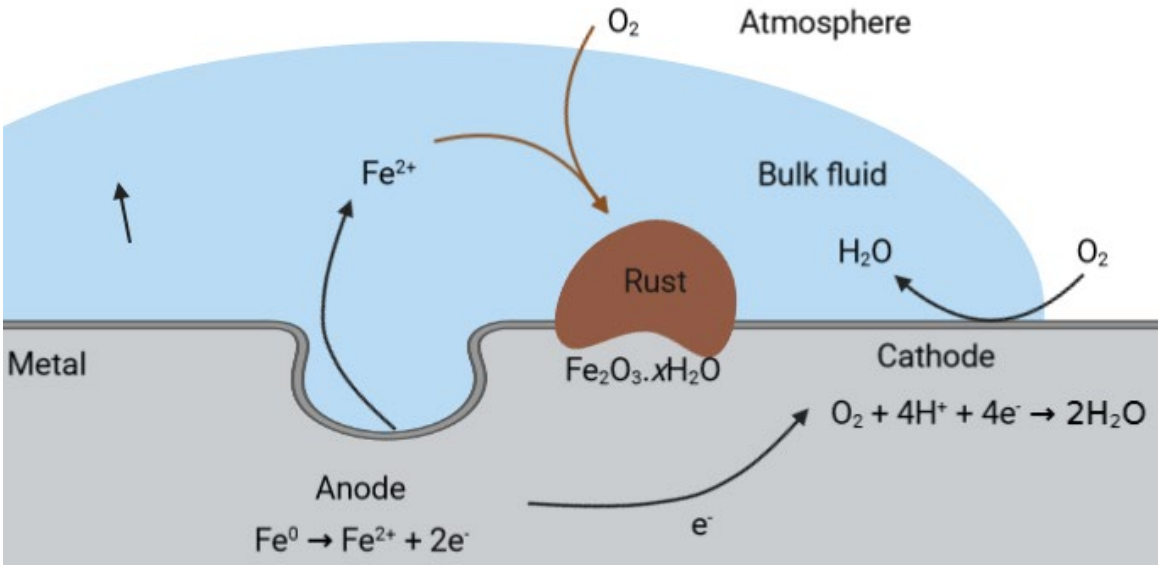

Figure 1.5. Illustration of oxygen corrosion. The process of iron dissolution occurs at the interface of the metal surface and bulk fluid by BioRender.com (2022).

$$\mathrm{H}_2 \rightarrow 2\mathrm{H}^{+} + 2\mathrm{e}^{-} \quad \ldots\ldots (1.6)$$

$$\mathrm{O}_2 + 4\mathrm{H}^{+} + 4\mathrm{e}^{-} \rightarrow 2\mathrm{H}_2\mathrm{O} \quad \ldots\ldots (1.7)$$

The abiotic O_2 corrosion mechanism involves the cathodic depolarisation of the metal surface, where O_2 reacts by consuming electrons at the cathode. Depolarisation removes the H_2 surrounding the cathode (Eqn. 1.6) and speeds up the corrosion process [80]. The anodic reaction involves the formation water ($\mathrm{H}_2\mathrm{O}$) molecules in acidic solutions (Eqn. 1.7) or hydroxide anion (OH^{-}) ions in basic solutions (Eqn. 1.8).

This is not to be confused with the O_2 concentration cell theory, where aerobic biofilms create an environment underneath the biofilm that excludes O_2. This creates anodic sites with low O_2 concentrations and leads to localised O_2 corrosion. Areas with higher O_2 concentrations serve as cathodic sites for O_2 reduction. The metal surface is the electron donor (Eqn. 1.3) and O_2 the terminal electron acceptor (Eqn. 1.8) that forms OH^{-} ions [90].

$$O_2 + 2H_2O + 4e^- \rightarrow 4OH^- \quad \ldots\ldots (1.8)$$

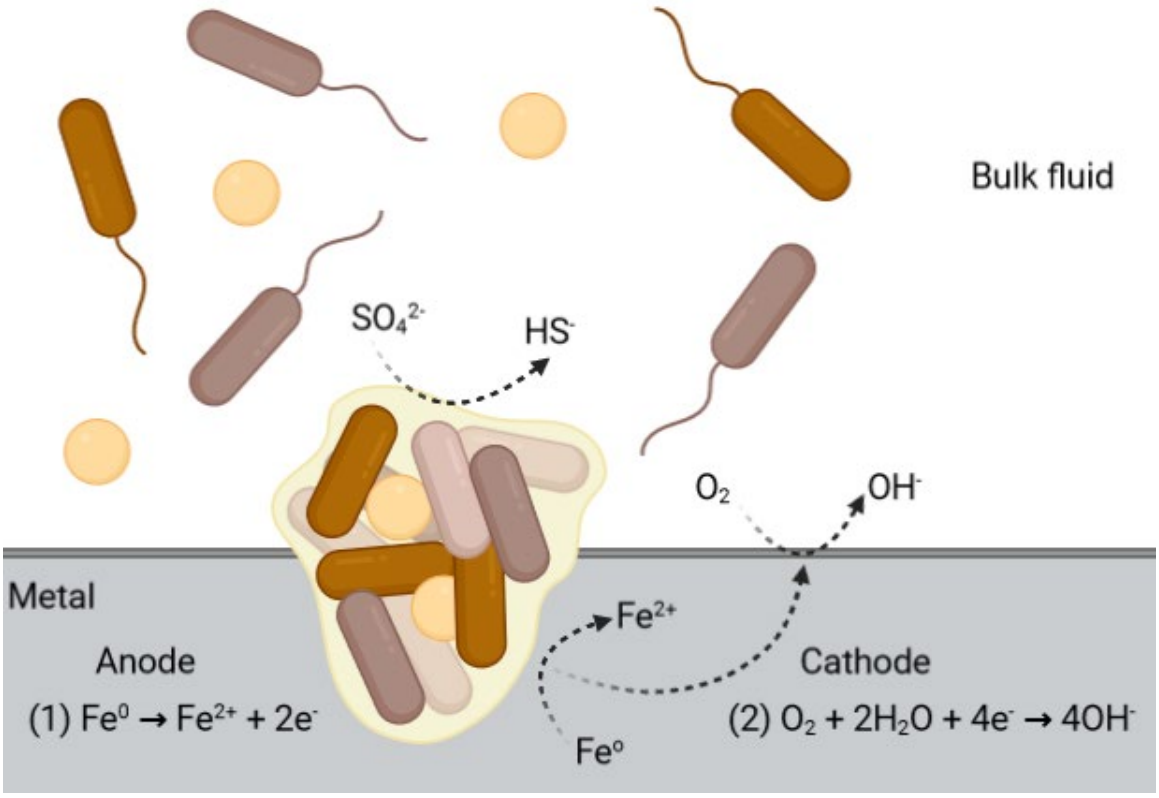

Figure 1.6. Illustration of pitting corrosion due to the creation of an oxygen concentration cell. The process of iron dissolution occurs at the interface of the metal surface and biofilm by BioRender.com (2022). Figure adapted from Jia *et al*., 2019.

Galvanic corrosion is the process in which one metal corrodes preferentially when it is in electrical contact with another, in the presence of an electrolyte. The more noble metal acts as the cathode, whilst the more active metal acts as the anode. The anode metal corrodes more quickly than it otherwise would, while the cathode metal corrodes more slowly and, in some cases, may not corrode at all [91, 92, 93]. Due to the proliferation of new metallurgy, corrosion resistant alloys (CRA), and greater complexity of equipment, the opportunities for galvanic corrosion have increased in the energy sector [94, 95]. Microorganisms can change the reaction kinetics of both anodic and cathodic components in a galvanic couple, thus changing the galvanic performance when compared to sterile/abiotic conditions.

UDC is a type of localised corrosion in which deposits or a collection of material form on a metal surface. The Schikorr reaction is an example of this phenomenon. This refers to the chemical transformation of ferrous hydroxide $(Fe(OH)_2)$ into magnetite $(\gamma - Fe_2O_3/Fe_3O_4)$ under anaerobic conditions, accompanied by the release of H_2 [91, 98, 99]. UDC occurs around or under an irregular deposit on metals. In the energy sector there are several reactive components mainly

CO_2 and H_2S, which react with the pipeline steel to give $FeCO_3$ and FeS products respectively, along with oxides [97]. The mechanism for UDC is not fully understood and is dependent upon the environmental conditions. Though, studies have observed a large increase in electrical potential difference that occurs between anodic and cathodic sites [63, 64, 65, 66, 67, 68, 98]. The area with the lower potential becomes the anode, while the area with the higher potential becomes the cathode. Current will flow from metals with a lower E_{corr} to materials with a higher E_{corr}, causing corrosion at the anode. Therefore, a material with a naturally high E_{corr} is likely to be the cathode. The system will rather take up electrons than lose electrons, so a reduction is more likely. If the E_{corr} is dropping, it means that the sample is oxidising, and negative charges are accumulating in it [99].

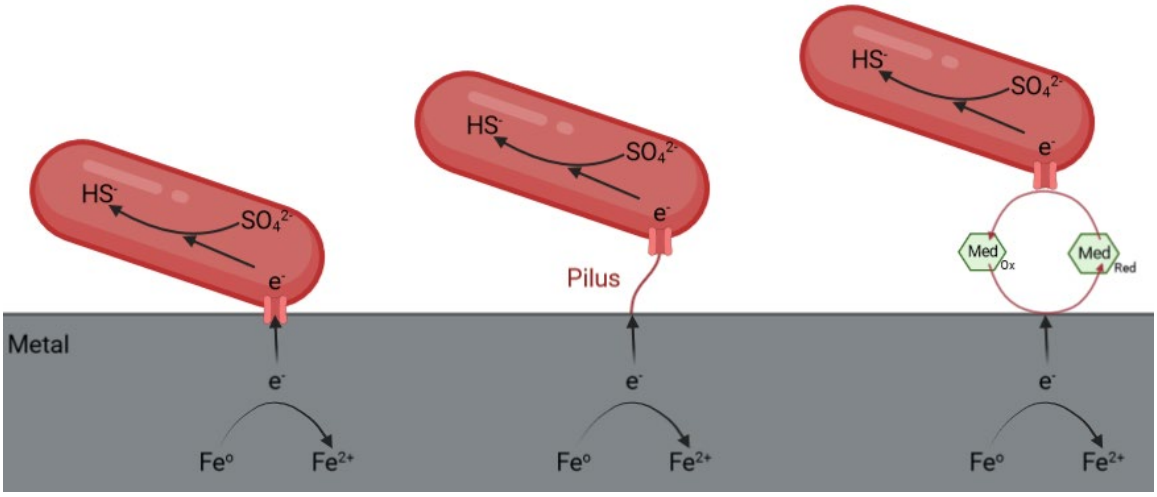

Figure 1.7. Illustration of extracellular electron transfer in microbiologically influenced corrosion, through both direct and mediated electron transfer by BioRender.com (2022). Figure adapted from Jia *et al*., 2019.

Biotic corrosion or MIC involves the deterioration of a surface because of the metabolic activity of various microorganisms. This corrosion is directly or indirectly influenced by microorganisms, typically chemoautotrophs. This includes corrosion through EMIC and CMIC in anaerobic conditions, as well as through a few mechanisms under aerobic conditions [6, 25].

In EMIC (Figure 1.7) sessile cells in a biofilm use metal as an electron donor, and a non-O_2 oxidant such as SO_4^{2-} or NO_3^- as the terminal electron acceptor [6]. EET for electron transfer between a metal surface and the cell wall has two possible routes. DET, where sessile cells have direct contact with a metal surface; MET, where soluble electron transfer mediators shuttle electrons from a metal surface and release them to the cell wall [100, 101, 102]. This is because the reduction of the terminal electron acceptors occurs inside a cell's cytoplasm, whilst the oxidation of the electron donor occurs extracellularly. As such, the extracellular electrons must be transported to the cytoplasm for the reduction reaction. Xu and Gu [103] have previously demonstrated that under carbon source starvation, elemental Fe^0 is used by SRB as an electron

donor, corresponding to more weight loss against CS. Similarly, Jia *et al*. [104] demonstrated that starvation of pre-grown mature NO_3^- reducing *P. aeruginosa* biofilms on CS was shown to trigger more aggressive weight loss, supporting this theory.

Conversely, CMIC is caused by the production of corrosive metabolites. For example, sulphide formation occurs when (SRB) reduce SO_4^{2-} to H_2S, which reacts with metal surfaces to form metal sulphides, leading to localized corrosion through de-passivation, acidification, and the formation of cathodic and anodic sites that accelerate metal dissolution [26]. Additionally, fermentative microorganisms such as APB and fungi can produce corrosive metabolites when an exogenous oxidant is not present. Fermentative microorganisms use the metabolite as the electron acceptor to achieve redox balance [38, 56]. Different organic acids produced by these microorganisms generate an acidic environment underneath a biofilm, which in turn leads to the generation of separate anodic and cathodic sites. Depending on the environment and the metal, different anodic and cathodic reactions may be identified [35, 104]. However, in general, corrosive metabolites accelerate the rate of cathodic reduction through the buffering effect theory, as mentioned earlier. Similarly, to other mechanisms, the source of organic acid can be both abiotic and/or biotic. Moreover, both aerobic and anaerobic microorganisms can produce enough organic acids to cause MIC. Thus, it is important to distinguish between the source of the corrosion to mitigate effectively. Additionally, biofilms can secrete enzymes which can degrade organic matter, such as plasticisers or polymers, to obtain small organic molecules as nutrients. Both aerobic and anaerobic microorganisms can cause MIC depending on the type of biodegradation. Though, this type of corrosion does not concern metallic corrosion. Consequently, it is not a focus area for MIC researchers in the energy sector [108].

1.2.3 Mitigation Strategies

Several strategies are available to mitigate MIC related threats in the energy sector. These include chemical treatment, mechanical cleaning/pigging, adjustment of operational parameters, asset design alterations, and appropriate materials selection. However, the effectiveness of any mitigation strategy should be evaluated and adjusted based on regular monitoring by investigating the microbiology, materials, and corrosion products, as well as the physical and chemical environment of any system in which MIC is a threat.

Biocides, corrosion inhibitors, surfactants, O_2/H_2S scavengers, scale inhibitors, and quorum sensing inhibitors (QSI) are few of the possible chemical mitigation alternatives to support MIC management. Though, compatibility is an important consideration when selecting a mitigation

strategy, particularly when it comes to chemical treatment, as undesirable or unintended interactions may arise which neutralise their effectiveness or even promote microbial growth through facilitating certain metabolic pathways.

Biocides are commonly used in several industries and can be either synthetic or natural. They act to control harmful microorganisms through both chemical and biological means by inhibiting the growth and reproduction of microorganisms in a variety of ways. Some alter the permeability of the cell walls, thereby interfering with the vital life processes of the microorganism. Others penetrate the cell into the cytoplasm and destroy the protein or complex with other compounds to kill the cell. Whilst some damage the cell through affecting its differential permeability, disrupting the normal flow of nutrients into the cell and the discharge of wastes from the cell. In the energy sector both oxidising and non-oxidising biocides are used. Chlorine-yielding chemicals and ozone are oxidising biocides that have been used historically. However, oxidising biocides may corrode equipment. Furthermore, other limitations include ineffectiveness at high pH, inactivation by sunlight and aeration [109]. Due to the limitations of chlorine and other oxidising biocides, non-oxidising biocides are becoming more widely used as a primary microorganism control treatment [110]. Tetrakis hydroxymethyl phosphonium sulphate (THPS) and glutaraldehyde are two non-oxidising biocides commonly used due to their broad-spectrum efficacy, biodegradability, safety, and cost effectiveness [111, 112]. Glutaraldehyde is known to crosslink amino groups in the cell wall of microorganisms thereby altering the permeability of the cell walls and ultimately interfering with the vital life processes of the microorganism [113]. The most widely used type of non-oxidising biocide are quaternary ammonium salts. Quaternary ammonium compounds (QACs) are a type of lytic biocide which damage cell membranes [114] and may also act as corrosion inhibitors and cationic surfactants. Other non-oxidising biocides include isothiazolones, organobromines, oxazolidines and triazines amongst others [115, 116, 117]. In the energy sector, a cyclic biocide treatment is required. Though, repeated treatments using the same biocide may promote those species that are more tolerant to the biocide, causing biocide dosage escalation over time [118]. Thus, it is often appropriate to enhance the biocide with adjunctive strategies. Surfactants or chelating agents are commonly employed to enhance the efficacy of biocide treatments.

A surfactant is a chemical that acts to reduce the surface tension on a material's surface. Surface tension is the force that causes the molecules on the surface of a liquid to be pushed together and form a layer or film. Chelating agents such as ethylenediaminetetraacetic acid (EDTA) and ethylenediaminedisuccinate (EDDS) inhibit the formation of biofilms [119, 120]. The key vital action of corrosion inhibition is the adsorption of the surfactant's functional group onto the material's surface. Conversely, surfactant absorption is generally related to aggregation and increased surface tension is attributed to pitting corrosion. Wen *et al*. demonstrated that a

trisodium salt of EDDS at 2000 ppm enhanced 30 ppm glutaraldehyde in the treatment of a SO_4^{2-} reducing *D. desulfuricans* biofilm on CS [121]. Though, due to the abundance of ions in the bulk fluid, the concentration and type of surfactant used needs to be carefully considered and the impact on the environment monitored [6].

A corrosion inhibitor is a substance which, when added to an environment effectively reduces the *CR* of a metal exposed to that environment by decreasing the anodic process rate. There are three types of corrosion inhibitors, anodic, cathodic, and mixed inhibitors. Similarly, there are three mechanisms which generally result in corrosion inhibition. First, the inhibitor molecule is adsorbed on the metal surface by the process of chemisorption, forming a thin protective film either by itself or in conjunction with metallic ions. Second, the inhibitor causes a metal to form its own protective film of metal oxides, thereby increasing its resistance. Third, the inhibitor reacts with a potentially corrosive substance in the water. Anodic inhibitors form a protective layer of oxide film on the surface of metals at anodic sites. When present in low concentrations the inhibitor blocks weak anodes. As the concentration increases, inhibitors react with the strong anodes, forming a passive layer and leading to reduction in *CR*. Examples of anodic inhibitors include but are not limited to chromate, molybdate, and NO_2^-. Conversely, cathodic inhibitors slow the reaction at the cathode or precipitate cathodic areas to increase the impedance on the surface. Impedance is the measure of the opposition that a circuit presents to a current when a voltage is applied. Examples of cathodic precipitates include zinc, calcium, and magnesium. They are precipitated on the surface of the metal to form a protective layer [122, 123].

O_2 scavengers are a type of cathodic inhibitor, which react with *DO*. An O_2 scavenger is a chemical substance that is used to reduce or completely remove O_2 in fluids to prevent O_2-induced corrosion. An O_2 scavenger is a corrosion-inhibiting substance that is added to an environment that is prone to O_2-based corrosion. Its cathodic nature enables it to combine with O_2 and form harmless compounds/salts. It is this process which reduces the *CR* in the system [124, 125, 126]. H_2S scavengers are a specialised chemical which selectively reacts with and removes H_2S from a system. As discussed, H_2S corrosion can cause damage through both abiotic and biotic mechanisms, either by reacting directly with steel to create an FeS corrosion film, or by increasing the acidity of the bulk fluid in the system. Thus, depending on the nature of the H_2S problem being addressed the application of H_2S scavengers to mitigate corrosion is important [127].

QSI are another type of chemical treatment that can interrupt quorum sensing (QS). QS is a mechanism of communication among microorganisms. Studies in bacteria have shown how QS is utilised to coordinate their behaviour. For example, some common phenotypes include biofilm

formation, virulence factor expression, and motility [128, 129, 130, 131, 132]. There are several different strategies for inhibition. First, QSI may inhibit or reduce the activity of the gene controlling the synthesis QS signal molecules. Second, QSI can degrade the signal molecule. Third, QSI may modulate the binding of the signal to receptor sites. Fourth, QSI can block receptor sites with antagonistic signal analogues [133, 134, 135]. Many natural and chemically synthesised inhibitors have been reported to disrupt QS mechanisms. For example, vanillin, quinones, and alkaloids [136, 137]. However, most of the natural QSI are produced in very small quantities and may have associated toxicity. Moreover, in industrial microbial systems, microbial species are diverse. Their population structures will adapt to QSI with surviving species not responsive to the QSI. Whilst quorum quenching may be an attractive strategy for preventing QS by disrupting signalling, studies typically focus on single-species biofilms which are not representative of mixed-species consortia found in natural environments. Thus, multiple QSI will likely be needed for mixed-species industrial biofilms.

A scale inhibitor can be a chemical or mechanical treatment used to prevent the precipitation and aggregation of slightly insoluble compound formation. The formation of scales depends on the pressure, temperature and the chemical composition or properties of the bulk fluid. Some common deposits include calcium carbonate (calcite), calcium sulphate dehydrate (gypsum), zinc sulphide, and magnesium carbonate. Chemical scale inhibition involves the chelation of carbonate and sulphate scales using phosphorous and inorganic compounds. Though, scaling can be remedied by using mechanical methods like milling, drilling, and jetting. Scale inhibitors help to improve flow rate within a system by not allowing certain corrosive materials to settle and adhere to the surface [138, 139].

Pigging, mechanical cleaning, flushing and sand jetting are common mitigation methods used in the energy sector to control MIC. These methods act to physically remove any trapped debris or biofilm on the internal surface of pipes. The pigging process removes built-up debris, which ultimately helps to protect from degradation of the pipe wall over time. The removal of the biofilm layer is an effective method to control MIC. Though, it may be appropriate to use physical cleaning coupled with chemical treatment with solvents and/or surfactants to penetrate some deposits such as oily hydrocarbons like paraffin [140].

Operational controls within a system can also be employed as a mitigation strategy. Common examples of operational controls used to minimise the threat of MIC include controlling fluid velocity, improvement of fluid quality process parameters, or adding preservative fluids such as corrosion or scale inhibitors. Maintaining a minimum velocity within a system helps to keep water and solids entrained thereby preventing accumulation. Though, it may sometimes be appropriate

to increase velocity within a system to effectively flush/sweep pipelines or dead legs occasionally to remove water. An example of a fluid quality process parameter improvement is reducing oil in water concentration in produced water (PW) to lower organic carbon levels [141].

Other mitigation strategies that asset holders can consider include design-based controls. Design based controls involve both appropriate material selection and asset design to reduce features that lead to water accumulation which may ultimately provide a threat of MIC, such as dead legs. Materials that possess resistance to corrosion may have also have a beneficial effect in reducing MIC. For example, CRAs and SS show greater resistance when compared to CS due to greater stability and protective layer formation on surfaces. The addition of chromium, nickel or molybdenum have been shown to increase SS and CRA resistance against MIC. CS are often selected due to lower capital cost, but often require regular corrosion mitigation, which increases its life cycle operating costs. CRAs typically do not require continuous mitigation, but have a higher capital cost as compared to CS. While CRAs have higher resistance to general corrosion, they can also be susceptible to localised corrosion under certain conditions, which may lead to the need for additional mitigation [142, 143, 144].

1.2.4 Threat Assessment – Current Standards

In the energy sector, it is becoming more widely understood that any investigation of MIC requires a multidisciplinary focus on multiple lines of evidence (MLOE) [145]. Yet, when industries today are attempting to understand the impact of MIC on their assets, many do not have experts from multiple disciplines on hand. The expertise to guide sampling, testing, and data integration to help solve complex MIC issues is critical [145]. While there are numerous standards available to guide specific types of testing, there are none that identify a truly unified multidisciplinary approach for combining MLOE. An international standard on biocide testing is still required that importantly includes the integration of biofilm testing. A new AMPP standard test method TM21495 is in the works by subcommittee 22, biodeterioration, for the laboratory evaluation of the effect of biocides on biofilms [146].

Current existing standards in industry provide some helpful guidance when it comes to the detection, testing and evaluation of MIC due to either external or internal corrosion. For example, NACE TM0212 [26] for internal MIC and NACE TM0106 [147] for external MIC of pipelines provide information about sampling and test methods that can be used to support corrosion investigations. ASTM G161-00 [148] also provides some helpful guidance for the corrosion failure analysis process. The framework for failure analysis is a three-step process. The first step is to collect appropriate

data from the location of failure [23]. Microbiological analysis plays a vital role in investigating the cause of failures and subsequently attributing the failures to MIC. Information on microbial abundance, composition of the microbial community, or microbial activity are vital for correctly diagnosing MIC. However, the microbial communities present in a system also interact with the materials and corrosion products in the environment to either initiate or accelerate corrosion reactions. Thus, it is also important to examine the materials and corrosion products associated with a failure to interpret the corrosion mechanisms. Moreover, information on the chemical environment near the failure location is important to establish the likelihood of MIC as a failure mechanism. Similarly, information on the physical environment of the system such as temperature, and use of physical cleaning methods, such as pigging, near the failure location are important to investigate the existence of a MIC threat [23].

Sampling can be performed to provide material to characterise the liquid phase, layers of deposits and biofilm on the metal surface, and the corroded metal surface itself. It is helpful to collect samples from corroded and uncorroded locations on the same sample, and from multiple locations for comparison. Sampling and preservation of biofilms from inside an operating pipeline is difficult, but those samples that are handled and preserved properly will provide reliable, accurate analytical results [149, 150]. In general, sampling and testing programmes should be designed to collect MLOE. Information about operating conditions such as pressure, temperature, flow rate, treatment chemical injection rates and pigging frequency, along with *CR* data from probes or routine inspections, microbiological conditions, as well as chemical composition data from the gas, liquid and solid samples should all be evaluated [26].

Table 1.1. Industry Standards for the energy sector.

Document	Title
AMPP TM21465-2024 [146]	Molecular Microbiological Methods— Sample Handling and Laboratory Processing
ASTM G1-03 [151]	Standard Practice for Preparing, Cleaning, and Evaluating Corrosion Test Specimens
ASTM G161-00 [148]	Standard Guide for Corrosion- Related Failure Analysis
ASTM G46-21 [152]	Standard Guide for Examination and Evaluation of Pitting Corrosion
ASTM G48-11 [153]	Standard Test Methods for Pitting and Crevice Corrosion Resistance of Stainless Steels and Related Alloys by Use of Ferric Chloride Solution
ASTM D8412-21 [154]	qPCR Quantification of Microbial Contamination in Liquid Fuels and Fuel Associated Water by Quantitative Polymerase Chain Reaction (qPCR)
DNV GL-RP-F116 [155]	Integrity management of submarine pipeline systems
DNV GL-RP-G101 [156]	Risk-based inspection of offshore topsides static mechanical equipment

Energy Institute [157]	Guidance on the use of Biocides in the Oil Industry
Energy Institute [158]	Guidelines on Managing Microbiologically Influenced Corrosion (MIC) in Water Injection Systems
Energy Institute [159]	Selection, applicability and use of molecular microbiological methods (MMM) in the Upstream and Downstream oil industry
Energy Institute [160]	Guidance for Corrosion Management in Oil and Gas Production and Processing
ISO 31000 [161]	Risk Management, Principles and Guidelines
ISO 55002 [162]	Asset management — Management systems — Guidelines for the application of ISO 55001
ISO 17776 [163]	Petroleum and natural gas industries — Offshore production installations — Major Accident hazard management during the design of new installations
ISO 21457 [164]	Petroleum, petrochemical and natural gas industries - Materials selection and corrosion control for oil and gas production systems
ISO 9712 [165]	Non-destructive testing - Qualification and certification of NDT personnel
NACE 31205 [166]	Application and Evaluation of Biocides in the Oil and Gas Industry
NACE 3T199 [167]	Techniques for Monitoring Corrosion and Related Parameters in Field Applications
NACE SP0169 [168]	Control of External Corrosion on Underground or Submerged Metallic Piping Systems
NACE SP0499 [169]	Standard Practice Corrosion Control and Monitoring in Seawater Injection Systems
NACE SP0775 [170]	Preparation, Installation, Analysis, and Interpretation of Corrosion Coupons in Oilfield Operations
NACE TM0106 [147]	Detection, Testing, and Evaluation of Microbiologically Influenced Corrosion on External Surfaces of Buried Pipelines
NACE TM0194 [27]	Field Monitoring of Bacterial Growth in Oil and Gas Systems
NACE TM0212 [26]	Detection, Testing, and Evaluation of Microbiologically Influenced Corrosion on Internal Surfaces of Pipelines
NACE SP0106 [171]	Control of Internal Corrosion in Steel Pipelines and Piping Systems
NACE TR 46107 [172]	Control of Corrosion, Deposition, and Microbiological Growth in Recirculating Water Systems in Buildings
NACE TR 11206 [173]	Biocide Monitoring and Control in Cooling Towers
NACE 1F192 [174]	Use of Corrosion-Resistant Alloys in Oilfield Environments
NACE SP21430 [175]	Standard Framework for Establishing Corrosion Management Systems

To determine the existence or significance of MIC, it is crucial to analyse the microbiology, physical and chemical conditions, and materials and corrosion products of the environment to determine if MIC is the actual cause of the failure [23]. Sampling data collection and analysis should be directed toward distinguishing the contributing effects of both abiotic and biotic factors on the likelihood, severity, location, and cause of corrosion [26]. Critically, existing standards recognise the importance of sessile microorganisms [26]. Though, sampling of sessile microorganisms can be difficult. Use of inconsistent sample collection and assay methods along with contamination of samples are common threats to attaining meaningful trends in sessile microorganism data.

It is recognised that current techniques and procedures for studying sessile microorganisms are limited and can produce variable results [26, 27, 147]. Conversely, samples of bulk fluids containing planktonic microorganisms are much easier to acquire and allow for the quantification and identification of planktonic microorganisms. However, collection and testing of bulk samples for MIC assessment should always be accompanied with other data collected concurrently. Changes in detectable numbers and types of microorganisms can occur rapidly after removal of samples from the environment. Thus, preservation and transport requirements are an important consideration wherever field testing is not practical or available for both sessile and planktonic samples [26].

The most commonly used microbiological techniques in the energy sector include culture-based testing, enzyme and immunological assays, microscopy-based methods, and molecular microbiological methods (MMM). Each of these methods reveal different types of microbiological information. Culture-based methods such as serial dilution tests and most probable number (MPN) tests, DNA-based methods such as quantitative polymerase chain reaction (qPCR) and DNA sequencing, and enzyme-based methods such as adenosine triphosphate (ATP) tests and enzyme tests for SO_4^{2-} reducers are the commonly used methods in MIC-related investigations. These methods provide information on microbial abundance, composition of the microbial community, or microbial activity. The quality of microbiological information obtained from the failure depends on the sample type and method used. DNA-based methods such as qPCR and DNA sequencing provide the most reliable information on the microbial abundance and composition [23]. The major challenge in transporting samples for microbiological testing is to ensure that microorganisms remain alive and active without multiplication. Sample collection may expose microorganisms to changes in pressure, temperature, salinity, dissolved gases, and light, causing changes in the number and type of microorganisms in the original sample. Moreover, sample exposure may lead to the oxidation or degradation of many chemical species associated with microbial metabolism [26].

In addition to characterising the microbiology of an environment in which corrosion has occurred, the chemistry of the environment, both on the surface and in the bulk fluids, should also be determined to gain a holistic understanding of potential MIC mechanisms. MIC cannot be diagnosed solely with microbiological data. NACE SP0775 [170] and ASTM G46 [152] provide some helpful guidance regarding the use of coupon monitoring and analytical procedures, along with the selection of procedures that can be used in the identification and examination of pits. The elemental and mineral composition of the corrosion products and surface deposits are important to determine whether MIC is a likely failure mechanism. Various analytical methods, such as energy dispersive X-ray spectroscopy (EDS) and X-ray diffraction (XRD), are available to analyse the

composition of deposits and corrosion products. The comparison of the corrosion products and deposits between the failure location and the non-corroded location can provide meaningful insights on the uniqueness of the corrosion threat and the mechanism of failure [23].

Investigating the chemical environment near the failure location is also important to establish the likelihood of MIC as a failure mechanism, as the chemical environment will be affected by the composition of the operating fluid and by the influence of microorganisms, which may deplete and/or add chemical compounds due to their metabolic activity. Some corrosion products can be formed by both biotic and abiotic driven mechanisms. Thus, to distinguish MIC from abiotic corrosion, analytical methods such as liquid chromatography mass spectrometry (LC-MS) and high-performance liquid chromatography (HPLC) are available to analyse the chemical composition of fluids. It is important to characterise the pH, total alkalinity, and dissolved gases of liquid samples immediately after sample collection as these parameters can change quickly. Likewise, organic acids can quickly degrade, so preservation of samples may be appropriate. Overall, the chemical environment is characterised by the presence of dissolved gases, organic acids, the presence of electron acceptors/donors, availability of carbon sources, pH, and the presence of production chemicals in the system [23]. As discussed earlier, dissolved gases such as CO_2, H_2S, and O_2 not only promote abiotic corrosion, but can also be associated with MIC. Similarly, organic acids such as acetic acid, and lactic acid can be generated as products of microbial metabolism and can indirectly promote corrosion. The source of these organic acid can be both abiotic and/or biotic. The presence of different electron acceptors or electron donors will greatly influence the mechanisms causing corrosion. For example, SO_4^{2-} or NO_3^- will promote the metabolism of SRB and NRB in the presence of Fe^0 as the electron donor, increasing the likelihood of MIC. Equally, other electron donors such as acetate, lactate, and H_2 can be associated with the metabolism of MIC causing microorganisms like methanogens or acetogens. Moreover, the availability of a carbon source is a crucial determining factor for microbial metabolism. Hydrocarbons and production chemicals present in the system can provide a source of carbon. In some cases, these production chemicals can be utilised by microorganisms as organic carbon sources or electron acceptors or donors to facilitate their metabolism. The inappropriate application of a biocide could have the opposite effect, by facilitating the growth of certain microorganism and exacerbating the threat of MIC. The pH of the system can also offer some useful insights into the cause of corrosion. A pH closer to neutral offers an ideal environment for microbial growth, which may indicate that MIC is the likely mechanism. Whilst, abiotic acid gas corrosion is typically associated with a low pH, due to increased H^+ dissociation. All these parameters that are characteristic to the chemical environment impact microbial metabolism and their interactions with the corroding metal and

corrosion products, subsequently resulting in MIC. Examining the chemical environment between the failure location and non-corroded locations, along with historical changes to these chemical parameters, can reveal valuable information to interpret the cause of failure [23].

Finally, evaluating the physical environment of the system can also provide some useful insights. Monitoring the temperature and use of any physical cleaning methods such as pigging near the failure location are important to investigate the existence of a MIC threat. The temperature of a system in the range of 25°C to 45°C provides an ideal environment for microbiological growth. However, MIC has frequently been reported in environments with temperatures outside of this range. As mentioned previously, many extremophiles like archaea can tolerate extreme conditions such as very high temperatures, salinity, and pressures [71], and methanogens have been shown to contribute to biocorrosion [72, 73, 74]. Water is a fundamental factor required for corrosion in general. Hence, the possibility of water wetting and duration of water wetting near the failure location is essential to investigate the cause of failure. Further, the absence of flow in the system will promote water settlement, subsequently increasing the likelihood of corrosion. All these parameters that are characteristic to the physical environment impact the microbiology and corrosion products, along with their interactions with the chemical environment, and subsequently can lead to MIC. Comparing the physical environment between the failure location and non-corroded locations in the system along with historical changes to the physical environment can reveal valuable information to interpret the cause of failure [23].

The second step in the failure analysis framework is to integrate all the data collected from the failure location and non-corroded locations. Once all this data is integrated, the last and the most important step is to determine the corrosion mechanism and to interpret the cause for the failure. Based on the available data, all the possible abiotic corrosion mechanisms should be considered and weighted against MIC and finally, the cause of failure should be assessed. This step requires careful consideration along with comprehensive examination of all information available. Abiotic and biotic threats in the system should be considered based on the historical corrosion susceptibilities of the system and the data collected at the time of failure. As stated earlier, the evidence for MIC in the system should not be determined solely based on high microbial abundance or high microbial activity or presence of usual suspects of MIC like SRB, APB, and methanogens. Rather, the evidence for MIC should be ascertained using MLOE by investigating whether microbiology, materials and corrosion products, physical and chemical environment highlight the existence of a MIC threat. Once MIC has been identified as a possible failure mechanism, all the threats in the system should be weighed against each other based on the data collected at the time of failure to determine the corrosion mechanisms.

There is currently a lack of recommendations or best practices at the time of writing. It is vital to be able to identify various microorganisms from a system, and subsequently have a reproducible model biofilm system that is representative of operating conditions that can cultivate mixed-species consortia whilst also utilising the most appropriate analytical methods to be able to fully understand different MIC mechanisms.

1.3 Methods for Assessing Biocorrosion

Historically, in the energy sector MIC has primarily been a concern when it comes to traditional oil and gas systems. As a significant number of pipeline failures, due to either external or internal corrosion, have resulted from MIC. However, corrosion represents one of the largest challenges when it comes to renewable energy too. Most renewable energy fit within the brackets of wind, marine, solar, hydro, geothermal, and bioenergy [176], with hydropower, wind, and solar being the three largest sources of renewable energy generation. In marine environments, structures can be exposed to a range of conditions with microorganisms forming damaging biofilms. The nature of the marine environment also makes maintenance and repair of structures more difficult and often expensive and not feasible. Because of this, corrosion proves to be an expensive challenge for the maritime, offshore renewables, and energy industries [177]. In recent years, it has become apparent that MIC poses a larger challenge to the offshore wind farm industry than initially estimated due to the discovery that the environment is considerably different to that which was assumed in the original design specifications for many offshore wind turbines [178]. The initial design specifications worked under several assumptions that predicted low rates of corrosion. However, these assumptions have proven to be wrong, as the development of anaerobic biofilms have caused accelerated rates of localised corrosion [179]. Current predictive measures are insufficient at adequately determining the threat to marine infrastructure. Thus, research into the development of biofilms, on metallic surfaces in different media, such as seawater is critical [180]. This should empower asset owners to improve sustainability and produce better designs and improve future maintenance techniques. The operating history of offshore wind farms is only recent, so the full scale of the problems brought about by MIC, as well as the costs associated with it, are yet to be fully understood.

1.3.1 How to establish and test biofilms in the lab

There are a range of test methods that can be used for the detection, testing and evaluation of MIC. Though, different testing companies or laboratories will use different analyses techniques to

investigate a failure, as there will be different expertise and access restrictions when it comes to specific methods/techniques. However, the hardest challenge first comes from how to establish and test a mixed-species biofilm in the laboratory.

There are several key considerations when it comes to how to establish and test mixed-species biofilms in a laboratory. The reactor system, chemical composition of the fluids/media including any dissolved gases, the microbial inoculum, test conditions, experimental design, and biocide treatment regime. There are several different experimental reactor systems available such as batch reactors, flow through reactors, recirculating reactors, and operational side stream devices. Here, we focus on one device, the CDC (Centre for Disease Control and Prevention) biofilm reactor, which is a recirculating reactor.

Figure 1.8. CBR 90-3 Anaerobic CDC Biofilm Reactor® (key dimensions: 22 cm reactor height and 12 cm internal diameter; 21 cm coupon holder rod; 1.27 cm coupon diameter) Includes seals around each rod and between lid and vessel. The anaerobic CBR includes coupon holder rods, polycarbonate coupons, coupon removal tool, coupon manipulation tool, and glass flow breaks [181].

The CDC reactor, illustrated in Figure 2.1, is uniquely positioned as it has previously been optimised and validated for *Pseudomonas aeruginosa* or *Staphylococcus aureus* biofilm growth. ASTM E2871-21 [182] is the 'Standard Test Method for Determining Disinfectant Efficacy Against Biofilm Grown in the CDC Biofilm Reactor Using the Single Tube Method'. Thus, there is precedence for cultivating single-species biofilms in the CDC reactor and testing disinfectant efficacy. The important distinction here is cultivating a reproducible mixed-species biofilm, one that closely

resembles real-world and operating environments and testing biocide efficacy. If available, environmental/field samples from the field are preferable rather than a single strain, as a mixed-species consortium taken from the field will be more representative. Similarly, PW or fluid samples taken from the field will always be more representative than any synthetic media. Though it may be appropriate to filter out hydrocarbons if growth is inhibited in the reactor system or even supplement the bulk fluid. Any synthetic media selected, or supplement added may preferentially favour the growth of certain microorganisms, which may not be the dominant species found in the operating environment. The experimental parameters will need to be optimised and validated for each different inoculum. Another advantage of using the CDC reactor, is the ability of using different surface substrates such as SS or CS amongst others. It is possible to tailor the surface substrate to match that of the operating environment. Moreover, a single reactor allows up to 24 coupon samples for replicates. An abiotic reactor can be run in tandem with experimental biotic reactors, where the test conditions or parameters can be changed to test certain hypothesis; test conditions such as the temperature, flow rate, pressure, and anaerobic conditions. The gas mixture that comprises the anaerobic conditions in the reactor could also impact the community dynamics. Careful consideration needs to be made regarding the ratio of N_2, CO_2, and H_2 gases. Again, it is possible to change the test conditions to closely mimic the operating environment from which the initial biofilm inoculum was collected. The length of test and frequency of data collection need to also be considered. The biofilms need to be mature and ready for testing. Each different microbial community will need to be optimised and validated prior to biocide treatment. The reproducibility of different technical and biological repeats using the same initial microbial consortium is also critical. If it is possible, it is recommended to run all repeats in tandem at the same time to minimise changes between reactor systems. However, if this is not possible it is important to first establish frozen stocks (-80°C glycerol stocks) of the source microbial consortium, or alternatively to use samples from the same location. Only once all these parameters have been validated can the biocide treatment regime be considered. A batch or continuous application of biocide can be employed. Though, the frequency and concentration of biocide should simulate field treatment conditions. Following the establishment of biofilms in the lab the analytical methods and information to collect need to be carefully chosen.

1.3.2 Analytical methods and information to collect

There is a lack of recommendations or best practices when it comes to what specific analytical methods and information to collect. Here, a special focus was placed on integrating MLOE [145]

and adopting a multi-disciplinary strategy, that accounts for materials and corrosion products, microbiology, and both the chemical and physical environment.

Microbiological assays/molecular microbiological methods. Microbiological assays have been commonly used in the energy sector for the isolation, cultivation, identification, and quantification of microorganisms present at corroded areas and other locations without corrosion. Culture-based testing, by the MPN method is a common method used for the quantification of microorganisms. MPN is used to approximate the size of the variable microorganism population in a solid or liquid sample using semi-quantitative estimates. It is important to note, that the type of medium selected to culture the inoculum largely determines the numbers and types of microbial species. No artificial culture medium can approximate the complexity of a natural environment. Under ideal circumstances, liquid culture provides favourable growth conditions for 1 to 10% of the natural population [26]. Consequently, the MPN method is not very accurate and lacks precision. Culture methods cannot provide sufficient information about the metabolic activity of microorganisms.

The most advanced and reliable method to characterise microbiological samples are MMM. MMM are a suite of technologies that are used to characterise the activity, diversity and abundance of microorganisms using enzymatic or genomics-based approaches. MMM are culture-independent approaches that provide direct analysis of samples without the bias introduced by the growth process during culturing. Enzyme and immunological assays are helpful tools for detecting and quantifying microorganisms associated with MIC. Biochemical methods such as ATP bioluminescence assays, aim to investigate the activity of microorganism populations. ATP is present in all living cells and the quantity of ATP in samples is approximately proportional to the number of living microorganisms in any given sample. This may give an indication of the viable biomass present in a microbial consortium. Detection of adenosine monophosphate (AMP) can provide further information about metabolic activity. Generally, metabolically more active cells have a higher content of ATP compared to AMP. ATP assays are extremely sensitive and provide an accurate measure of total cellular activity from samples. ATP assays quantify all active microorganisms present in a sample, irrespective of their functionality or metabolic pathway [26]. Metabolites can also be used to quantify growth activities. For example, gas chromatography (GC) is a sensitive method to measure biogenic H_2S levels. Ion chromatography is a high resolution, but more expensive method [6]. Similarly, microsensors can be used for studying H_2S production and oxidation concurrently. Determination of metabolic activity of samples will be helpful in the assessment of the effectiveness of MIC control measures, as microorganisms must be active for MIC to occur [26].

Next generation sequencing (NGS) is a qualitative, DNA-based method that characterises the diversity of the microorganisms found in each sample, as a relative proportion of each taxonomic group. This test is run after DNA amplification, then microbiological taxonomic groups are identified by comparing their 16S rRNA genes to sequences in available databases. NGS is a laboratory-based method that can be used to identify the diversity of MIC-causing microorganisms in a sample. qPCR is a DNA-based method that quantifies the number of specific microorganisms per unit sample/microbiological abundance. Very small amounts of sample be that planktonic or sessile, with or without live bacteria, are needed. DNA-based methods such as qPCR and DNA sequencing provide the most reliable information on the microbial abundance and composition of the microbial community and hence are recommended as compared to serial dilution tests for obtaining information on microbial presence, abundance, and composition. qPCR measures living, inactive and dead microorganisms or a specific genus/species of microorganisms. The qPCR method does not underestimate organisms that do not grow in culture. Reverse transcriptase (RT)-qPCR can be performed as a way of enumerating only those metabolically active microorganisms in a sample. DNA sequencing involves the extraction of DNA from all microorganisms in sample. Most commonly, the 16S rRNA gene, a gene present in all bacteria and archaea, is amplified. Sequencing of 16S rRNA genes provides a full inventory of all microorganisms that are present as well as indications of their relative abundances. Such information can be used to identify the presence of microorganisms implicated in MIC [26].

MMM are vital in investigating the cause of failures and subsequently attributing the failures to MIC. Each of these methods reveal different types of microbiological information. These methods provide information on microbial abundance, composition of the microbial community, or microbial activity.

Image analyses. Microscopy-based methods are also commonly employed to determine the overall numbers of microorganisms present without regard to their viability or species. Epifluorescent microscopy is a useful tool that can help to distinguish microorganisms from debris or may be used to examine specific cellular structures. Fluorescent *in situ* hybridisation (FISH) is an example, in which only living and active cells are stained with a fluorescent dye. The quantitative FISH method differentiates active/live microorganisms from dead microorganisms. Moreover, FISH probes may be designed to attach only to selected groups of microorganisms, such as SRB. Conversely, the DAPI method quantifies all intact microorganisms, both living and inactive cells, containing DNA. DAPI can be used in combination with FISH analysis to help distinguish the total cell count from the number of cells that are labelled using the FISH probe.

Scanning electron microscopy (SEM) is a method for the observation of biofilm morphologies and corrosion products which provides high-resolution images that can distinguish different cell shapes in a mixed-species biofilm consortium [183, 184]. In combination with an energy dispersive X-ray spectroscopy (EDS) accessory, the chemical composition of biofilms and corrosion products can be characterised. Moreover, biofilm treatment efficacy can be assessed through identifying any detachment from the coupon surface. Though, there are some limitations that arise through the preparation of biofilm samples. Images are obtained from a dehydrated sample under high vacuum. Samples are dehydrated using alcohol followed by drying using supercritical CO_2 [185]. This process may result in a cracked film due to drying, rather than a fractured film produced by the corrosion process [35]. Potentially giving a false positive or misleading information regarding the MIC mechanism.

Confocal laser scanning microscopy (CLSM) is an epifluorescence microscopy technique that allows the three-dimensional (3D) visualisation and analysis of biofilm samples. In combination with appropriate fluorescent stains, a more comprehensive analysis of the entire biofilm is possible [26]. CLSM can be used to measure a biofilm's thickness. CLSM can also reveal whether dead cells are only in the top layer of a biofilm or also in deeper places [186]. This is particularly important in biofilms, as the EPS can limit the penetration and effectiveness of antimicrobial agents or biocides as well as offering protection from physical disturbances [3].

Other methods are also available for coupon surface analyses. XRD can be applied to identify the crystal structure and chemical composition of corrosion products [187]. XRD may be limited however as the technique may not be able to penetrate to the bottom of a thick film [188]. Transmission electron microscopy (TEM) can provide very high-resolution images in the analysis of biofilm structures and element distributions [88, 189]. Profilometers such as Infinite focus microscopy (IFM) and Atomic force microscopy (AFM) use a microprobe that detects the surface topography of a biofilm [10, 190] and can also be used to measure pit depth information. 3D surface profilometry can provide valuable information regarding surface roughness measurements and any resulting corrosion because of MIC. Biocide efficacy can be assessed through identifying the changes in biocorrosion compared to a control. Raman spectroscopy and infrared spectroscopy can also be used to study biofilm formation and to identify different microorganisms [10, 191]. Both Raman spectroscopy and infrared spectroscopy can be applied to wet samples, which removes some of the limitations of other imaging techniques [6].

Imaging analysis can provide valuable information concerning biofilm structure, overall numbers of microorganisms present and in combination with epifluorescence is a useful tool that can help to distinguish microorganisms from debris. Biofilm treatment efficacy can be assessed

through identifying any detachment from the coupon surface and identifying whether dead cells are only in the top layer of a biofilm.

Corrosion tests. Weight loss is a simple and dependable test for measuring corrosion in MIC studies which can be directly converted into a uniform CR. In combination with pitting analysis, a metric for relative pitting severity (*RPS*) can be calculated [192]. Weight loss offers direct evidence for corrosion. Though, some materials are far less prone to MIC and do not show detectable weight loss in short term tests [6]. Profilometers can be used in these instances to provide pit depth information. Typically, the concept of averaged maximum pit depth is used to reduce error. By averaging several of the largest pit depth values, the average maximum pit depth can be calculated [193]. Both weight loss and maximum pit depth are useful in quantifying MIC threats.

$$RPS = \frac{\text{maximum pit growth rate}}{\text{uniform corrosion rate based on specific weight loss}} \quad \ldots\ldots (2.1)$$

Using RPS, maximum pit depth can be estimated from specific weight loss (mg cm^{-2}) during the same corrosion period and metal density (mg cm^{-3}) [6, 194].

$$\text{Maximum pit depth} = \frac{\text{specific weight loss} \times RPS}{\text{metal density}} \quad \ldots\ldots (2.2)$$

Weight loss and pit depth analysis require at least several days to become measurable. They are done in a one-shot manner, meaning coupons can no longer be put back to continue testing due to biofilm removal [6].

Electrochemical measurements. Electrochemical measurements, such as open-circuit potential (OCP) or E_{corr}, linear polarisation resistance (LPR), electrochemical impedance spectroscopy (EIS), and potentiodynamic polarisation can be monitored *in-situ* and provide transient corrosion information over the entire test duration. These techniques can also be used to determine biocide efficacy through determining changes in corrosion current density (j_{corr}), polarisation resistance (R_p, Ω cm^2) and inversely CR [6].

E_{corr} is defined as the potential that exists at open-circuit. This potential ultimately defines the equilibrium potential between the anodic and cathodic processes. A typical three-electrode electrochemical cell consists of (Figure 2.2) a working electrode (WE), counter electrode (CE) and reference electrode (RE) immersed in an electrolyte.

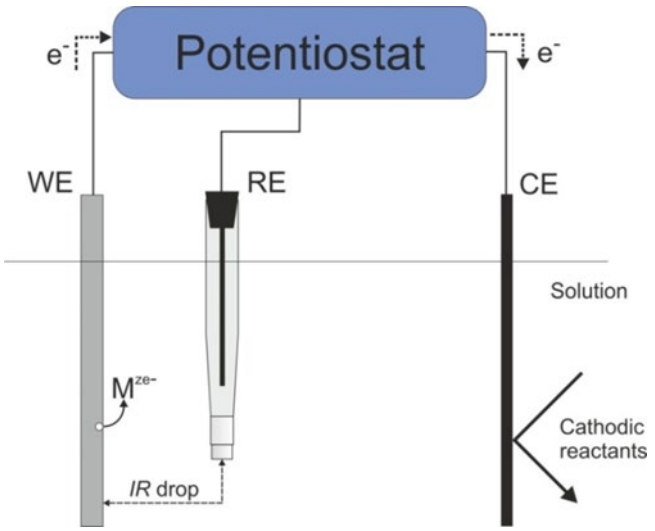

Figure 1.9. Schematic view of a three-electrode setup.

An OCP will be adopted between the CE and WE. The measured current flows between the CE and the WE. The potential difference is controlled between the WE and the CE and measured between the RE. It is important that the RE is kept at close proximity to the WE to minimise ohmic losses or IR drop, which is the electrical potential difference between the two electrodes. This configuration allows the potential across the electrochemical interface at the WE to be controlled with respect to the RE. Despite the difference in their name, OCP is the same as E_{corr}. Generally, in biotic conditions a more negative shift in OCP will be observed compared to abiotic control conditions. This can be attributed to the attachment of microorganisms and the formation of a biofilm on the surface of the working electrode.

LPR is a non-destructive technique commonly used in MIC studies. It provides near-real time corrosion data. A linear direct current (DC) potential scan is performed relative to the OCP, once a steady-state has been reached, which allows the R_p and j_{corr} to be calculated. The combined measurement of potential and current relationships for an operating corrosion cell over a wide range of oxidising conditions results in polarisation curves that describe the electrochemical reactions. The combined measurement of potential and current at potentials that are very close to the freely corroding potential of the system gives rise to linear polarisation curves. Both, potential and current measurements have useful applications in corrosion control [195, 196]. Transient R_p data can be used for monitoring biocide efficacy over time, as R_p is inversely proportional to the *CR*. The data can be used to determine when a biocide treatment starts to take effect and when the effect tapers off [194]. Moreover, R_p gives an indication of early biofilm formation. An initial increase in R_p is indicative of biofilm formation on the surface of the working electrode surface, as the presence of biofilm can act as a barrier to prevent the diffusion of H^+ from the environment to the working electrode surface [197].

EIS is another non-destructive technique used in studying MIC and is one of the most modern techniques available to characterise the electrical properties of electrode/electrolyte interfaces and has emerged as the most powerful of electrochemical techniques for defining reaction mechanisms, for investigating corrosion processes, and for exploring distributed impedance systems [198]. Electrochemical impedance tests apply an alternating current (AC) potential over a very large frequency range. This data is then used to determine the impedance (Z) of the test specimens, which is often displayed as Bode and Nyquist plots. A Nyquist plot shows real impedance (Z') against imaginary impedance (Z''). Impedance or resistance is the measure of the opposition that a circuit presents to a current when a voltage is applied. It is the ability of a circuit element to resist the flow of electrical current. Whereas capacitance is defined as the ratio of the amount of electric charge stored. In a Nyquist plot the impedance can be represented as a vector of length $|Z|$. The angle between this vector and the x-axis, commonly called the phase angle gives an indication of corrosion resistance. A greater phase angle will correspond to a larger plot diameter, and thus indicates a higher corrosion resistance or lower CR [43]. The limitation of a Nyquist plot is that you cannot tell what frequency was used to record that point. Conversely, the Bode plots provide frequency information. The impedance is plotted with log frequency against both the absolute values of the impedance and the phase-shift, that is, the changes in magnitude and phase as a function of frequency. The resistances in a circuit can be summed up to yield a corrosion resistance [43]. For phase-shift, high frequencies do not allow electrons to interact with any capacitor, and thus only ohmic resistance is measured. As frequency increases, from 10^{-2} to 10^{5} Hz, phase-shift peaks may be identified. These may indicate the presence of a charge transfer processes but can also indicate diffusion limitations [198]. In a biotic system, a phase-shift in lower frequencies is indicative of active pit growth [199]. Bode plots also demonstrate the total magnitude of impedance. Impedance is the opposition to AC presented by the combined effect of resistance and reactance. The magnitude at high frequency gives an indication of solution resistance. In a biotic system, the greater the magnitude of impedance the greater the corrosion resistance. Alternatively, the less susceptible the working electrode surface is to localised corrosion.

A potentiodynamic polarisation curve employs a DC voltage range around a stable OCP to examine the overall corrosion behaviour of a system. Tafel slopes of the anodic curve and the cathodic curve yield β_a and β_c values. The point at which the anodic and the cathodic currents are equal defines the E_{corr}. As mentioned previously, OCP is the same as E_{corr}. Whilst a negative shift can be attributed to biofilm formation that does not necessarily mean a greater j_{corr}, which can be obtained from the Tafel analysis and can be used to calculate the CR. Unlike LPR and EIS,

potentiodynamic polarisation can cause significant damage to biofilms and should therefore be used with caution [6].

1.3.3 Data interpretation for biocide efficacy

As discussed, there is a range of different analytical methods and information to collect. However, the microbial communities present in a system also interact with the materials and corrosion products as well as the environment to either initiate or accelerate corrosion reactions. Thus, it is also important to examine the materials and corrosion products associated with a failure to interpret the corrosion mechanisms along with monitoring environmental conditions [23]. A combination of the analytical techniques discussed will allow for a holistic understanding of the corrosion mechanisms causing MIC along with biofilm data for interpreting biocide efficacy.

1.4 Aims and Objectives

This project aims to develop and validate a representative model system in which inoculate relevant to industry, can be cultured to enhance the fundamental understanding of the role that biofilms play within MIC. Once key performance characteristics of the model have been evaluated, commercially available biocides as well as novel antimicrobial compounds can then be introduced into the model system and investigated using a combination of techniques including standard microbiological assays, molecular tools, electrochemical methods, and chemical and metallurgical assays. In accordance with these primary aims, specific objectives of this research are outlined as listed below:

- Evaluate the changes in prevalence and activity of different species within the biofilm using molecular microbial methods such as NGS.
- Evaluate the changes in *CR* of the underlying metal with methods used across academia and industry to gain a holistic understanding of what is happening physically at the metal/electrolyte interface.
- Investigate the impact that biocides have on the viability of the biofilm using MLOE, to determine their efficacy, and to establish whether their use is sustainable.
- Determine the mechanistic relationships between the above through the data collected, providing novel insights into the specific effects of different biocides, and potentially highlighting new approaches to biocide development.

Other key questions to consider are as follows:

- Is the influence of biofilm growth primarily metabolic through the combined action of organisms present as a consortium, or physical through the development of diffusion gradients and microenvironments?
- Do the corrosion products themselves have an influence on the nature and extent of any further corrosion?
- Are microorganisms involved in the creation of an electrochemical cell?
- Do they affect principally the anodic or cathodic reaction?
- What is the identity of the cathodic electron acceptor, particularly under anaerobic conditions?
- Can pitting corrosion be the consequence of colonial growth or development of a patchy biofilm?

1.5 Overview of Research Design

This thesis, guided by existing literature [200, 201] and knowledge gaps identified, outlines a standard protocol for a novel dual anaerobic reactor model to study mixed-species biofilm and MIC interactions on UNS G10180 CS. Several methods were used in this investigation to assess the critical stages associated with abiotic and biotic corrosion mechanisms. A special emphasis was placed on integrating MLOE, employing a multi-disciplinary approach. Broadly, culture independent methods were employed using a range of MMM, image analysis, corrosion tests and electrochemical methods. These techniques were selected to develop a holistic understanding of the mechanistic relationship at the interface of the biofilm and metal during the critical stages of corrosion. An environmental, mixed-species, consortium was chosen which would exhibit key metabolic traits and demonstrate metabolic capabilities to best simulate an industry relevant biofilm. Bacterial attachment and biofilm formation was evaluated on CS material for all experiments. Anaerobic experiments were conducted using pure O_2-free N_2 gas, and reactors were established by initially using batch conditions for three-days, followed by continuous flow conditions. This was to allow settlement and to facilitate biofilm formation in the biotic reactor. Two anaerobic CDC biofilm reactors were used, an abiotic and biotic reactor. Baseline corrosion data was established using abiotic experiment for all relevant studies, whist biotic experiments were used to establish microbial corrosion data. Importantly, design and engineering modifications were made to the anaerobic CDC biofilm reactor setup for these laboratory studies. Typically, these reactors hold up to eight rods which accommodate three coupons each. Though, in this model three rods were replaced with an electrochemical cell setup and a microsensor. Additionally, two

rods in each reactor were engineered to allow for the creation of working electrodes for a three-electrode cell setup. These modifications can be seen in Appendix A. The base test solution used varies between laboratory studies depending on the objectives of these studies. These include a well-defined artificial seawater (ASW) adapted from the literature [202], MB media for the enumeration of SRB and PW from an offshore system to simulate environmental conditions. Once key performance characteristics of the model had been evaluated, the ASW test solution was selected to investigate commercially available biocides. The working temperature of the laboratory studies also varied. For the study using PW as the test solution (chapter 5), the working temperature was 40°C, to better simulate the environmental condition of the offshore system. Otherwise, a working ambient temperature of 20 - 24°C was used across the other laboratory studies (chapters 3, 4 and 6). This was to maximise microbial recovery and simulate mesophilic conditions. Exposure times, of 28 days, were consistent across the laboratory studies, and the detailed methodology and materials are outlined herein.

1.6 Significance of the Research and Contribution

MIC is a major problem in many industries which leads to large economic losses and major environmental issues across different industrial sectors. Fundamental research evaluating mixed-species biofilms and the mechanisms that lead to MIC within these heterogeneous microbiomes is limited. Whilst existing standards can be helpful, ultimately, they do not address the problem at the source, biofilms. Similarly, available literature primarily focuses on single-species biofilms, which are not relevant in an industrial context. The first stages of conditioning film formation, bacterial attachment and bacterial colonisation represent topics of current scientific interest. Equally, the second stages of maturing corrosion film and mixed-species biofilm growth are key topics. Finally, understanding the mechanistic relationship during the third stage which may cause uniform and pitting corrosion under patchy corrosion deposits and/or bacteria clusters is critical. By understanding these critical stages, more effective and sustainable mitigation strategies can be developed.

However, how to establish and test mixed-species biofilms, which are representative of their environment within the lab, is a major challenge. And the current regulatory standards for biofilm culture testing provide limited insight. Moreover, what analytical methods to use, and what information to collect are important considerations. Furthermore, how to interpret the data to evaluate the effectiveness of any mitigation strategy employed is essential. This is because there are numerous microorganisms that may be part of a mixed-species biofilm with distinct metabolic pathways which may directly or indirectly lead to MIC. Environmental biofilms participating in MIC are known to be heterogeneous in industry. This broad functional diversity of natural biofilms

compared to many laboratory simulations has led to underestimations of biofilm tolerance acquisition, a serious global economic and health concern. However, almost nothing is known about these mixed communities on CS. A holistic understanding, incorporating MLOE is essential for effective MIC management. Chapter 2 outlines a standard protocol for a dual anaerobic reactor model to study biofilm and MIC interactions on UNS G10180 CS. The model system outlined serves as the model system used for research chapters 3, 4, 5 and 6, which broaden the fundamental scientific knowledge on mixed-species biofilms and the mechanisms that lead to MIC.

Chapter 3 contributes valuable insight into environmental mixed-species communities, developed on CS and exposed to simulated marine conditions. Similarly, chapter 4 explores the selective pressure that ATCC 1249 Modified Baar's (MB) media has on the community dynamics of an environmental mixed-species biofilm, and the corresponding corrosion mechanisms. Whilst, chapter 5 investigates the impact that environmental conditions, more closely mimicking an offshore oilfield system, has on natural mixed-species biofilm communities. Importantly, from this research we can start to rationalise an idealised representation of the mixed-species biofilm and the microbial mechanisms that lead to corrosion of CS under anoxic conditions at the metal/electrolyte interface under these different simulated conditions. Critically, with a holistic understanding of mixed-species biofilms we can enhance predictive measures for identifying the relative contributions of different microbial mechanisms. Moreover, from simulating the environmental conditions of an offshore oilfield system within the laboratory we can bridge the gap between experimental and real-world scenarios of mixed-species biofilms and MIC. Being able to identify and characterise specific microorganisms under simulated environmental conditions is critical to understanding the threat of MIC.

Using chapter 3 as a foundation, Chapter 6 explores the biocidal efficacy of glutaraldehyde. Real-world application of biocidal compounds invariably results in enhanced biofilm chemical tolerance. There is limited research evaluating approaches to enhance biocidal efficacy in a sustainable way. Chapter 6 acknowledges the importance of biocide efficacy, as well as consideration of biofilm tolerance acquisition and environmental sensibility to introduce a targeted approach to mitigation MIC. Using the innovative dual bioreactor protocol, we can optimise biocidal treatment strategies by understanding their efficacy against mixed-species biofilms. By refining biocidal application under simulated environmental conditions, a move towards evidence-based biocide dosing can be achieved. Ultimately, this will allow for more sustainable prevention and mitigation strategies to be designed.

Together, this thesis introduces a novel standard protocol for a dual anaerobic reactor model to study mixed-species biofilm and MIC interactions on UNS G10180 CS. The proposed protocol is also an effective method to evaluate and optimise biocidal treatment strategies. This research enhances the fundamental understanding of the initial stages of biofilm development, including conditioning film formation, microbial attachment, and colonisation. Additionally, it furthers the understanding of corrosion film maturation and the growth of mixed-species biofilms. Finally, it advances the understanding surrounding the mechanistic relationships in the later stages that may lead to uniform and pitting corrosion under patchy corrosion deposits and/or heterogeneous biofilms under both abiotic and biotic conditions.

Chapter 2 Materials and Methods

Test conditions. Two anaerobic CDC biofilm reactors (Biosurface Technologies Corporation) were used: an abiotic control reactor and a biotic test reactor (key dimensions: 22 cm reactor height and 12 cm internal diameter; 21 cm coupon holder rod; 1.27 cm coupon diameter). Sterile CS coupons were fixed in reactors and exposed to two separate conditions for 28 days. Anaerobic conditions were maintained throughout the test by initially sparging the system with N_2 (BOC Nitrogen (O_2-Free), 44-W) over an initial three-day batch phase. Anaerobic conditions, considered to be hypoxic or low O_2, are characterised as a system with low concentrations ranging between 1 and 30% saturation. Strict obligate anaerobes will not survive if there is more than half a percent O_2 in the environment, while moderate obligate anaerobes can still grow in a 2 to 8% O_2 environment [203]. For research chapters 3, 4, and 6 *DO* (Hanna Instruments) concentrations were measured on day 28. For chapter 6, the flow of N_2 was maintained throughout the 28 day study. The base test solution used varies between laboratory studies depending on the objectives of these studies. For chapters 3 and 6, a well-defined ASW+YE adapted from the literature was used [202]; for chapter 4, MB media for the enumeration of SRB was used; whilst for chapter 5, PW from an offshore system to simulate environmental conditions. Where different test solutions have been used, the components can be found in the appendices of each research chapter. It was acknowledged for the studies which used yeast extract, that yeast extract contains redox mediators that may adsorb onto the electrode surfaces and chelate metal ions and the test matrix was designed to highlight any significant interference [204]. Resazurin (0.1%, 0.5 mL L^{-1}) was added as a redox indicator, as it is colourless under O_2-free conditions but changes to a pink colour in an O_2-containing environment. Agitation of the reactor baffles was set to 50 rpm to maintain a homogeneous solution. Additionally for chapter 6, the reactors were dosed twice weekly with a biocide on days 4, 7, 10, 13, 16, 19, 22, and 25 using 5 mL of 214 – 250 ppm of glutaraldehyde (Merck, 340855-1L). The range accounts for the variations in working volume of the reactors between 300 – 350 mL.

Primarily, a working ambient temperature of 20 – 24°C was used across most laboratory studies (chapters 3, 4 and 6). This was to maximise microbial recovery and simulate mesophilic conditions. However, for chapter 5 the working temperature was 40°C, to better simulate the environmental condition of the offshore system. Prior to inoculating the biotic reactor, a three-day pre-culture was prepared in a blue-cap flask (50 mL), consisting of 10% marine sediment with the remainder fresh test solution depending on the laboratory study. The biotic reactor was inoculated using a sterile syringe, where 10% of the working reactor volume (35 mL) was added as the inoculum. Initial ATP measurements were taken from the pre-culture and long-term frozen stocks were prepared using 20% glycerol. Figure 2.3(a) shows a schematic of a full experimental setup, with Figure 2.3(b) illustrating the three-electrode cell setup within each anaerobic CDC biofilm reactor. Both reactors were operated in batch mode for the first three days to allow settlement and to facilitate biofilm formation in the biotic reactor. After this period, the reactors were switched to continuous flow of fresh media at a rate of 0.2 mL min^{-1}, which replaced about 50% of the 600 mL total volume daily (288 mL day^{-1}).

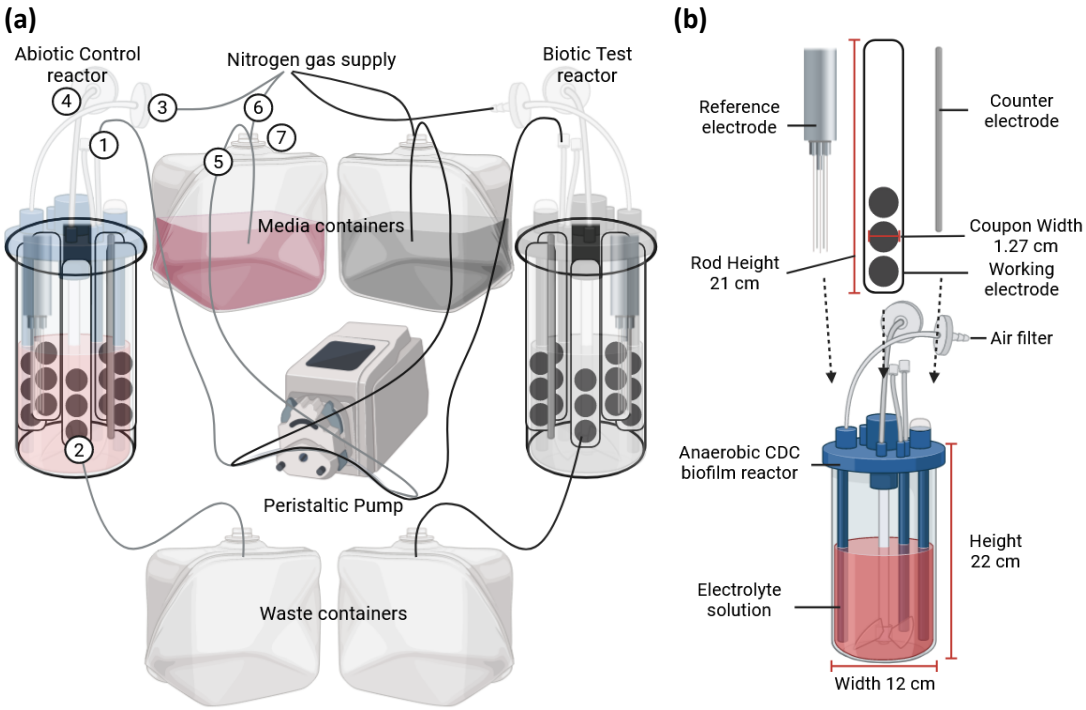

Figure 2.1. (a) The dual anaerobic biofilm reactor system (abiotic and biotic reactors) comprising 10 L media containers, peristaltic pump, magnetic stirrer/hot plate, sulphide microsensor, and the three electrode cell setup. Each reactor has five rods, with three coupons in each rod (15 coupons in total). Each reactor has four inlets. ① The first inlet is connected to the peristaltic pump and then the media container. ② The outlet is connected to the waste containers. ③ Connection to the nitrogen gas source. ④ Air filter (Millex, 0.2 µm) that acts as the exit for excess gas in the reactors. ⑤ The 10 L media container is connected via the peristaltic pump and feeds the first inlet in the reactor. ⑥ Connection to the nitrogen gas source. ⑦ Air filter (Millex, 0.2 µm) that acts as the exit for excess gas in the media containers. **(b)** detailed three-electrode cell setup in an anaerobic CDC biofilm reactor: There are three separate carbon steel coupon working electrodes that can be measured per rod. Each reactor had two rods that were modified for electrochemical analysis, *n* = 3 for both as-received (AR) and polished (P) UNSG10180 carbon steel coupons. Created by BioRender.com.

Microbial consortia. Prior to each experiment (research chapters 3, 4, 5 and 6) different samples were collected from the same location. A 50 mL falcon tube was used to collect the sediment samples. The sheltered zone littoral sediment microbial consortia were collected at a depth between 10 – 15 cm below the sediment surface during low tide from Langstone Harbour, United Kingdom (50°50'11.9"N 0°58'47.5"W). The coastal/estuarine marine sediment (very fine and cohesive mud and silt deposits) was selected to sample microorganisms living under low O_2 conditions. The environmental conditions on the day the marine sediment was collected is presented in the appendices of each research chapter. The sediment samples were added to 500 mL of the medium and stored at 37°C in an anaerobic chamber to maximise the recovery of the diverse microbial populations. Mesophilic bacteria can survive and grow in temperatures between 10 – 50°C. Thus, a tropic strategy to promote cell growth and viability was employed to maximise microbial recovery. From the sediment sample, pre-cultures were prepared prior to inoculation of biotic reactors. 5 mL of the sediment sample was added to 45 mL of fresh medium and allowed to grow for three days under anaerobic conditions. The anaerobic chamber gas mixture consisted of 85% N_2, 10% CO_2 and 5% H_2 (BOC Anaerobic Growth Mix, 290563-L). Long-term storage of sediment samples and microbial consortia was employed to create frozen stocks at –80°C.

Carbon steel coupon preparation. UNS G10180 (AISI 1018) CS disc coupons (Biosurface Technologies – RD128 CS), with dimensions of 12.7 mm diameter × 3.8 mm thickness were used for all laboratory studies. These were used either as-received (AR) (R_a = 1.35652 ± 0.76193 μm) or polished (P) (R_a = 0.44068 ± 0.03206 μm) with a Kemet 15 Lapping machine using 25 μm Type K diamond slurry depending on the laboratory study. The surface profiles and weights for all coupon samples were assessed prior to starting the experiment, on Day 0. Surface profilometry and gravimetric analysis was also performed at the completion of the experiment after Day 28. 3D surface profiles were taken using a 3D optical profilometer (Alicona imaging infinite focus microscope IFM G4 3.5). A Mettler AT201 was used to take five measurements of the initial weights of all coupons.

Experimental setup. Before autoclaving, the two anaerobic CDC biofilm reactors were cleaned with detergent and allowed to dry. The empty reactors with attached tubing were placed in autoclavable bags; all tube openings and air filters (Millex, 0.2 μm) were covered in aluminium foil, with tube openings clamp shut. The empty assembled reactors were autoclaved for 15 mins at 121°C. For laboratory studies using ASW or MB test solutions, the media was also autoclaved to ensure sterility. The PW was not autoclaved, so not to disrupt the chemical nature of the environmental test solution. Instead, the PW was filter sterilized using a 0.2 μm Vivaflow® TFF Cassette, PES (Sartorius). After cooling the reactors were transferred into a sterilised microbiological safety cabinet (MSC), along with all rods, CS test coupons, as well as any sensors

and electrodes. Working electrode rods were prepared in advance. For each working electrode rod, wires were soldered to each coupon separately. The coupon face with the soldered wire was then covered with a lacquer solution (Polishing Shop, Type 45 Stop Off Lacquer) and allowed to dry. To assemble the reactors, all rods with coupons were submerged in 99% ethanol for at least 10 s, then inserted into the autoclaved reactors within the MSC. Any sensors or electrodes used in place of a rod were also inserted, after also being sterilised with 99% ethanol for at least 10 s. The medium bottles and all tubing were connected in an MSC. Once both reactors were fully assembled, they were transferred to the working area, with access to a N_2 gas supply. The gas was run through a variable are flow meter (RS Components 198-2975) at a flow rate of approximately 90 mL min^{-1}. The tubing was evenly split into each reactor to equalise the pressure gradient caused by the peristaltic pump (Matson Marlow 300 series).

Sulphide microsensor. H_2S concentrations were monitored daily in each reactor using a Unisense, *SULF*-50 sulphide microsensor (50 µm diameter) and amplifier (Unisense, H_2S UNIAMP). The microsensor measures the partial pressure of H_2S gas, and the total concentration is a function of pH and temperature. The microsensor limit of detection is 0.3 µM, with a range from 0-300 µM H_2S in water. Calibration utilised the H_2S and *SULF* sensor calibration kit (Unisense, CALKIT-H_2S). Due to the nature of the experimental setup, it was not possible to calibrate the microsensors during the experiment. However, calibrations were performed both prior to starting the experiment and once the experiment had finished to confirm that the sensors were still calibrated. The SensorTrace Suite software was used to collect the H_2S microsensor data. The sensor has a higher signal for zero right after it has been connected to the amplifier, thus each microsensor collected readings concurrently whilst all electrochemical measurements were performed. This was to allow the sensor to stabilise. For each time point, measurements were taken for up to 5 minutes at a rate of 1 measurement per second. These technical replicates were used to generate error bars.

Surface profilometry and visual inspection. Corrosion products and biofilms were removed from select sample surfaces using the cleaning protocol as described for the gravimetric analysis below. 3D profiling of the CS surfaces was reconstructed using an Alicona imaging infinite focus microscope IFM G4 3.5. For each sample analysed areas were scanned at randomly distributed areas over the sample surface (n=15). The images allowed assessment of changes in surface roughness compared to the surface profiles obtained prior to testing. Additionally, ImageJ/Fiji was used for the quantitative determination of pit depth, width, height, percentage area, and to assess pit rate (*PR*) and pit density (*PD*). Prior to the analysis, it is important to calibrate the pixel scale to

the scale bar on each image. The method involved applying a colour threshold to depths greater than 5 µm. Then, the images were converted to a binary mask. Next, measurement parameters were selected for areas greater than 650 µm^2. Finally, the images were analysed to display counts, area, and average size of pits. The pit parameters were adapted from ASTM G48-11 [153]. For *PR* analysis, the deepest pits from each image were captured using the Alicona. From this the *PR*s were calculated using the following formula [170]:

$$PR\ (\mathrm{mm\ y^{-1}}) = \frac{depth\ of\ deepest\ pit\ (\mathrm{mm}) \times 365}{exposure\ time\ (\mathrm{days})} \quad \ldots\ldots (2.3)$$

Gravimetric analysis. Corrosion products and biofilms were removed following the ASTM G1-03 standard with a 15% inhibited hydrochloric acid described in NACE SP0775-2023 [151, 170]. A stock solution was made of 37.5% HCl (Merck, Suprapur, 1.00318.0500) to which 10 g/L of 1,3-di-n-butyl-2 thiourea (DBT) (Merck, 8.20423.0250) was added. Immediately prior to use, the stock solution was diluted by slowly adding a measured volume of stock solution to an equal volume of deionised water with stirring. A Mettler AT201 was used to take five measurements of all coupons. *CR* were determined by the gravimetric technique that considers the weight loss and surface area of the metal samples, using the following formula [170]:

$$CR\ (\mathrm{mm\ y^{-1}}) = \frac{(KW)}{(ATD)} \quad \ldots\ldots (2.4)$$

Where:

CR = average corrosion rate, millimetres per year $(\mathrm{mm\ y^{-1}})$

K = constant depending on desired units. For millimetres per year $(\mathrm{mm\ y^{-1}})$ $K = 8.763104 \times 10^4$

W = mass loss, grams (g)

A = initial exposure time, days (d)

T = exposure time, days (d)

D = density of coupon metal, grams per cubic centimetre $(\mathrm{g\ cm^{-3}})$

Corrosion product analysis. Analysis of the corrosion products and biofilms were performed by XRD using a Rigaku SmartLab thin film and materials diffractometer for chapter 3. Four coupons were extracted from each reactor on day 28, two AR and two P, and stored and allowed to dry under anaerobic conditions. Spectra were collected using a Rigaku SmartLab thin film and materials diffractometer. For chapter 4, no corrosion product analysis could be performed as the XRD instrument was out of order. However, for chapters 5 and 6, both SEM-EDS and Raman microspectroscopy were performed. For SEM, all images and Energy dispersive X-ray spectroscopy (EDS) measurements were taken using a Hitachi S-3400N II SEM and attached energy-dispersive X-ray spectrometer (Oxford Instruments). Imaging was performed at approximately 15 kV with a

working distance of 10 mm at various magnifications (71×, 1000×, and 3000×). EDS analysis used the same parameters and magnifications. For each sample analysed areas were scanned at randomly distributed areas over the sample surface (n=15). EDS data was analysed using AZTEC software before being compiled in Microsoft Excel. Raman microspectroscopy experiments were conducted using a Renishaw InVia Raman microscope (Renishaw, UK), with a Leica DM 2500-M bright field microscope and an automated 100 nm-encoded XYZ stage. The samples were excited using a 532 nm laser directed through a Nikon 50× long working distance air objective (NA = XX). Raman-scattered signals were separated from the laser illumination at 532 nm using a Rayleigh edge filter, and a diffraction grating (532nm: 1800 L/mm) dispersed the Raman-scattered light onto a Peltier-cooled CCD (1024 pixels × 256 pixels). Calibration of the Raman shift was carried out using an internal silicon wafer using the peak at 520 cm^{-1}. Spectra were acquired over two or three accumulations of between 5 and 20 s each, using laser power of up to 3 mW. Spectra were acquired from a selection of points manually determined using the brightfield imaging mode of the microscope. The spectra obtained were processed using MATLAB (MathWorks).

Electrochemical analysis. Electrochemical measurements were performed using a Gamry Instruments potentiostat (Ref 600 Plus). The electrochemical behaviours of the CS coupons were evaluated using a three-electrode system consisting of a UNS G10180 CS coupon as the working electrode, graphite rod (Alfa Aesar, 99.9995%, 6.15mm diameter, 152mm long) as the CE, and a silver/silver chloride (Ag/AgCl, 3.5 M KCl) reference electrode (Sentek, (AgCl) Double junction Reference Electrode).

① R1+(Q1/Q2+R2)

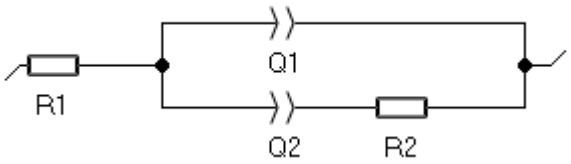

② R1+(Q1+R2)

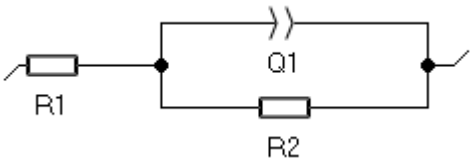

③ R1+Q1/(R2+Q2/R3)

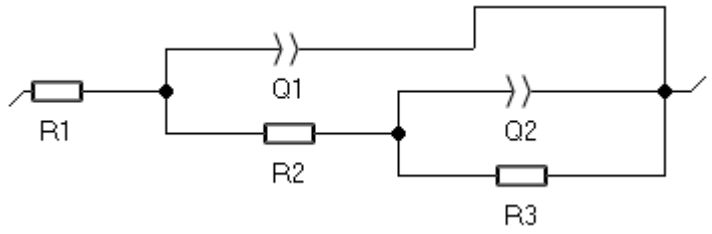

④ R1+Q1+(Q2/R3)

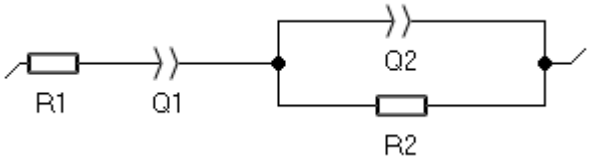

Figure 2.2. Equivalent circuit models used to generate EIS parameters. The element '*R*' corresponds to a resistor and represents either the solution resistance, the resistance of the biofilm or the corrosion product film, and the charge transfer resistance, respectively. The element '*Q*' represents a constant phase element, which characterises the 'non-ideal' capacitance behaviour of either the biofilm or the corrosion product film layer, and the charge transfer capacitance.

On day 1, after the biotic reactor was inoculated, both reactors were left for at least 1 h prior to performing any electrochemical measurements. OCP were recorded for each coupon on day 1 prior to measuring LPR and EIS. LPR and EIS were measured daily for each sample. LPR measurements were performed from ±10 mV with respect to E_{OCP} using a scan rate of 0.167 mV s^{-1}. EIS measurements were performed at OCP with an applied 10 mV_{rms} sinusoidal potential signal with a frequency range of 10^{-2} to 10^{5} Hz. Potentiodynamic polarisation measurements were performed at the end of the experiment on day 28 for each coupon from –0.200 mV to +0.200 V using the scan rate of 0.5 mV s^{-1}. Standard procedures were followed when selecting an equivalent circuit best-fit using the Gamry Echem Analyst software: (*i*) the chi-squared (χ^2) error was suitably minimised ($\chi^2 \leq 10^{-4}$) and (*ii*) the errors associated with each element were ranged between 0 % and 5 %. Figure 2.4 outlines the equivalent circuit models (ECM) used.

Confocal laser scanning microscopy and post-image analysis. The distribution of live and dead cells within biofilms was studied using CLSM. Coupons were gently rinsed with sterile anaerobic PBS, with the following composition: NaCl 8 g, KCl 0.2 g, Na_2HPO_4 1.44g, KH_2PO_4 0.245 g, deionised water 1 L. and stained using the FilmTracer Live/Dead biofilm viability kit (Invitrogen) according to the manufacturer's instructions. Before imaging with a Leica SP8 confocal microscope, coupons were rinsed with sterile deionised water to remove the excess of dyes and fixed using mowiol. Mowiol had the following composition: 2.4 g Mowiol, 6 mL deionised water, 12 mL 0.2 M Tris (pH 8.5), 0.01 g sodium azide, and 6 g glycerol. Images were obtained with a 63× magnification and glycerol immersion. The dyes used stained live cells with a green-fluorescent colour (SYTO 9) and dead cells with a red colour (propidium iodide). The *z*-stacked images were analysed using Imaris software (Oxford Instruments).

Microbial community analysis. After 28 days, three coupons from each sample type used in each laboratory study, were gently rinsed with phosphate buffered saline (PBS) and then placed in a Falcon tube containing 10 mL of test solution. Long-term frozen stocks were prepared using 20% glycerol for the bulk fluid, and biofilm samples from the biotic reactor. The sediment, three-day pre-culture, day 28 bulk fluid, and biofilm frozen stocks were sent in triplicate for DNA extraction and 16S rRNA amplicon sequencing. Library preparation and sequencing were performed for the V3 and V4 regions of the 16S rRNA gene targeting both bacteria and archaea. The microbiome analysis pipeline along with DNA extraction was performed by Eurofins Genomics LLC. Taxonomic classification method using Kraken2 (v 2.1.1). Bioinformatics and data analysis was performed using the Qiime2 (version 2023.5) software. To visualise the multivariate dispersion of the community composition, a principal component analysis (PCA) analysis was conducted employing GraphPad (version 10.0.2).

ATP assay. The ATP concentration in both the abiotic and biotic reactors was determined by luminescence after reaction with luciferin-luciferase using the BacTiter-Glo™ Microbial Cell Viability Assay kit (Promega). The assay provides a method for determining the number of viable microbial cells in culture based on quantitation of the ATP present. ATP is the energy source of all living cells and is involved in many vital biochemical reactions. When cells die, they stop synthesising ATP, and the existing ATP pool is quickly degraded. Higher ATP concentration indicates higher number of living cells. All assays were performed according to the manufacturer's instructions. Both total ATP (tATP) and dissolved ATP (dATP) were measured. tATP represents the total ATP in a surface-associated biofilm or on a solid substrate. It includes both intracellular ATP from active microbial cells and extracellular ATP released due to cell lysis or metabolic activity. It is measured per unit area (cm^2) and is commonly used to assess biofilm activity, biomass, and microbial contamination on surfaces in industrial, medical, and environmental settings. dATP refers to ATP that is free in solution (i.e., planktonic), typically measured in a liquid sample such as water, wastewater, or industrial process fluids. It mainly represents extracellular ATP released from lysed cells or actively secreted by microorganisms. It is measured per unit volume (mL) and is often used to monitor microbial contamination, system cleanliness, and biocide efficacy in fluid systems. Both metrics are important in MIC monitoring, as high tATP suggests biofilm-driven corrosion, while high dATP may indicate microbial stress, cell lysis, or contamination in industrial fluid systems. Six coupons were gently rinsed with PBS and then immersed in a Falcon tube containing 10 mL of test solution. Any cells were detached from the metal coupons using a cell scraper (Biologix). Both planktonic and sessile samples were processed with the BacTiter-Glo™ Microbial Cell Viability Assay kit, which measures ATP from as few as 10 microbial cells. The ATP concentrations were determined by

measuring luminescence with a Clariostar Plus Multimode Microplate Reader (BMG Labtech). Planktonic cells in each reactor were determined following the same method described before; in this case, 10 mL of the bulk test solution was processed with the BacTiter-Glo™ Microbial Cell Viability Assay kit. Negative controls of PBS, deionised water and sterile test solution were used to indicate no ATP activity.

Statistical analysis. All statistical analysis was performed using the Mann-Whitney test (also known as the Wilcoxon rank-sum test), to compare the differences between two independent groups when the dependent variable is either ordinal or continuous, but not normally distributed. As such, the following assumptions were made: (*i*) the observations from both groups are independent, (*ii*) the dependent variable is either ordinal or continuous, and (*iii*) the distributions of the two groups are identical under the null hypothesis. The statistical software GraphPad (version 10.0.2) was utilised. The results were reported with the p-value, with the significance level also stated. Any assumptions that were met or violated would have been flagged in the software. The Mann-Whitney test provides a robust method for comparing two independent groups when the data do not meet the assumptions required for parametric tests. By ranking the data and comparing the rank sums, this test determines whether there is a statistically significant difference in the distributions of the groups under study.

Chapter 3 Investigating the effects of surface roughness and nutrient-enriched artificial seawater on anaerobic marine biofilm formation and microbiologically influenced corrosion of UNS G10180 carbon steel

3.1 Introduction

MIC is a complex process that causes structural and operational degradation, especially in the energy and maritime sectors. Understanding the precise MIC mechanism is not straightforward as there can be numerous competing abiotic and biotic corrosion mechanisms taking place at any given time. As such, understanding and predicting MIC is a particular challenge, since there is a lack of robust and reproducible physical biofilm model systems that reflect real-world and operating environments. With the recent operating history of the offshore wind farm industry, the scale problems and associated costs are yet to be fully understood, but it has become apparent the actual

environmental corrosivity can be very different from that originally assumed in the design specification. Early monopile design assumptions anticipated low, uniform *CR* in sealed compartments that would be completely air- and water-tight. However, operational experience has shown anaerobic (anoxic) microbial conditions can quickly develop negating the original installation protection strategies leading to structural deterioration [205].

Detailed knowledge of how microorganisms behave within mixed biofilm communities is limited [24, 206, 207]. Additionally, the extent to which abiotic or biotic conditions lead to corrosion is also complex. Abiotic corrosion is linked to physical and non-biological factors. Whilst biotic (microbial) corrosion involves the deterioration of a surface because of the metabolic activity of microorganisms, either directly or indirectly through EET, metabolites or biodegradation. A marine biofilm will typically comprise of a mixed-species consortium that form synergistic relationships enabling the mixed-species biofilm to be more recalcitrant, compared to single-species biofilms and planktonic microorganisms [6]. A wide diversity of microorganisms, typically growing as biofilms, has been implicated in corrosion. Biofilms are aggregates of microorganisms that are typically surface adherent, due to the presence of EPS [2, 3]. Protection from physical disturbances and antimicrobial agents, along with increased environmental stability are two important advantages afforded to biofilm communities. Furthermore, these sessile microorganisms within a biofilm have greater access to nutrients and other resources accumulating at surfaces, along with enhanced opportunities for interactions such as horizontal gene transfer and co-metabolism which may greatly influence the community dynamics within a biofilm and the threat of MIC [16, 208].

The broad functional diversity of microorganisms apparent in anaerobic soils, sediments, and subsurface environments play an important ecological and biogeochemical role in nature and can lead to intrinsically heterogeneous biofilms under simulated conditions. However, it is the presence of electroactive microorganisms, capable of exchanging electrons with their extracellular environment, which play a key role in EET associated EMIC [29]. These electroactive microorganisms can be further classified as being either electrogens, capable of donating electrons to natural extracellular electron acceptors, or electrotrophs, capable of accepting electrons from natural extracellular electron donors. Though, some electroactive microorganisms can switch between functioning as electrogens or electrotrophs, depending on environmental conditions. The full diversity of electroactive microorganisms is still poorly understood and new electroactive microorganisms are continually being identified [29]. In the context of anaerobic sediments and the surface of corroding metals, the relationship between respiratory and fermentative electrogens

can have a significant effect on the electromicrobiome, the surrounding environmental chemistry and any corrosion mechanisms, specifically the extent of EET [29].

EET is typically much greater for respiratory electrogens, such as SRB and IRB. SRB obtain energy by oxidising H_2 or a range of organic compounds to reduce SO_4^{2-}, the terminal electron acceptor, to biogenic H_2S [30]. For SRB, electrons can be directly withdrawn from the metal surface through membrane-bound redox proteins for SO_4^{2-} reduction [209, 210]. Since H_2S readily combines with Fe^{2+} ions from the primary dissolution of Fe^0, the net reaction (including bicarbonate that is readily available in many water systems) is as follows [211]:

$$4Fe + SO_4^{2-} + 3HCO_3^- + 5H^+ \rightarrow FeS + 3FeCO_3 + 4H_2O \quad \ldots\ldots (3.1)$$

This net reaction is commonly referred to as EMIC and allows SRB to utilise Fe^0 more efficiently as an electron donor by direct uptake of electrons from Fe^0 oxidation [25, 210]. The formation of corrosion products, such as FeS or $FeCO_3$, can increase the *CR* by generating a localised corrosion cell on the metal surface [209]. In contrast, IRB utilise Fe^{3+} ions as efficient electron acceptors that are capable of out-competing electron acceptors of lower potential, such as SO_4^{2-} [62, 63]. IRB are thought to accelerate the corrosion of steel by removing the ferric oxide passivating layer through iron respiration. Biomineral dissolution reactions by metal reducing microorganisms remove oxide layers or force mineral replacement reactions that lead to further dissolution of metals. The rate of dissolution depends on many aspects and parameters, such as chemical nature of the solvent and solute, temperature, and interfacial surface area [212].

Existing industrial standards, such as the NACE TM0212-2018, [26] acknowledge that sessile microorganisms are the most important biological component. As data based on planktonic microorganisms are of limited value, since planktonic microorganisms are not directly representative of sessile microorganisms which form the biofilms which cause MIC [170]. It is however recognised that techniques and procedures for studying sessile microorganisms are limited and can produce variable outcomes [27, 170]. Various assays and test methods have been used for the investigation, diagnosis, and treatment of MIC. Though, a more holistic understanding that accurately evaluates the effects of biocides on biofilms, and not of planktonic microorganisms, is needed. The difficulty comes in how to establish and test biofilms in the lab, analytical methods, and information to collect, and data interpretation for biocide efficacy [213, 214]. A key objective for this thesis is to explore recent advances in biofilm testing and MIC research, for instance, to provide recommendations for future standards being drafted by the AMPP for the testing of biocides. As there are not nationally or internationally recognised standards or test methods with which to evaluate control strategies effective against biofilm-mediated corrosion.

This study demonstrates the applicability of a novel dual bioreactor protocol to investigate biofilms under conditions that mimic the MIC environment of interest. It is important to note that this is the first experiment in our lab using the proposed experimental setup. Overall, the aim is to develop a reproducible bioreactor-based model for MIC that will be able to: (*i*) gain new scientific insight and mechanistic MIC understanding that will improve predictive measures including next-generation sequencing of the MIC-associated microbiome and (*ii*) progress the first standard model and biofilm-relevant test method for the industry. Moreover, the novelty of this protocol is in using a mixed-species environmental biofilm which also importantly also incorporates a multi-disciplinary approach, using MLOE [145] to gain a holistic understanding of biofilms and MIC.

3.2 Results

Over the initial three-day batch phase, the abiotic media had no apparent visual changes, and the coupons maintained the silver-grey appearance of the CS. Once the flow of fresh media was started on day 4, the sterile abiotic reactor ASW media became reddish-brown in colouration with increased turbidity (increasing suspended matter). Generally, the abiotic coupons had a reddish-brown corrosion product over the 28 days. Conversely, after inoculation of the biotic reactor ASW media, a black surface film was present on the steel coupons (day 1), with a low level of turbidity. After the flow of fresh ASW media was started on day 4, the ASW media had visible black particulates settling at the bottom of the reactor, with the bulk media being green in appearance. After two weeks, there was a visible crust at the ASW surface, and the media was black in appearance with high turbidity. Over the following two weeks, up to 28 days, the biotic media was dark green/black in colouration. Upon dismantling of the reactors on day 28, and retrieval of the coupon rods, there was an evident difference in the coupon appearances, see Appendix B Figure B3. The abiotic surfaces were covered in a thick reddish-brown corrosion product. Whilst the biotic surfaces were only partially covered around the centre with a dark green/black deposit.

Sulphide microsensor. Figure 3.1 shows the aqueous H_2S concentrations monitored in the abiotic and the biotic anaerobic nutrient-enriched ASW media over the test duration. For the sterile abiotic condition, there was a generally low H_2S concentration (mean: 29.2 µmol L^{-1}). Whereas for the biotic condition, the H_2S concentration steadily increased resulting a maximum of about 150 µmol L^{-1} after two weeks, before decreasing to similar levels detected for the abiotic media. *DO* concentrations measured on day 28 were: 4.4 ppm in the 10 L media containers, 2.6 ppm in the abiotic and 0.2 ppm in the biotic reactor. The pH was not measured on completion of the experiment.

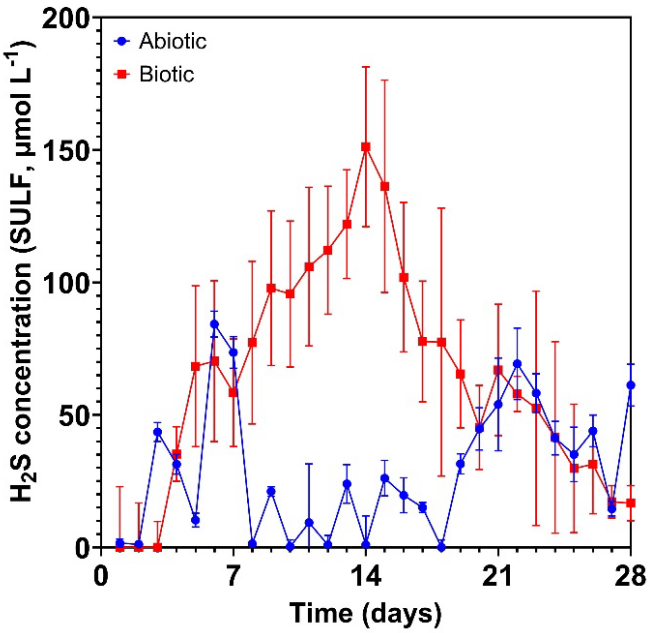

Figure 3.1. Aqueous sulphide measurements (*SULF*, µmol L^{-1}) for the abiotic and biotic conditions over 28 days (nb. measured the anaerobic nutrient-enriched artificial seawater media *in situ* adjacent to corroding UNS G10180 carbon steel).

Carbon steel surface analysis. Appendix B Figure B4 shows the CS surfaces on day 0. Appendix B Table B5 summarises the quantitative surface roughness profiles on both day 0 and day 28. Prior to testing, the AR and P coupons had markedly different surface profiles, owing primarily to the clearly evident machine marks on the AR surfaces. The machine marks were still evident on day 28. However, both coupon samples exhibited similar surface roughness profiles on day 28. Figure 3.2 shows the cleaned CS surfaces after 28 days, with biofilms and corrosion products removed to reveal the morphology of the surface degradation and to facilitate corrosion assessment. Surface profilometry revealed that both abiotic and biotic anaerobic ASW media led to localised pitting, with the biotic condition more extensively pitted. The abiotic average pit depths were 39 µm and 46 µm, and average pit areas of 1533 μm^2 and 1939 μm^2, for the AR and P coupons, respectively. The biotic average pit depths were 47 µm and 52 µm, with the average pit areas of 1943 μm^2 and 2398 μm^2, for the AR and P coupons, respectively. For this study, a pit was classified as having a depth greater than 5 µm and an area greater than 650 μm^2 [153].

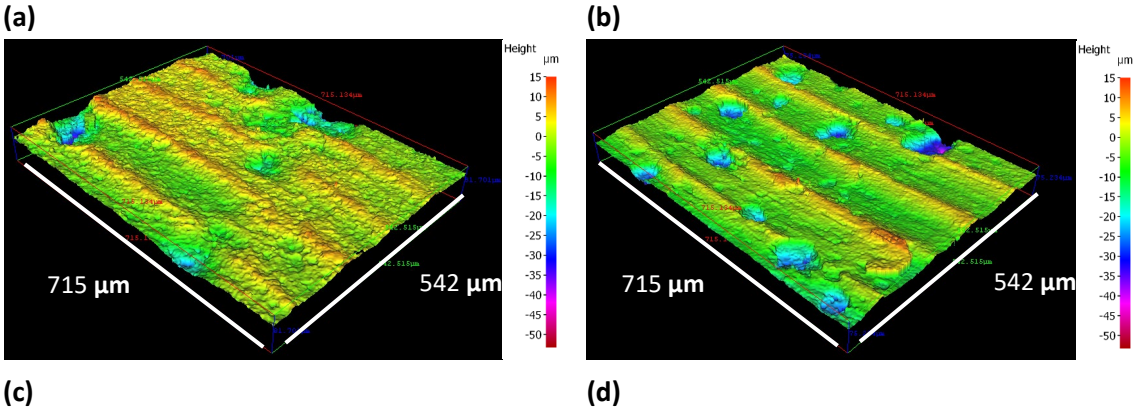

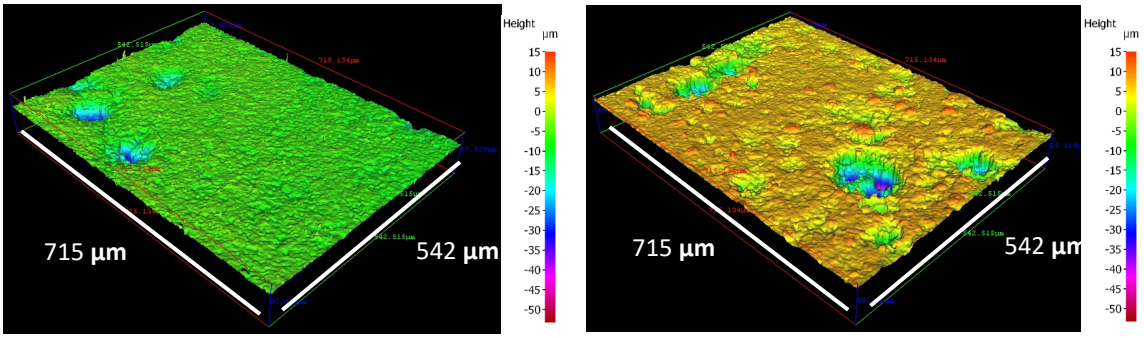

Figure 3.2. Three-dimensional optical surface profilometry of the cleaned UNS G10180 surfaces at day 28. AR coupons for: **(a)** abiotic and **(b)** biotic conditions; and P coupons for: **(c)** abiotic and **(d)** biotic conditions, after exposure to anaerobic nutrient-enriched artificial seawater media for 28 days.

Figure 3.3a provides an evaluation of the CS coupon *CR* (with the caveat that such an assessment assumes uniform corrosion). For the abiotic condition, there was a higher *CR* when compared to the biotic condition, though there was no significance. Furthermore, when comparing between the two surface roughness types, AR and P coupons within each reactor, there was also no significance ($n = 3$). According to the NACE SP0775-2023 assessment criteria, there was a severe *CR* (> 0.25 mm y^{-1}) in the abiotic and a moderate *CR* (between 0.025 and 0.12 mm y^{-1}) in the biotic (Figure 3.3a); whilst a severe *PR* (> 0.38 mm y^{-1}) was assessed for both the abiotic and biotic conditions (Figure 3.3b) [170].

Further analysis of the surface profilometries in Figure 3.2, allowed a quantitative determination of the *PR* Figure 3.3b and *PD* Figure 3.3c of the CS coupons. For the biotic condition, though there was a higher *PR*, although there was no significant difference evident between the abiotic and biotic conditions. Moreover, there was a significant increase in the incidence of pitting. There was an average *PD* of 13 pits mm^{-2} and 10 pits mm^{-2} in the abiotic condition, with 31 pits mm^{-2} and 26 pits mm^{-2} in the biotic condition, for AR and P coupons, respectively. Again, there were no significant differences when comparing between the two surface roughness types within each reactor.

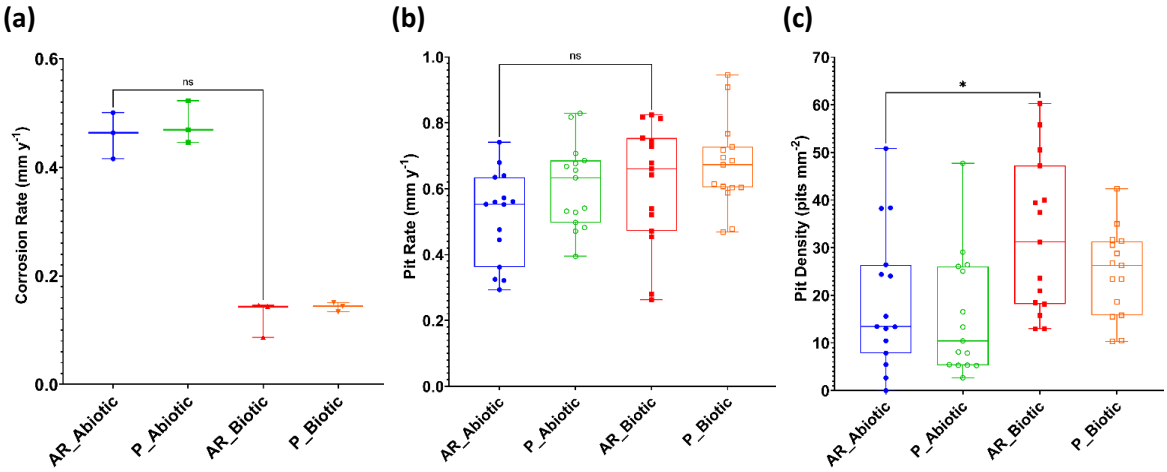

Figure 3.3. Abiotic and biotic corrosion performance after exposure to anaerobic nutrient-enriched artificial seawater media for 28 days: **(a)** corrosion rate via gravimetric analysis and surface profilometry assessed **(b)** pit rate and **(c)** pit density ($P < 0.05$), for the AR and P coupons.

Electrochemical measurements. Figure 3.4 shows clear differences between the abiotic and biotic anaerobic nutrient-enriched ASW media for the OCP (*i.e.*, E_{corr} for UNS G10180 CS) and R_p. The abiotic condition, Figure 3.4a, had a distinct +0.100 V increase in the E_{corr} during the first seven days that can be linked with the presence of a conditioning film (i.e., an adsorbed organic layer) and the formation of inorganic corrosion product layer. A pseudo-steady state E_{corr} was attained in the following 18 days (where AR had a slightly greater variation in potential). Conversely, for the biotic condition, there was a gradual electronegative shift in the E_{corr} after seven days, until Day 14, after which E_{corr} swiftly increased by +0.070 V. The potentials for both abiotic and biotic in the latter stages (Day 16 to 28) were generally similar and ranged between –0.610 V and –0.660 V *vs*. Ag/AgCl.

In Figure 3.4b the LPR derived R_p after Day 3 remained low at approx. 500 Ω cm^2 for the sterile abiotic condition, indicative of a uniform corrosion across a porous corrosion film. Whereas a periodic response over several days was evident for the biotic condition, with R_p ranging between 5000 and 15000 Ω cm^2. The pioneering bacterial attachment/colonisation, biofilm formation and growth kinetics will lead inevitably to a more complex electrochemical response. Overall, there were no significant differences when comparing between the two surface roughness's (AR and P) within both the abiotic and biotic reactor environments.

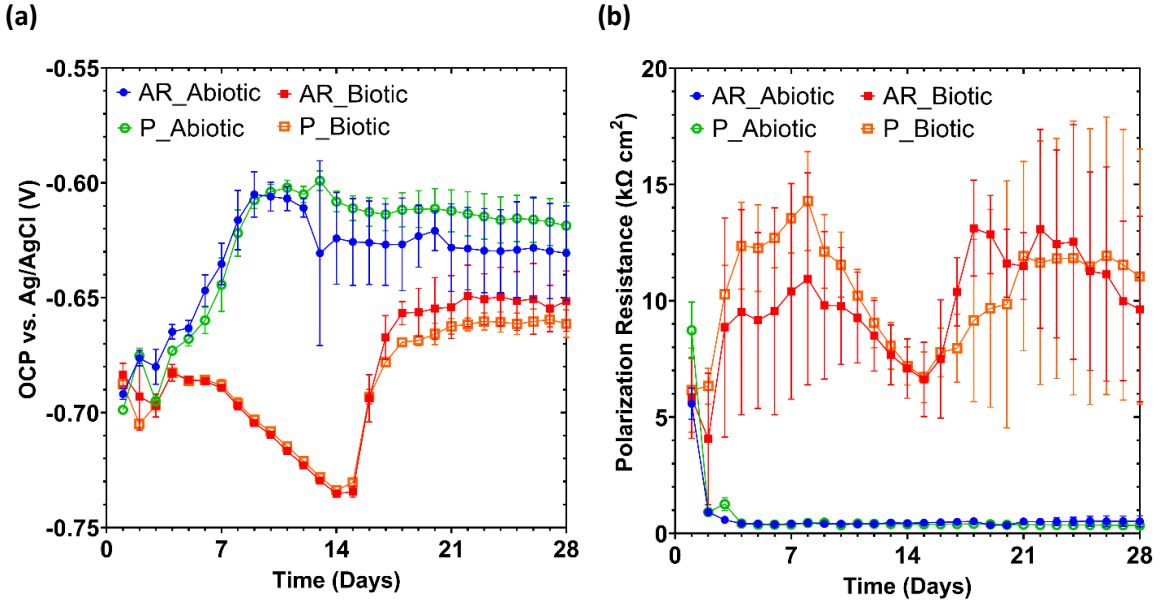

Figure 3.4. LPR data for UNS G10180 carbon steel: **(a)** open-circuit potentials and **(b)** polarisation resistance in anaerobic nutrient-enriched artificial seawater media (abiotic and biotic conditions), for the as-received (AR) and polished (P) coupons (data points represent mean ± standard deviation, $n = 3$). Reactor stirrer at 50 rpm.

Figure 3.5 shows the EIS data for UNS G10180 CS in the anaerobic nutrient-enriched ASW media presented in three forms: Nyquist, Bode phase angle and Bode impedance modulus plots. The sterile abiotic condition on Day 1 typifies an electrochemical response for the formation of a

porous interface, with diffusion of soluble electroactive species across an organic conditioning film [207] and nascent inorganic corrosion product layer. The diffusive behaviour is associated with linear features having a roughly 45° slope (a Warburg impedance response) and phase angles close to 45° in low frequency region (10^{-2} – 10^{0} Hz), see Fig. 3.5a and 3.5c. At Day 7, a depressed Nyquist semicircle and phase angles tending towards zero are evident, indicative of a more prominent resistive component operating within the low frequency region.

Subsequently, the abiotic impedance spectra shift towards lower frequencies (10^{-2} – 10^{0} Hz), with a combined diffusive/resistive behaviour. The biotic condition had a consistently uniform EIS response over the 28 day test, with only minor variation in the spectra and suggests the absence of significant detectable electrochemical changes with time. Notably, there are no discernible Nyquist semicircles (Fig 3.5b), with Day 1 being more capacitive/diffusive in character relates to the well-established double-layer concept (*i.e.*, interfacial charge distribution) and diffusion of electroactive species. Here a wider low frequency region (10^{-1} – 10^{2}) is likely to be subject to a greater influence of adsorption processes, associated with the adhesion of the pioneering bacteria on a conditioning film [215, 216] and biofilm formation.

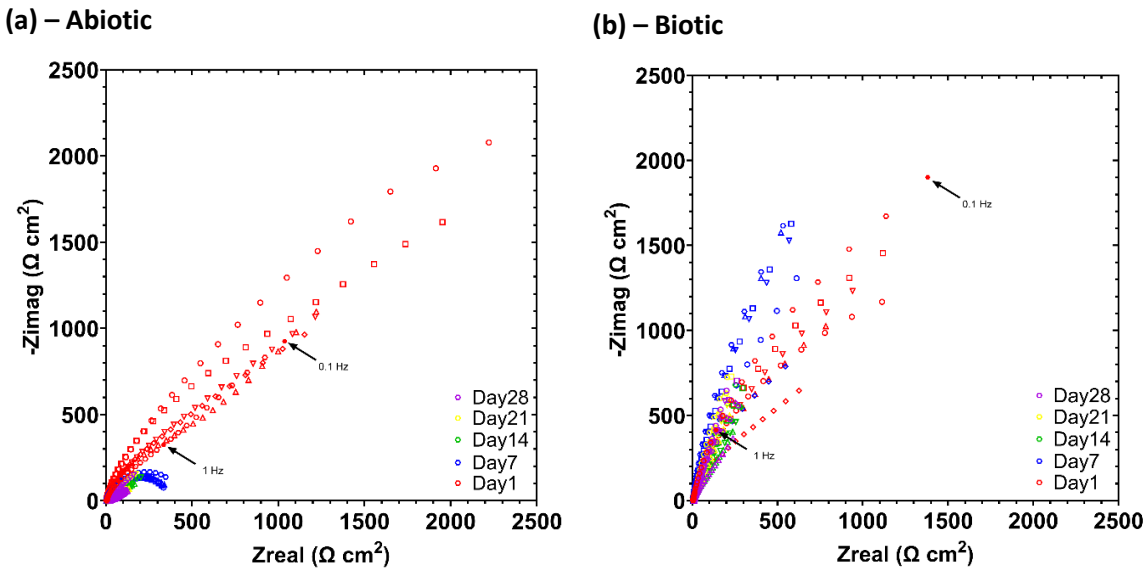

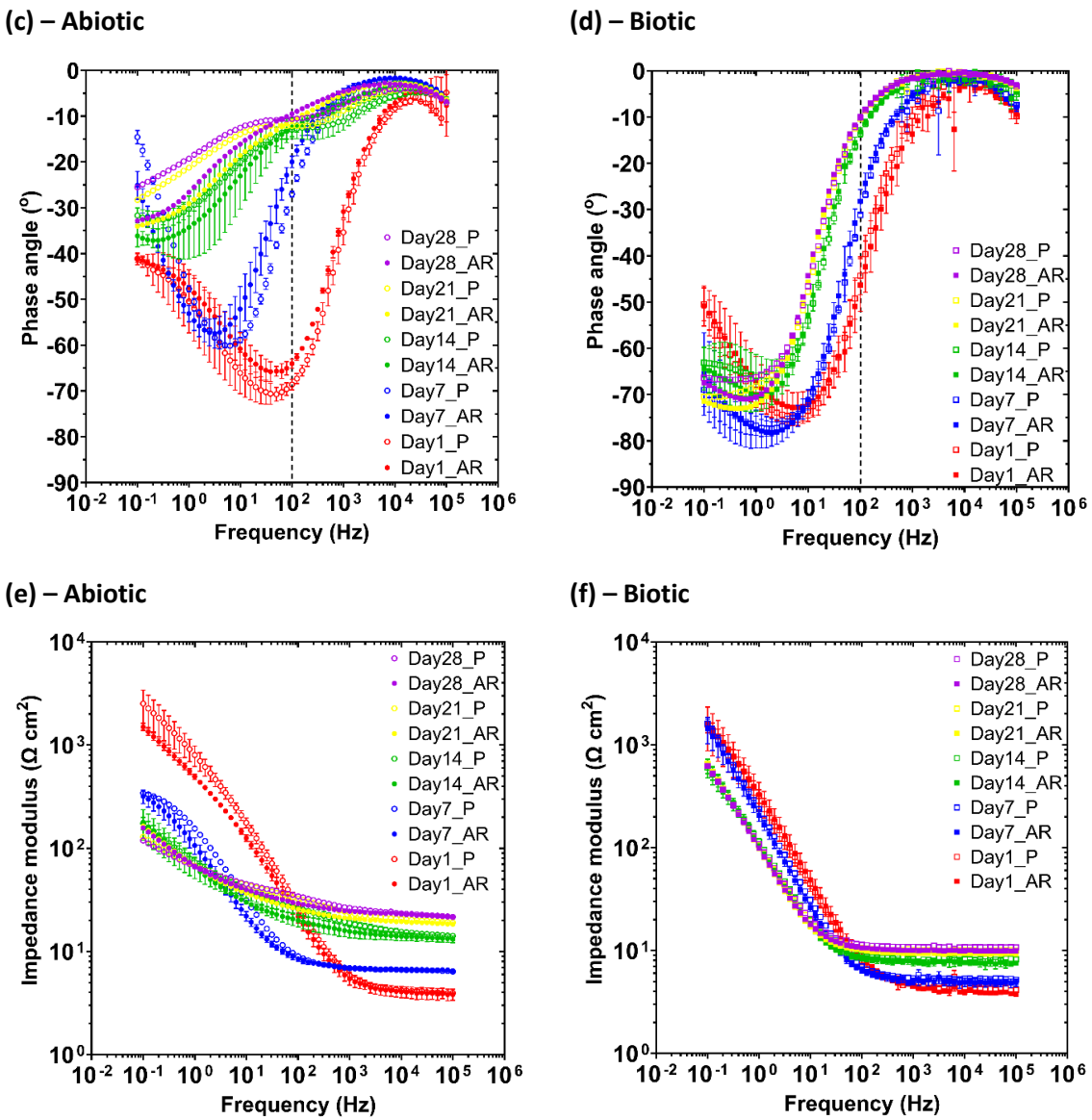

Figure 3.5. EIS data for UNS G10180 carbon steel in anaerobic nutrient-enriched artificial seawater media at OCP: **(a, b)** Nyquist, **(c, d)** Bode phase angle (q vs. f), and **(e, f)** Bode impedance modulus (|Z| vs. f) over 28-days. (*n* = 3). Reactor stirrer at 50 rpm.

The EIS spectra were fitted using an ECM shown in Figure 2.4. Both the abiotic and biotic data generally had a good fit, with the quantitative fitting results shown in Appendix Table B6. R_s, R_{film} and R_{ct} are the solution resistance, the resistance of the biofilm or the corrosion product film, and the charge transfer resistance, respectively. The constant phase element (CPE) characterises the 'non-ideal' capacitance behaviour of either the biofilm or the corrosion product film layer, and the charge transfer capacitance. In the Appendix Table B6, *Q* and *n*, are admittance and exponent parameters from the CPE. For the abiotic condition, there is a capacitive behaviour over the first week, with a diffusive behaviour over the final three weeks in the film layer (reflecting ion adsorption). Whilst there was a diffusive behaviour in the double layer, which reflects charge transfer, due to the formation of corrosion products (rust, porous oxide layer). The exponent

parameter in the double layer reflects a non-ideal capacitance, which is indicative of resistive and inductive parasitics, because of a more prominent resistive component. R_{film} is consistently low over the 28 days, and there are no significant changes in R_{ct}. For the biotic condition, there is a capacitive behaviour in both the film layer and double layer due to the presence of the biofilm. There are no significant changes in the R_{ct} in the double layer over time. The exponent parameter for the film layer is greater than 0.8 at most time points, which indicates a non-ideal capacitance response. This is true for the first two weeks in the double layer. However, during the final two weeks of the experiment, the exponent parameter is closer to 1 for the AR coupons in the double layer, which indicates a strong capacitive behaviour. The ECMs and EIS both have general agreement with the LPR data.

Figure 3.6 shows the potentiodynamic polarisation curves for UNS G10180 CS for the abiotic and biotic reactors in anaerobic nutrient-enriched ASW media after 28 days. Table 3.1 shows the corrosion parameters obtained from the polarisation curves. From the Tafel slopes, there is a similar cathodic behaviour (reduction) when comparing the abiotic and biotic ASW media, which is linked to the predominant hydrogen evolution reaction (HER) under anaerobic conditions. Conversely, the anodic Tafel slopes (oxidation) are greater, demonstrating almost limiting current densities, in the biotic compared to the abiotic media. Thus, after 28 days the biofilm hindered the Fe^0 dissolution reactions. Overall, the abiotic condition had a higher j_{corr} compared to the biotic condition. This is consistent with the more uniform corrosion morphology seen for the abiotic coupon surfaces, see Figure 3.2. Similarly, the sterile abiotic condition had a more electropositive E_{corr} when compared to the biotic condition. The polarisation results corroborate the LPR and EIS data, with no significant differences when comparing between the two surface roughness types within each reactor.

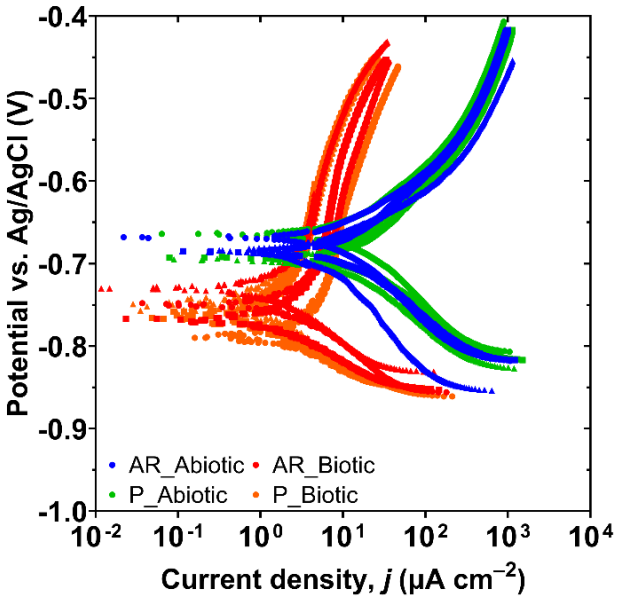

Figure 3.6. Potentiodynamic polarisation curves for the abiotic and biotic AR and P UNS G10180 carbon steel coupons at ambient temperature after exposure to anaerobic nutrient-enriched artificial seawater media for 28 days. Scan rate of 0.5 mV s^{-1} and reactor stirrer at 50 rpm. Dissolved oxygen levels were 2.6 ppm (abiotic) and 0.2 (biotic), at Day 28.

Table 3.1. Fitted electrochemical parameters from polarisation curves; comparison between the abiotic and biotic AR and P UNS G10180 coupons after exposure to anaerobic nutrient-enriched artificial seawater media for 28 days.

	Coupon	j_{corr} / µA cm^{-2}	E_{corr} *vs.* Ag/AgCl / V	β_a (mV dec^{-1})	β_c (mV dec^{-1})
Abiotic	AR	14.5 ± 4.8	-0.679 ± 0.010	123 ± 20	146 ± 11
	P	22.1 ± 5.3	-0.684 ± 0.017	129 ± 32	108 ± 144
Biotic	AR	2.99 ± 1.04	-0.749 ± 0.019	317 ± 24	86 ± 9
	P	1.93 ± 1.47	-0.769 ± 0.019	263 ± 53	66 ± 6

Biofilm characterisation. CLSM with differentiation of live and dead biofilm cells was performed and can be found in the supplementary material Appendix B Figure B7. The heterogeneous biofilm distribution over the surface of the CS coupons did not allow measurements of the maximum biofilm thickness. Therefore, the thickness of biofilms was not determined. It was also difficult to identify significant differences in the structure and distribution of live and dead cells in the biofilms across the two surface roughness types, AR and P coupons, within the biotic

condition. In general, both surfaces had similar live and dead cell ratios (approximately 98% live to 2% dead).

Active microorganism evaluation of the environmental marine sediment, the initial and final biotic ASW media planktonic samples (Day 0 and Day 28), and the biotic AR and P biofilms, was undertaken via 16S rRNA amplicon sequencing with two target region, V3-4 for bacteria and archaea. A total of 2,422,833 high-quality sequences were obtained after bioinformatics processing of the raw reads. From these, 95.8% was classified for the sediment sample with 99.99% classified for the Day 0 and Day 28 planktonic samples, AR and P biofilm samples. These sequences were taxonomically classified into microbial genera. The top 25 microbial genera are presented in Appendix B Table B8 in the supplemental material. Figure 3.7 summarises the sequencing data, showing a PCA (a) and a stacked bar plot (b) illustrating the relative abundances for the top 25 genera. Molecular identification of the microorganisms showed that the initial sediment sample had a very diverse microbial composition. Most genera had low relative abundances less than 2%. The dominant genera included *Sulfurovum*, *Candidatus Prometheoarchaeum*, *Candidatus Methanoplasma*, *Desulfosarcina*, *Desulfuromonas* and *Thiohalobacter*. The sediment sample had low or negative Spearman correlation coefficients (Appendix B Figure B9) with the other samples which was attributed to changes in conditions such as temperature and media composition from the natural marine environment. There was much less diversity in the Day 0 sample, with *Sulfurovum*, *Candidatus Prometheoarchaeum*, *Candidatus Methanoplasma*, and *Thiohalobacter* all exhibiting lower relative abundances (<1%). Whilst genera from *Vibrio*, *Oceanicoccus*, *Serpentinicella* and *Methanococcoides* made-up approximately 75% of the relative abundance. Again, the Day 0 planktonic sample had mostly negative Spearman correlation coefficients with the other samples. After 28 Days, there was a distinct shift in the microbial composition, with substantially lower abundances of methanogenic species. *Malaciobacter*, *Vibrio*, and *Draconibacterium* were the dominant genera making up approximately 80% of the relative abundance. The Day 28 planktonic sample had a Spearman correlation coefficient of 0.11 with the sediment sample, -0.10 with the Day 0 planktonic sample and 0.75 with both biofilm samples. Both biofilm samples exhibited similar microbial populations on both the AR and P coupons. The relative abundances of *Vibrio* decreased to between 3% and 6%, and *Draconibacterium* reduced to approximately 3.5%. *Sulfurovum*, *Candidatus Prometheoarchaeum*, *Candidatus Methanoplasma*, and *Thiohalobacter* which were the dominant genera from the sediment sample all had lower relative abundances (<1%) in the biofilm samples and Day 28 planktonic sample. Both biofilm samples were similar, with a Spearman correlation coefficient of 0.94. The dominant genera included *Malaciobacter*, *Crassaminicella*, *Maridesulfovibrio*, *Desulfomicrobium* and *Halarcobacter*

making up approximately 60% of the relative abundance. There were no methanogenic archaea in the biofilm samples.

(a)

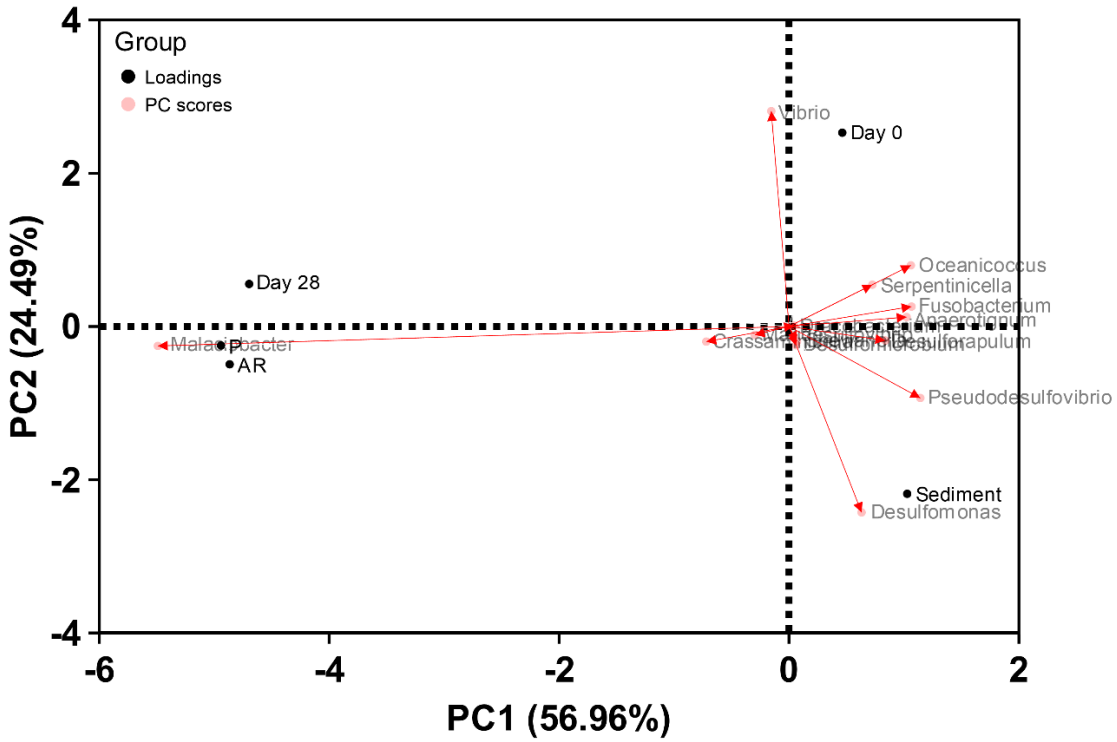

(b)

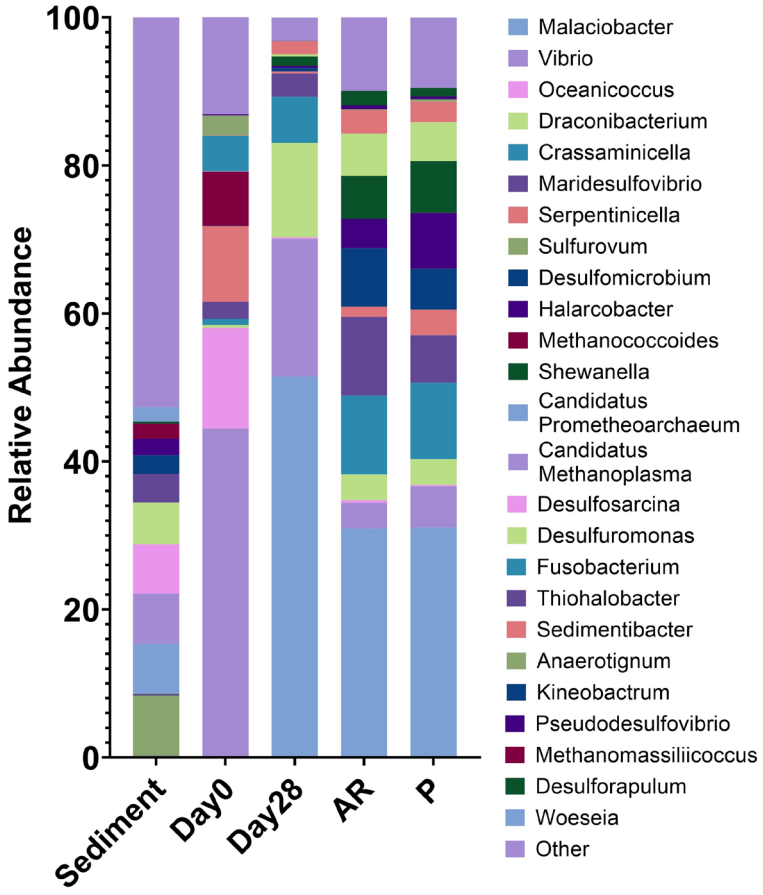

Figure 3.7. Principal Component Analysis biplot **(a)**; Microbial community. The results show the mean relative abundances of microbial communities classified at the genus level, for the top 25 genera, from 16S rRNA amplicon sequencing **(b)**; for environmental marine sediment, Day 0, and Day 28 planktonic samples, AR and P biofilm samples after exposure to anaerobic nutrient-enriched artificial seawater media for 28 days.

The microbial activity was determined by the ATP concentrations (dissolved and total, dATP and tATP, respectively) in both the bulk fluid and biofilms, see Figure 3.8. It should be noted, for the sterile abiotic condition, the dATP concentration did not exceed the negative control concentrations, which were used to indicate no ATP activity, and was thus omitted from the figure. For the biotic ASW media (bulk fluid), there was no significant change in the dATP concentration when comparing Day 0 and Day 28, with dATP values of on the order of 1 pg mL^{-1}. Again, for the sterile abiotic condition, the tATP concentration did not exceed the negative control concentrations and was thus omitted from the figure. Also, for the biotic condition there was no significant change in the concentration of tATP over the surface of the CS coupons (tATP of about 100 pg mL^{-1}). There were no significant differences when comparing between the two surface roughness types within each reactor. As expected, there was a significantly greater ATP concentration for the biotic compared to the abiotic condition.

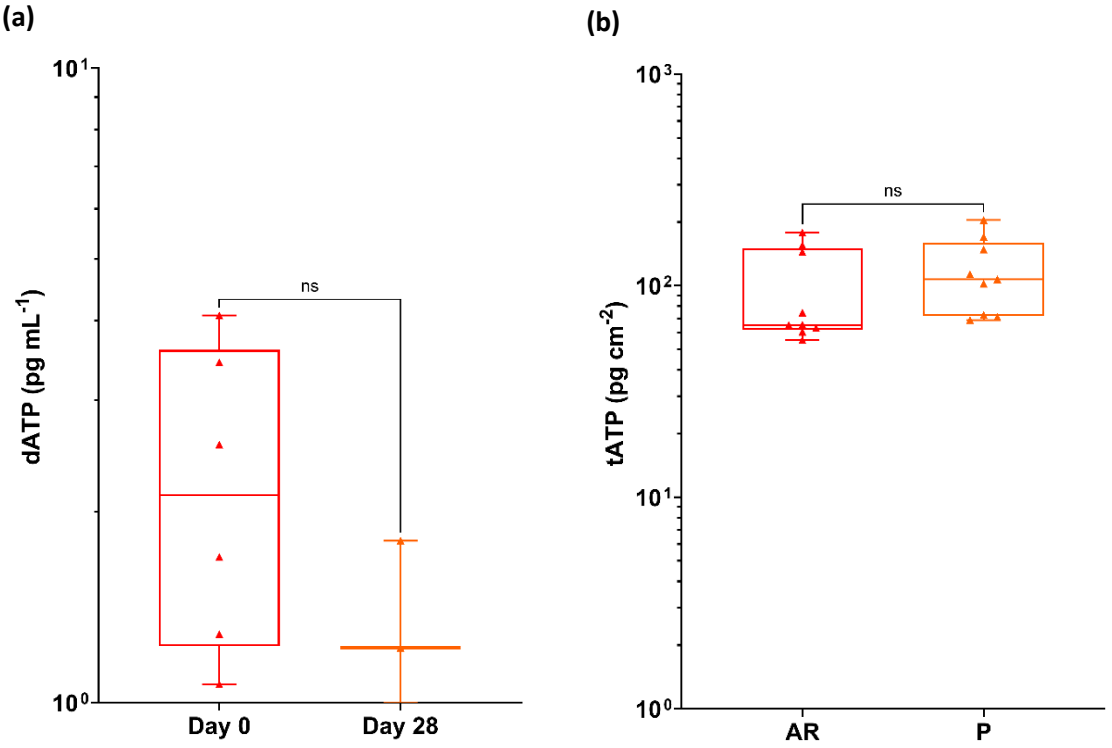

Figure 3.8. **(a)** Dissolved ATP (dATP) concentrations comparing the anaerobic nutrient-enriched artificial seawater media taken on Day 0 and Day 28 and **(b)** Total ATP (tATP) concentration comparing the biofilm of the AR and P coupons, from the biotic condition, after exposure to anaerobic nutrient-enriched artificial seawater media for 28 days.

3.3 Discussion

Previous studies, which generally investigate single-species biofilms, have shown that bacteria tend to cause an increase in the uniform *CR* on CS coupons compared to abiotic controls [16, 103, 217, 218]. Typical *CR*s of CS in anoxic environments are reported to be between 0.2 and 0.4 mm y^{-1} [25]. As such, CS corrosion is often considered to be insignificant in anoxic environments, such as marine sediments [25, 219, 220]. However, under either stagnant or low hydrodynamic flow conditions, microorganisms tend to form thicker biofilms on solid surfaces [197]. Ultimately, this results in higher *CR*s due to microbial corrosion mechanisms which generate anodic and cathodic regions that affect the passive film on the material surface. *CR*s for SRB have been reported to be 0.9 mm y^{-1} [196]. During the initial stages of biofilm formation, heterogeneous patches form on material surfaces, inducing the formation of differential concentration gradients. The periodic detachment or formation/growth of the biofilm facilitates the removal of the protective films which changes the passive film structure and/or increases the dissolution [17]. Additionally, when the biofilm builds up, the diffusion of nutrients from the environment to the microorganisms in the biofilm matrix is limited, which leads to nutrient deprivation. The interfacial microenvironment is altered, changing the diffusivity of metabolites and nutrients through the biofilm layer [196]. Here, the biofilm affects

the transportation of chemical species at the steel/ASW interface [17]. This has been shown to cause a shift in metabolism which exacerbates *CR*s [103].

However, studies which have investigated mixed-species biofilms have challenged these observations. Due to the presence of a mixed-species biofilm formed on the material surface, uniform *CR*s have been shown to decrease [221, 222]. The main mechanism of corrosion inhibition is the biofilm induced formation of green rust (GR) compounds, such as siderite, $\mathrm{GR}(\mathrm{CO}_3^{2-})$, and iron sulphide compounds ($\mathrm{GR}(\mathrm{S}^{2-})$ [221]. The presence of biogenic FeS acts as a barrier by impeding the diffusion of Fe^{2+} ions from the metal surface to the aqueous environment [25]. This impediment has been linked to organotrophically grown SRB. Whereas, in organic matter-free cultures, where the predominant corrosion mechanism is EMIC, no significant slowing of corrosion due to the formation of corrosion products in the crust layer has been observed [25, 219, 220]. In combination with the formation of GR, the mixed-species biofilm acts as a protective layer which results in decreased uniform *CR*s [197]. At the same time the mixed-species biofilm has been shown to aggravate localised pitting corrosion. Here, patchy distribution of the biofilm may be causing differential aeration effects on the steel surface, which in turn affects the oxidation–reduction conditions at the steel/ASW media interface [17]. Through the generation of microenvironments, whether that is primarily influenced through metabolic activity or through physical gradients, localised pitting has been shown to be accelerated [222].

Figure 3.9 provides an illustration of the proposed corrosion mechanisms for both the abiotic and biotic conditions during the initial stages, as they evolved over time during this present study. For the abiotic control, during the first few days a conditioning film is developing as redox mediators adsorb onto the surface and a corrosion film is beginning to develop [196, 198]

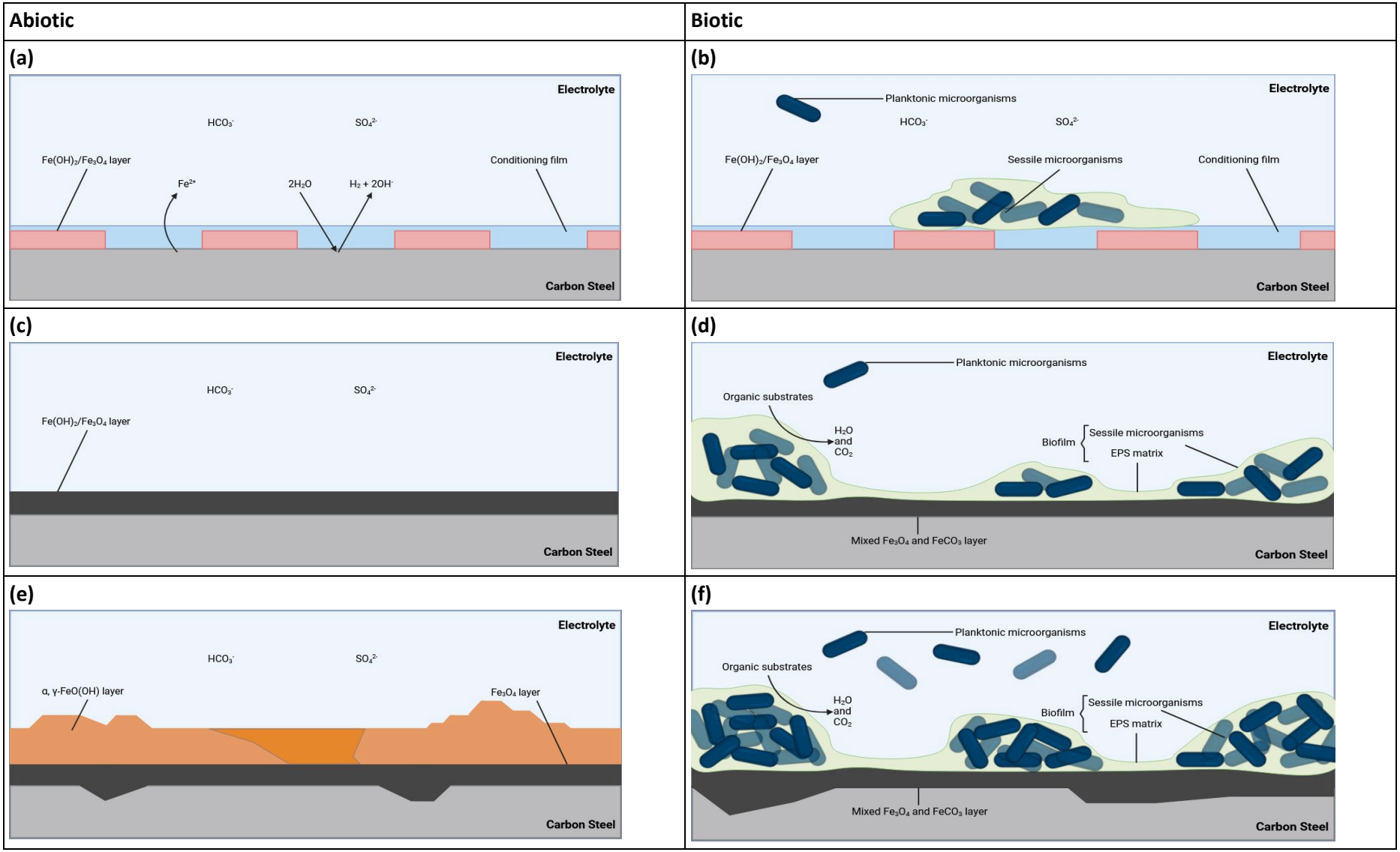

Figure 3.9. Schematic of the initial stages for UNS G10180 carbon steel in anaerobic abiotic and biotic nutrient-enriched artificial seawater media. corrosion mechanisms, **(a, b)** the formation of nascent inorganic corrosion film and the organic conditioning film with pioneering bacterial attachment; **(c, d)** maturing corrosion film under the abiotic condition and biofilm growth and colonisation under the biotic condition; **(e, f)** uniform and pitting corrosion under patchy corrosion deposits and bacteria clusters. BioRender.com (2023).

Abiotic reactor: - Under anaerobic conditions, the corrosion of Fe^0 produces $Fe(OH)_2$. This may then transform via the Schikorr reaction into Fe_3O_4, releasing more H_2 [91, 221, 222]. This results in anodic polarisation over the first week, until the E_{corr} reaches an equilibrium. From the ECMs, there is initially a capacitive behaviour observed over the first week, which reflects ion adsorption and the development of a nascent $Fe(OH)_2/Fe_3O_4$ film. Subsequently, there was a diffusive behaviour during the final three weeks in the film layer. Moreover, there was a diffusive behaviour in the double layer, which reflects charge transfer, due to the formation of corrosion products, such as lepidocrocite ($\gamma - FeO(OH)$), $Fe(OH)_2$, and $\gamma - Fe_2O_3/Fe_3O_4$. Generally, there was a relatively high level of uniform corrosion of the steel surface for the abiotic media. The presence of Fe^{3+}orange corrosion products suggest that the abiotic condition was not completely anaerobic, and minor O_2 ingress may be an influencing factor here. *DO* was measured at 2.6 ppm in the abiotic condition and 0.2 ppm in the biotic condition. The presence of the biofilm may have been acting as a passive layer to mitigate uniform corrosion but exacerbate localised pitting. In corrosion systems, a salt film may cover an electrode that is itself covered by a porous oxide layer [223]. This may explain why some localised pitting corrosion was observed in the abiotic media. Additionally, the presence of elemental sulphur, due to the minor O_2 ingress that can oxidise H_2S, may have been a contributing factor [224, 225, 226]. SO_4^{2-} adsorption onto Fe_3O_4 has been extensively studied [227] and in the presence of reducing conditions of H_2 has been shown to be involved in redox reactions to produce FeS and H_2S [228]. Cations such as Ca^{2+} have also been shown to enhance SO_4^{2-} adsorption from alkaline solutions [229]. This may also explain why low H_2S concentrations were observed in the abiotic control.

Biotic reactor: - Conversely, in the biotic condition the E_{corr} exhibited an electronegative shift during the first two weeks. This can be attributed to the initial attachment of microorganisms and subsequent biofilm formation on the steel surface [197]. Bacterial cell surfaces also possess net negative electrostatic charge on the outer cell envelope that is exposed to the extracellular environment. Moreover, they are generally negatively charged due to the EPS microenvironment [230]. There was also an initial R_p increase during the first week that is indicative of biofilm formation on the steel surface, as the presence of biofilm can act as a physical barrier preventing the diffusion of ionic species (*e.g.*, H^+) from the environment to the metallic surface [197]. For the biotic condition, there is a capacitive behaviour in both the film layer and double layer due to the presence of the biofilm. Over the final two weeks, the E_{corr} increased after the biofilm had been established. This is associated with a decrease in the anodic reaction (depolarisation) with the growth of a passive film and an increase in the cathodic reaction (polarisation) through localised

pitting corrosion. ECMs indicated an ideal capacitive behaviour over the final two weeks. Here, we can infer that there are different electrochemical reactions that are taking place at the interface of the metal/electrolyte. This may be caused by diffusion limitations due to the biofilm and changes in the prevailing metabolic activity in the system due to the availability of terminal electron acceptors. In general, the biofilm appears to accelerate localised pitting corrosion.

Surface profilometry analysis further highlighted that the biofilm induced greater localised pitting corrosion, with significantly greater *PD*, compared to the abiotic control. Generally, the shape and pit morphology were different in coupons exposed to biotic conditions compared to abiotic conditions. Whilst the pit depths were relatively similar in this present study, the average pit sizes and the percentage area of pitting was significantly greater for the biotic condition. Previous research [16, 197, 231] has found that pits were narrow and deep under abiotic conditions, but wide and shallow in the presence of microorganisms [232, 233]. In those experiments, it was hypothesised that under biotic conditions, the binding of Fe^{2+} ions and S^{2-} ions can act as a protective film on the surface of materials along with the biofilm to prevent H^+ and chloride (Cl^-) attack. Whilst for the abiotic control, there was no such protective film to prevent corrosion of the material [197]. Additionally, previous studies have also suggested that SRB and possibly also the IRB in anaerobic biofilms participate in the corrosion and rust mineralization of steel in seawater environments [221]. It is hypothesised that the deterioration observed in this present study could have been a combination of the patchy distribution of the biofilm formed under flow conditions and the formation of different corrosion products which will have affected the prevailing oxidation-reduction reactions taking place over the 28 days.

Analysis of the community dynamics revealed a marked change in the predominant relative abundances of microorganisms. The dominant genera from the sediment sample were generally anaerobic, halophilic, and obligately chemolithoautotrophic, obtaining energy by oxidizing inorganic compounds (SO_4^{2-}, NO_3^-, etc.) through respiration. However, the dominant genera from the planktonic samples taken from the bulk fluid were generally facultative anaerobes known to be chemoheterotrophic, utilising organic compounds through fermentation. The ASW supplemented with yeast extract clearly had a large impact on the community dynamics. For example, *Methanococcoides*, which had a greater relative abundance in the planktonic samples, exhibited a decrease in relative abundance over time in the planktonic day 28 sample and in the biofilm samples. Another microorganism of interest from the planktonic samples was *Fusobacterium* which has been shown to help facilitate the aggregation and establishment of several other species [235]. This may have played an important role in early biofilm formation [236]. From the biofilm samples, the dominant genera were generally anaerobic, halophilic, SRB and IRB with a relative increase in the prevalence of respiratory electroactive microorganisms. Interestingly, there were distinctly

lower relative abundances of methanogenic species in both the day 28 bulk fluid and biofilm samples. This can be attributed to an inhibition by SRB, as methanogens and SRM are known to compete for energy sources, with SRM outcompeting methanogens in sulphate-rich environments [237]. *Malaciobacter*, *Crassaminicella*, *Maridesulfovibrio*, and *Halarcobacter* made-up approximately 50% of the relative abundance. These genera are integral to the biogeochemical cycles in marine ecosystems, particularly in sulphur and carbon cycling. Not much is known about the specific functions of *Malaciobacter*. However, like other Proteobacteria in marine environments, they are likely involved in sulphur and nitrogen cycles. Together, these bacteria contribute to maintaining the balance of nutrients and energy flow in marine environments. As previously mentioned, there was an increase in the relative abundance of respiratory electroactive bacteria, such as *Desulfomicrobium*, *Shewanella*, and *Desulfuromonas* in the biofilm samples. These respiratory electrogens have been reported to play a key role in EET [29], which is an important process in MIC. In EMIC sessile cells in a biofilm use metal as an electron donor, and a non-O_2 oxidant such as SO_4^{2-} as the terminal electron acceptor [6]. However, careful consideration needs to be given to both abiotic and biotic corrosion mechanisms that may be taking place.

Under anoxic conditions, both abiotic and biotic corrosion usually leads to the dissolution of Fe^{2+} cations, which precipitate as $Fe(OH)_2$ and has reddish-brown appearance. Nonetheless, $Fe(OH)_2$ is reported to only be metastable in solution and will oxidise to form Fe_3O_4 [238] via the Schikorr reaction [91, 236, 237]. The abiotic coupons were observed to have a reddish-brown corrosion product over the 28 days, which was believed to be lepidocrocite. Lepidocrocite has been identified to form in the outer layer on CS coupons permanently immersed in natural seawater [239]. It is difficult to definitively state one abiotic corrosion mechanism as several mechanisms may be occurring simultaneously. Figure 3.10 highlights several possible abiotic reaction mechanisms [210].

However, the scenario described above for abiotic corrosion changes in the presence of microorganisms, some of which may dramatically accelerate the corrosion kinetics. Figure 3.10 also illustrates the diversity and heterogeneity of microorganisms within a biofilm that are involved in MIC. Possible biotic reaction mechanisms that may be occurring are hypothesised [29, 25, 209, 210]. Though, it is important to note that through the generation of concentration gradients along with the diffusion of organics, the availability of electron acceptors from the environment and electron donors from the metallic Fe^0, the community dynamics within the biofilm will be constantly shifting. This results in heterogeneity within the biofilm which will ultimately affect the predominant metabolic mechanisms and prevailing corrosion mechanisms [210].

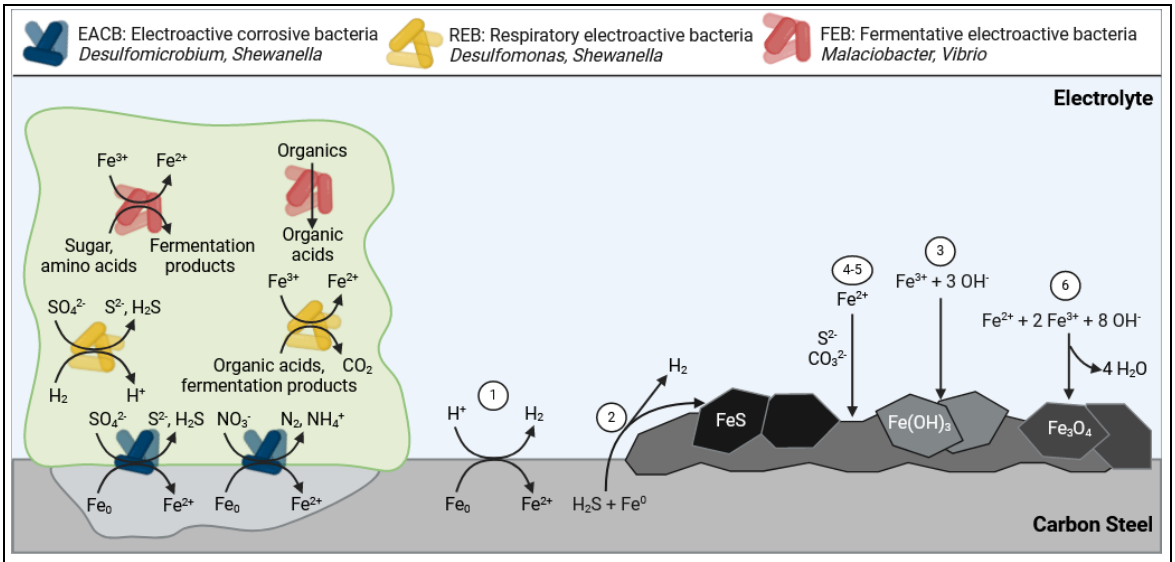

Abiotic Reactions

(1) $Fe^0 + 2H^+ \rightarrow Fe^{2+} + H_2$

(2) $Fe^0 + H_2S \rightarrow FeS + H_2$

(3) $Fe^{3+} + 3OH^- \rightarrow Fe(OH)_3$

(4) $Fe^{2+} + S^{2-} \rightarrow FeS$

(5) $Fe^{2+} + CO_3^{2-} \rightarrow FeCO_3$

(6) $Fe^{2+} + 2Fe^{3+} + 8OH^- \rightarrow Fe_3O_4 + 4H_2O$

Biotic Reactions

Sulphate reduction

Electrical Microbial Influenced Corrosion (EMIC)

$4Fe^0 + SO_4^{2-} + 3HCO_3^- + 5H^+ \rightarrow FeS + 3FeCO_3 + 4H_2O$

Chemical Microbial Influenced Corrosion (CMIC)

$3(CH_2O) + 2Fe^0 + 2SO_4^{2-} + H^+ \rightarrow 2HCO_3^- + 2FeS + 2H_2O$

Iron reduction

$Fe^{3+} + H_2 \rightarrow 2Fe^{2+} + 2H^+$

Figure 3.10. Schematic overview of key reactions and diversity of microorganisms within a biofilm involved in metal corrosion. It is important to note that the reactions illustrated may occur simultaneously. Numbers 1–6 refer to abiotic reactions associated with corrosion. Biotic reactions involved in corrosion of ferrous metals are also shown for electroactive corrosive bacteria, respiratory electroactive bacteria, and fermentative electroactive bacteria. BioRender.com (2023).

Over the first two weeks, there appears to have been a shift towards SO_4^{2-} reduction based on the H_2S microsensor data. After the first week, the reactor had visible black particulates settling at the bottom of the reactor, with the bulk of the fluid being green in appearance. After two weeks, there was a visible scum layer, and the reactor was black in appearance with increased turbidity. Biogenic H_2S production will have provided a source of dissolved Fe^{2+} through Fe^0 oxidation coupled with an increase in the alkalinity of the reactor through consuming H^+ with the reduction of H^+ to H_2. For SRB, electrons can either be directly withdrawn from the steel surface through membrane-bound redox proteins via DET or indirectly transferred through redox mediators via MET. It is hypothesised that EMIC was the predominant biotic corrosion mechanism during the first two weeks [209]. Initially, biogenic H_2S can be oxidised by Fe^{3+} ions and thus not be able to

precipitate all dissolved Fe^{2+} in the system. However, over the course of the 28 days, the biotic condition appeared to be black, green in appearance, which was believed to be GR compounds. This has been identified to form in the inner layer on CS coupons permanently immersed in natural seawater according to references, which is linked to cathodic zones (accelerating cathodic reduction), SRB activity and localised corrosion [239], such as $GR(CO_3^{2-})$ and $GR(S^{2-})$ compounds [221]. The local microbial SO_4^{2-} reduction generates alkalinity which helps in increasing the ion activity product (specifically the concentration of carbonate ions) for siderite formation [240]. There was subsequently a steady decline in the concentration of H_2S over the final two weeks of the experiment. When Fe^{3+} ions are available, SO_4^{2-} reducers such as *Desulfomicrobium* and *Desulfuromonas* spp. may divert electron flux to Fe^{3+} reduction rather than reducing SO_4^{2-} [29]. Moreover, *Shewanella* sp., which were prevalent in the biofilm samples, have been shown to utilize Fe^{3+} as efficient electron acceptors and are capable of out-competing electron acceptors of lower potential, such as SO_4^{2-} [29]. Amorphous Fe^{3+} oxide compounds can provide a source of Fe^{3+} ions. Moreover, Fe^{3+} oxides can protect metallic Fe^0 from corrosion because they are an insulating layer preventing DET. Additionally, Fe^{3+} oxide compounds can restrict access to organic acids and other sources of H^+, thus limiting Fe^0oxidation coupled to H^+ reduction [210]. Though, the formation of corrosion products can also increase the *CR* by generating a localised corrosion cell on the surface of the coupon which can exacerbate pitting [209]. When Fe^{3+} reducers remove Fe^{3+} oxides, Fe^0 oxidation coupled to H^+ reduction is possible again. This allows H_2 oxidisers, such as SO_4^{2-} reducers, to resupply H^+ for Fe^0 oxidation [210]. Active microbial iron reduction increases the dissolved Fe^{2+} in the system which also increase the ionic activity product favouring siderite precipitation, which was observed by analysing the corrosion products of the test coupons using XRD (Appendix B Figure B.10) [240]. At the same time, CMIC, which refers to the sulphidogenic degradation of organic matter in anoxic environments may be occurring. Here, biogenic H_2S may initially stimulate the anodic part of the corrosion reaction by chemisorption and direct reaction with metallic Fe^0. However, once the metallic surface is covered with inorganic corrosion products such as siderite cathodic reactions become more important drivers of metal oxidation [25].

3.4 Summary

The 28 day dual bioreactor protocol represents a pioneering approach to investigating biofilms, specifically tailored to mimic the MIC environment, thus providing a reproducible model for advancing understanding, enhancing predictive measures while employing a multi-disciplinary approach with MLOE to comprehensively unravel the complexities of biofilm formation and MIC

initiation mechanism. In this study, the dual bioreactor explored the development of MIC on UNS G10180 CS in anaerobic ASW using a marine sediment microbial consortium.

- Concurrent electrochemical methods were used to determine when initial biofilm attachment and formation occurred, and the influence that the biofilm had on the surface of the CS coupons. However, whilst these methods provide insights into the redox processes and can quantify corrosion and the influence of the biofilm, they provide limited information about the extent of pitting.
- At the biofilm/steel interface, knowledge of the pitting incidence is critical in the context of a deeper understanding of the MIC initiation and growth processes. Surface profilometry demonstrated the microbial impact when comparing the abiotic and biotic conditions. Coupon analysis showed the biotic condition had a significantly greater *PD* ($P < 0.05$), with a greater pit depth and size when compared to the sterile abiotic ASW media.
- Biofilm characterisation using sequencing showed a relative increase in respiratory electrogens, specifically SRB and IRB, such as *Desulfomicrobium*, *Shewanella* and *Desulfuromonas*, within the biofilm. Importantly, these respiratory electrogens play a key role in EET, which is an important MIC process.

From this, we can start to rationalise an idealised representation of the mixed-species biofilm and the microbial mechanisms that lead to corrosion of CS under anoxic conditions at the metal/electrolyte interface. The innovative dual bioreactor protocol allows new insights, establishing a standard model and biofilm-relevant test method for biocide efficacy testing. The development of such a model will support a move towards evidence-based biocide dosing, empowering asset owners to reduce the effect of MIC leading to reduced cost, increased sustainability, and increased asset lifetime.

Chapter 4 Investigating the effects of surface roughness and ATCC 1249 Modified Baar's media on anaerobic marine biofilm formation and microbiologically influenced corrosion of UNS G10180 carbon steel

4.1 Introduction

SRM are ubiquitous anaerobes, with SRB being the most studied corrosive microorganisms in the MIC literature [241, 242]. The mechanism of SO_4^{2-} respiration involves the reduction of SO_4^{2-} to sulphide species (H_2S, HS^-) with natural organic compounds, such as lactate, as electron donors that are oxidised to CO_2 [211]. Under pH-neutral conditions, the Schikorr reaction predicts that the predominant sulphur species would be H_2S and HS^-, depending on the exact pH and equilibrium dynamics. H_2S is dominant in environments with slightly acidic to neutral pH. Whereas, HS^- becomes more significant as pH approaches the neutral range (above pH 6.5). Thus, under neutral pH conditions, both H_2S and HS^- are present, with their relative proportions governed by the dissociation constant [91, 240, 241].

Many SRB can also utilise H_2, which is a common by-product produced by other bacteria involved in the biological breakdown of organic compounds in O_2-free aquatic systems such as marine sediments [211]. This is particularly relevant in the energy and maritime sectors where environmental mixed-species biofilms are present. Within such mixed biofilm communities' synergistic relationships that may be mutualistic or competitive in nature are established. These relationships likely impact the availability of nutrients, whether primarily through metabolic activity or physical through the development of diffusion gradients and microenvironments. Moreover, the formation of corrosion products themselves may have an influence on the nature and extent of any further corrosion, through the generation of electrochemical cells which may subsequently affect the anodic or cathodic reactions. Understanding the influence that the mixed-species biofilms and the formation of any inorganic corrosion products, has on growth, spatial and community dynamics, and potential corrosion mechanisms is critical.

The mechanisms by which SRB interact with metallic Fe^0 have been a topic of debate in the literature, with two prevailing corrosion mechanisms proposed [243, 244, 245], EMIC and CMIC [25, 211]. EMIC is a cathodic reaction, that is kinetically impossible under sterile abiotic conditions, which is characterised by the direct electron uptake of electrons from Fe^0 oxidation by SRB and the formation of large amounts of inorganic corrosion products [25]. CMIC is fundamentally different and is characterised by the indirect activity of metabolic end products. Through SRB respiration, the biogenic production of H_2S initially stimulates the anodic part of the corrosion reaction by chemisorption and direct reaction with metallic Fe^0 to form inorganic corrosion products (Equations 4.1 & 4.2) [246, 247]. However, cathodic reactions become more important drivers of Fe^0 oxidation once the metallic surface is covered with inorganic corrosion products such as FeS [248, 249].

$$H_2S + Fe^0 \rightarrow H_2 + FeS \quad \ldots\ldots (4.1)$$

$$3(CH_2O) + 2Fe^0 + 2SO_4^{2-} + H^+ \rightarrow 2HCO_3^- + 2FeS + 2H_2O \quad \ldots\ldots (4.2)$$

Traditionally, the literature has primarily focused on single-species studies. Whilst these types of studies provide clear, simple, and reproducible results; ultimately, they lack ecological relevance and do not consider microbial interactions within established microbiomes. However, distinguishing between abiotic and biotic corrosion mechanisms is simpler in these types of studies. Moreover, identifying key electron acceptors and donators is less complex. It was speculated by early investigators that a H_2 film develops at the metal surface in the absence of microorganisms leading to polarisation and impeding Fe^0 dissolution [243]. Yet, in the presence of microorganisms with the capability of H_2 utilisation, it was suggested that through the HER these microorganisms would lead to depolarisation, allowing Fe^0 dissolution to proceed. In turn, this makes the metal surface more reactive, thus accelerating the overall corrosion process. This was known as the 'cathodic depolarisation theory' [211]. However, whilst this reaction can proceed spontaneously from a thermodynamic perspective, early investigators did not consider environmentally relevant conditions or account for kinetic considerations [211].

Several cultures of SRB were shown to stimulate the cathodic current on mild steel electrodes in early studies [244, 250]. The authors attributed this to bacterial H_2 uptake from the electrode surface and, interpreted the observation in favour of the 'classical' depolarisation theory [211]. However, an experimental misconception in the early electrochemical study of the postulated direct mechanism involving H_2 with conventional SRB strains was the addition of lactate, which represents a competitive electron donor in addition to 'cathodic' H_2 [211, 244, 250]. More importantly, lactate leads to excessive concentrations of aggressive H_2S which cause chemical corrosion [211]. Studies which omitted lactate showed that SRB became more corrosive even

though such starvation led to reduced sessile cell densities on metallic Fe^0 [103]. Additionally, cathodic depolarisation was shown not to occur in SRB cultures with metallic Fe^0 as the only source of electrons for the organisms [243, 245]. This was because SRB biofilms switched to elemental Fe^0 as a substitute for organic carbon as an electron donor in their respiration [35]. Conversely, acceleration of the cathodic reaction was shown to result from the reactivity of dissolved H_2S [211]. In another approach towards a mechanistic understanding of anaerobic corrosion, SRB were directly enriched and isolated with metallic Fe^0 as the only source of electrons, without an organic substrate such as lactate [211, 251]. In these studies, the SRB severely corroded the metallic surface with a rate of up to 0.7 mm y^{-1}. This *CR* could not be explained by dependency on H_2 alone [251]. Their findings indicated a direct electron uptake through EMIC.

The BCSR theory is a more specific mechanism, which considers the direct influence that SRB have on corrosion and explains the bioenergetics of MIC in SRB respiration specifically when SO_4^{2-} is the terminal electron acceptor [52]. As mentioned earlier, SRB reduce SO_4^{2-} to H_2S, HS^- under anaerobic conditions. The reduction of SO_4^{2-} to H_2S is catalysed by the metabolic activity of SRB. This microbial process can influence the electrochemical reactions at the metal surface. The production of S^{2-} ions can react with Fe^{2+} ions to form FeS, which can influence corrosion processes [35]. This film can lead to the generation of electrochemical cells which may affect the anodic or cathodic reactions to inhibit or accelerate corrosion under different environmental conditions. In SRB corrosion, both planktonic and sessile cells produce H_2S. However, under an SRB biofilm, the concentration of H_2S is likely higher than that in the bulk fluid due to cell density. Furthermore, the biofilm is a diffusion barrier that slows down the escape of H_2S [35]. Though, parallel to SRB corrosion, other abiotic and biotic corrosion mechanisms will influence corrosion overall in mixed-species biofilms. Mixed-species studies provide a holistic understanding of microbial interactions which are ecologically relevant. Though, the increased complexity makes interpreting any data and identifying the appropriate corrosion mechanism challenging.

This study aimed to demonstrate the applicability and reproducibility of a novel dual bioreactor protocol to investigate the influence of a mixed-species SRB biofilm on UNS G10180 CS corrosion. A key focus was placed on enumerating SRM using selective MB media, to evaluate the influence of a mixed-species biofilm on the prevailing corrosion mechanisms. Critically, MLOE [145], incorporating microscopy-based methods, MMM, and electrochemical techniques was employed to gain a holistic understanding of the underlying corrosion mechanisms.

4.2 Results

Throughout the 28 days, the abiotic media had no visual changes, and the CS coupons maintained their silver-grey metallic lustre appearance. The sterile abiotic reactor MB media was orange/pink in colouration with no apparent turbidity. However, after inoculation of the biotic reactor MB media, a black surface film was evident on the steel coupons (day 1), with a low level of turbidity. After the flow of fresh MB media was started on day 4, over the following days up to day 7, black particulates in the MB media started to precipitate at the reactor bottom, with the bulk media being green in appearance. After two weeks, there was a visible surface crust at the MB interface, and the media was black in appearance with high turbidity. Over the following two weeks, up to 28 days, the biotic media was dark green/black in colouration. Upon dismantling of the reactors on day 28, and retrieval of the coupon rods, there was a significant difference in the coupon appearances, see Appendix C Figure C3. The abiotic surfaces had no apparent corrosion products. Whilst the biotic surfaces were covered with a thick slimy biofilm with a dark green/black granular deposit.

Sulphide microsensor. Figure 4.1 shows the aqueous H_2S concentrations monitored in the abiotic and the biotic anaerobic MB media over the test duration. For the sterile abiotic condition, there was a generally low H_2S concentration (mean: 5.1 µmol L^{-1}). Whereas for the biotic condition, the H_2S concentration drastically increased after the flow of fresh MB media on day 3, to a maximum of 523.4 µmol L^{-1}, before ultimately decreasing to similar levels detected for the abiotic media after two to three weeks. *DO* concentrations measured on day 28 were: 4.6 ppm in the 10 L media containers, 0.5 ppm in the abiotic and 0.0 ppm (below the limit of detection) in the biotic reactor. The pH was not measured on completion of the experiment.

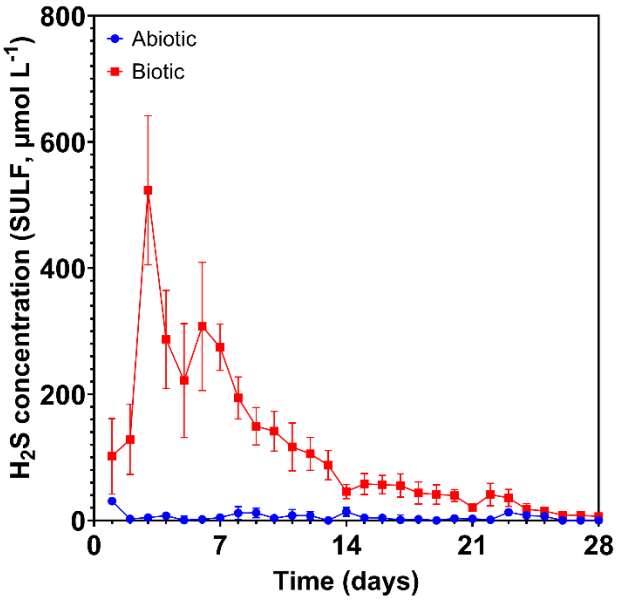

Figure 4.1. Aqueous sulphide measurements (*SULF*, µmol L^{-1}) for the abiotic and biotic conditions over 28 days (nb. measured the anaerobic MB media *in situ* adjacent to corroding UNS G10180 carbon steel).

Carbon steel surface analysis. Appendix C Figure C4 shows the CS surfaces on day 0. Appendix C Table C5 summarises the quantitative surface roughness profiles on both day 0 and day 28. Figure 4.2 shows the cleaned CS surfaces after 28 days, with biofilms and corrosion products removed to reveal the morphology of the surface degradation and to facilitate corrosion assessment. Surface profilometry revealed that both abiotic and biotic anaerobic MB media led to localised pitting, with the biotic condition more extensively pitted. The abiotic average pit depths were 39 µm and 31 µm, and average pit areas of 1212 μm^2 and 1022 μm^2, for the AR and P coupons, respectively. The biotic average pit depths were 38 µm and 41 µm, with the average pit areas of 1571 μm^2 and 1530 μm^2, for the AR and P coupons, respectively. Again, for this study a pit was classified as having a depth greater than 5 µm and an area greater than 650 μm^2 [153].

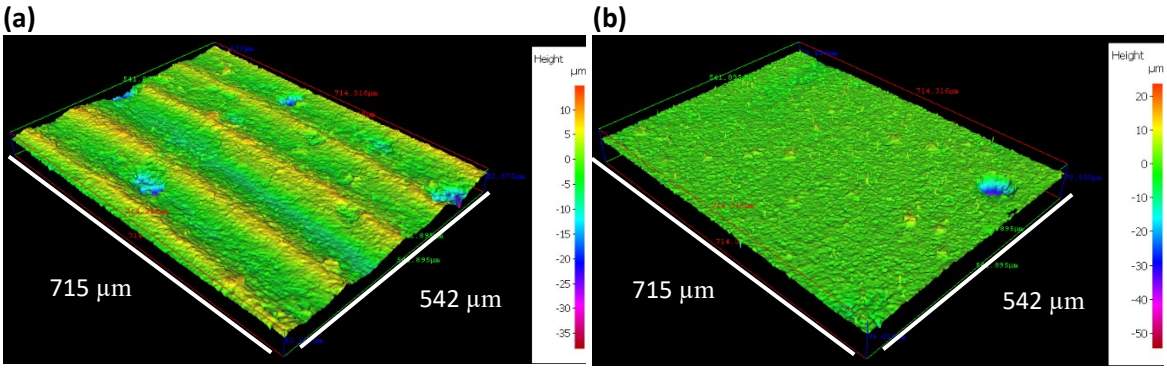

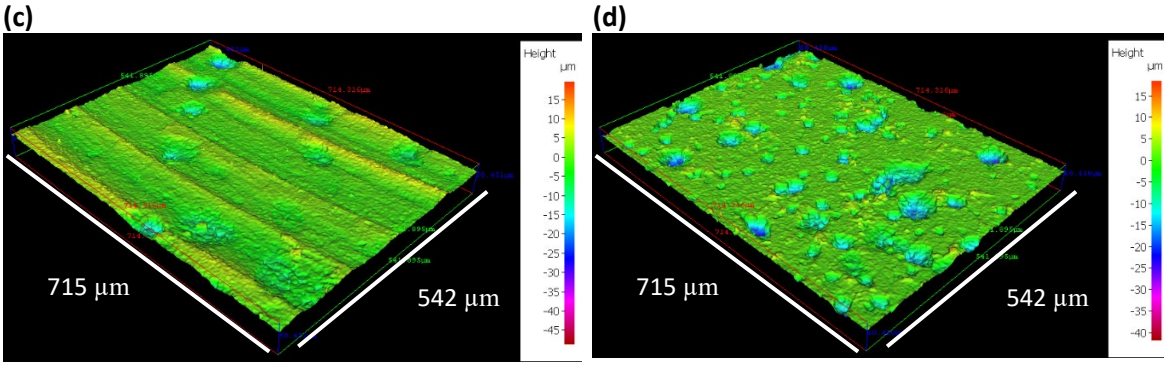

Figure 4.2. Three-dimensional optical surface profilometry of the cleaned UNS G10180 surfaces at day 28. AR coupons for: **(a)** abiotic and **(b)** biotic conditions; and P coupons for: **(c)** abiotic and **(d)** biotic conditions, after exposure to anaerobic MB media for 28 days.

Figure 4.3a provides an evaluation of the CS coupons *CR*. For the abiotic condition, there was a higher *CR* when compared to the biotic condition, though there was no significance. Furthermore, when comparing between the two surface roughness types, AR and P coupons within each reactor, there was also no significance (n = 3). According to the NACE SP0775-2023 assessment criteria, there was a high *CR* (between 0.13 and 0.25 mm y^{-1}) in the abiotic and a moderate *CR* (between 0.025 and 0.12 mm y^{-1}) in the biotic (Figure 4.3a); whilst a severe *PR* (> 0.38 mm y^{-1}) was assessed for both the abiotic and biotic conditions (Figure 4.3b) [170].

Further analysis of the surface profilometries in Figure 4.2, allowed a quantitative determination of the *PR* Figure 4.3b and *PD* Figure 4.3c of the CS coupons. For the biotic reactor, though there was a higher *PR*, although there was no significant difference evident between the abiotic and biotic conditions. Though, *PR* is calculated based on the deepest pits. Whilst *PR* had no significant difference, there was a significant increase in the incidence of pitting ($P < 0.05$). There was an average *PD* of 3 pits mm^{-2} in the abiotic reactor for both AR and P coupons, with 15 pits mm^{-2} and 47 pits mm^{-2} in the biotic reactor, for AR and P coupons, respectively. Again, there were no significant differences when comparing between the two surface roughness types within each reactor.

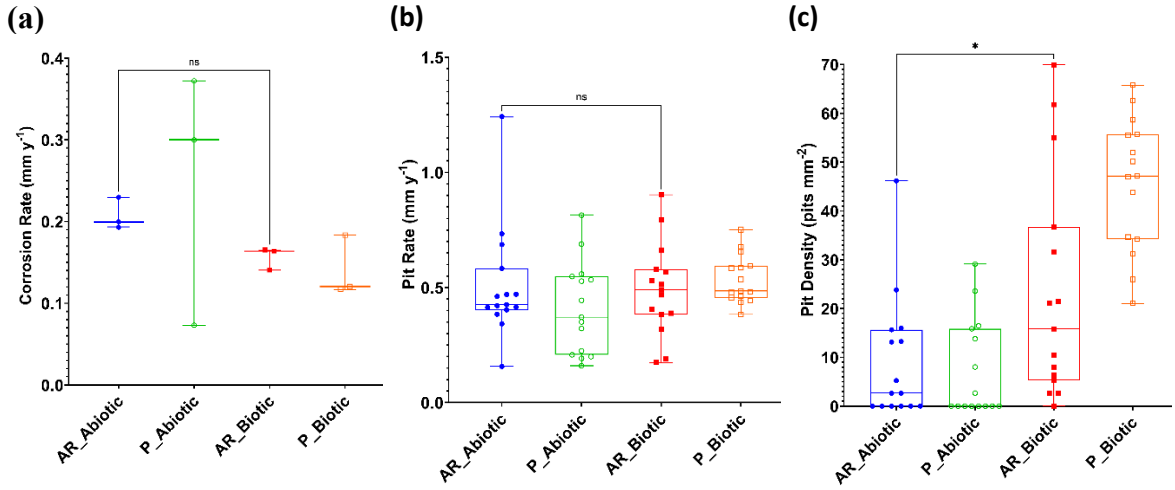

Figure 4.3. Abiotic and biotic corrosion performance after exposure to anaerobic MB media for 28 days: **(a)** corrosion rate via gravimetric analysis and surface profilometry assessed **(b)** pit rate and **(c)** pit density ($P <$

0.05 for the abiotic and biotic AR coupons, P <0.0001 for the abiotic and biotic P coupons, P < 0.0066 for the biotic AR and biotic P coupons), for the AR and P coupons.

Corrosion product analysis. Note for this study, no chemical analysis was performed on the corrosion products due to access to the XRD being unavailable as it was out of order. Thus, the hypothesised presence of FeS was inferred from the literature. For research chapters 5 and 6, this oversight was addressed by getting further training and utilising Raman spectroscopy and SEM-EDS.

Electrochemical measurements. Figure 4.4 shows the changes in E_{corr} and R_p between the abiotic and biotic anaerobic MB media, for the UNS G10180 CS coupons. The abiotic condition, Figure 4.4a, had a distinct +0.100 V increase in the E_{corr} during the first three days that can be linked with the presence of a conditioning film (i.e., an adsorbed organic layer). Generally, a pseudo-steady state E_{corr} was attained in the days following with some odd electronegative shifts. Conversely, for the biotic condition, there was a gradual electronegative shift in the E_{corr} after the first day, until Day 9, after which E_{corr} steadily increased by +0.070 V to around -0.610 V on Day 28. The potential for the abiotic condition in the latter stages was generally around -0.610 V *vs*. Ag/AgCl too.

In Figure 4.4b the LPR derived R_p remained low at approx. 300 Ω cm^2 for the sterile abiotic condition. Whereas there was a gradual increase for the biotic condition over the 28 Days, with R_p ranging between 5000 and 40000 Ω cm^2. The pioneering bacterial attachment/colonisation, biofilm formation and growth kinetics will lead inevitably to a more complex electrochemical response. Overall, there were no significant differences when comparing between the two surface roughness's (AR and P) within both the abiotic and biotic reactor environments.

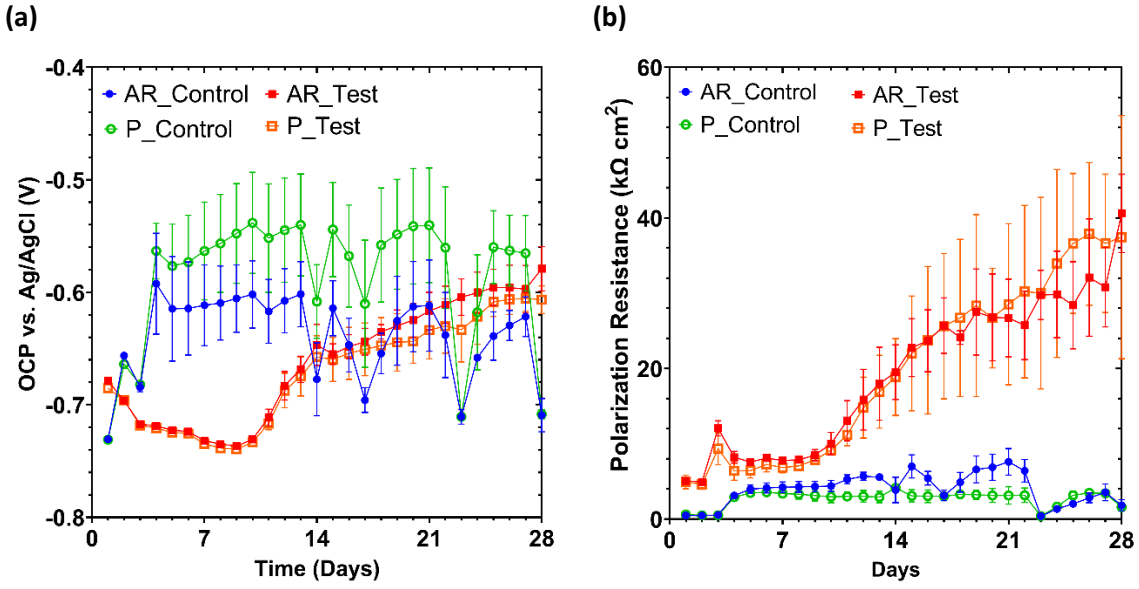

Figure 4.4. LPR data for UNS G10180 carbon steel: **(a)** open-circuit potentials and **(b)** polarisation resistance in anaerobic MB media (abiotic and biotic conditions), for AR and P coupons (data points represent mean ± standard deviation, *n* = 3). Reactor stirrer at 50 rpm.

Figure 4.5 shows the EIS data for UNS G10180 CS in the anaerobic MB media presented in three forms: Nyquist, Bode phase angle and Bode impedance modulus plots. The sterile abiotic condition on Day 1 has a depressed Nyquist semicircle and phase angle close to zero, which is indicative of a resistive response. However, on the subsequent days up until Day 28 the abiotic condition exhibits a typical electrochemical response for the formation of a porous interface, with diffusion of soluble electroactive species across an organic conditioning film [207]. The diffusive behaviour is associated with linear features having a roughly 45° slope (a Warburg impedance response) and phase angles close to 40° in low frequency region (10^{-2} – 10^{0} Hz), see Fig. 4.5a and 4.5c. The abiotic impedance spectra shift towards lower frequencies (10^{-2} – 10^{0} Hz), with a combined diffusive/resistive behaviour. The biotic condition had a consistently uniform EIS response over the 28 day test, with only minor variation in the spectra and suggests the absence of significant detectable electrochemical changes with time. On Day 1 there is a more capacitive/diffusive behaviour which relates to the well-established double-layer concept (*i.e.*, interfacial charge distribution) and diffusion of electroactive species. Subsequently, there are no discernible Nyquist semicircles (Fig 4.5b). Here a wider low frequency region (10^{-1} – 10^{2}) is likely to be subject to a greater influence of adsorption processes, associated with the adhesion of the pioneering bacteria on a conditioning film [215, 216] and biofilm formation.

The EIS spectra were fitted using an ECM shown in Figure 2.4. Both the abiotic and biotic data generally had a good fit, with the quantitative fitting results shown in Appendix C Table C6.

(a) – Abiotic **(b) – Biotic**

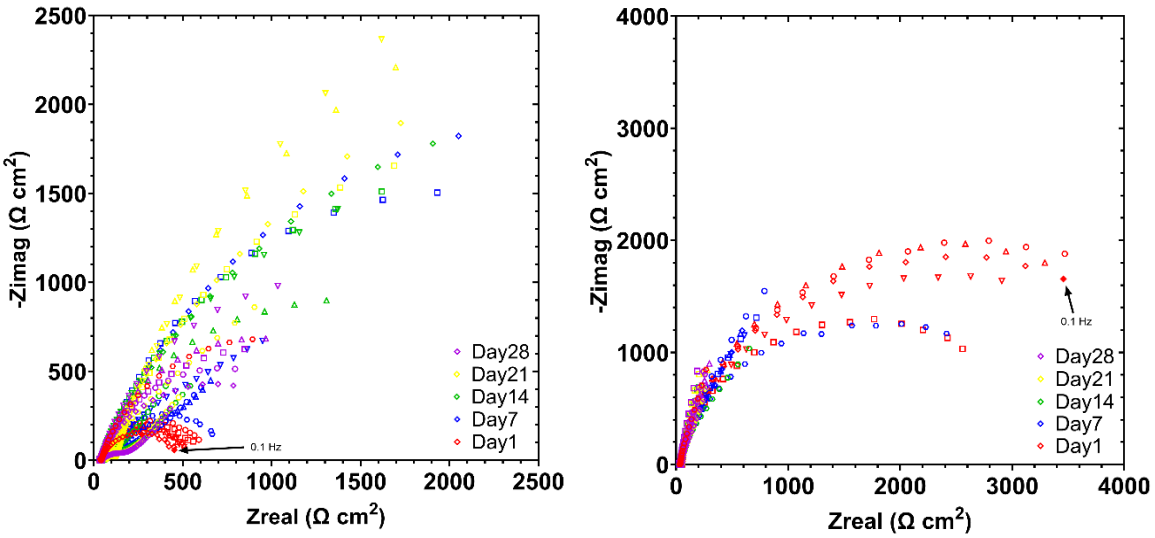

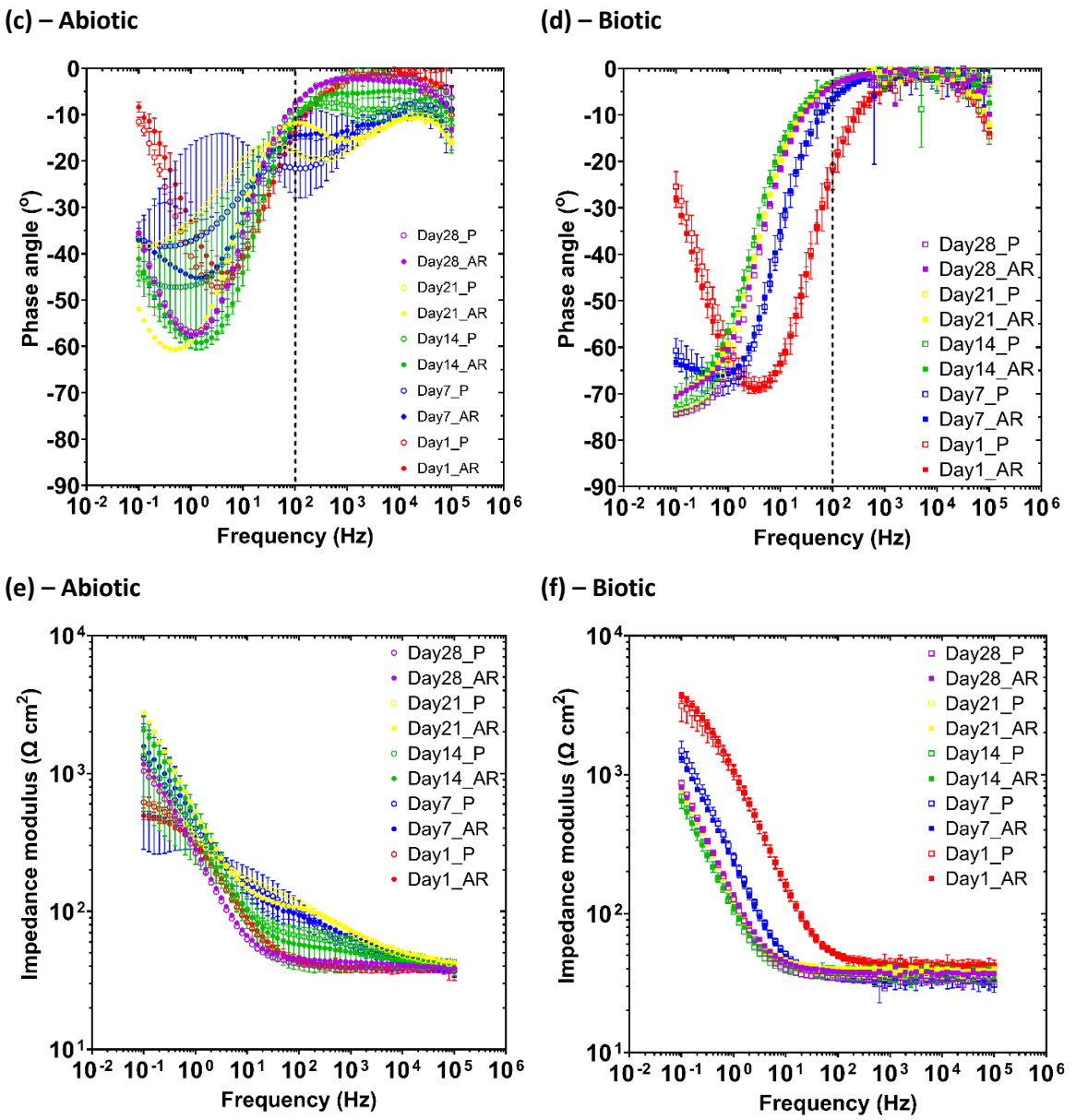

Figure 4.5. EIS data for UNS G10180 carbon steel in anaerobic MB media at OCP: **(a, b)** Nyquist, **(c, d)** Bode phase angle (θ *vs.* f), and **(e, f)** Bode impedance modulus ($|Z|$ *vs.* f) over 28-days. (n = 3). Reactor stirrer at 50 rpm.

For the abiotic control, there is initially a diffusive behaviour over the first week with a diffusive/resistive behaviour over the final three weeks in the film layer. Whilst there was initially a resistive behaviour over the first week in the double layer with a capacitive behaviour over the final three weeks, which reflects the accumulation of charge. The thin layer of ions that contacts the electrode surface serves as a dielectric, insulating the surface. The exponent parameter in the double layer reflects ideal capacitance over the final three weeks, which is indicative of a more prominent capacitive component. R_{film} has a large shift on Day 14 and again on Day 28, which indicates high R_p. There are no significant changes in R_{ct}. For the biotic test reactor, there is a capacitive behaviour in both the film layer and double layer due to the presence of the biofilm. There are no significant changes in the R_{ct} in the double layer over time. The exponent parameter

for the film layer is greater than 0.8 at most time points, which indicates non-ideal capacitance. This is true for the first two weeks in the double layer. However, during the final two weeks of the experiment, the exponent parameter is equal to 1 for the AR coupons in the double layer, which indicates an ideal capacitive behaviour. Whilst the exponent parameter is indicative of a diffusive behaviour for the P coupons on Days 12 and 21, with a more capacitive behaviour by Day 28. This may reflect differences in biomass of the biofilm associated with biofilm attachment and growth. The ECM and EIS both have general agreement with the LPR data.

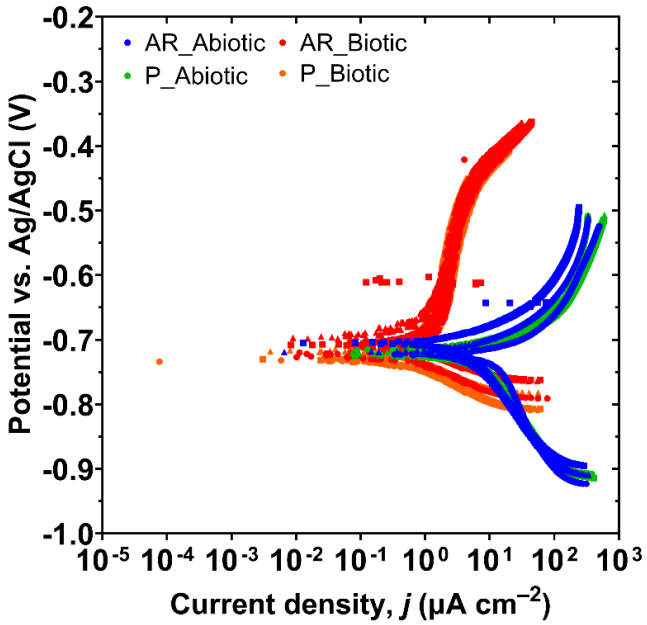

Figure 4.6. Potentiodynamic polarisation curves for the abiotic and biotic AR and P, UNS G10180 carbon steel coupons, at ambient temperature after exposure to anaerobic MB media for 28 days. Scan rate of 0.5 mV s^{-1} and reactor stirrer at 50 rpm. Dissolved oxygen levels were 0.5 ppm (abiotic) and 0.0 ppm (biotic), at Day 28.

Figure 4.6 shows the potentiodynamic polarisation curves for UNS G10180 for the abiotic and biotic reactors in anaerobic MB media after 28 days. Table 4.1 shows the corrosion parameters obtained from the polarisation curves. From the Tafel slopes, there is a decrease in cathodic current (reduction) for the biotic condition. The abiotic condition has an increased cathodic current which indicates a greater accumulation of charge. Conversely, the anodic Tafel slopes (oxidation) are greater in the biotic compared to the abiotic media. Thus, after 28 days the biofilm hindered the iron dissolution reactions. Overall, the abiotic condition had a higher j_{corr} compared to the biotic condition. This is consistent with the more uniform corrosion morphology seen for the abiotic coupon surfaces, see Figure 4.2. Both conditions exhibited similar E_{corr} on Day 28. The polarisation results corroborate the LPR and EIS data, with no significant differences when comparing between the two surface roughness types within each reactor.

Table 4.1. Fitted electrochemical parameters from polarisation curves; comparison between the abiotic and biotic AR and P UNS G10180 carbon steel coupons after exposure to anaerobic MB media for 28 days.

	Coupon	j_{corr} / μA cm^{-2}	E_{corr} *vs.* Ag/AgCl / V	β_a (mV dec^{-1})	β_c (mV dec^{-1})
Abiotic	AR	22.4 ± 20.1	-727 ± 3	157 ± 52	268 ± 67
	P	15.7 ± 2.49	-720 ± 4	125 ± 12	266 ±39
Biotic	AR	0.44 ± 0.22	-710 ± 15	213 ± 52	38 ±11
	P	0.70 ± 0.33	-727 ± 7	276 ± 54	54 ± 15

Biofilm characterisation. CLSM with differentiation of live and dead biofilm cells was performed and can be found in the supplementary material Appendix C Figure C7. The heterogeneous biofilm distribution over the surface of the CS coupons did not allow measurements of the maximum biofilm thickness. Therefore, the biofilm thickness was not determined. It was also difficult to identify significant differences in the structure and distribution of live and dead cells in the biofilms across the two surface roughness types, AR and P coupons, within the biotic reactor. In general, both surfaces had similar live and dead cell ratios (approximately 91% live to 9% dead).

Active microorganism evaluation of the environmental marine sediment, the initial and final biotic MB media planktonic samples (Day 0 and Day 28), and the biotic AR and P biofilms, was undertaken via 16S rRNA amplicon sequencing with two target region, V3-4 for bacteria and archaea. A total of 2,398,327 high-quality sequences were obtained after bioinformatics processing of the raw reads. From these, 95.9% was classified for the sediment sample with 99.99% classified for the Day 0 and Day 28 planktonic samples, AR and P biofilm samples. These sequences were taxonomically classified into microbial genera. The top 25 microbial genera are presented in Appendix C Table C8 in the supplemental material. Appendix C Figure C7 summarises the sequencing data, showing a PCA (a) and a stacked bar plot (b) illustrating the relative abundances for the top 25 genera. Molecular identification of the microorganisms showed that the initial sediment sample had a very diverse microbial composition. Most genus had low relative abundances less than 2%. The dominant genera included *Sulfurovum*, *Desulfuromonas*, *Candidatus Prometheoarchaeum*, *Desulfosarcina*, *Thiohalobacter* and *Candidatus Methanoplasma* which made-up approximately 33% of the total relative abundance. Interestingly, there were relatively high numbers of archaea in the sediment sample compared to the other samples. The sediment sample had low or negative Spearman correlation coefficients (Appendix C Figure C9) with the other

samples which was attributed to changes in conditions such as temperature, but primarily media composition which was selective for the enumeration of SRB. There was much less diversity in the Day 0 sample, with *Sulfurovum*, *Candidatus Prometheoarchaeum*, *Candidatus Methanoplasma*, and *Thiohalobacter* all exhibiting lower relative abundances (<1%). Whilst genera from *Clostridium*, *Klebsiella*, *Escherichia*, *Paracabacteroides*, *Veillonella*, *Anaerotignum* and *Terrisporobacter* made-up approximately 60% of the relative abundance. The relative abundances of *Veillonella* and *Terrisporobacter* were particularly high in the initial Day 0 planktonic sample but had lower concentrations for the Day 28 planktonic sample and both AR and P biofilms. The Day 0 planktonic had negative Spearman correlation coefficients with the sediment and Day 28 planktonic samples but had approximately 50% Spearman correlation coefficients with both AR and P biofilms. After 28 Days, there was a substantial shift in the microbial composition, with substantially lower abundances of methanogenic species. *Desulfovibrio* was the dominant genera, with a relative abundance of approximately 32%. *Parabacteroides*, *Sulfurospirillum*, *Salmonella* and *Enterobacter* made-up approximately another 23% of the relative abundance. Again, the Day 28 planktonic had low or negative Spearman correlation coefficients with the sediment and Day 0 planktonic samples but had approximately 50% Spearman correlation coefficients with both AR and P biofilms. The Day 28 planktonic sample had a Spearman correlation coefficient of 0.17 with the sediment sample, –0.10 with the Day 0 planktonic sample and 0.45 with both biofilm samples. Both biofilm samples exhibited similar microbial populations on both the AR and P coupons. The relative abundances of *Desulfovibrio* increased further to approximately 55% and 53% for both AR and P biofilms respectively. *Sulfurovum*, *Candidatus Prometheoarchaeum*, *Candidatus Methanoplasma*, and *Thiohalobacter* which were the dominant genera from the sediment sample all had lower relative abundances (<1%) in the biofilm samples and Day 28 planktonic sample. Both biofilm samples were similar, with a Spearman correlation coefficient of 0.99. Other genera with relatively high abundances included *Clostridium*, *Klebsiella*, *Escherichia* and *Paracabacteroides* making up approximately 13% of the relative abundance. There were no methanogenic archaea in the biofilm samples.

(a)

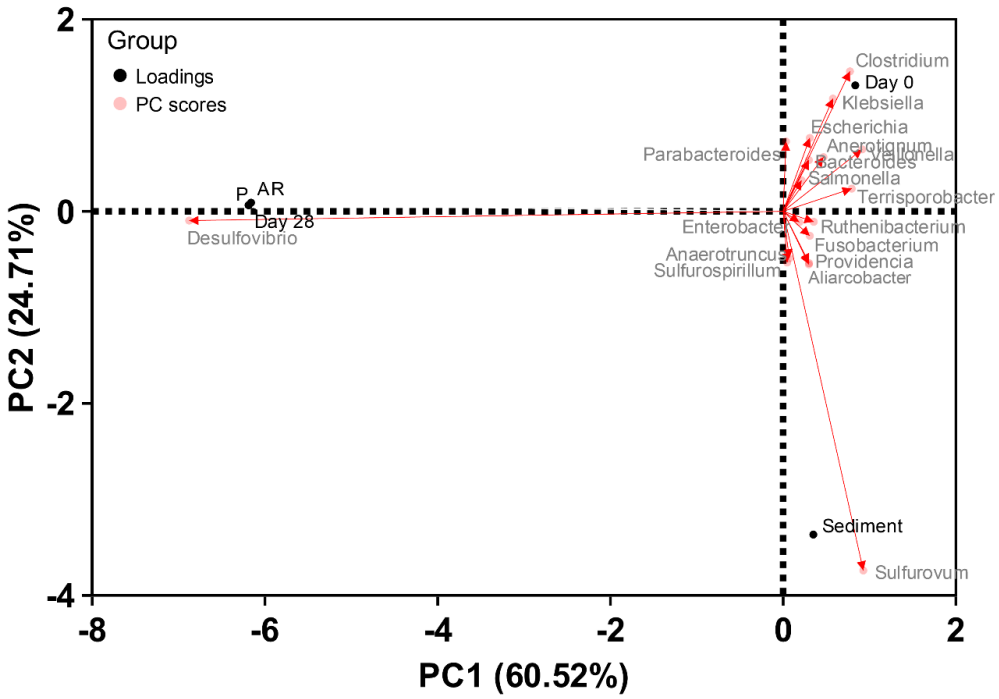

(b)

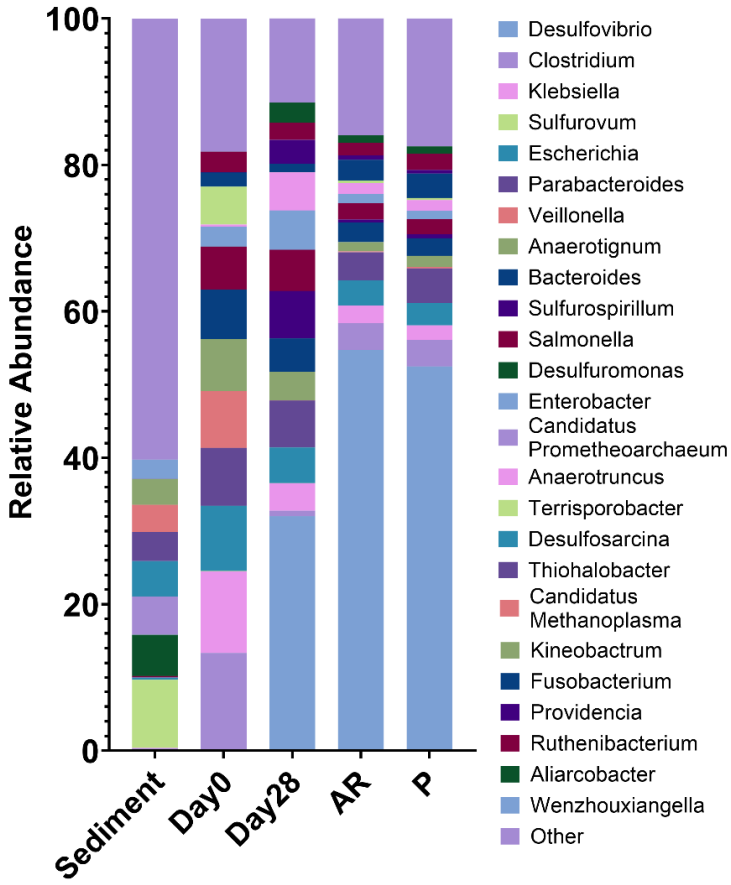

Figure 4.7. Principal Component Analysis biplot **(a)**; Microbial community. The results show the mean relative abundances of microbial communities classified at the genus level, for the top 25 genera, from 16S rRNA amplicon sequencing **(b)**; for environmental marine sediment, Day 0, and Day 28 planktonic samples, AR and P biofilm samples after exposure to anaerobic MB media for 28 days.

The microbial activity was determined by the ATP concentrations (dissolved and total, dATP and tATP, respectively) in both the bulk fluid and biofilms, see Figure 4.8. For the biotic MB media (bulk fluid), there was a significant change ($P < 0.05$) in the dATP concentration when comparing Day 0 and Day 28, with dATP values increasing on the order of 10 pg mL^{-1}. Also, for the biotic condition there was a significant change ($P < 0.05$) in the concentration of tATP over the surface of the CS coupons (tATP of about 100 pg mL^{-1}), when comparing between the two surface roughness types within each reactor.

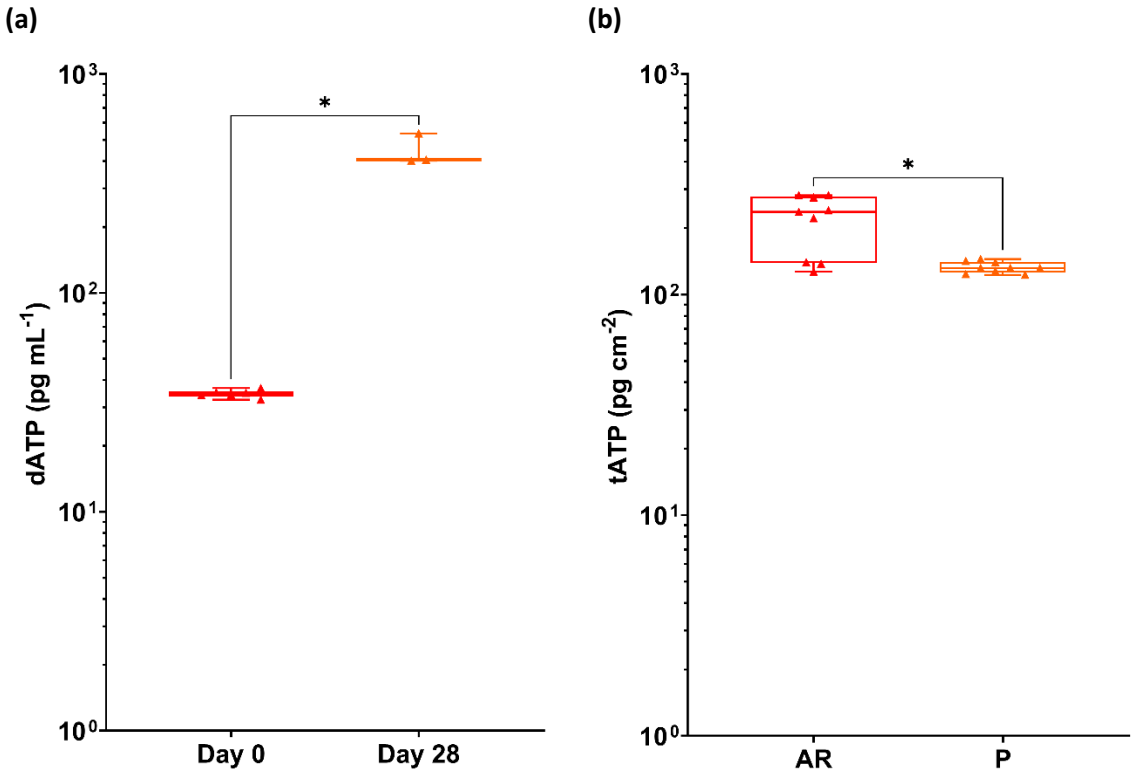

Figure 4.8. **(a)** Dissolved ATP (dATP) concentrations comparing the anaerobic MB media taken on Day 0 and Day 28 ($P < 0.05$) and **(b)** Total ATP (tATP) concentration comparing the biofilm of the AR and P coupons ($P < 0.05$), from the biotic condition, after exposure to anaerobic MB media for 28 days.

4.3 Discussion

Figure 4.9 provides an illustration of the initial stages for UNS G10180 CS in anaerobic abiotic MB media and the proposed corrosion mechanisms during the initial stages, and as they evolved over time during this present study. For this study, the abiotic surfaces were observed to have no apparent corrosion film upon retrieval, only minimal loose deposits were present. Moreover, there was no apparent turbidity within the abiotic reactor itself. As stated earlier, the abiotic condition exhibited a typical electrochemical response for the formation of a porous interface, with diffusion of soluble electroactive species across an organic conditioning film [207].

Abiotic	Biotic
(a)	(b)
(c)	(d)
(e)	(f)

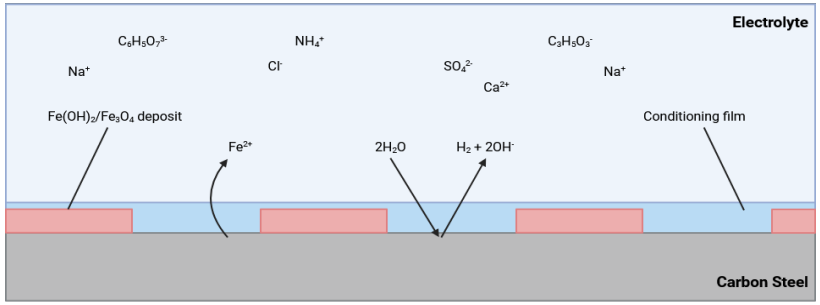

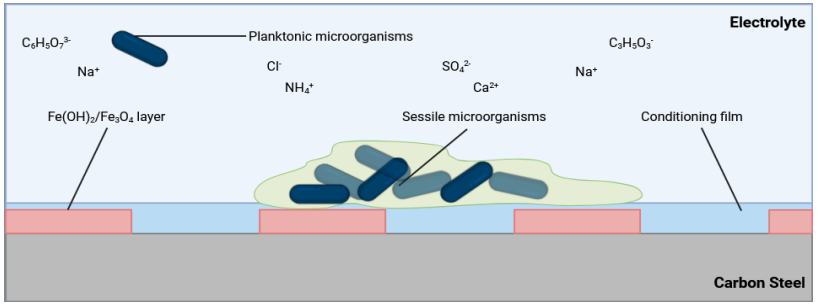

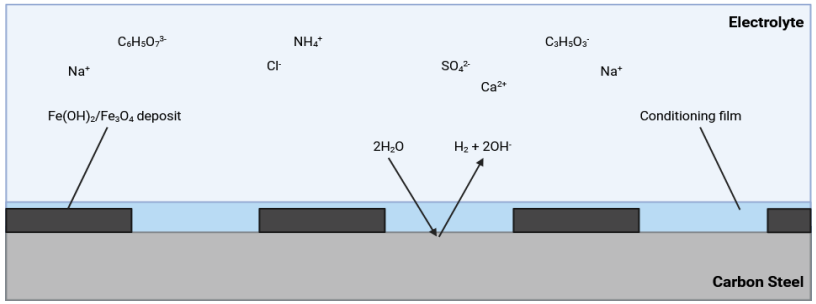

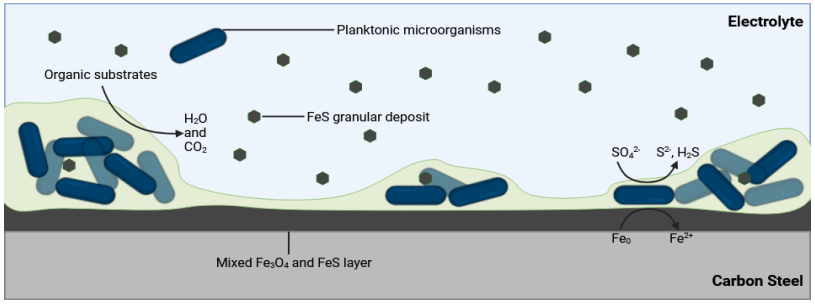

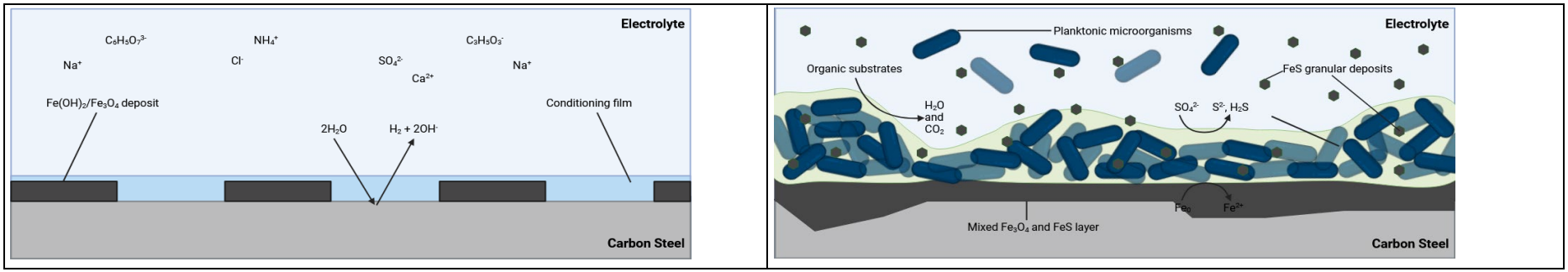

Figure 4.9. Schematic of the initial stages for UNS G10180 carbon steel in anaerobic abiotic ATCC 1249 MB media. Corrosion mechanisms, **(a, b)** the formation of nascent inorganic corrosion film and the organic conditioning film with pioneering bacterial attachment; **(c, d)** general absence of a maturing corrosion film under the abiotic condition with a prolonged period of charge accumulation; whilst there was sustained biofilm growth and colonisation for the biotic condition **(e, f)** moderate uniform and pitting corrosion for both conditions; under patchy corrosion deposits and a thick slimy biofilm with black granular deposits for the biotic condition. BioRender.com (2024).

Though, the absence of any inorganic corrosion products would indicate that the primary abiotic corrosion mechanism was the HER. Figure 4.9 also illustrates the proposed biotic reaction mechanisms during the initial stages of biofilm formation, and as they evolved over time on CS.

Abiotic reactor: - Over the first three days, the abiotic condition exhibited anodic polarisation until reaching a pseudo-steady state. The MB media contains many organic substrates, which will have adsorbed onto the electrode surface forming a conditioning film. From the ECMs, there is initially a diffusive behaviour over the first week. Moreover, there was initially a resistive behaviour over the first week in the double layer. The thin layer of ions that contacts the electrode surface serves as a dielectric, insulating the surface. Subsequently, there was a diffusive/resistive behaviour over the final three weeks in the film layer. The abiotic condition exhibits a typical electrochemical response for the formation of a porous interface, with diffusion of soluble electroactive species across an organic conditioning film [207]. Additionally, the exponent parameter in the double layer reflects ideal capacitance over the final three weeks, which is indicative of a more prominent capacitive component. The abiotic condition had an increased cathodic current which indicates a greater accumulation of charge. Generally, there was a moderate level of uniform corrosion of the steel surface for the abiotic media, which was consistent with the electrochemistry data. Interestingly, the abiotic surfaces had no apparent corrosion products upon retrieval. For the sterile abiotic condition, there was also generally a low H_2S concentration.

Biotic reactor: - Under biotic conditions, there was a gradual electronegative shift in the E_{corr} after the first day, until Day 9. This can be attributed to the initial attachment of microorganisms and subsequent biofilm formation on the steel surface [197]. A small decrease in R_p was observed after the initial 3 day batch phase was ended, and the flow of fresh media began. However, there was generally a gradual increase in R_p over the 28 Days. This was attributed to increasing sessile cell density within the biofilm. For the biotic reactor, there was a consistently uniform EIS response over the 28 day test. This suggest that there was an absence of significant detectable electrochemical changes with time. From the ECMs, there was a capacitive behaviour in both the film layer and double layer due to the presence of the biofilm. A more capacitive/diffusive behaviour was initially observed on Day 1. This is associated with the adhesion of the pioneering bacteria on a conditioning film and biofilm formation [215, 216]. Yet, over time there were no significant changes in the double layer. The film layer was behaving as a non-ideal capacitor at most time points. This was also true for the first two weeks in the double layer. However, during the final two weeks of the experiment, there was some ideal capacitance

behaviour specifically for the AR coupons. Conversely, there was a more diffusive behaviour for the P coupons after two to three weeks, with the capacitive behaviour only observed after four weeks. This may reflect differences in biomass of the biofilm associated with biofilm attachment and growth. Upon dismantling of the reactors on day 28, the biotic coupon surfaces were covered with a thick slimy biofilm but lacked the presence of a protective corrosion film. Instead, there were fine granular deposits with a dark green/black appearance, which is associated more with CMIC than EMIC.

Surface profilometry analysis further highlighted the impact of the biofilm on the CS surfaces. Generally, the shape and pit morphology were different in coupons exposed to biotic conditions compared to abiotic conditions. This difference was more pronounced when comparing the P coupons exposed to the biotic condition. Further, in this study there was a significant difference when comparing between the two surface roughness types under the biotic condition. Again, the P coupons exhibited a significantly greater *PD* compared to the AR coupons. The interactions between a surface and a bacterial cell have been shown to follow the principles of colloidal physics described by the DLVO theory [5]. Depending on the topographical features and nanostructure of the material surface, the actual contact area of the material surface with the bacterial cell can either be increased or decreased [5]. It is hypothesised that the AR coupons would have a greater surface area than the P coupons, and thus allow for greater surface attachment of sessile cells. Subsequently, this would translate to an increased incidence of pitting. However, in this present study the opposite was true. A more in depth analysis of the nanostructure of the coupon surfaces is therefore necessary to get a better understanding. Initially, it was hypothesised that the deterioration observed in this present study is primarily a result of CMIC, rather than EMIC due to the activity of the biofilm and the availability of lactate. CMIC of Fe^0 by $\mathrm{H_2S}$ from microbial $\mathrm{SO_4^{2-}}$ reduction has been shown to occur when organic substrates are available [25].

Analysis of the community dynamics revealed a marked change in the predominant relative abundances of microorganisms. The dominant genera from the sediment sample were generally anaerobic, halophilic, and obligately chemolithoautotrophic, obtaining energy by oxidizing inorganic compounds. However, the dominant genera from the planktonic samples taken from the bulk fluid were generally facultative anaerobes known to be chemoheterotrophic, utilising organic compounds, such as lactate, through fermentation. The relative abundances of *Veillonella* and *Terrisporobacter* were particularly high in the initial Day 0 planktonic sample but had lower concentrations after 28 Days. *Veillonella* spp., are known to require lactate for growth as they are unable to metabolise normal dietary carbohydrates [252]. Another microorganism of interest from the Day 0 planktonic sample was *Clostridium*. *Clostridium* spp., have genes for EET and/or demonstrated EET capabilities [253, 254]. Isolates are typically fermentative electrotrophs that

produce organic acids from fermentable substrates [29]. The MB media, for the enumeration of SRB, clearly had a large impact on the community dynamics. After 28 Days, there were significantly lower relative abundances of methanogenic species. This can be attributed to the MB media, selective for the enumeration of SRB species. Methanogens and SRM are known to compete for energy sources, with SRM outcompeting methanogens in sulphate-rich environments [237]. Predictably, SRB were the dominant genera in both the day 28 bulk fluid and biofilm samples. *Desulfovibrio* was the dominant genera, and both biofilm samples exhibited similarly high relative abundances. Generally, the microbial populations on both the AR and P coupons were very similar. *Desulfovibrio* is a recognised electroactive corrosive microorganism, found in electromicrobiomes on the corroding surface of Fe^0- containing metals under anaerobic conditions. *Desulfovibrio* can extract electrons from the metallic Fe^0 in structural materials to support anaerobic respiration [29]. Fe^0 oxidation may be coupled to the reduction of electron acceptors that commonly support anaerobic respiration [255]. Electroactivity within mixed-species biofilm communities is an important process. Electroactivity, between fermentative electroactive bacteria (FEB) and respiratory electroactive bacteria (REB), enables food chains to be established. These electroactive microorganisms cooperate to oxidise organic compounds to CO_2 with the reduction of Fe^{3+} [29]. However, this proposed direct Fe^0- to- microorganism electron transfer has not been rigorously demonstrated in the literature, with limited examples [256, 257]. Understanding the role of EET in corrosion is critical.

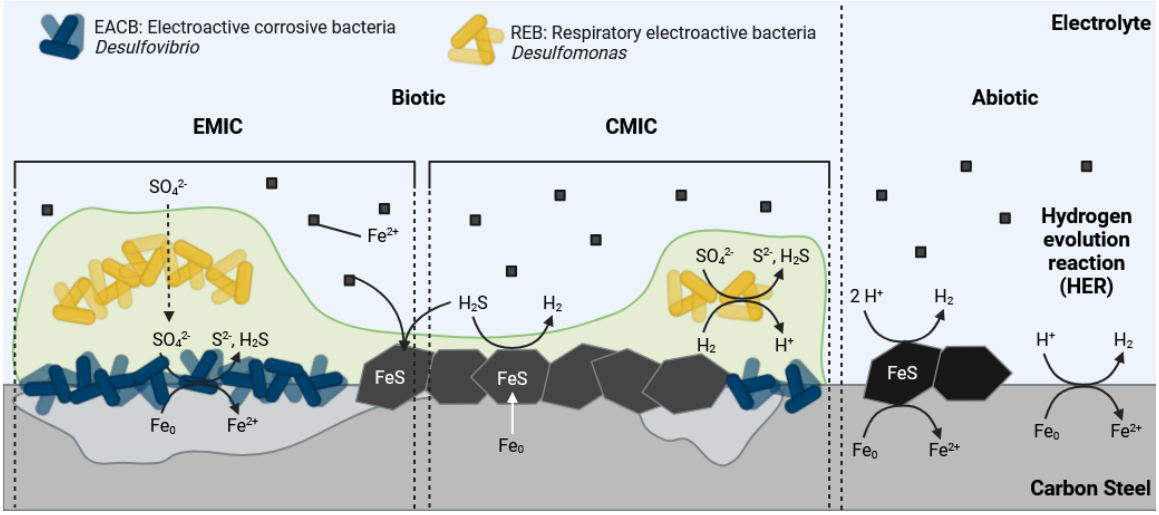

Figure 4.10. Schematic overview of key reactions for both abiotic and biotic conditions involved in metal corrosion. Abiotic reactions were associated with the hydrogen evolution reaction, as there was a general lack of a corrosion film. Biotic reactions were associated with both EMIC and CMIC. BioRender.com (2024).

Naturally, for the biotic condition, with MB media for the enumeration of SRB, the prevailing corrosion mechanisms were both EMIC and CMIC. Figure 4.10 illustrates the proposed abiotic and biotic reaction mechanisms. Initially, CMIC may have been the dominant corrosion

mechanism when H_2S concentrations were high and organic substrates were more readily available [35]. Over the first week, there was a relatively high H_2S concentration, which gradually decreased to similar levels observed in the abiotic reactor after two to three weeks. During this time visible black particulates could be seen settling at the bottom of the reactor. After two weeks, there was a visible crust on the surface of the MB media. Moreover, the media was black in appearance with increased levels of turbidity. EMIC, via the direct uptake of electrons from the metal surface [25], may have been the primary corrosion mechanism during this period. The increased turbidity was attributed to a combination of increased Fe^{2+} ions and fine suspensions of FeS produced in the bulk fluid rather than as a film on metal surface. This was due to the presence of a thick biofilm which covered a greater surface area than corrosion products on the metal surface. Additionally, the decreasing concentration of H_2S may also be attributed to the large headspace within the reactor system. A large headspace has been shown in other studies to allow for more H_2S to escape from the bulk fluid. In turn, the environment within the bulk fluid becomes less cytotoxic further supporting biofilm growth [35]. This could have also contributed to a lack of FeS passivation on the metal surface. Conversely, the concentration of H_2S is likely higher under the biofilm compared to the bulk fluid due to cell density. Furthermore, the biofilm is a diffusion barrier that slows down the escape of H_2S. Thus, CMIC could still be a contributing factor to localised pitting corrosion. However, organic substrates are likely at lower concentrations under the biofilm. Based on visual observation of the coupons taken from the biotic condition, there was an inorganic corrosion product on the metal surface, but there were also distinct dark green/black granular deposits present. EMIC by SRB is characterised by the formation of large amounts of inorganic corrosion products [25]. However, the biotic surfaces were covered with a thick slimy biofilm.

In sulphate-containing anoxic environments, previous studies have demonstrated that CMIC and EMIC are the likely primary processes that drive Fe^0 corrosion [25]. However, determining the relative contributions of EMIC and CMIC in different anoxic environments is challenging. Moreover, there are certain situations in which SRB-induced biocorrosion can be further exacerbated [25]. For example, ingress of molecular O_2 [258, 259, 260] into previously anoxic systems can lead to the formation of highly corrosive sulphur species from the partial oxidation of dissolved H_2S and biogenic FeS deposits on steel surfaces [261, 262]. CMIC and EMIC produce corrosion products with inherently different relative amounts of sulphidic (containing H_2S, HS^-, S^{2-}) and non-sulphidic iron. FeS are the characteristic products of SRB-induced corrosion [25]. While CMIC produces FeS as the sole mineral product, FeS has been found to account for only about 25% of the total iron minerals formed by the EMIC mechanism [35, 184]. Biogenic dissolved H_2S have been shown to be a key determining factor in whether CMIC or EMIC are the primary corrosion mechanism [35]. It was hypothesised that direct electron uptake via EMIC rather than

biogenic H_2S metabolites produced via CMIC was the primary corrosion mechanism during the later stages of this study [35]. There have been several studies performed with pure laboratory-grown SRB cultures that have reported lower *CR*s in media with organic electron donors [263, 264, 265, 266]. Similarly, these studies have speculated that the presence of microorganisms capable of EMIC play a critical role in MIC. EMIC is hypothesised to be a widespread mechanism amongst corrosive microorganisms [219, 251].

The presence of biogenic FeS appears to also play a central role in CMIC and EMIC. Newman *et al*. stated that formation of a protective FeS film usually occurs at high concentrations of dissolved H_2S which exceed the concentration of dissolved Fe^{2+} ions at the unreacted metal surface [267]. The presence of biogenic FeS may hinder further Fe^0 corrosion. The formation of a tightly adherent FeS film on the metal surface may act as a passive layer [267, 249]. Such films act as an effective process barrier by impeding the diffusion of Fe^{2+} ions from the metal anode to the aqueous environment [25, 267]. Several studies have observed impediment of the anodic half-reaction in cultures of SRB grown in the presence of organic substrates [244, 268, 269]. However, in organic matter-free cultures, where the predominant corrosive mechanism is EMIC, no significant slowdown of corrosion due to crust formation has been observed to date [25]. Enning *et al*. demonstrated that the bulky black crusts formed through EMIC are electrically conductive [219]. Electrons can flow from the corroding Fe^0 through the electroconductive mineral crust to the crust-attached cells reducing SO_4^{2-} [25, 219]. Yet, disruption of the FeS film can occur. CMIC has been demonstrated in lactate-based media with high concentrations of Fe^{2+} salts, to prevent the formation of the protective FeS film and instead deposit fine suspensions of the mineral on the metal [25, 270]. Rupture of the FeS film and local re-exposure of metallic Fe^0 subsequently results in rapid pitting corrosion. Understanding the relative contributions of EMIC and CMIC within mixed-species biofilms is critical, as given the dual role of FeS films in corrosion, resulting *CR* in sulphidic SRB cultures can vary significantly.

4.4 Summary

This protocol is designed to improve predictive measures by utilising a multidisciplinary approach and MLOE to thoroughly investigate the complexities of biofilm formation and the mechanisms that initiate MIC. The study employed a novel dual bioreactor system to explore the development of MIC on UNS G10180 CS in anaerobic MB media, focusing on the enumeration of SRB using a marine sediment as the inoculum.

- The environmental conditions in this study supported continuous biofilm growth. Electrochemical methods were concurrently employed to identify the onset of biofilm attachment and formation, as well as to assess the biofilm's impact on the surface of the CS coupons.
- Surface profilometry in this study revealed that biotic conditions resulted in a significantly higher *PD* ($P < 0.05$ for abiotic and biotic AR coupons, $P < 0.0001$ for abiotic and biotic P coupons, $P < 0.0066$ for biotic AR and biotic P coupons) with deeper and larger pits compared to sterile abiotic conditions.
- Additionally, biofilm characterisation through sequencing indicated a significant increase in SRB, particularly the electroactive and corrosive *Desulfovibrio* spp., within the biofilm. This microorganism plays a crucial role in EET, a key process in MIC.

These findings contribute to a deeper understanding of the relative contributions of EMIC and CMIC within a mixed-species biofilm. Identifying the microbial mechanisms that drive the corrosion of CS under anoxic conditions at the metal/electrolyte interface is essential, as *CR*s in sulphidic SRB cultures can vary widely. By employing MLOE, a comprehensive understanding of the role SRB play in MIC can be developed. In turn, this can inform the design of more sustainable prevention and mitigation strategies.

Chapter 5 Investigating the effects of produced water on anaerobic marine biofilm formation and microbiologically influenced corrosion of UNS G10180 carbon steel

5.1 Introduction

The formation and behaviour of biofilm communities in oil and gas systems, particularly those involving CS surfaces in contact with PW, is a critical area of study due to its implications for material and infrastructure integrity. The presence of certain types of microorganisms can contribute to infrastructure complications, such as corrosion, souring, and biofouling [219, 271]. While some metal loss is expected and accounted for during the design of the infrastructure, higher rates of corrosion, unless detected and mitigated early, can necessitate costly repairs or replacements [272]. PW is one of the most common sampling sources within oilfield systems but is often characterised by low biomass and diversity [273]. Moreover, environmental samples are notoriously difficult to culture using standard laboratory techniques. This is because PW typically contains a diverse and complex mixture of organic compounds, including hydrocarbons and organic acids. Whereas, PW does not contain rich carbon sources, including amino acids, peptides, and sugars. Thus, simulating the environmental conditions of an offshore system within the laboratory, whilst supporting growth of environmental cultures, can be challenging. Consequently, laboratory studies on biofilms have typically been conducted under simplified conditions. However, there is a need to replicate the complex environmental parameters of offshore systems more closely to ensure the relevance of findings and any mitigation strategies employed.

MIC is notoriously difficult to detect and monitor within industry. Despite the advent of molecular tools and improved microbial monitoring strategies for oil and gas operations, specific underlying MIC mechanisms in pipelines remain largely enigmatic [272]. Consequently, MIC is a particularly difficult corrosion mechanism to manage. Oilfield systems contain multiphase fluids, including crude oil, gas, as well as PW [274]. This multifaceted ecological niche consists of many undetermined thermophilic and mesophilic archaea/bacteria [274]. These uncharacterised microorganisms may metabolise organic and inorganic compounds in the crude oil and metal pipelines under extreme environmental conditions [275, 276]. Moreover, these microbial communities have the potential to change the redox chemistry within oilfield systems [277, 278].

Furthermore, PW may also contain high concentration of minerals, such as Cl^- and SO_4^{2-}, which may influence the community dynamics within the biofilm. This will impact initial biofilm formation and influence the predominant microbial metabolisms present. Therefore, any MIC processes at the interface of the biofilm and the metal surface will be affected [278, 279, 280].

The most common corrosion mechanisms reported in oilfield systems are linked to H_2S and/or CO_2 acid gases. These gases readily dissolve into PW, resulting in aqueous corrosive environments [272]. However, these are abiotic corrosion mechanisms. Abiotic corrosion mechanisms, such as acid gas corrosion, can be modelled *in silico* [281] or alternatively, they can be simulated in laboratory reactors [282] to understand the rates of metal loss expected under specific field conditions. This is critical for industry, as field conditions such as flow rate, temperature, water chemistry, and partial pressure of acid gases will all impact reported *CR*s [272]. Additionally, laboratory testing of abiotic corrosion mechanisms provides a robust approach for testing the efficacy of different mitigation strategies. Conversely, biotic corrosion mechanisms have not been adequately modelled within the laboratory for mixed-species biofilms from an industrial perspective. Similarly, the efficacy of biocides, applied to control MIC, have also not been adequately modelled. Thus, the development of such a model protocol is important for the effective management of MIC mechanisms. Currently, field-based detection and monitoring is primarily employed for the effective management of MIC corrosion mechanisms [272]. Microbiological assessment is routinely performed to detect the presence of MIC causative microorganisms and to evaluate the effectiveness of biocide treatments used to mitigate against MIC [144]. Though, by the time MIC is detected and diagnosed as the root cause, it may already be too late to effectively mitigate due to the recalcitrant nature of biofilms.

It is well documented that it is sessile microorganisms within biofilms that attach to metal surfaces which lead to electrochemical MIC processes. Additionally, it is widely accepted that there are distinct phylogenetic groups such as IRB, SRB, and APB, which actively participate in MIC [274, 283, 284, 285]. However, long-term studies on the influence of mixed-species biofilms on MIC in oilfield systems are limited. Most laboratory studies on MIC are typically short- to medium-term, often focusing on specific aspects of the corrosion process, such as biofilm formation, *CR*, or the identification of corrosive microbial species. While these studies provide valuable insights, they may not fully capture the long-term dynamics and cumulative effects of microbial corrosion, particularly under conditions that closely mimic real-world environments. Recent studies from Elumalai *et al.* found that crude oil reservoirs were dominated by Proteobacteria, Actinobacteria, and Firmicutes classes [274, 286]. Proteobacteria biofilms have been associated with various types of corrosion, with *Pseudomonas* sp. being shown to form a thin biofilm with corrosion deposits and causing the reduction of Fe^{3+} to Fe^{2+} on the metal surface [287, 288]. Moreover, Proteobacteria

species have been reported to consume hydrocarbons as a nutrient source and have the proficiency to degrade aromatic hydrocarbons for their metabolic pathways [289].

Long-term studies are challenging to conduct due to the time, resources, and complexities involved in replicating the dynamic and multifaceted conditions found in oil and gas systems. However, the need for such studies is increasingly recognised, as they can provide more comprehensive data on how biofilms evolve over time, how microbial communities interact with materials, and how these interactions contribute to long-term corrosion processes. Understanding these factors is crucial for developing effective mitigation strategies to protect infrastructure in the oil and gas industry.

This study investigates the impact of these more realistic environmental conditions on natural mixed-species biofilm communities, aiming to provide deeper insights into their development, community dynamics, and potential to induce MIC within a novel dual bioreactor protocol that simulates offshore oil and gas environments. By aligning laboratory conditions with those encountered *in situ*, this research seeks to bridge the gap between experimental and real-world scenarios, ultimately enhancing the reliability of biofilm management strategies in the industry. Importantly, utilising MLOE [145], the protocol incorporates a multi-disciplinary approach to gain a holistic understanding of biofilms and MIC.

5.2 Results

Over the initial three-day batch phase, the abiotic media was pink in appearance, and the coupons maintained the silver-grey metallic lustre of CS. After the first week, the abiotic media was beginning to become cloudier, but it was not until Day 11 that the abiotic PW became orange-pink in colouration. Similarly, over the initial three-day batch phase, the biotic coupons maintained the silver-grey appearance of the CS. However, the PW quickly became dark green/black in colouration on Day 3. After the flow of fresh PW media was started on day 4, the bulk fluid became pink in appearance. Similarly, it was not until Day 11 that the biotic PW became orange-pink in colouration. Upon dismantling of the reactors on day 28, and retrieval of the coupon rods, there was a significant difference in the coupon appearances, see Appendix D Figure D.2. Additionally, the appearance of the waste from the different reactor conditions was significantly different. The abiotic waste media was orange-pink in colouration with reddish-brown granular deposits, whilst the biotic waste media was dark green/black in colouration. The abiotic surfaces had the presence of a black corrosion product across the entire coupon surfaces, with some reddish-brown granular deposits. Whereas, the biotic surfaces were only partially covered by a black corrosion product, with the presence of a

heterogeneous dark green/black biofilm. The silver-grey appearance of the CS was also partially visible upon retrieval.

Sulphide microsensor. All values were detected as below zero, as such it was assumed that no H_2S was present throughout the experiment. Alternatively, the PW poisoned the microsensors. Nonetheless, both conditions experienced similar readings. Unfortunately, *DO* concentrations could not be measured as the probe was not working. However, the pH was measured on day 28 for the media containers, waste containers and reactor systems. All values recorded were between 7.01 and 7.47.

Carbon steel surface analysis. Appendix D Figure D.3 shows the CS surfaces on day 0. Appendix D Table D.4 summarises the quantitative surface roughness profiles on both day 0 and day 28. Figure 5.1 shows the cleaned CS surfaces after 28 days, with biofilms and corrosion products removed to reveal the morphology of the surface degradation and to facilitate corrosion assessment. Surface profilometry revealed that there were low levels of uniform or localised pitting corrosion present for both the abiotic and biotic condition. The abiotic average pit depths were 12 µm, with an average pit area of 971 µm^2 for any classified pits. The biotic average pit depths were 7 µm, with an average pit area of 1501 µm^2 for any classified pits. Again, for this study a pit was classified as having a depth greater than 5 µm and an area greater than 650 µm^2 [153].

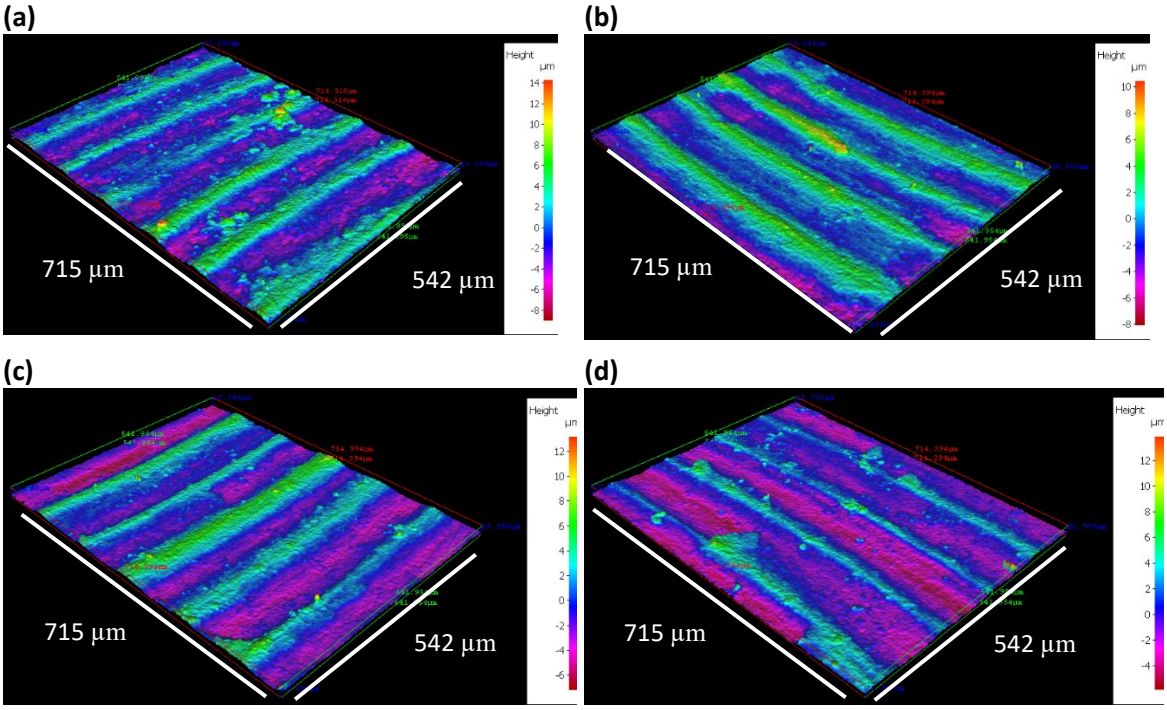

Figure 5.1. Three-dimensional optical surface profilometry of the cleaned UNS G10180 surfaces at day 28. AR coupons for: **(a,b)** abiotic and **(c,d)** biotic conditions, after exposure to anaerobic produced water media for 28 days.

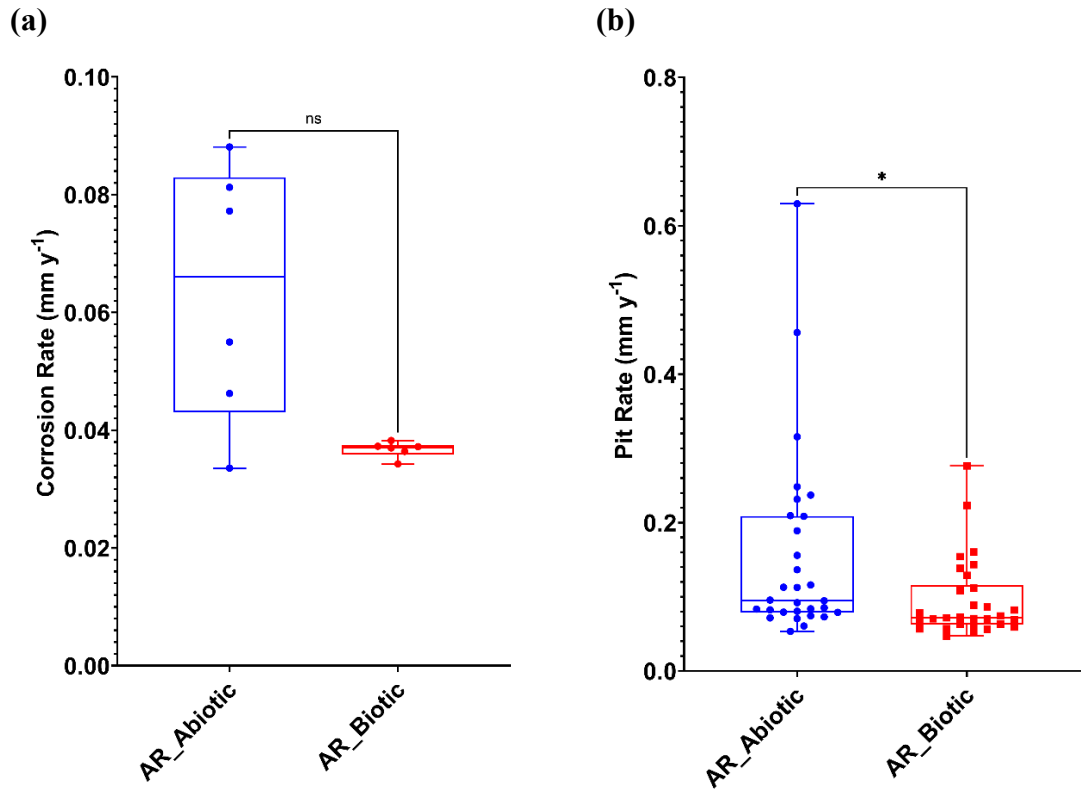

Figure 5.2. Abiotic and biotic corrosion performance after exposure to anaerobic produced water media for 28 days: **(a)** corrosion rate via gravimetric analysis and surface profilometry assessed and **(b)** pit rate ($P < 0.05$), for the AR coupons.

Figure 5.2a provides an evaluation of the CS coupons *CR*. For the abiotic condition, there was a higher *CR* when compared to the biotic condition, though there was no significance. According to the NACE SP0775-2023 assessment criteria, there was a moderate *CR* (between 0.025 and 0.12 mm y^{-1}) in both the abiotic and biotic reactors (Figure 5.2a). Whereas a moderate *PR* (0.13 – 0.20 mm y^{-1}) was assessed for the abiotic condition, with a low *PR* (<0.13 mm y^{-1}) for the biotic condition (Figure 5.2b) [170].

Further analysis of the surface profilometries in Figure 5.1, allowed a quantitative determination of the *PR* Figure 5.2b of the CS coupons. For this study, it was not possible to quantitatively determine *PD* values, due to the general absence of pitting across the coupon surfaces upon retrieval after 28 days.

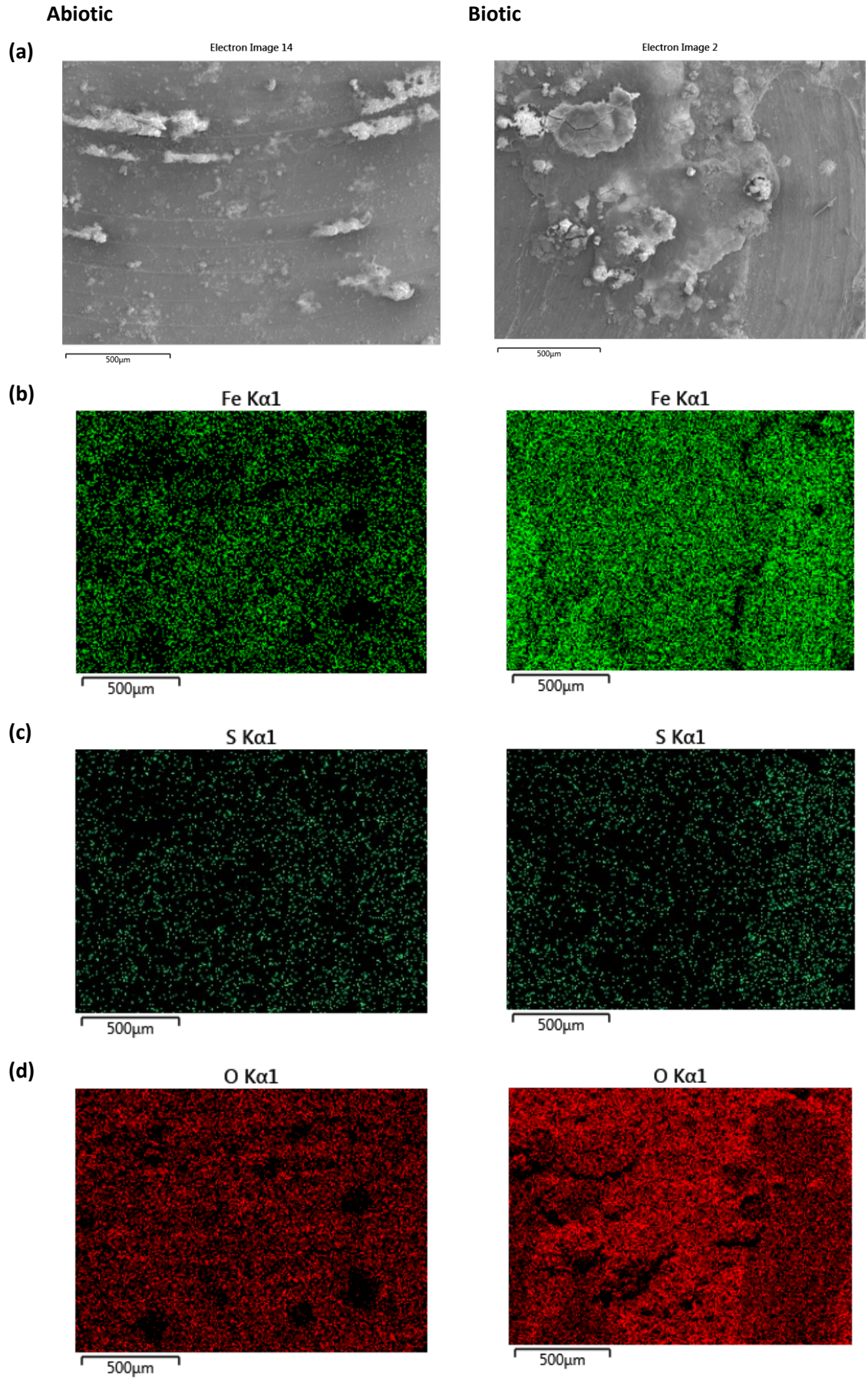
Abiotic
Biotic
(a)
Electron Image 14
500µm
Electron Image 2
500µm
(b)
Fe Kα1
500µm
Fe Kα1
500µm
(c)
S Kα1
500µm
S Kα1
500µm
(d)
O Kα1
500µm
O Kα1
500µm

Figure 5.3. SEM-EDS elemental mapping of the UNS G10180 carbon steel, AR surfaces, after exposure to anaerobic produced water media, taken on day 28. **(a)** SEM image; **(b)** iron map; **(c)** sulphur map; **(d)** oxygen map.

Corrosion product analysis. Figure 5.3 shows SEM-EDS elemental mapping of the UNS G10180 CS surfaces for both the abiotic and biotic conditions. The images of corrosion products and biofilms attached to the metal samples demonstrate the heterogeneity of distribution over the surface. Coupons exposed to the biotic condition were observed to exhibit greater surface coverage. The SEM-EDS elemental maps are shown in Figure 5.3b – d. The major elements detected in coupons exposed to all conditions were iron (Fe), sulphur (S), and oxygen (O). Corroded areas of all coupons were mainly covered by Fe and O, with heterogeneous distribution of S. A cross-sectional image of the corrosion products was not performed.

Additional analysis of the corrosion products using Raman spectroscopy are shown in Figure 5.4. According to Raman bands of reference corrosion products in previous papers [290, 291, 292], the corrosion products are identified to be primarily mackinawite (bands 208, 282 cm^{-1}) for both the abiotic and biotic condition. There were also additional bands which may be attributed to sulphur, as well as reference iron oxide compounds such as magnetite, goethite ($\alpha - \mathrm{FeO(OH)}$), lepidocrocite, or hematite ($\alpha - \mathrm{Fe_2O_3}$). The composition of this black compact layer was identified at mid-strong bands 250, 380, 1307 cm^{-1} associated with lepidocrocite. Additionally, bands at 298, 399, 481, 554, 675 and 1002 cm^{-1} have previously been shown to be associated with goethite, whilst bands at 222, 244, 298, 501, 615 and 1318 cm^{-1} are associated with hematite. Magnetite has previously been shown to be associated with bands at 675 and 550 cm^{-1} [290, 291, 292]. The coverage of the metal sample with a black precipitate was indicative of the successful growth of corrosion products film containing FeS compounds. The Raman spectrum of the sample is in good agreement with literature spectra attributed to mackinawite.

(a) - Abiotic

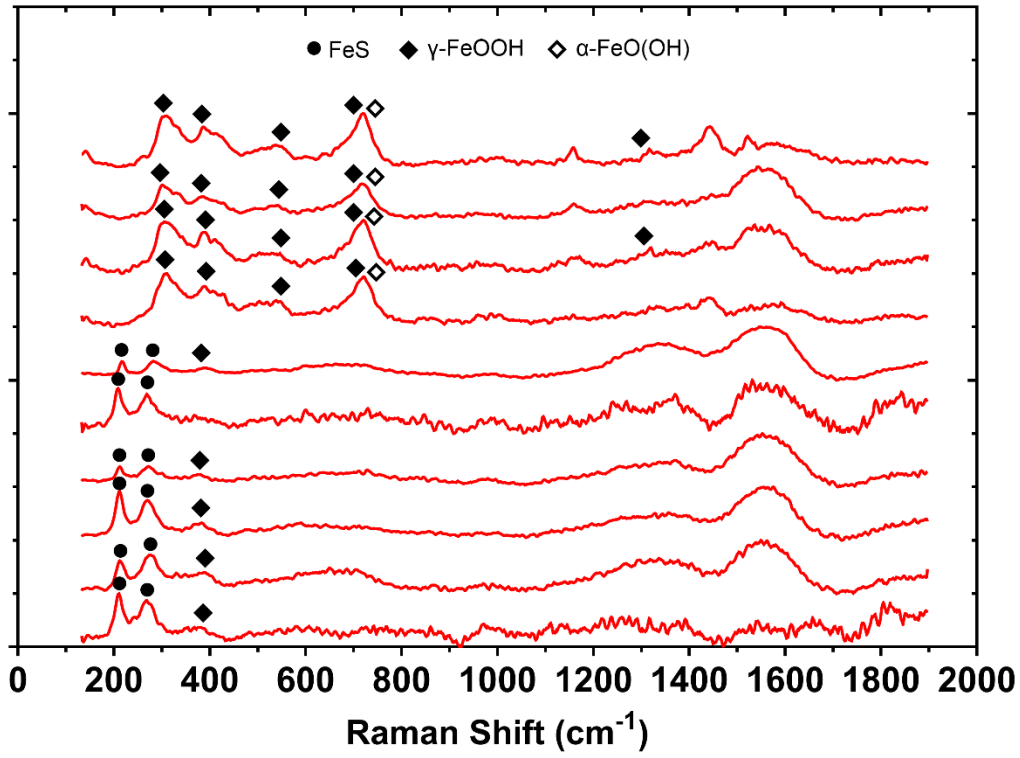

(b) - Biotic

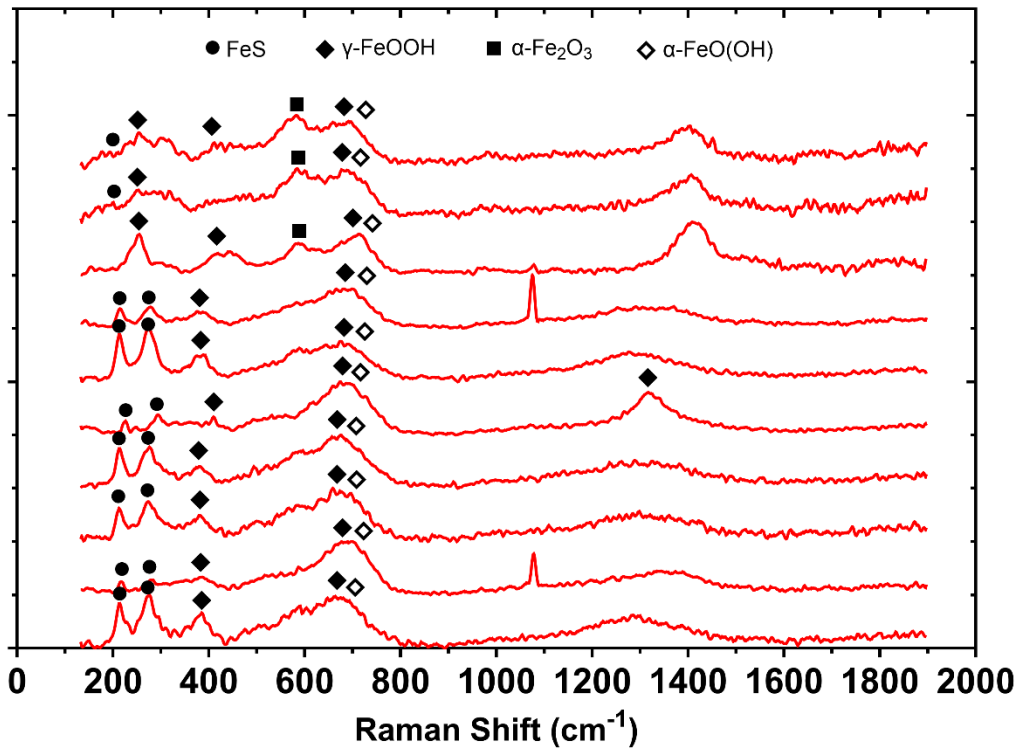

Figure 5.4. Raman spectra of the UNS G10180 carbon steel surfaces after exposure to anaerobic produced water media, taken on day 28. For the AR **(a,b)** abiotic and; **(c, d)** biotic condition.

Electrochemical measurements. Figure 5.5 shows the changes in E_{corr} and R_p between the abiotic and biotic anaerobic PW media, for the UNS G10180 CS coupons. For the abiotic condition, Figure 5.5a, there was a swift increase of +0.040 V on Day 3 after the end of the batch phase. This was subsequently followed by swift decrease of -0.050 V on Day 4. This can be attributed to the flow of fresh PW. Otherwise, there was a gradual +0.090 V electronegative shift in the E_{corr} between days 4 and 28. This can be linked with the presence of a conditioning film (i.e., an adsorbed organic layer) and the formation of inorganic corrosion product layer. A pseudo-steady state E_{corr} had not been attained after 28 days. Similarly, for the biotic condition, there was a swift increase of +0.050 V on Day 3 after the end of the batch phase. This was subsequently followed by swift decrease of -0.030 V on Day 4. Then, there was a gradual electronegative shift in the E_{corr}, until Day 24. After which, the E_{corr} swiftly decreased by -0.040 V. The potentials for both abiotic and biotic in the latter stages were generally similar and ranged between –0.610 V and – 0.670 V *vs*. Ag/AgCl.

In Figure 5.5b the LPR derived R_p after Day 10 remained low at approx. 400 Ω cm^2 for the sterile abiotic condition, indicative of a uniform corrosion across a porous corrosion film. Similarly, for the biotic condition, the R_p remained low at approx. 400 Ω cm^2. The pioneering bacterial attachment/colonisation was difficult to detect for this study. However, biofilm formation and growth kinetics will lead inevitably to a more complex electrochemical response. Overall, there were no significant differences when comparing between the abiotic and biotic reactor environments.

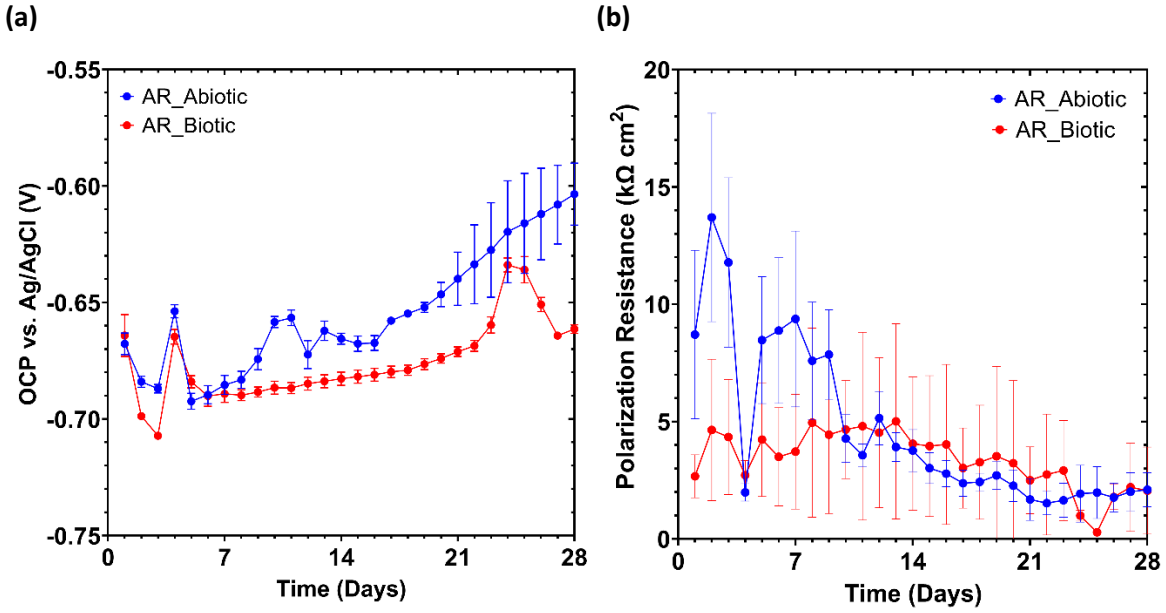

Figure 5.5. LPR data for UNS G10180 carbon steel: **(a)** open-circuit potentials and **(b)** polarisation resistance in anaerobic produced water media (abiotic and biotic conditions), for AR and P coupons (data points represent mean ± standard deviation, *n* = 6). Reactor stirrer at 50 rpm.

Figure 5.6 shows the EIS data for UNS G10180 CS in the anaerobic PW media presented in three forms: Nyquist, Bode phase angle and Bode impedance modulus plots. The sterile abiotic condition on Day 1 typifies an electrochemical response for the formation of a porous interface, with diffusion of soluble electroactive species across an organic conditioning film [207] and nascent inorganic corrosion product layer. The diffusive behaviour is associated with linear features having a roughly 45° slope (a Warburg impedance response) and phase angles close to 45° in low frequency region (10^{-2} – 10^{0} Hz), see Fig. 5.6a and 5.6c. This electrochemical response did not really change over the 28 days. Similarly, the biotic condition had a consistently uniform EIS response over the 28 day test, with only minor variation in the spectra and suggests the absence of significant detectable electrochemical changes with time. Notably, there are no discernible Nyquist semicircles (Fig 5.6b). Here a wider low frequency region (10^{-1} – 10^{2}) is likely to be subject to a greater influence of adsorption processes, associated with the adhesion of the pioneering bacteria on a conditioning film [215, 216] and biofilm formation.

The EIS spectra were fitted using an ECM shown in Figure 2.4. Both the abiotic and biotic data generally had a good fit, with the quantitative fitting results shown in Appendix D Table D.6. For the abiotic control, there is a capacitive behaviour over the first week, with a diffusive behaviour over the final three weeks in the film layer (reflecting ion adsorption). Whilst there was a diffusive behaviour in the double layer, which reflects charge transfer, due to the formation of corrosion products (rust, porous oxide layer). The exponent parameter in the double layer reflects a non-ideal capacitance, which is indicative of resistive and inductive parasitics, because of a more prominent resistive component. R_{film} is relatively low over the 28 days, and there are no significant changes in R_{ct}. Similarly, for the biotic condition, there was a capacitive behaviour over the first week, with a diffusive behaviour over the final three weeks in the film layer. Whereas there was a diffusive behaviour over the initial two week, followed by a capacitive behaviour over the final two weeks in the double layer. This capacitive behaviour is attributed to the biofilm. There are no significant changes in the R_{ct} in the double layer over time. The exponent parameter for the film layer is greater than 0.8 only on day 28, which indicates a non-ideal capacitance response. This is true for the final two weeks in the double layer. The ECM and EIS both have general agreement with the LPR data.

(a) – Abiotic

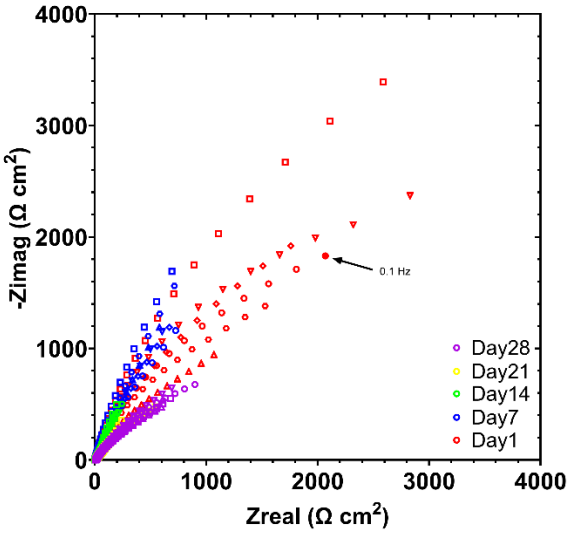

(b) – Biotic

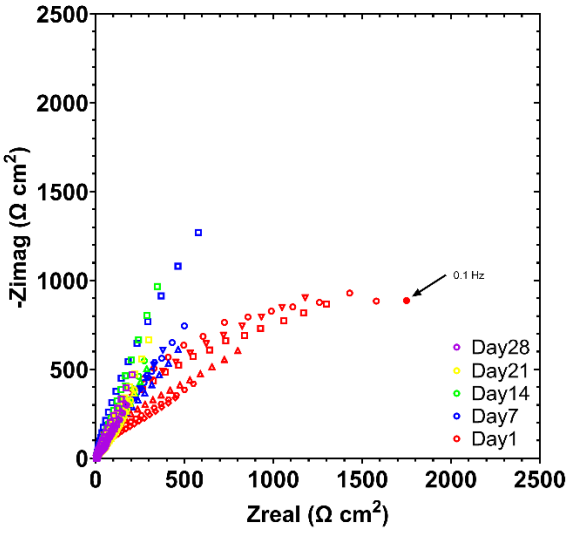

(c) – Abiotic

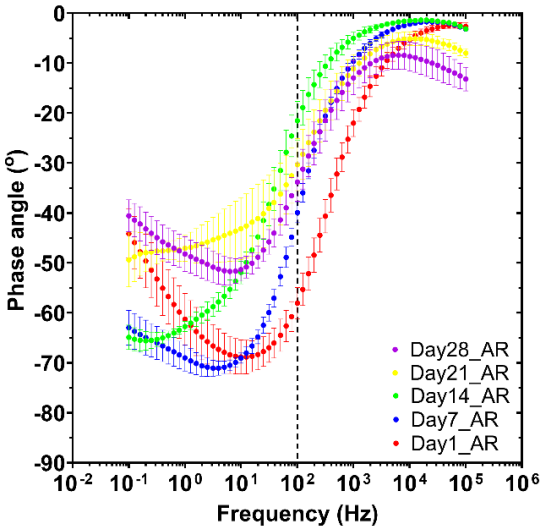

(d) – Biotic

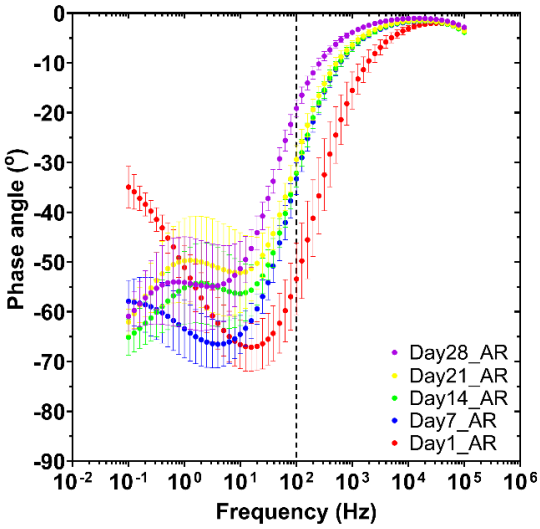

(e) – Abiotic

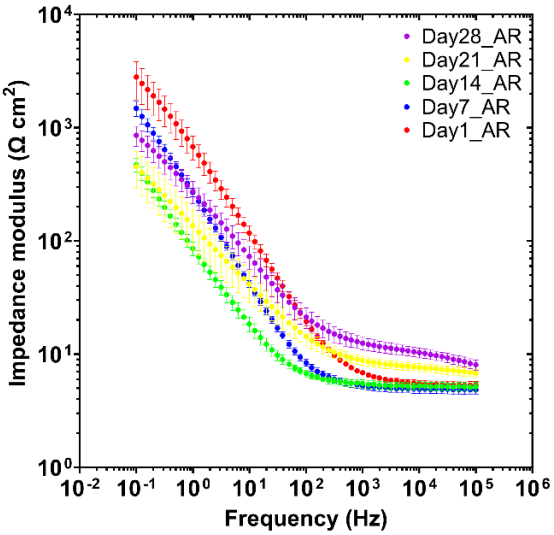

(f) – Biotic

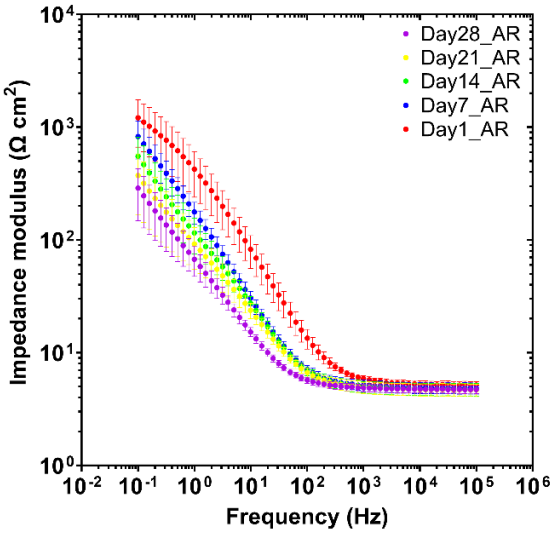

Figure 5.6. EIS data for UNS G10180 carbon steel in anaerobic produced water media at OCP: **(a, b)** Nyquist, **(c, d)** Bode phase angle (θ *vs.* f), and **(e, f)** Bode impedance modulus ($|Z|$ *vs.* f) over 28-days. (n = 6). Reactor stirrer at 50 rpm.

Figure 5.7 shows the potentiodynamic polarisation curves for UNS G10180 CS for the abiotic and biotic reactors in anaerobic PW media after 28 days. Table 5.1 shows the corrosion parameters obtained from the polarisation curves. From the Tafel slopes, there is a similar cathodic behaviour (reduction) when comparing the abiotic and biotic conditions, which is linked to the predominant HER under anaerobic conditions. Conversely, the anodic Tafel slopes (oxidation) are greater, demonstrating almost limiting current densities, in the abiotic compared to the biotic media. Overall, the abiotic condition had a higher j_{corr} compared to the biotic condition. This is consistent with a more uniform corrosion morphology. Similarly, the sterile abiotic condition had a more electropositive E_{corr} when compared to the biotic condition. The polarisation results corroborate the LPR and EIS data.

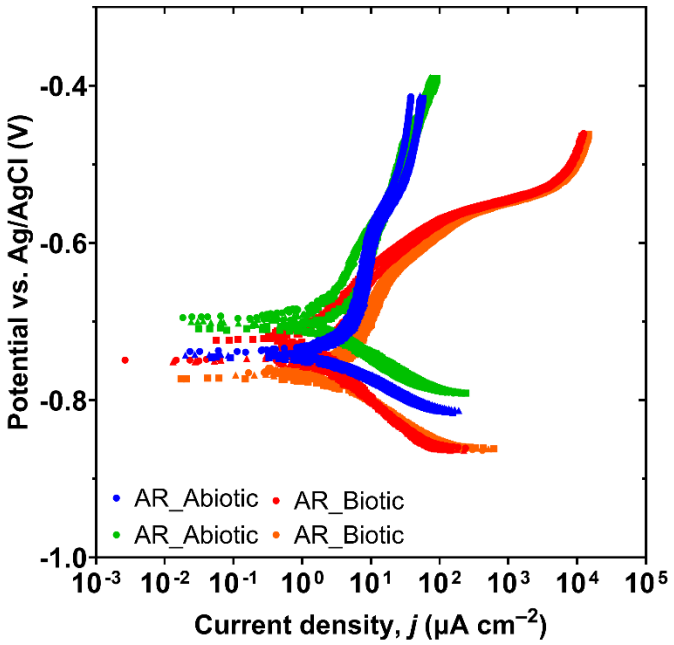

Figure 5.7. Potentiodynamic polarisation curves for the abiotic and biotic AR, UNS G10180 carbon steel coupons, at ambient temperature after exposure to anaerobic produced water media for 28 days. Scan rate of 0.5 mV s^{-1} and reactor stirrer at 50 rpm.

Table 5.1. Fitted electrochemical parameters from polarisation curves; comparison between the abiotic and biotic AR, UNS G10180 carbon steel coupons, after exposure to anaerobic produced water media for 28 days.

	Coupons	j_{corr} / µA cm^{-2}	E_{corr} *vs.* Ag/AgCl / V	β_a (mV dec^{-1})	β_c (mV dec^{-1})
Abiotic	AR	3.1 ± 0.8	-723 ± 23	240 ± 36	54 ± 7
Biotic	AR	0.7 ± 0.2	-748 ± 16	64 ± 2	51 ± 15

Biofilm characterisation. CLSM with differentiation of live and dead biofilm cells was performed and can be found in the supplementary material Appendix D Figure D.7. The heterogeneous biofilm distribution over the surface of the CS coupons did not allow measurements of the maximum biofilm thickness. Therefore, the thickness of biofilms was not determined. From the images captured, there was a live/dead cell ratio of approximately 87% live to 13% dead.

Active microorganism evaluation of the environmental marine sediment, the initial and final biotic PW media planktonic samples (Day 0 and Day 28), and the biotic AR biofilm, was undertaken via 16S rRNA amplicon sequencing with two target region, V3-4 for bacteria and archaea. A total of 2,293,909 high-quality sequences were obtained after bioinformatics processing of the raw reads. From these, 97.7% was classified for the sediment sample with 99.99% classified for the Day 0 planktonic sample and 100% classified for the Day 28 planktonic sample and AR biofilm sample. These sequences were taxonomically classified into microbial genera. The top 25 microbial genera are presented in Appendix D Table D.8 in the supplemental material. Figure 5.8 summarises the sequencing data, showing a PCA (a) and a stacked bar plot (b) illustrating the relative abundances for the top 25 genera. Molecular identification of the microorganisms showed that the initial sediment sample had a very diverse microbial composition. Most genus had low relative abundances less than 2%. The dominant genera included *Sulfurovum*, *Candidatus Prometheoarchaeum*, *Desulfosarcina*, *Desulfuromonas* and *Thiohalobacter*. Interestingly, there were relatively high numbers of archaea in the sediment sample compared to the other samples. The sediment sample had negative Spearman correlation coefficients (Appendix D Figure D.9) with the other samples which was attributed to changes in conditions such as temperature and media composition from the natural marine environment. There was much less diversity in the Day 0 sample, with *Sulfurovum*, *Candidatus Prometheoarchaeum* and *Thiohalobacter* all exhibiting lower relative abundances (<1%). Whilst genera from *Vibrio*, *Methanococcoides*, *Apibacter*, and *Methanococcus* made-up approximately 55% of the relative abundance. Again, the Day 0 planktonic sample had negative Spearman correlation coefficients with the other samples. After 28 Days, there was a substantial shift in the microbial composition, with substantially lower abundances of methanogenic species. Conversely, there was a significant increase in Proteobacteria species. *Marinobacter*, *Pseudomonas*, and *Halomonas* were the dominant genera making up approximately 80% of the relative abundance. The Day 28 planktonic sample had a Spearman correlation coefficient of -0.43 with the sediment sample, -0.38 with the Day 0 planktonic sample and 0.89 with the AR biofilm sample.

(a)

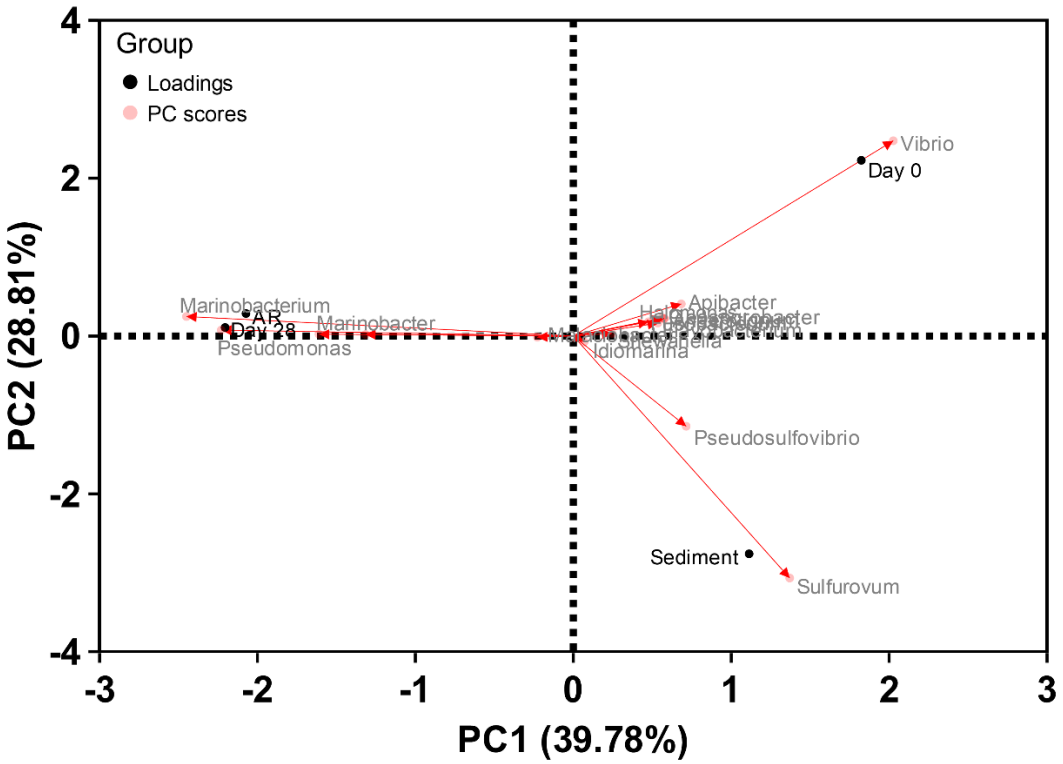
Group
Loadings
PC scores
Vibrio
Day 0
Marinobacterium
Marinobacter
Pseudomonas
Apibacter
Idiomarina
Pseudosulfovibrio
Sediment
Sulfurovum
PC2 (28.81%)
PC1 (39.78%)
4
2
0
-2
-4
-3
-2
-1
0
1
2
3

(b)

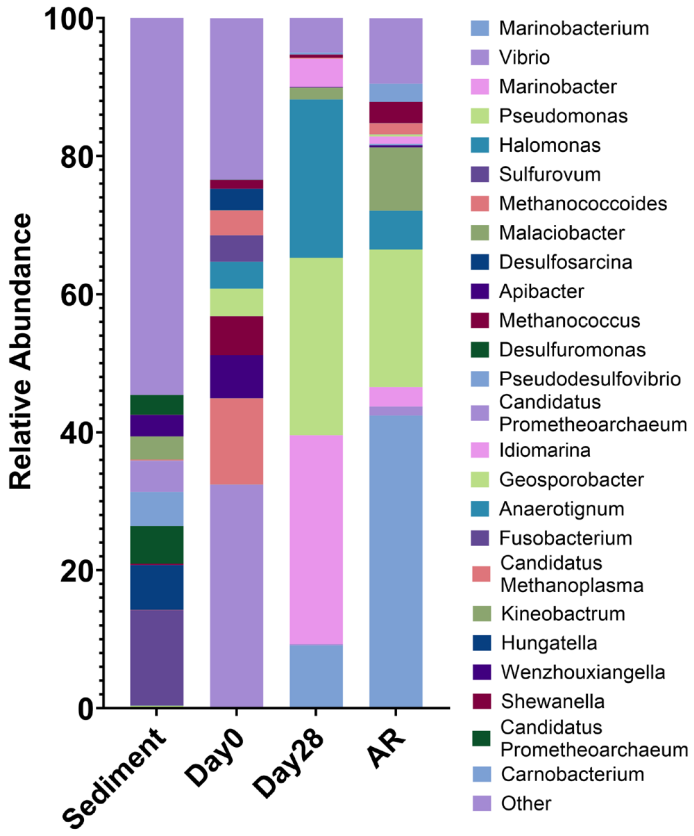

Figure 5.8. Principal Component Analysis biplot **(a)**; Microbial community. The results show the mean relative abundances of microbial communities classified at the genus level, for the top 25 genera, from 16S rRNA amplicon sequencing **(b)**; for environmental marine sediment, Day 0, and Day 28 planktonic samples, and AR biofilms, after exposure to anaerobic produced water media for 28 days.

The relative abundances of *Vibrio* decreased to approximately 1%, with the relative abundances of *Methanococcoides*, *Apibacter*, and *Methanococcus* also decreasing to lower values (<1%) in the AR biofilm. Moreover, *Sulfurovum*, *Candidatus Prometheoarchaeum*, *Desulfosarcina*, *Desulfuromonas* and *Thiohalobacter* which were the dominant genera from the sediment sample all had lower relative abundances (<1%) in the biofilm sample. The dominant genera included *Marinobacterium*, *Pseudomonas*, and *Malaciobacter* making up approximately 70% of the relative abundance. There were no methanogenic archaea in the biofilm sample.

The microbial activity was determined by the ATP concentrations (dissolved, dATP) in the bulk fluid, see Figure 5.9. The ATP assay did not measure any ATP from the biofilm sample. The biofilm may have been loosely adherent to the coupon surfaces are may have been rinsed off during sample preparation. For the biotic PW media (bulk fluid), there was a significant change ($P < 0.05$) in the dATP concentration when comparing Day 0 and Day 28, with dATP values of on the order of

100 pg mL^{-1}. As expected, there was a significantly greater ATP concentration for the biotic compared to the abiotic condition.

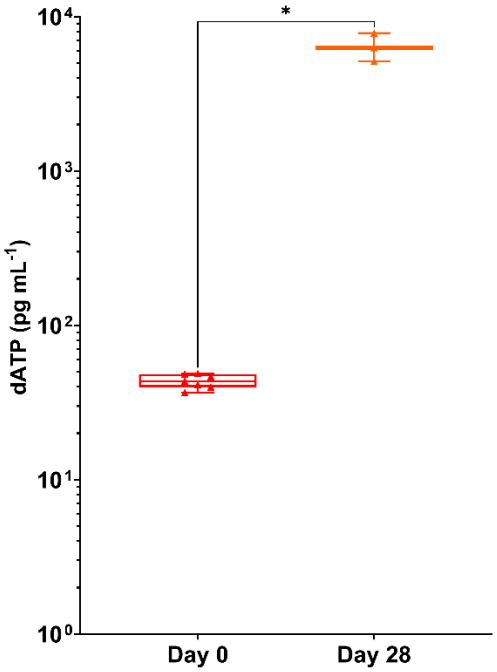

Figure 5.9. Dissolved ATP (dATP) concentrations comparing the anaerobic produced water media, taken on Day 0 and Day 28 ($P < 0.05$).

5.3 Discussion

Case studies from offshore oilfield systems have consistently demonstrated that environmental factors such as temperature, salinity, O_2 levels, and the composition of PW play a crucial role in the development of biofilms and the severity of MIC on CS surfaces [214]. These studies underscore the importance of implementing tailored corrosion management strategies that include regular monitoring, biocide application, material selection, and maintenance to mitigate the threat of MIC in offshore oil and gas operations. However, there are limitations and challenges when testing *in situ*. Offshore environments are often remote and difficult to access, making it challenging to collect samples and monitor corrosion processes over time. Environmental variability, including changes in temperature, pressure, salinity, and flow rates can further complicate the identification of specific factors driving MIC. Continuous long-term monitoring is essential to fully understand the dynamics of biofilm development and MIC in offshore systems. However, maintaining long-term studies in such harsh environments is challenging. Consequently, this leads to a reliance on shorter-term studies that may miss important trends. This can make it difficult to identify and characterise the full range of microorganisms involved in MIC, as well as understand their interactions. These limitations underscore the need for more robust and innovative approaches to studying MIC using more realistic laboratory simulations of offshore environments.

Figure 5.10 provides an illustration of the proposed corrosion mechanisms for both the abiotic and biotic conditions during the initial stages, as they evolved over time during this present study.

Abiotic reactor: - After the initial batch phase, there was a general electronegative shift associated with anodic polarisation for the abiotic condition. A pseudo-steady state E_{corr} had not been attained after 28 days. PW often contains various organic compounds, including hydrocarbons and organic acids [293]. Additionally, PW typically contains inorganic compounds such as salts, minerals, and metal ions. Both organic and inorganic substances can precipitate on metal surfaces, contributing to the formation of a conditioning film. This film can affect the electrochemical properties of the steel surface, potentially making it more susceptible to corrosion or providing passivation. From the EIS ECMs, there is initially a capacitive behaviour observed over the first week, which reflects ion adsorption and the development of a conditioning film (mixed organic and inorganic interfacial layer). Subsequently, there was a diffusive behaviour during the final three weeks in the film layer. Moreover, there was a diffusive behaviour in the metallic interface double layer, which reflects charge transfer, due to the formation of corrosion products. The primary corrosion product identified was mackinawite. There were also additional bands which may be attributed to sulphur, as well as reference iron oxide compounds such as magnetite, goethite, lepidocrocite and hematite. Additional analysis identified that corroded areas were mainly covered by Fe and O, with heterogeneous distribution of S. Generally, there was a moderately low level of uniform corrosion of the steel surface for the abiotic media.

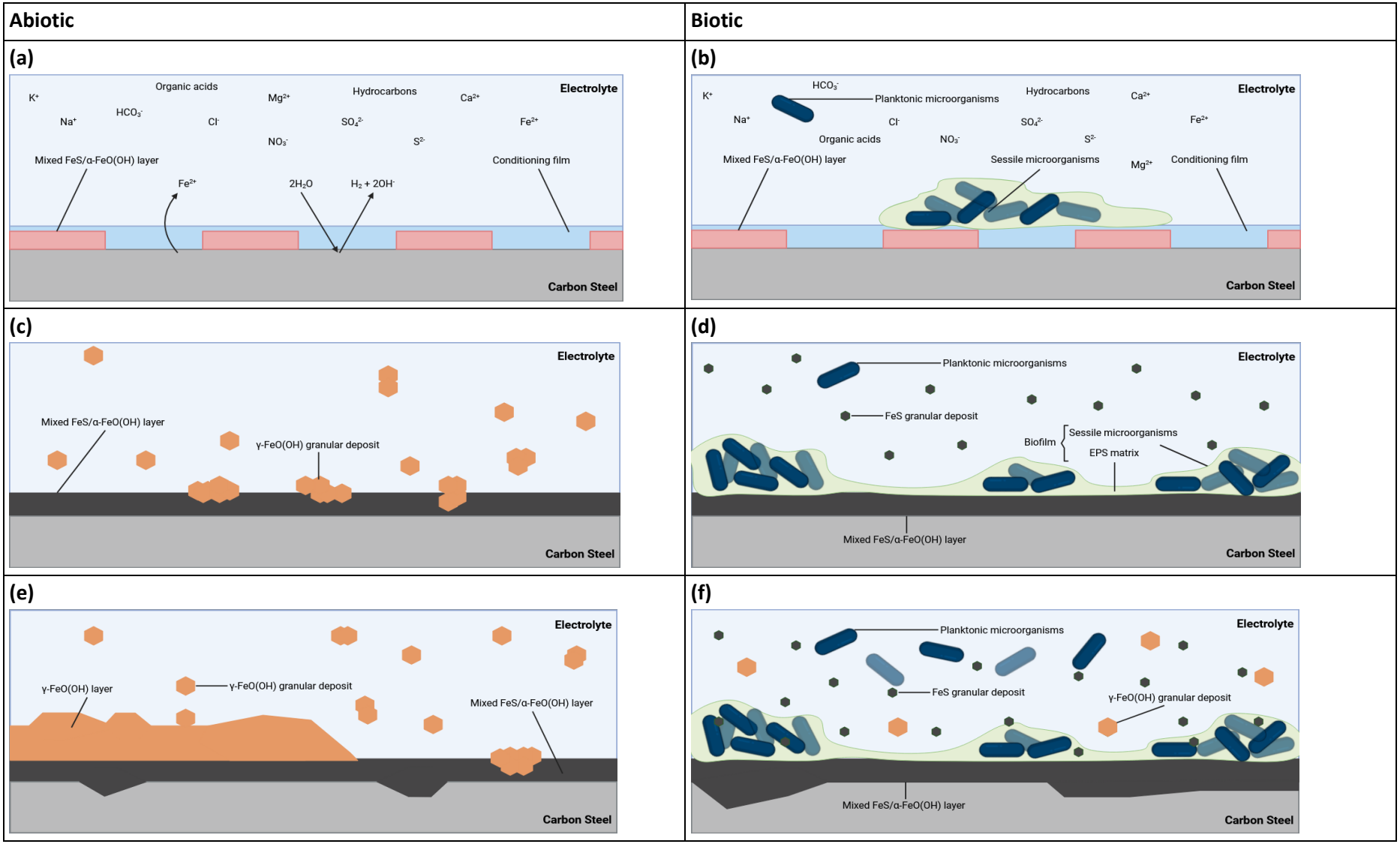

Figure 5.10. Schematic of the initial stages for UNS G10180 carbon steel in anaerobic abiotic and biotic PW media. corrosion mechanisms, **(a, b)** the formation of nascent inorganic corrosion film and the organic conditioning film with pioneering bacterial attachment during the initial batch phase; **(c, d)** maturing corrosion film under the abiotic condition with reduced biofilm growth and colonisation under the biotic condition due to the limited availability of organic carbon; **(e, f)** moderately low uniform and pitting corrosion under patchy corrosion deposits and thin biofilm with increasing granular deposits. BioRender.com (2024).

Biotic reactor: - During the initial batch phase, where additional organics were available via supplementation with yeast extract in the pre-culture, an electronegative shift in the E_{corr} was observed. This can be attributed to the increased organics and/or biofilm formation on the CS, as the PW became dark green/black in colouration with visible black precipitates and increased turbidity. However, once the flow of fresh media was initiated, there was a similar electronegative shift which was observed for the abiotic condition. The potentials for both abiotic and biotic conditions in the latter stages were generally similar. Additionally, the R_p was generally low for both conditions. For the biotic condition, there is initially a capacitive behaviour observed over the first week, with a diffusive behaviour over the final three weeks in the film layer. This was similar to the abiotic condition. Whereas there was a diffusive behaviour over the initial two weeks, followed by a capacitive behaviour over the final two weeks in the double layer. This capacitive behaviour may be attributed to a biofilm, which may cause diffusion limitations. Likewise, the formation of corrosion products, which were primarily identified as mackinawite, will also be impacting the possible electrochemical reactions that are taking place at the interface of the metal/electrolyte.

Surface profilometry analysis provided further insights and revealed that there were low levels of uniform or localised pitting corrosion present for both the abiotic and biotic condition. However, after 28 days, the biotic condition did exhibit pits with a greater average area. This is characteristic of localised pitting caused by biofilms [232, 233]. Whilst localised pitting corrosion did not appear to be significantly exacerbated by the biotic condition, longer-term studies may reveal critical stages of biofilm maturation and corrosion progression. For this study, it was not possible to quantitatively determine *PD* values, due to the general absence of pitting across the coupon surfaces.

Analysis of the community dynamics revealed a marked change in the predominant relative abundances of microorganisms. The dominant genera from the sediment sample were generally anaerobic, halophilic, and obligately chemolithoautotrophic, obtaining energy by oxidizing inorganic compounds. Interestingly, the relative total archaea from the Day 0 planktonic sample still accounted for approximately 20% of the relative abundance. *Methanococcoides*, and *Methanococcus*, are both known methanogenic archaea that play an important role in the production of methane in anaerobic environments [294, 295]. The primary metabolic pathway in *Methanococcus* involves the reduction of CO_2 with H_2 to form methane [294]. Whereas *Methanococcoides* utilise methylotrophic methanogenesis, where methylated compounds serve as the primary substrates for methane production [295]. *Vibrio* was the dominant genera in these

samples at approximately 30% relative abundance and are typically found in marine and estuarine environments. *Vibrio* sp. are known for their ability to form biofilms on various surfaces, including metals [296]. After 28 Days, there was a significant increase in *Marinobacter*, *Pseudomonas*, and *Halomonas*, making up approximately 80% of the relative abundance. *Marinobacter* species are known for forming biofilms on metal surfaces in marine environments. These biofilms can influence the corrosion process by altering the local chemical environment [297]. Moreover, *Marinobacter* species can degrade hydrocarbons, making them important for the bioremediation of oil spills in marine environments. They are well-adapted to high-salinity environments and play a role in iron cycling in marine environments, impacting the availability of iron [298, 299]. *Pseudomonas* species are prolific biofilm formers, and these biofilms can enhance corrosion by creating microenvironments that promote differential aeration and localized corrosion [104]. *Halomonas* species thrive in high-salinity environments and can reduce SO_4^{2-} to H_2S. Additionally, *Halomonas* species participate in nitrogen cycling, including denitrification, which is important for maintaining the balance of nitrogenous compounds in marine ecosystems [300]. The AR biofilm sample also had relatively high abundances of Proteobacteria species, namely *Marinobacterium* which made-up approximately 40%. Generally, the dominant species were halophilic or halotolerant and are known to be heterotrophic. They are well-adapted to marine conditions, playing roles in organic matter degradation, nutrient cycling, and interactions with marine organisms. Though the specific role of *Marinobacterium* and *Malaciobacter* are less characterised compared to other bacteria like *Pseudomonas* or *Halomonas,* they occupy a similar phenotypic niche [301]. Interestingly, there was an increase in the relative abundance of *Shewanella* within the AR biofilm. *Shewanella* species are known for their unique role in microbial corrosion, primarily due to their ability to reduce metal ions and interact directly with metal surfaces. In the presence of other bacteria, *Shewanella* can enhance corrosion through indirect mechanisms, such as H_2S production and the formation of FeS. Moreover, *Shewanella* have a demonstrated ability for EET [29], which is an important process in MIC. It would be interesting to conduct longer-term studies with the same experimental setup to observe the threat of *Shewanella*.

For the conditions used in this study, more closely mimicking the environmental conditions of an offshore oilfield system, the abiotic surfaces had the presence of a black corrosion product across the entire coupon surfaces with some reddish-brown granular deposits. As stated earlier, the primary corrosion product identified was mackinawite; with reference iron oxide compounds also detected. Mackinawite can form under anoxic or reducing conditions in environments containing H_2S. H_2S can be present in natural waters due to the reduction of SO_4^{2-}. Moreover, mackinawite formation is favoured in anaerobic environments. Conversely, iron oxides are typically formed in the presence of O_2 and water through oxidation reactions. Several types of iron oxides

can form depending on environmental conditions. Initial electrochemical reactions produce iron hydroxides which are subsequently oxidised further to iron oxides. Nonetheless, there appeared to be a passivation of the metal surface as *CR*s were moderately low.

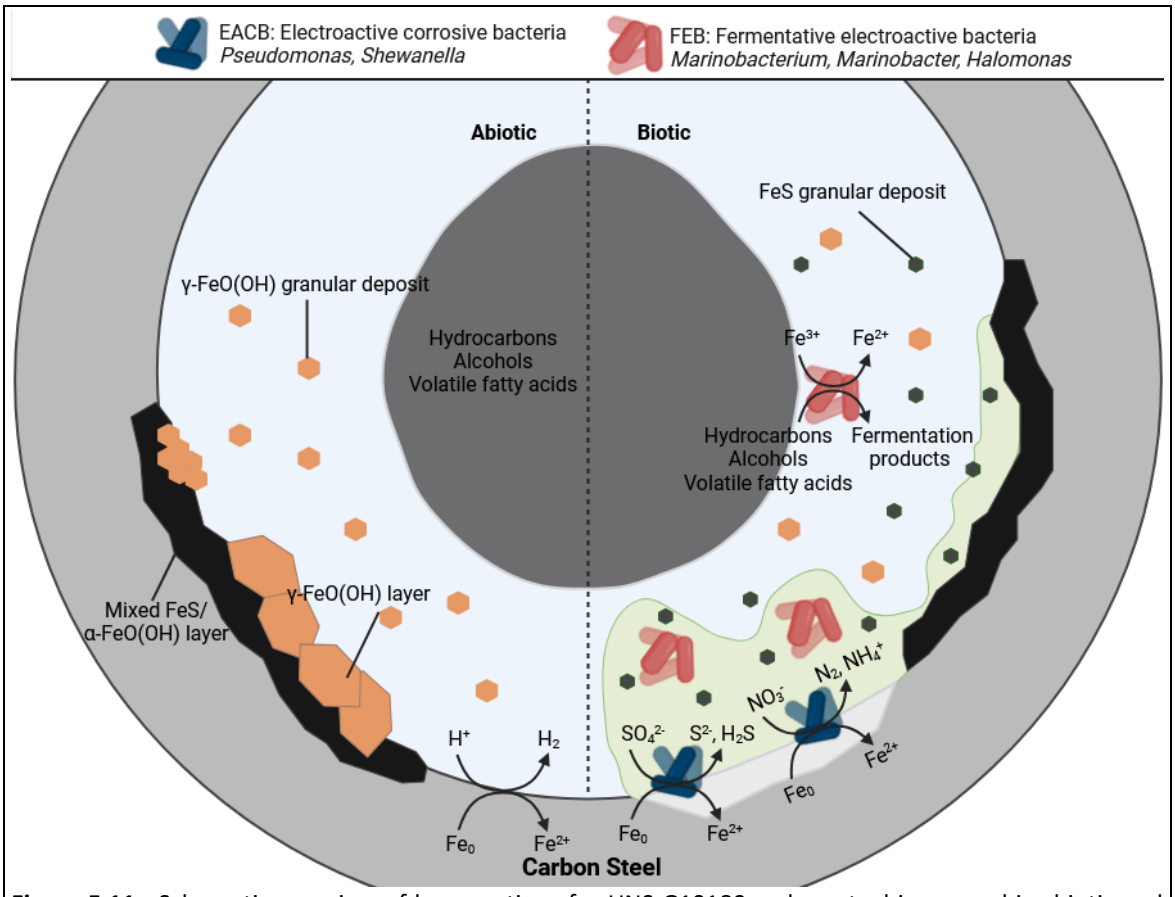

Figure 5.11. Schematic overview of key reactions for UNS G10180 carbon steel in anaerobic abiotic and biotic PW media. It is important to note that the reactions illustrated may be complementary or antagonistic processes, particularly within the heterogeneous biofilm.

For this study, the electrochemical response under biotic conditions was not too dissimilar to the abiotic condition. However, surface observations and analysis of the biofilm suggest a different scenario. The biotic surfaces were only partially covered by a black corrosion product, with the presence of a heterogeneous dark green/black biofilm. As stated earlier, the mixed-species biofilm contained *Marinobacterium*, *Malaciobacter*, *Pseudomonas*, and *Halomonas* which all contribute to biofilm formation in high salinity marine environments. They are important players in nutrient cycling within marine ecosystems and are crucial in creating microenvironments. In mixed microbial communities, these bacteria can work synergistically by altering environmental conditions [298, 299, 104, 300]. Through the production of organics and other metabolites, that can influence the redox potential or pH, they can create microenvironments which may support SO_4^{2-} and Fe^0 reduction over long-term studies. It is hypothesised that the mixed-species biofilm is acting as a diffusion barrier and providing some passivation of the metal surface. Figure 5.11

proposes possible abiotic and biotic reaction mechanisms, associated primarily with the formation of mackinawite.

Previous laboratory studies have generally found that environmental conditions that mimic offshore oilfield systems, such as salinity, temperature, nutrient levels, and fluctuating O_2 concentrations, have a profound impact on the formation, structure, and threat of corrosion from mixed-species biofilm communities on CS [302]. These studies emphasise the importance of replicating real-world offshore conditions in laboratory experiments to accurately assess and mitigate the threat of MIC in oil and gas systems. However, like *in situ* studies, there are limitations and challenges when it comes to designing laboratory studies. One of the primary challenges in these studies is accurately replicating the complex and dynamic environmental conditions found in offshore systems, such as fluctuating temperatures, pressures, and chemical compositions. Laboratory settings often simplify these conditions, which can limit the relevance of the findings to real-world applications. Many studies are constrained by time, making it difficult to observe long-term biofilm development and the full extent of MIC. Corrosion is a slow process, and short-term studies may miss critical stages of biofilm maturation and corrosion progression. Maintaining a stable and representative microbial community in laboratory settings is also challenging. In industrial environments, microbial communities are constantly evolving, and this dynamic nature is difficult to capture in a controlled environment. Laboratory studies often struggle to replicate the scale and flow conditions of actual pipelines. The differences in flow dynamics can significantly impact biofilm formation and corrosion patterns, meaning lab results may not fully translate to field conditions. Thus, designing experiments that closely mimic real-world conditions as much as possible is critical. Furthermore, long-term studies are needed to fully understand the impacts of biofilm communities on MIC in oil and gas systems.

5.4 Summary

In conclusion, by utilizing a marine sediment microbial consortium and replicating the environmental conditions of an offshore oilfield system within the laboratory, we gained valuable insights into biofilm development, community dynamics, and the potential for inducing MIC within a novel dual bioreactor protocol.

- The electrochemical response under both abiotic and biotic conditions was found to be similar. An initial conditioning film appeared to form, influencing the electrochemical properties of the steel surface. However, the PW in this study did not support rapid biofilm growth, likely due to the absence of rich carbon sources such as amino acids, peptides, and sugars.

- Mackinawite was identified as the primary corrosion product. Additionally, there were bands that may correspond to sulphur and reference iron oxide compounds, including magnetite, goethite, lepidocrocite, and hematite, observed under both conditions.
- Both conditions exhibited a moderately low uniform *CR* and limited localized pitting. Consequently, it was challenging to quantitatively assess *PD* values due to the general lack of pitting across the coupon surfaces. However, the biotic condition did display pits with a larger average area, indicative of MIC.
- Sequencing-based biofilm characterisation revealed that *Marinobacterium*, *Malaciobacter*, *Pseudomonas*, and *Halomonas* played critical roles in biofilm formation under conditions simulating an offshore oilfield system. These microorganisms are essential in nutrient cycling within marine ecosystems and contribute to the creation of microenvironments.

This study begins to bridge the gap between experimental findings and real-world scenarios involving mixed-species biofilms and MIC. The innovative dual bioreactor protocol, which leverages MLOE, enables a comprehensive understanding of initial biofilm formation and the metabolic changes occurring within the biofilm over time. Identifying and characterizing specific microorganisms under simulated environmental conditions is crucial for understanding the threat posed by MIC. If not detected and mitigated early, the microbial mechanisms can lead to significant costs. Ultimately, the aim is to enhance the effectiveness of biofilm management strategies in the industry, thereby improving sustainability.

Chapter 6 Investigating the effects of glutaraldehyde on anaerobic marine biofilm formation and microbiologically influenced corrosion of UNS G10180 carbon steel

6.1 Introduction

To control the threat of MIC, various mitigation strategies have been employed in the energy sector. These include chemical treatment with biocides [16, 199, 303, 304, 305], corrosion inhibitors [306], and surfactants [120], as well as physical treatments using paints and coatings [307], and mechanical cleaning/pigging. Additionally, adjustment of operational parameters, asset design alterations, and appropriate materials selection can also be employed to mitigate the threat of MIC. Among chemical treatments, all of which are based on the inhibition of bacterial growth and excessive biofilm formation, biocides are the most widely used [303]. However, many traditional oxidising biocides are environmentally hazardous and may exert adverse effects on aquatic species due to the release of chemical byproducts [303]. Biocidal compounds, such as glutaraldehyde and THPS, which are non-oxidising control treatments, have been widely employed to mitigate MIC [111, 112]. Yet, over time, sessile biofilm communities often develop increased tolerance to these chemical biocides [308]. Thus, there has been an increase in the development of novel eco-friendly biocidal compounds over recent years [309, 310]. Understanding not only how these chemicals interact at the biofilm/metal interface where corrosion-promoting species drive microbial corrosion mechanisms, but also understanding how they are degraded, what chemical byproducts they produce, and how they subsequently interact with the environment is critical when trying to understand efficacy and improve sustainability.

Whilst the use of traditional biocides may initially be effective at reducing microbial populations and slowing the progression of MIC, through disrupting biofilm formation and microbial metabolic activity, the use of these biocides often results in the development of enhanced biofilm chemical tolerance, undermining their long-term effectiveness. This enhanced tolerance can be due to factors like the protective nature of the biofilm EPS, genetic adaptation of the microbial community, and the presence of resistant species within the mixed-species biofilm [311]. And although biofilms are ubiquitous, studies have shown that the structure, composition, and spatial

distribution of biofilms in different locations, even in the same environmental niche, are different, and their corrosion behaviour is also different [312, 313]. This is because MIC is the result of the joint action of different microorganisms. Within a mixed-species biofilm, microorganisms will exhibit different corrosion behaviours compared to single-species biofilms [309]. Thus, understanding biofilm formation, the spatial community dynamics within a mixed-species biofilm, and what synergistic and/or antagonistic relationships are present is fundamental.

The biofilm structure can affect the diffusion of antimicrobial compounds through the stratified biofilm layers, thereby reducing the concentration of antimicrobial compounds reaching the cells at the bottom of biofilms at the metal interface, which are often the corrosion-promoting species [16]. Therefore, these cells will be exposed to sublethal concentrations of biocidal compounds and will have sufficient time to switch on the expression of antimicrobial-resistant factors and antimicrobial-degrading enzymes [16, 314]. Biocides frequently fail to completely eradicate biofilm communities, leading to the persistence of microbial populations, as the energy sector commonly uses a cyclic biocide treatment protocol [118]. These residual biofilm communities can then regenerate when there is no biocidal treatment and continue to drive microbial corrosion mechanisms. Additionally, the efficacy of biocides can vary significantly depending on the starting composition of the mixed-species biofilm. As different biocides have different modes of action. Moreover, some microbial species within a mixed-species biofilm may be resistant to biocides than others. There are diverse strategies which microorganism can employ to enable survival. These include efflux pumps, enzymatic degradation, modification of membrane permeability, QS and horizontal gene transfer to name a few. Therefore, despite biocidal treatment, corrosion can persist due to the resilience and adaptability of microbial communities within mixed-species biofilms.

Despite the widespread application of biocides, there is limited research which investigates the efficacy of such chemicals against mixed-species biofilms [16, 303]. Whilst there are many studies which evaluate the antimicrobial efficacy of biocides against single-species microorganisms [199, 315, 316, 317]. Sharma *et al.* demonstrated that glutaraldehyde alone was the most ineffective biocide tested against *D. ferrophilus* IS5, a model SRB known to utilise electrons directly from metal. Whereas benzalkonium chloride (BAC) was the most effective biocide in preventing biofilm formation and pitting on the CS coupons [199]. However, they noted that MIC in the natural environment is due to the action of a mixed-species biofilm. And while pure microbial strains can provide insight to better understand MIC mechanisms, ultimately biocidal efficacy must be validated against mixed-species biofilms [199]. Salgar-Chaparro *et al.* stressed the importance of assessing mixed-species biofilms under different nutrient conditions to understand the effectiveness of biocide treatments [16]. Their results demonstrated that thicker biofilms, grown

under continual nutrient replenishment, exhibited greater survival against a glutaraldehyde treatment compared to a biofilm grown under batch conditions without nutrient replenishment [16]. In this instance, it may be appropriate to enhance the biocide treatment with an adjunctive strategy. The efficacy of an adjunctive strategy using a combination of phenolic and QACs has been reported against a mixed-species biofilm [303]. Chang *et al*. demonstrated a strong antimicrobial effect against a mixed-species biofilm isolated from the environment. The combination treatment demonstrated a synergistic effect to reduce bacterial growth compared to individual treatments [303]. These types of studies highlight the importance of evaluating the efficacy of different biocide treatments against mixed-species biofilms.

This study further proposes a targeted approach to MIC mitigation by utilising a novel dual bioreactor protocol to evaluate and optimise biocidal treatment strategies. By utilising MLOE [145], the protocol incorporates a multi-disciplinary approach to gain a holistic understanding of biofilms, MIC, and biocidal efficacy. By refining biocidal application in a controlled environment and closely mimicking environmental conditions using a mixed-species biofilm, this approach aims to overcome the challenges of biofilm tolerance, offering a more sustainable and effective solution to mitigating the threat of MIC.

6.2 Results

Over the initial three-day batch phase, the abiotic media had no apparent visual changes, and the coupons maintained the silver-grey metallic lustre of the CS. It was not until the flow of fresh media was started on day 4, that any visual changes could be observed. The sterile abiotic reactor ASW media became reddish-brown in colouration with increased turbidity after the first week. Conversely, after inoculation of the biotic reactor ASW media, a black surface film was present on the steel coupons on day 1. At the end of the initial three-day batch phase there were low level of turbidity. After the flow of fresh ASW media was started on day 4, the ASW media was completely covered with black particulates and had a very high level of turbidity. On day 28, the biotic reactor was black/brown in appearance. Upon dismantling of the reactors on day 28, and retrieval of the coupon rods, there was a significant difference in the coupon appearances, see Appendix E Figure E.1. The abiotic surfaces were covered in a reddish-brown corrosion product. Whilst the biotic surfaces were generally also covered in a reddish-brown corrosion product, underneath this was a black deposit more closely adhered to the surface.

Sulphide microsensor. Figure 6.1 shows the aqueous H_2S concentrations monitored for the biotic anaerobic nutrient-enriched ASW media over the test duration. Unfortunately, whilst

calibrating the microsensors prior to starting the experiment, the second microsensor was discovered to be damaged and not in working order. Consequently, only one microsensor was used for this study. For the biotic condition, the H_2S concentration generally peaked prior to being dosed with glutaraldehyde, with a maximum concentration of 60 µmol L^{-1} measured on day 21. After each dose of biocide (every third day, starting on day 4) there was a decrease in the H_2S concentration. *DO* concentrations measured on day 28 were between 0.16 and 0.88 ppm in the 10 L media containers, 3.3 ppm in the abiotic and 0.2 ppm in the biotic reactor. The pH was not measured on completion of the experiment.

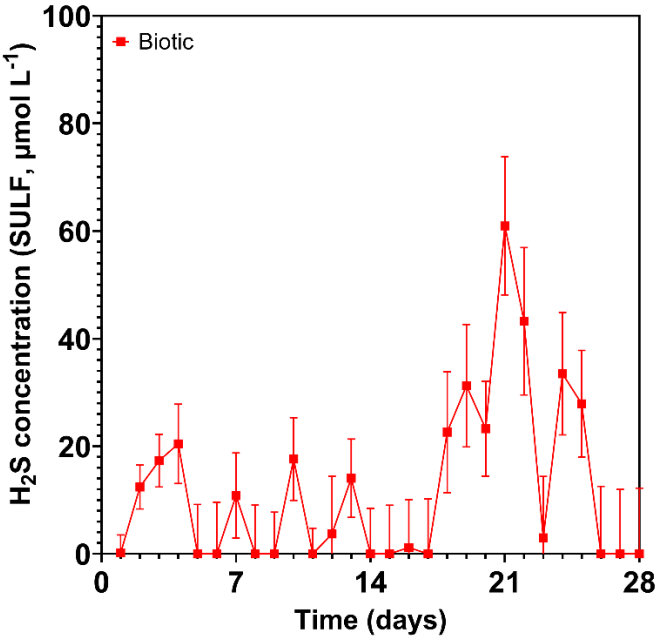

Figure 6.1. Aqueous sulphide measurements (*SULF*, µmol L^{-1}) for the biotic condition over 28 days (nb. measured the anaerobic nutrient-enriched artificial seawater media dosed bi-weekly with glutaraldehyde *in situ* adjacent to corroding UNS G10180 carbon steel).

Carbon steel surface analysis. Appendix E Figure E.2 shows the CS surfaces on day 0. Appendix Table E.3 summarises the quantitative surface roughness profiles on both day 0 and day 28. Figure 6.2 shows the cleaned CS surfaces after 28 days, with biofilms and corrosion products removed to reveal the morphology of the surface degradation and to facilitate corrosion assessment. Surface profilometry revealed that there were low levels of uniform or localised pitting corrosion present for both the abiotic and biotic condition. The abiotic average pit depths were 8 µm, with an average pit area of 2308 μm^2 for any classified pits. The biotic average pit depths were 9 µm, with an average pit area of 8684 μm^2 for any classified pits. However, only 2 – 3 % of the analysed surfaces observed pitting. Again, for this study a pit was classified as having a depth greater than 5 µm and an area greater than 650 μm^2 [153].

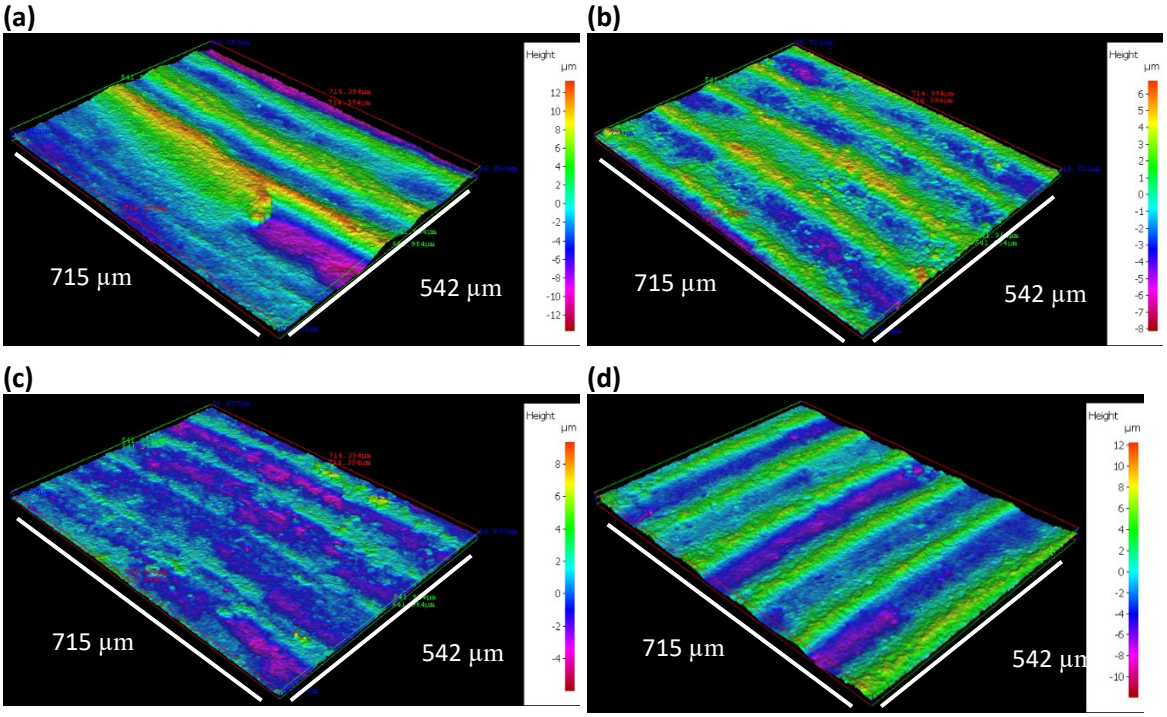

Figure 6.2. Three-dimensional optical surface profilometry of the cleaned UNS G10180 surfaces at day 28. AR coupons for: **(a,b)** abiotic and **(c,d)** biotic conditions, after exposure to anaerobic nutrient-enriched artificial seawater media dosed bi-weekly with glutaraldehyde for 28 days.

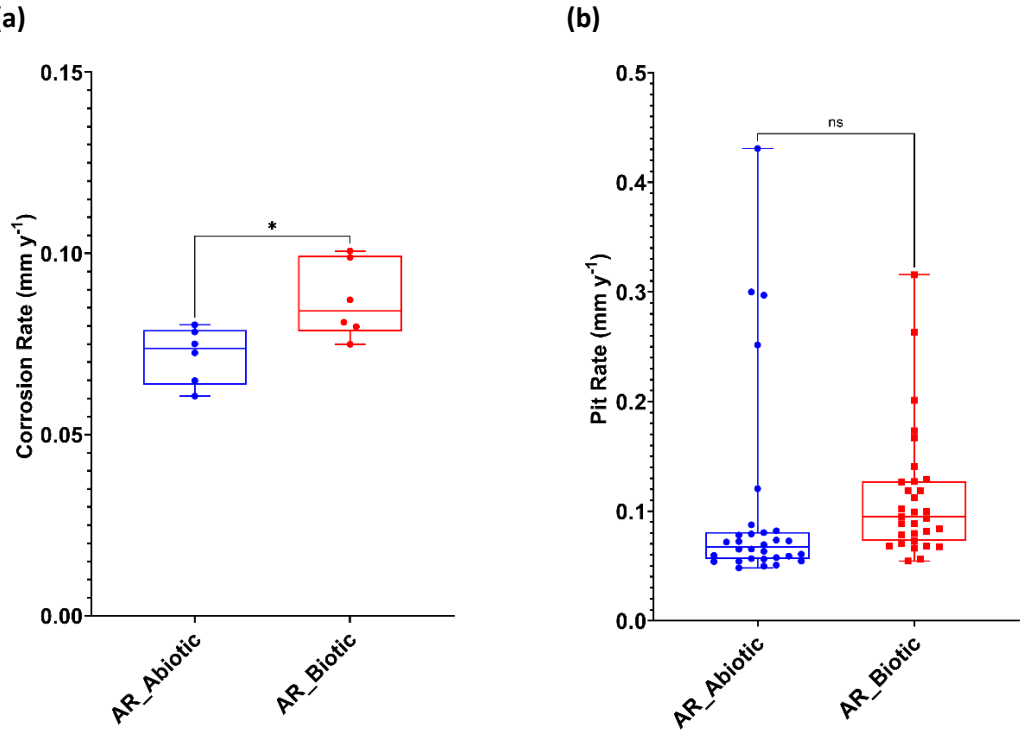

Figure 6.3. Abiotic and biotic corrosion performance after exposure to anaerobic nutrient-enriched artificial seawater media dosed bi-weekly with glutaraldehyde for 28 days: **(a)** corrosion rate via gravimetric analysis and surface profilometry assessed ($P < 0.05$) and **(b)** pit rate, for the AR coupons.

Figure 6.3a provides an evaluation of the CS coupons *CR*. For the abiotic condition, there was a significantly lower *CR* when compared to the biotic condition. According to the NACE SP0775-2023 assessment criteria, there was a moderate *CR* (between 0.025 and 0.12 mm y^{-1}) in both the abiotic and biotic reactors (Figure 6.3a). Similarly, there was a low *PR* (<0.13 mm y^{-1}) in both the abiotic and biotic reactors (Figure 6.3b) [170].

Further analysis of the surface profilometries in Figure 6.2, allowed a quantitative determination of the *PR* Figure 6.3b of the CS coupons. For this study, it was not possible to quantitatively determine *PD* values, due to the general absence of pitting across the coupon surfaces.

Corrosion product analysis. Figure 6.4 shows SEM-EDS elemental mapping of the UNS G10180 CS surfaces for both the abiotic and biotic conditions. The images of corrosion products and biofilms attached to the metal samples demonstrate the heterogeneity of distribution over the surface. Both conditions exhibited similar levels of surface coverage. The SEM-EDS elemental maps are shown in Figure 6.4b – d. The major elements detected in coupons exposed to all conditions were Fe, S, and O. Corroded areas of all coupons were mainly covered by Fe and O, with heterogeneous distribution of S. A cross-sectional image of the corrosion products was not performed.

Additional analysis of the corrosion products using Raman spectroscopy are shown in Figure 6.5. According to Raman bands of reference corrosion products in previous papers [290, 291, 292], the corrosion products are identified to be primarily mackinawite (bands 208, 282 cm^{-1}) for both the abiotic and biotic condition. There were also additional bands which may be attributed to sulphur, as well as reference iron oxide compounds such as magnetite, goethite, lepidocrocite, or hematite. The composition of this black compact layer was identified at mid-strong bands 250, 380, 1307 cm^{-1} associated with lepidocrocite. Additionally, bands at 298, 399, 481, 554, 675 and 1002 cm^{-1} have previously been shown to be associated with goethite, whilst bands at 222, 244, 298, 501, 615 and 1318 cm^{-1} are associated with hematite. Magnetite has previously been shown to be associated with bands at 675 and 550 cm^{-1} [290, 291, 292]. The coverage of the metal sample with a black precipitate was indicative of the successful growth of corrosion products film containing FeS compounds. The Raman spectrum of the sample is in good agreement with literature spectra attributed to mackinawite. After aging the products in air, a change in their colour from black to rust-red became visible. This is a clear indication for the oxidation of the initial products.

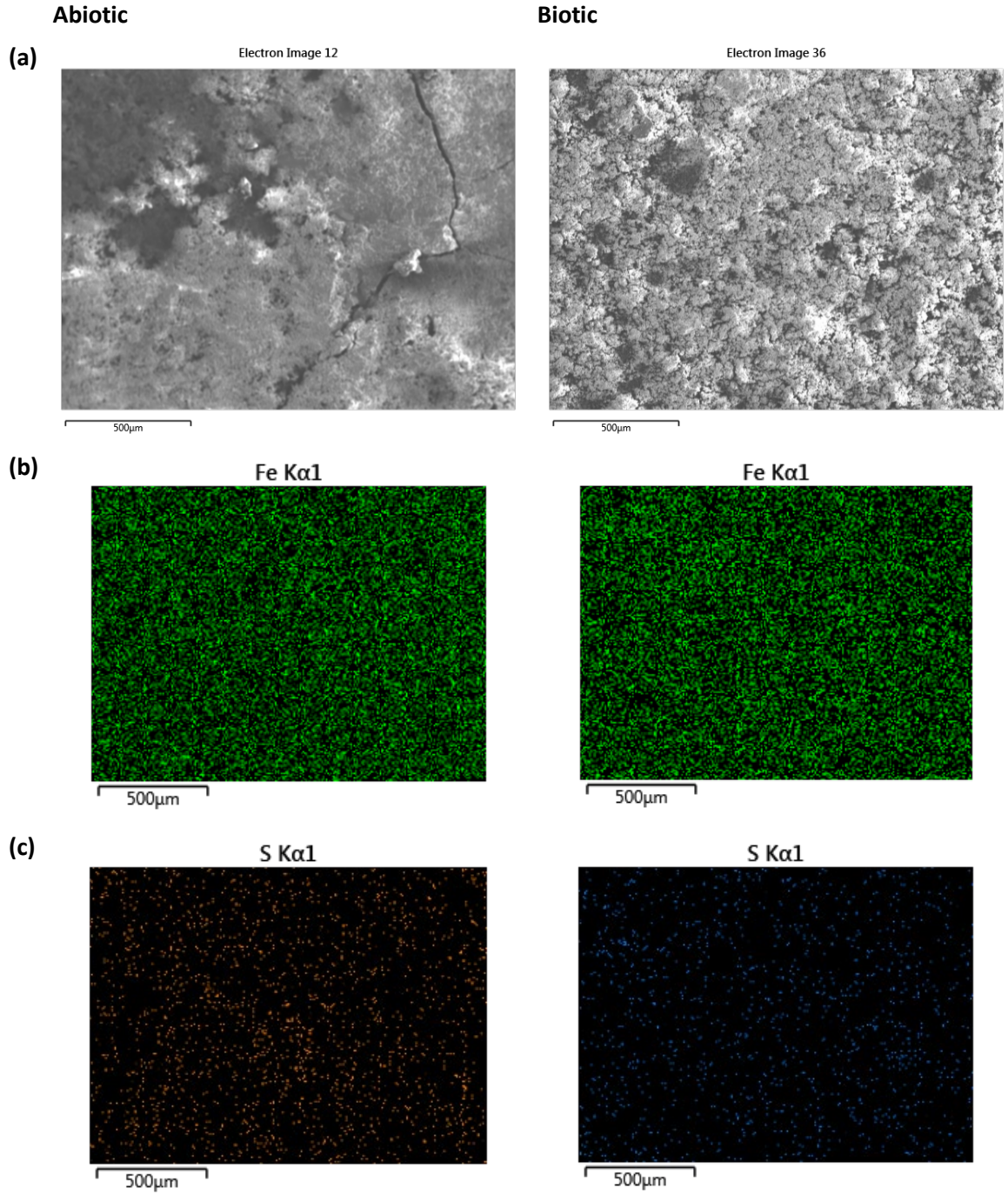
Abiotic
Biotic
(a)
Electron Image 12
Electron Image 36
500µm
500µm
(b)
Fe Kα1
Fe Kα1
500µm
500µm
(c)
S Kα1
S Kα1
500µm
500µm

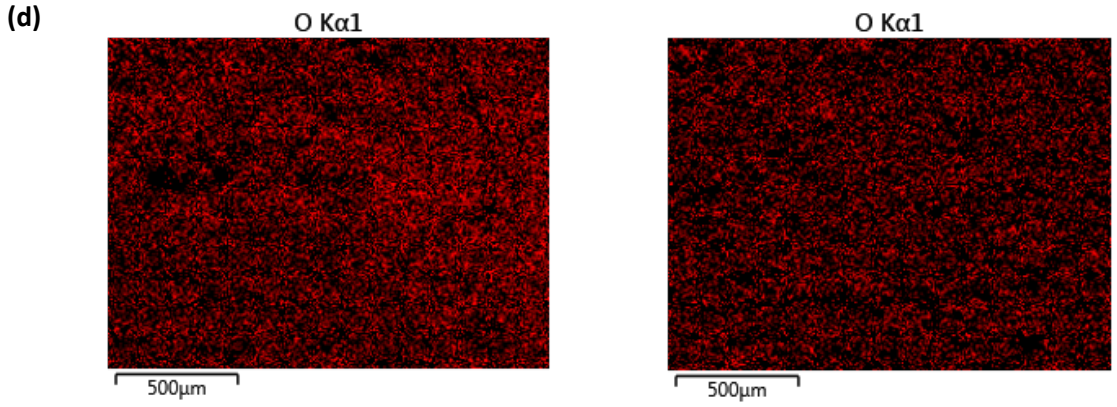

Figure 6.4. SEM-EDS elemental mapping of the UNS G10180 carbon steel, AR surfaces, after exposure to anaerobic nutrient-enriched artificial seawater media dosed bi-weekly with glutaraldehyde, taken on day 28. **(a)** SEM image; **(b)** iron map; **(c)** sulphur map; **(d)** oxygen map.

(a) - Abiotic

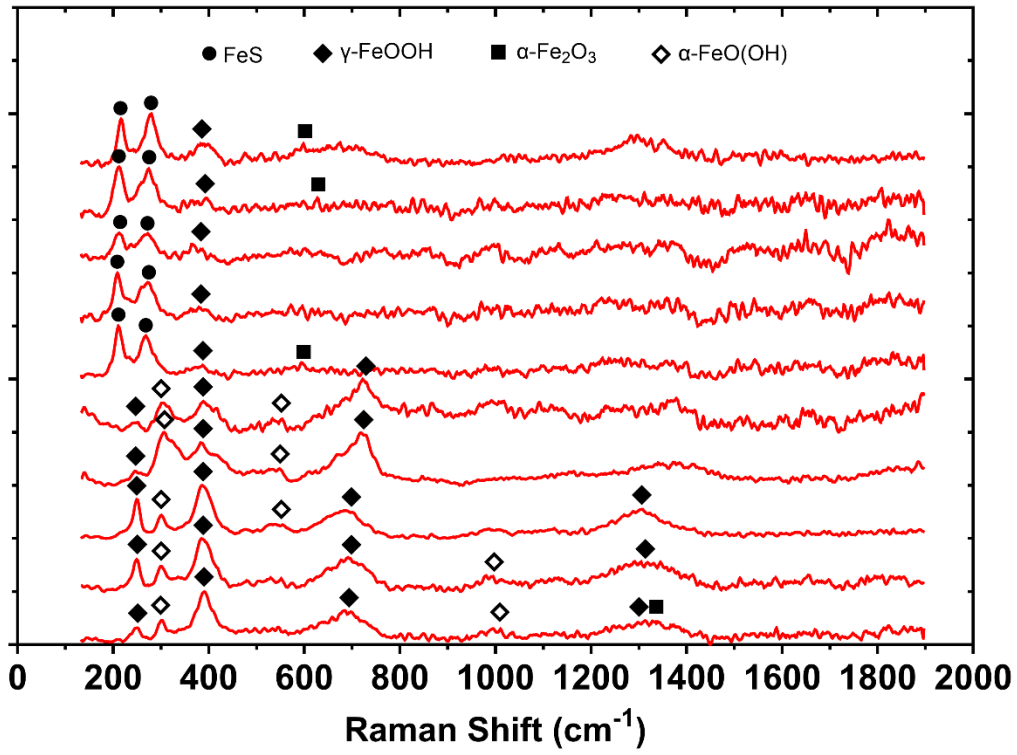

(b) - Biotic

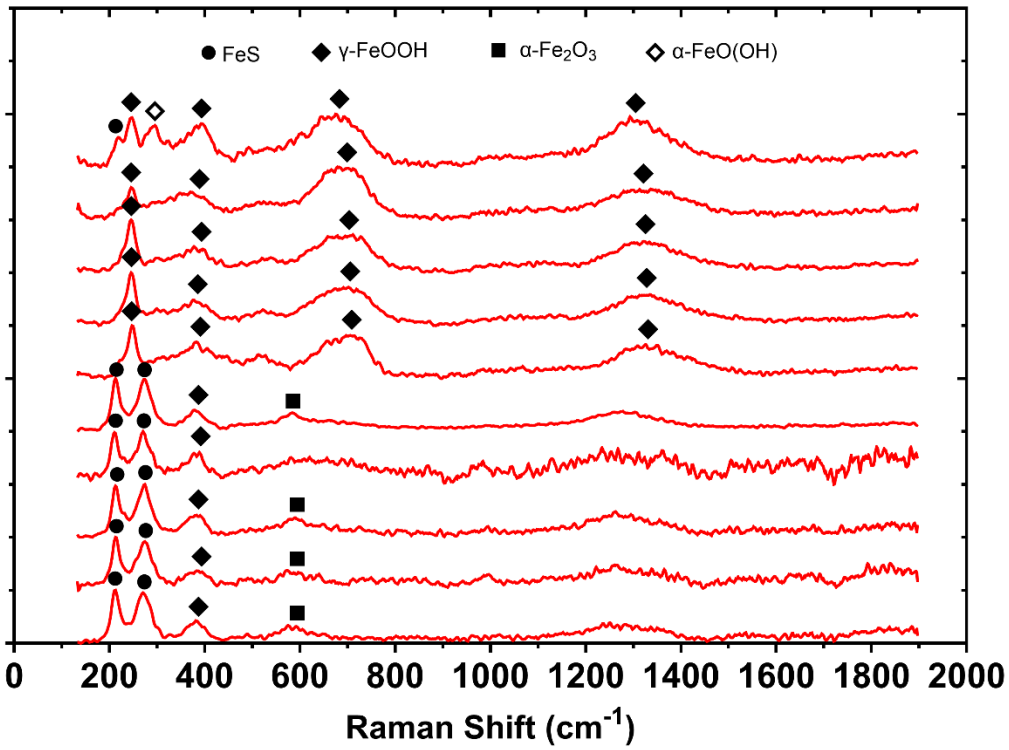

Figure 6.5. Raman spectra of the UNS G10180 carbon steel surfaces after exposure to anaerobic nutrient-enriched artificial seawater media dosed bi-weekly with glutaraldehyde, taken on day 28. For the AR **(a,b)** abiotic and; **(c, d)** biotic condition.

Electrochemical measurements. Figure 6.6 shows the changes in E_{corr} and R_p between the abiotic and biotic anaerobic nutrient-enriched ASW water media, for the UNS G10180 CS coupons. For the abiotic condition, Figure 6.6a, there was generally a pseudo-steady state for the E_{corr} up until day 25. Here, there was a swift increase of +0.100 V. This may be attributed to the presence of a conditioning film (i.e., an adsorbed organic layer) and the formation of inorganic corrosion product layer. Conversely, for the biotic condition, there was generally a gradual increase in the E_{corr} over the 28 days. Throughout the study, there were generally electronegative shifts after each dose of biocide. The potentials for both abiotic and biotic in the latter stages (Day 28) were generally similar and ranged between – 0.590 V and – 0.610 V *vs*. Ag/AgCl.

In Figure 6.6b the LPR derived R_p remained low at approx. 600 Ω cm^2 for the sterile abiotic condition, indicative of a uniform corrosion across a porous corrosion film. There was a swift drop after day 25 to approx. 100 Ω cm^2. Similarly, for the biotic condition, the R_p remained low at approx. 100 Ω cm^2. The pioneering bacterial attachment/colonisation was difficult to detect for this study. However, biofilm formation and growth kinetics will lead inevitably to a more complex electrochemical response.

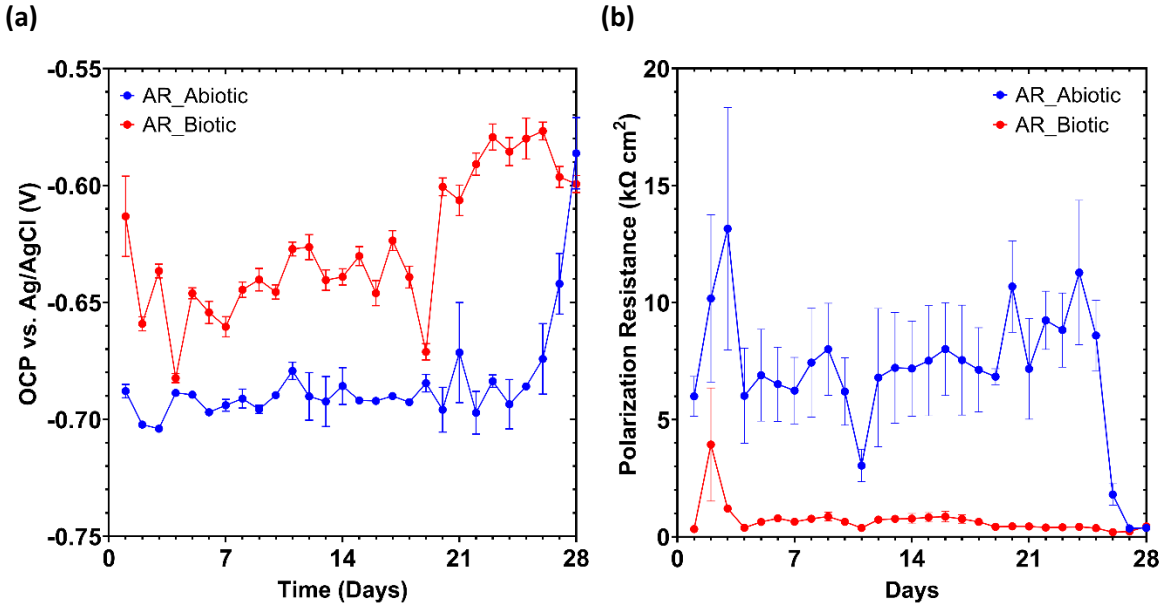

Figure 6.6. LPR data for UNS G10180 carbon steel: **(a)** open-circuit potentials and **(b)** polarisation resistance in anaerobic nutrient-enriched artificial seawater media dosed bi-weekly with glutaraldehyde (abiotic and biotic conditions), for AR coupons (data points represent mean ± standard deviation, *n* = 6). Reactor stirrer at 50 rpm.

Figure 6.7 shows the EIS data for UNS G10180 CS in the anaerobic nutrient-enriched ASW media presented in three forms: Nyquist, Bode phase angle and Bode impedance modulus plots. The sterile abiotic condition on Day 1 typifies an electrochemical response for the formation of a porous interface, with diffusion of soluble electroactive species across an organic conditioning film [207] and nascent inorganic corrosion product layer.

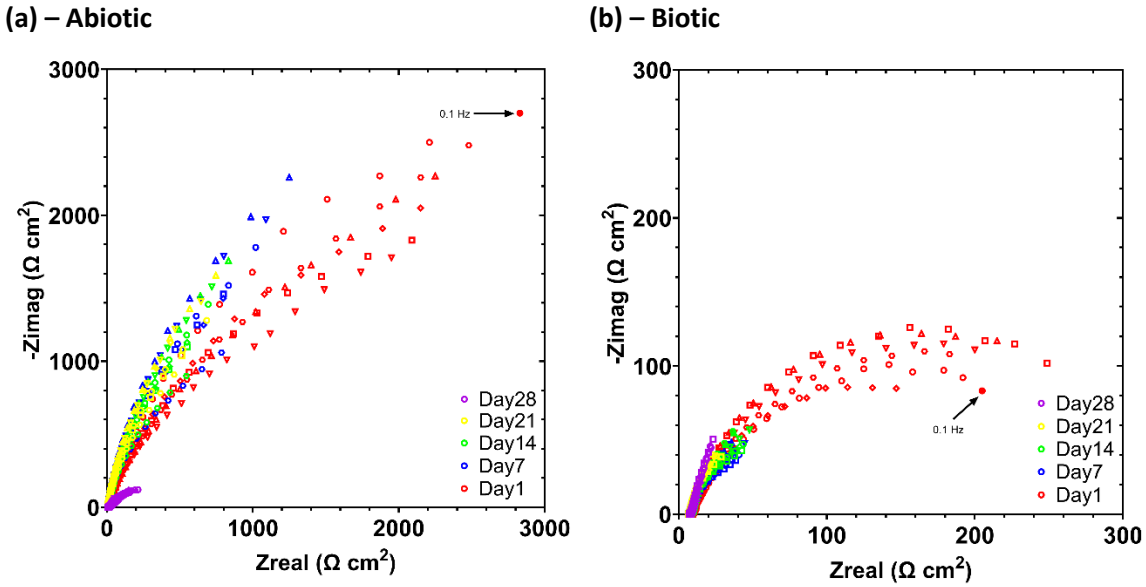

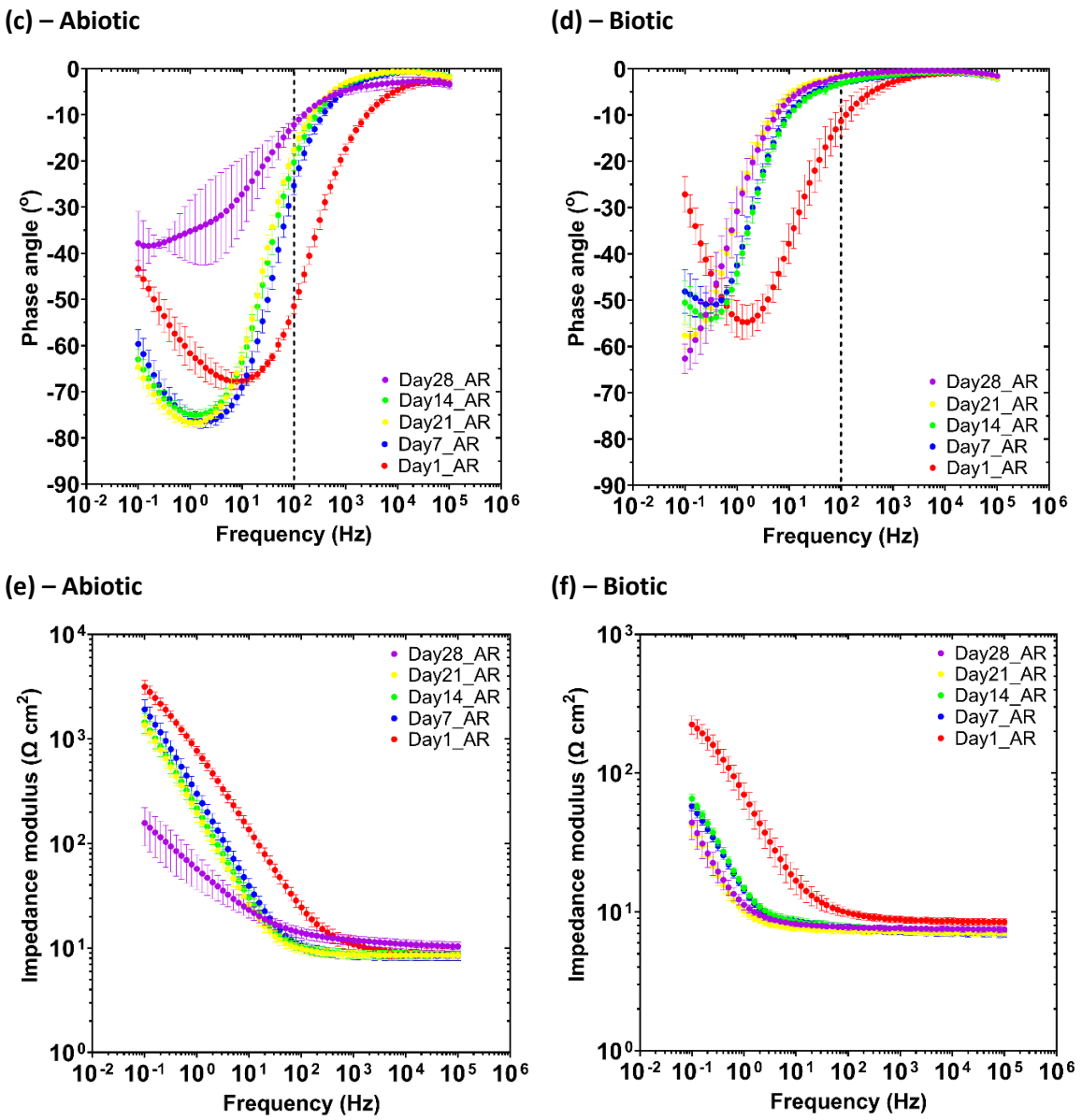

Figure 6.7. EIS data for UNS G10180 carbon steel in anaerobic nutrient-enriched artificial seawater media dosed bi-weekly with glutaraldehyde at OCP: **(a, b)** Nyquist, **(c, d)** Bode phase angle (θ *vs.* f), and **(e, f)** Bode impedance modulus ($|Z|$ *vs.* f) over 28-days. (n = 6). Reactor stirrer at 50 rpm.

The diffusive behaviour is associated with linear features having a roughly 45° slope (a Warburg impedance response) and phase angles close to 45° in low frequency region (10^{-2} – 10^{0} Hz), see Fig. 6.7a and 6.7c. At Day 28, a depressed Nyquist semicircle and phase angles tending towards zero are evident, indicative of a more prominent resistive component operating within the low frequency region. Subsequently, the abiotic impedance spectra shift towards lower frequencies (10^{-2} – 10^{0} Hz), with a combined diffusive/resistive behaviour. Equally, the biotic condition had a consistently uniform EIS response over the 28 day test, with only minor variation in the spectra attributed to the biocide. Notably, there are no discernible Nyquist semicircles (Fig. 6.7b). Here a wider low frequency region (10^{-1} – 10^{2}) is likely to be subject to a greater influence

of adsorption processes, associated with the adhesion of the pioneering bacteria on a conditioning film [215, 216] and biofilm formation.

The EIS spectra were fitted using an ECM shown in Figure 2.4. Both the abiotic and biotic data generally had a good fit, with the quantitative fitting results shown in Appendix E Table E.5. For the abiotic control, there is a capacitive behaviour over the first three weeks, with a diffusive behaviour over the final week in the film layer (reflecting ion adsorption). Whilst there was a diffusive behaviour in the double layer during the first and final week, which reflects charge transfer, due to the formation of corrosion products (rust, porous oxide layer). The exponent parameter in the double layer reflects a non-ideal capacitance, which is indicative of resistive and inductive parasitics, because of a more prominent resistive component. There were no significant changes in R_{ct}. R_{film} had a high error value, so not much could be determined from this.

For the biotic condition, there was a diffusive behaviour over the first three weeks, with a capacitive behaviour over the final week in the film layer. Conversely, there was a capacitive behaviour over the first three weeks, with a diffusive behaviour over the final week in the double layer. There are no significant changes in the R_{ct} in the double layer over time. The exponent parameter for the film layer is greater than 0.8 during the final week, which indicates a non-ideal capacitance response. This is true for the first three weeks in the double layer. However, during the final week of the experiment, the exponent parameter is closer to 0 for the AR coupons in the double layer, which indicates a strong diffusive behaviour. The ECM and EIS both have general agreement with the LPR data.

Figure 6.8 shows the potentiodynamic polarisation curves for UNS G10180 CS for the abiotic and biotic reactors in anaerobic nutrient-enriched ASW media after 28 days. Table 6.1 shows the corrosion parameters obtained from the polarisation curves. From the Tafel slopes, there is limited cathodic densities for the cathodic behaviour (reduction) for both the abiotic and biotic conditions. This phenomenon is caused by the rate of diffusion of ions being limited. This can be attributed to an inorganic corrosion film layer and is linked to the predominant HER under anaerobic conditions. Additionally, the anodic Tafel slopes (oxidation) are similar. Overall, the abiotic condition had a higher j_{corr} compared to the biotic condition. This is consistent with a more uniform corrosion morphology. Similarly, the sterile abiotic condition had a more electropositive E_{corr} when compared to the biotic condition. The polarisation results corroborate the LPR and EIS data.

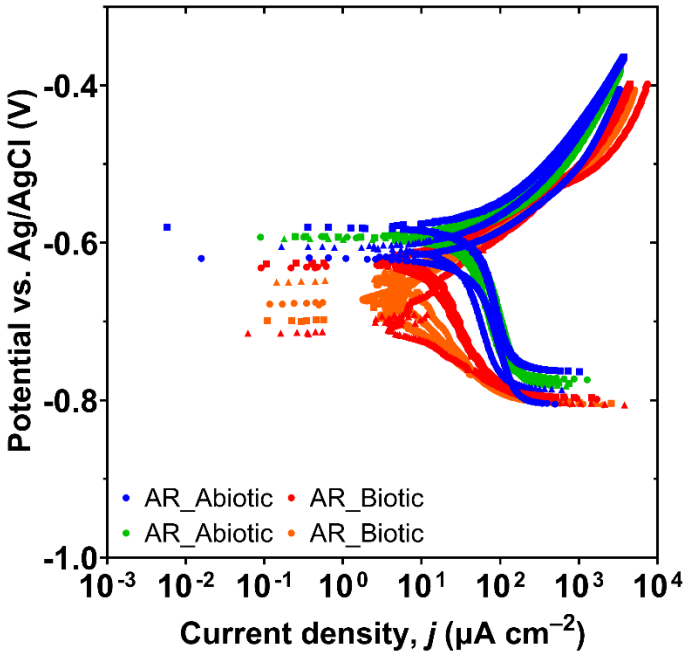

Figure 6.8. Potentiodynamic polarisation curves for the abiotic and biotic AR, UNS G10180 carbon steel coupons, at ambient temperature after exposure to anaerobic nutrient-enriched artificial seawater media dosed bi-weekly with glutaraldehyde for 28 days. Scan rate of 0.5 mV s^{-1} and reactor stirrer at 50 rpm.

Table 6.1. Fitted electrochemical parameters from polarisation curves; comparison between the abiotic and biotic AR, UNS G10180 carbon steel coupons, after exposure anaerobic nutrient-enriched artificial seawater media dosed bi-weekly with glutaraldehyde for 28 days.

	Coupons	j_{corr} / µA cm^{-2}	E_{corr} *vs.* Ag/AgCl / V	β_a (mV dec^{-1})	β_c (mV dec^{-1})
Abiotic	AR	0.169 ± 0.035	-599 ± 14	160 ± 6	-
Biotic	AR	0.044 ± 0.036	-663 ± 35	113 ± 12	-

Biofilm characterisation. CLSM with differentiation of live and dead biofilm cells was performed and the images can be seen in Figure 6.9. The heterogeneous biofilm distribution over the surface of the CS coupons did not allow measurements of the maximum biofilm thickness. Therefore, the thickness of biofilms was not determined. From the images captured, there was a live/dead cell ratio of approximately 41% live to 59% dead.

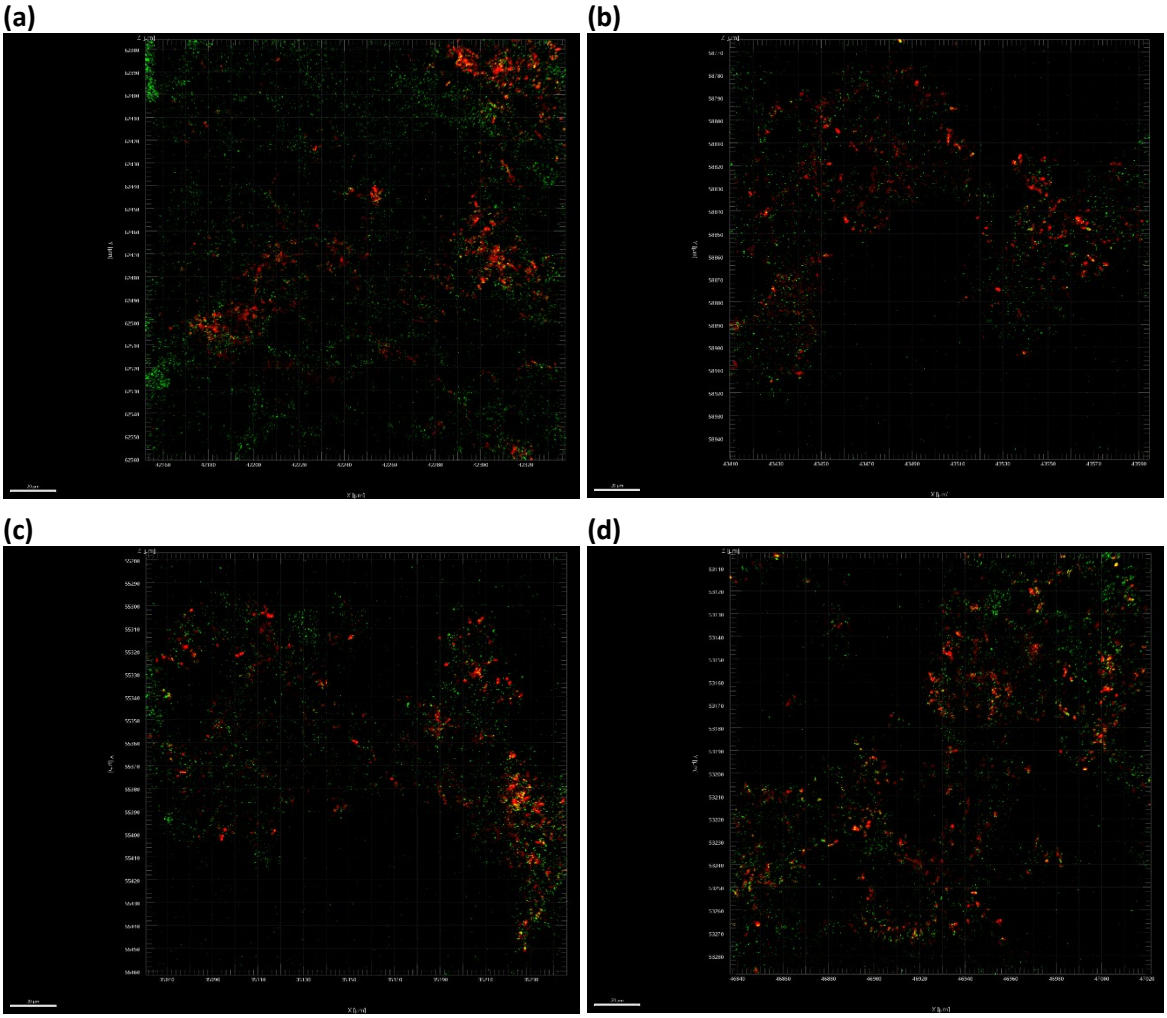

Figure 6.9. Confocal microscopy of biofilm formed over UNS G10180 carbon steel surfaces for AR **(a, b)** biotic coupon sample 1; **(c, d)** biotic coupon sample 2, after exposure anaerobic nutrient-enriched artificial seawater media dosed bi-weekly with glutaraldehyde for 28 days.

Active microorganism evaluation of the environmental marine sediment, the initial and final biotic nutrient-enriched ASW media planktonic samples (Day 0 and Day 28), and the biotic AR biofilm, was undertaken via 16S rRNA amplicon sequencing with two target region, V3-4 for bacteria and archaea. A total of 3,586,285 high-quality sequences were obtained after bioinformatics processing of the raw reads. From these, 97% was classified for the sediment sample with 99.99% classified for the Day 0 planktonic sample and 100% classified for the Day 28 planktonic sample and AR biofilm sample. These sequences were taxonomically classified into microbial genera. The top 25 microbial genera are presented in Appendix E Table E.6 in the supplemental material. Figure 6.10 summarises the sequencing data, showing a PCA (a) and a stacked bar plot (b) illustrating the relative abundances for the top 25 genera. Most genus had low relative abundances less than 2%. The dominant genera included *Sulfurovum*, *Candidatus Prometheoarchaeum*, *Candidatus Methanoplasma*, *Desulfosarcina*, *Desulfuromonas* and *Thiohalobacter*.

(a)

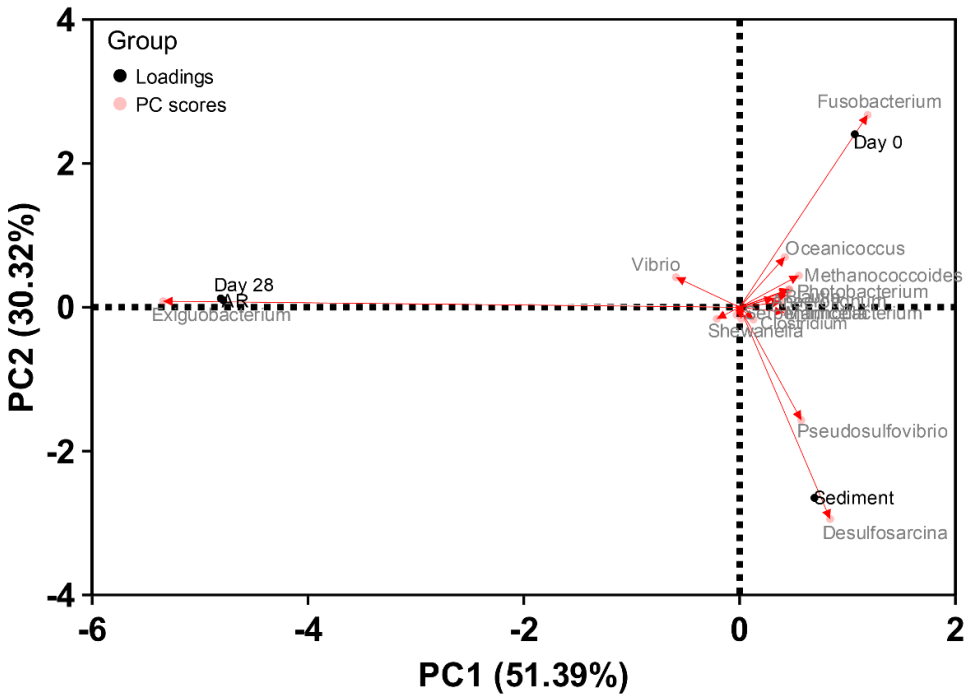

(b)

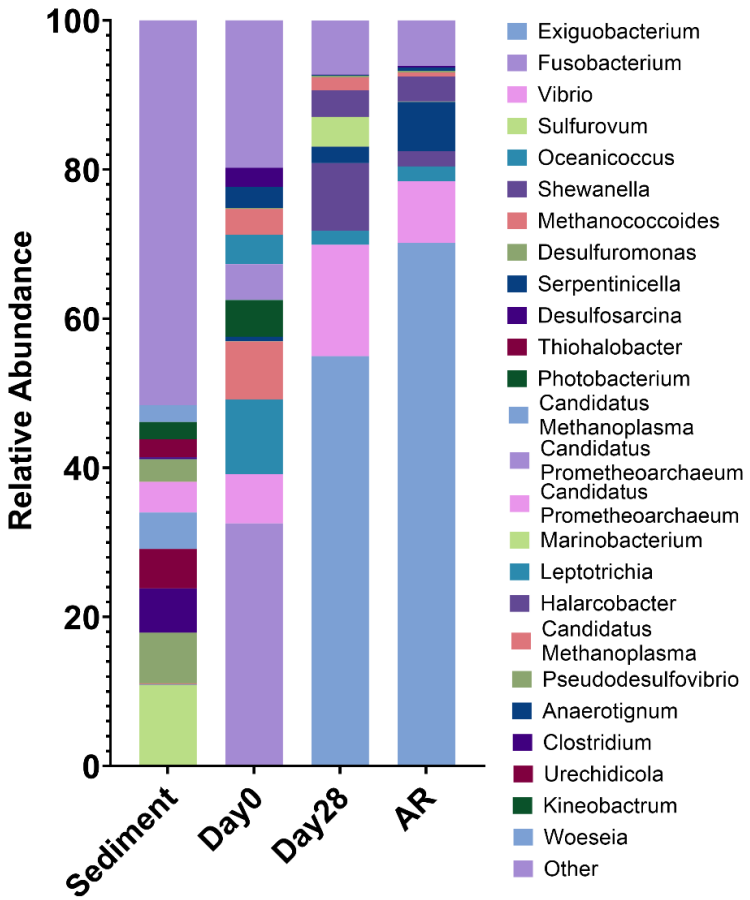

Figure 6.10. Principal Component Analysis biplot **(a)**; Microbial community. The results show the mean relative abundances of microbial communities classified at the genus level, for the top 25 genera, from 16S

rRNA amplicon sequencing **(b)**; for environmental marine sediment, Day 0, and Day 28 planktonic samples, and AR biofilms, after exposure anaerobic nutrient-enriched artificial seawater media dosed bi-weekly with glutaraldehyde for 28 days.

Interestingly, there were relatively high numbers of archaea in the sediment sample compared to the other samples. The sediment sample had a negative Spearman correlation coefficient (Appendix E Figure E.7) with the other samples which was attributed to changes in conditions such as temperature and media composition from the natural marine environment. There was much less diversity in the Day 0 sample, with *Sulfurovum*, *Candidatus Prometheoarchaeum*, *Candidatus Methanoplasma*, and *Thiohalobacter* all exhibiting lower relative abundances (<1%). Whilst genera from *Fusobacterium*, *Vibrio*, *Oceanicoccus*, and *Methanococcoides* made-up approximately 55% of the relative abundance. Genera from *Photobacterium*, *Blautia*, *Leptotrichia*, *Maridesulfovibrio*, *Anaerotignum* and *Clostridium* made-up another approximately 20% of the relative abundance. Again, the Day 0 planktonic sample had mostly negative Spearman correlation coefficients with the other samples. After 28 Days, there was a substantial shift in the microbial composition, with substantially lower abundances of methanogenic species. *Exiguobacterium*, *Vibrio*, and *Shewanella* were the dominant genera making up approximately 80% of the relative abundance. The Day 28 planktonic sample had a Spearman correlation coefficient of -0.47 with the sediment sample, 0.15 with the Day 0 planktonic sample and 0.88 with the AR biofilm sample. *Sulfurovum*, *Candidatus Prometheoarchaeum*, *Candidatus Methanoplasma*, and *Thiohalobacter* which were the dominant genera from the sediment sample all had lower relative abundances (<1%) in the AR biofilm sample and Day 28 planktonic sample. The dominant genera included *Exiguobacterium*, *Vibrio*, and *Serpentinicella* making up approximately 85% of the relative abundance. *Shewanella* also maintained a relative abundance of 2%. There were no methanogenic archaea in the biofilm sample.

The microbial activity was determined by the ATP concentrations (dissolved, dATP) in the bulk fluid, see Figure 6.11. The ATP assay did not measure any ATP from the biofilm sample. The biofilm may have been removed through the activity of glutaraldehyde. For the biotic nutrient-enriched ASW media (bulk fluid), there was a significant change ($P < 0.05$) in the dATP concentration when comparing Day 0 and Day 28, with dATP values of on the order of 10 pg mL^{-1}. As expected, there was a significantly greater ATP concentration for the biotic compared to the abiotic reactor.

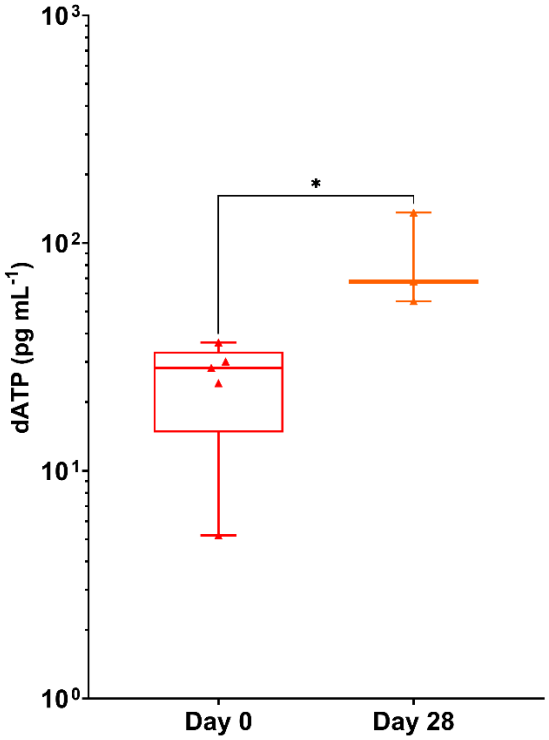

Figure 6.11. Dissolved ATP (dATP) concentrations comparing the anaerobic nutrient-enriched artificial seawater media dosed bi-weekly with glutaraldehyde, taken on Day 0 and Day 28 ($P < 0.05$).

6.3 Discussion

This current study is focused on understanding the efficacy of a biocide, glutaraldehyde, at mitigating MIC caused by a mixed-species biofilm cultured from a littoral marine sediment. The frequency and dosage concentration were determined by reported best practices within the offshore oilfield industry. Figure 6.12 provides an illustration of the proposed corrosion mechanisms for the abiotic condition during the initial stages, as they evolved over time during this present study. Overall, the primary corrosion mechanisms under the abiotic condition were attributed with the formation of iron oxide corrosion products, associated with the reddish-brown film layer observed on the coupon surfaces. These were identified as magnetite, goethite, lepidocrocite, or hematite. Lepidocrocite has been identified to form in the outer layer on CS coupons permanently immersed in natural seawater [239].

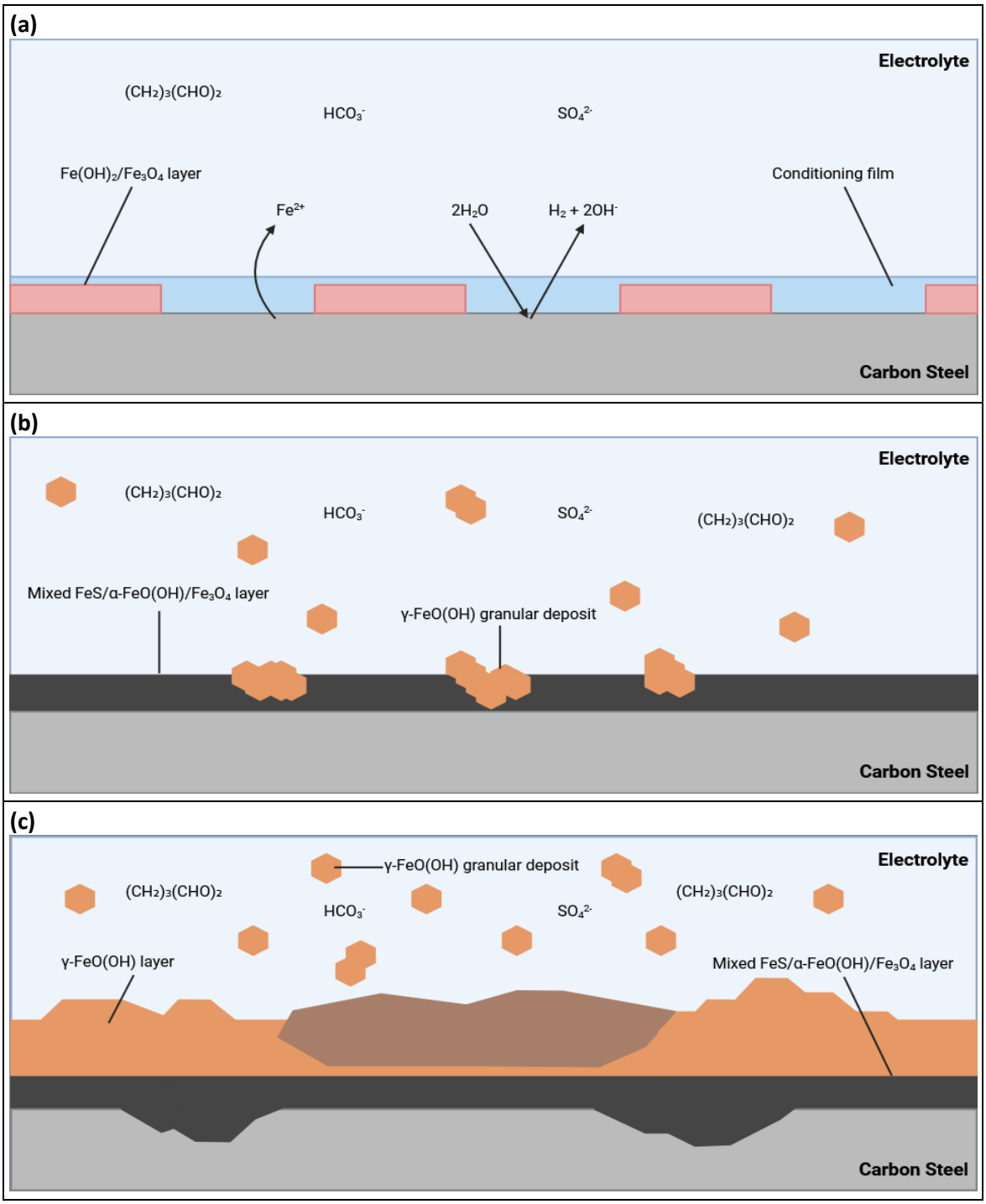

Figure 6.12. Schematic of the initial stages for UNS G10180 carbon steel in anaerobic abiotic and biotic artificial seawater media. corrosion mechanisms, **(a)** the formation of nascent inorganic corrosion film and the organic conditioning film; **(b)** maturing corrosion film under the abiotic condition; **(c)** moderate uniform and pitting corrosion under patchy corrosion deposits, with increasing granular deposits. BioRender.com (2024).

Abiotic reactor: - Generally, the sterile abiotic condition had a pseudo-steady state up until day 25. Then, there was a swift decrease in R_p after day 25. Overall, this may be attributed to the presence of a conditioning film and the formation of inorganic corrosion product layer. As upon dismantling of the reactors, the abiotic surfaces were covered in a reddish-brown corrosion product. Similarly, the abiotic reactor ASW media was reddish-brown in colouration. The primary corrosion products for the abiotic condition were attributed to iron oxide compounds such as

magnetite, goethite, lepidocrocite, or hematite. From the ECMs, there is initially a capacitive behaviour over the first three weeks, which reflects ion adsorption and the development of a nascent iron oxide film. Subsequently, there was a diffusive behaviour during the final week in the film layer. Moreover, there was a diffusive behaviour in the double layer during the first and final week, which reflects charge transfer, due to the formation of corrosion products such as lepidocrocite. Generally, there were low levels of uniform or localised pitting corrosion present for the abiotic condition. Interestingly, whilst both CR were similar, there was a significantly lower uniform CR for the abiotic condition when compared to the biotic condition. This can be attributed to the presence of a biofilm for the biotic condition.

Biotic reactor: - A black surface film was present on the steel coupons on day 1, immediately after inoculation with the pre-culture. Then, during the initial three-day batch phase there was an electronegative shift observed in the E_{corr}, which was attributed to biofilm formation on the CS coupons. After the flow of fresh media on day 4, there was a gradual increase in the E_{corr} associated with anodic polarisation. Interestingly, there were electronegative shifts observed after each dose of biocide. Similarly, a decrease in the concentration of H_2S was observed after each dosage, with a peak of 60 µmol L^{-1} measured on day 21. However, the biotic condition generally had a consistently uniform EIS response over the 28 day test, with only minor variation in the spectra attributed to the biocide. Additionally, the R_p was generally low for the biotic condition. For the biotic condition, there is initially a diffusive behaviour over the first three weeks. This is indicative of a non-ideal capacitance response. Whilst there is a capacitive behaviour over the final week in the film layer, which reflects ion adsorption and the development of a film layer. Conversely, there is a capacitive behaviour over the first three weeks, with a diffusive behaviour over the final week in the double layer. This indicates a strong diffusive behaviour and reflects charge transfer due to the formation of corrosion products. The coverage of the metal sample with a black precipitate was indicative of the successful growth of corrosion products film containing FeS compounds. However, after aging the products in air, a change in their colour from black to rust-red became visible. This is a clear indication for the oxidation of the initial products. The composition of this corrosion layer was associated with lepidocrocite, as well as mackinawite.

Microscopic analysis provided further insights into the surfaces of the CS coupons. The heterogeneous biofilm distribution over the surface of the CS coupons was captured using CLSM. From the images, it was clear to see that the biocide had a clear impact on the survivability of the biofilm. From a previous experiment in chapter 4, there was approximately 91% live to 9% dead without biocide. Whilst, there was a live/dead cell ratio of approximately 41% live to 59% dead

with the application of biocide. Once the surfaces had been cleaned, surface profilometry analysis revealed that there were low levels of uniform or localised pitting corrosion present for both the abiotic and biotic condition. It should be noted that only 2 – 3 % of the analysed surfaces observed pitting. However, after 28 days, the biotic condition did exhibit pits with a greater average area. There was approximately a 3.7× increase in pit area. It is important to note that these type of conclusions are hypothetical and that longer-term studies may reveal critical stages of biofilm maturation and corrosion progression. This is characteristic of localised pitting caused by biofilms [232, 233]. For this study, it was not possible to quantitatively determine *PD* values, due to the general absence of pitting across the coupon surfaces.

Analysis of the community dynamics revealed a marked change in the predominant relative abundances of microorganisms. The dominant genera from the sediment sample were generally anaerobic, halophilic, and obligately chemolithoautotrophic. They collectively play crucial roles in the biogeochemical cycles of carbon, sulphur, and methane in marine environments. There was much less diversity in the Day 0 sample, with Fusobacteriota, Proteobacteria, and Clostridia classes making up approximately 75% of the relative abundance. *Fusobacterium*, *Vibrio*, and *Oceanicoccus* alone made-up approximately 55% of the relative abundance. *Fusobacterium* is primarily known as a genus of bacteria that inhabit animal guts. They are fermentative bacteria that have been reported to produce butyrate and other short-chain fatty acids as metabolic byproducts [318]. *Vibrio* sp. are facultative anaerobes, known for their ability to form biofilms on various surfaces, including metals [296]. While *Oceanicoccus* sp. are relatively undocumented [319]. They likely contribute to the degradation of organic material in marine ecosystems. Genera from *Photobacterium*, *Blautia*, *Leptotrichia*, *Maridesulfovibrio*, *Anaerotignum* and *Clostridium* made-up another approximately 20% of the relative abundance. These genera represent a diverse group of bacteria contributing to processes such as fermentation, and sulphur cycling in marine environments [320, 321]. *Exiguobacterium*, *Vibrio*, and *Shewanella* were the dominant genera making up approximately 80% of the relative abundance in the bulk fluid. *Exiguobacterium* sp. are facultative anaerobes, capable of utilizing a variety of organic compounds for energy. They are known for their ability to survive under extreme environmental conditions, such as high salinity. In marine environments, *Exiguobacterium* contributes to the degradation of organic material [322]. Similarly for the AR biofilm sample, the dominant genera included *Exiguobacterium* and *Vibrio*. *Serpentinicella* also saw an increase in relative abundance. *Serpentinicella* represents a group of extremophilic bacteria which have been reported to be adapted to extreme environments characterised by high pH (alkaline conditions) and low availability of organic carbon [323]. Interestingly, *Shewanella* also maintained a relative abundance of 2% in the biofilm sample. *Shewanella* sp. are widely distributed in marine environments and play a crucial role in the

biogeochemical cycling of elements like iron and manganese in marine sediments. Additionally, *Shewanella* has been reported to play a key role in EET [29].

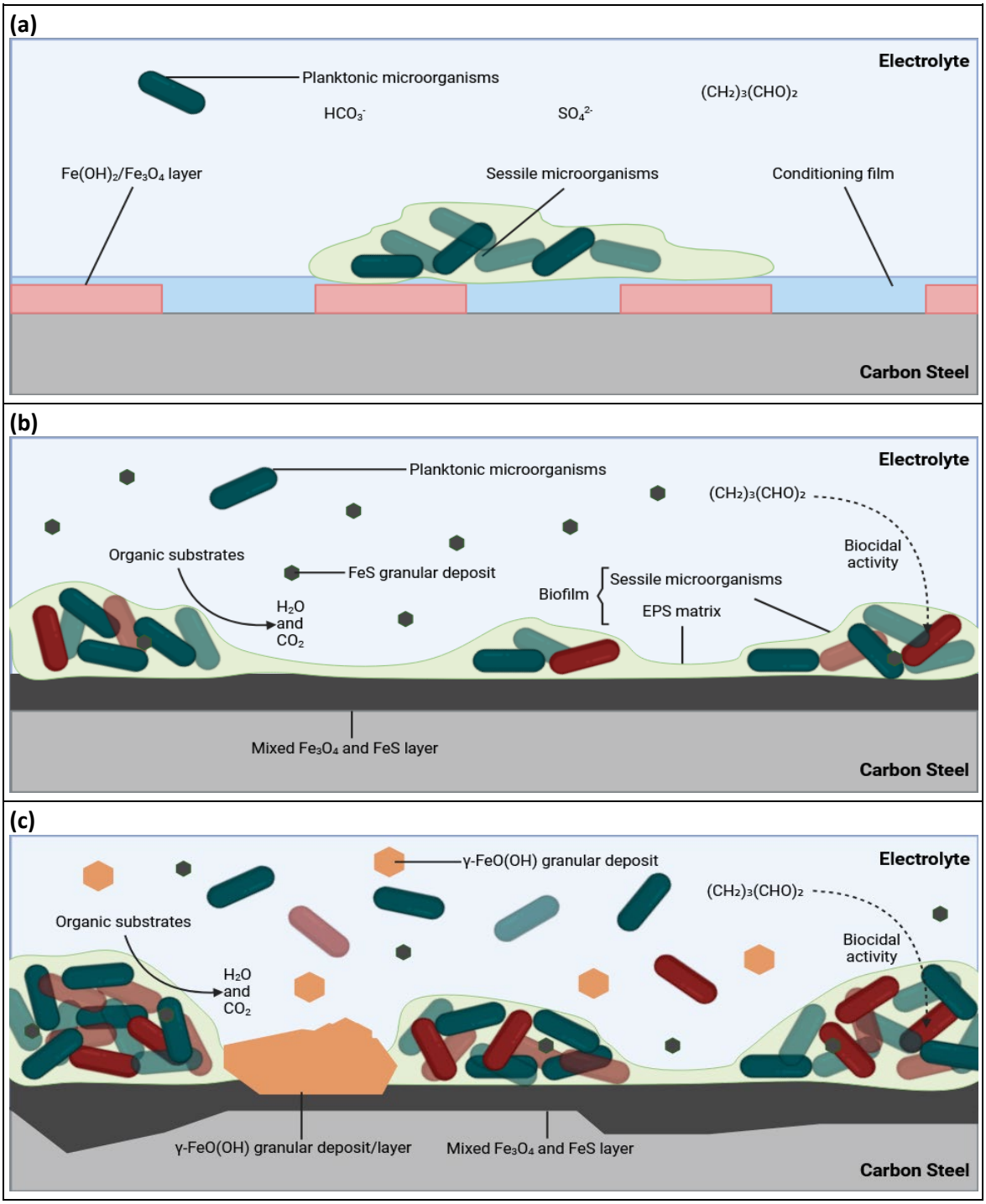

Figure 6.13. Schematic of the initial stages for UNS G10180 carbon steel in anaerobic abiotic and biotic artificial seawater media. Corrosion mechanisms, **(a)** the formation of nascent inorganic corrosion film and the organic conditioning film with pioneering bacterial attachment; **(b)** maturing corrosion film with inhibited biofilm growth and colonisation due to biocidal activity; **(c)** moderate uniform and pitting corrosion under patchy corrosion deposits, with increasing granular deposits, as well as patchy biofilm due to biocidal activity. BioRender.com (2024).

For this study, the electrochemical response under both abiotic and biotic conditions were distinct. For the biotic condition, whilst a reddish-brown corrosion product was also observed, this was largely a granular deposit that easily sloughed off the surface. Underneath the granular deposit was a black deposit more closely adhered to the surface. The composition of this corrosion layer was associated primarily with mackinawite. Figure 6.13 proposes biotic reaction mechanisms, associated primarily with the formation of mackinawite, as well as iron oxide corrosion products.

As stated earlier, the mixed-species biofilm contained *Exiguobacterium* and *Serpentinicella*. These species are known for their ability to survive under extreme stress, and in environmental conditions not conducive to growth such as high salinity. Critically, the mixed-species biofilm also contained *Vibrio* known for their ability to form biofilms on various surfaces, including metals. It is hypothesised that these genera were working synergistically to enhance chemical tolerance towards glutaraldehyde. Glutaraldehyde is known to kill bacteria by cross-linking proteins, inactivating enzymes, disrupting cell membranes, and damaging DNA. These combined effects lead to the disruption of essential cellular processes, resulting in bacterial death [113]. However, the formation of a biofilm can enhance chemical tolerance. The biofilm acts as a diffusion barrier, which limits the efficacy of biocidal treatments. Moreover, genetic adaptation and the presence of resistant species, such as *Exiguobacterium* and *Serpentinicella* may have been key determining factors. The cyclic biocide treatment protocol employed failed to completely eradicate the mixed-species biofilm community. It is hypothesised that longer-term studies may reveal critical stages of biofilm maturation and corrosion progression.

6.4 Summary

In summary, the proposed protocol provides a robust platform that integrates a multidisciplinary approach with MLOE to thoroughly investigate the complexities of biofilm formation, MIC initiation mechanisms, and the efficacy of biocides. In this study, the dual bioreactor was employed to assess the effectiveness of glutaraldehyde in mitigating the development of MIC on UNS G10180 CS in anaerobic ASW using a marine sediment microbial consortium.

- The electrochemical responses differed significantly between abiotic and biotic conditions. Under biotic conditions, electronegative shifts were observed following each biocide dose, alongside a decrease in H_2S concentration after each application.
- The primary corrosion product identified for the biotic condition was mackinawite. There were also additional bands which may be attributed to sulphur, as well as reference iron

oxide compounds such as magnetite, goethite, lepidocrocite and hematite for both conditions.

- Overall, a moderately low uniform *CR* and minimal localized pitting were observed for both conditions. Quantitative determination of *PD* was not feasible due to the general absence of pitting across the coupon surfaces. However, the biotic condition did exhibit pits with a larger average area, indicative of MIC.
- Finally, biofilm characterisation using sequencing demonstrated that *Exiguobacterium*, *Vibrio*, and *Serpentinicella* all appeared to play a critical role in enhancing chemical tolerance to glutaraldehyde.

These findings contribute to the optimization of biocidal treatment strategies by improving our understanding of their effectiveness against mixed-species biofilms. The innovative dual bioreactor protocol, which utilizes MLOE and a multidisciplinary approach, provides new insights into MIC. Identifying and characterizing specific microorganisms under simulated environmental conditions is crucial for understanding the threat of MIC. By refining biocide application under these conditions, a move toward evidence-based biocide dosing can be achieved. Ultimately, this will facilitate the development of more sustainable prevention and mitigation strategies.

Chapter 7 Conclusions, Limitations and Future Work

7.1 Conclusions

The main questions that this thesis sought to address were focused on the initial stages of biofilm development, including conditioning film formation, microbial attachment, and colonisation. Additionally, understanding the maturation of corrosion films and the growth of mixed-species biofilms were crucial areas of study. It was also vital to understand the mechanistic relationships in the later stages that may lead to uniform and pitting corrosion under patchy corrosion deposits and/or heterogeneous biofilms under both abiotic and biotic conditions. By understanding the influence of corrosion products, biofilm community dynamics, and any electron donors/acceptors a more fundamental understanding of the role that mixed-species biofilms play within MIC and the interactions at the interface of the metal/electrolyte could be gained. Thus, this thesis aimed to develop and validate a representative model system in which inoculate relevant to industry could be cultured. Then, once key performance characteristics of the model had been evaluated, commercially available biocides as well as novel antimicrobial compounds could then be introduced into the model system and investigated using MLOE. The expectation was that by gaining insights into these critical stages, more effective and sustainable mitigation strategies can be employed and/or developed.

The first objective of this thesis was to compile research in the area in the form of a literature review, which is included in chapter 1. The research area was further refined to form a succinct overview of relevant topics. Each individual research chapter (3, 4, 5 and 6) also provides additional context surrounding the available literature. From this, a critical analysis of contradictory research outcomes and knowledge gaps were identified.

Guided by existing literature and knowledge gaps identified in chapter 1, the second objective of this thesis aimed to outline a standard protocol for a novel dual anaerobic reactor model to study mixed-species biofilm and MIC interactions on UNS G10180 CS. Critically, the proposed standard protocol aimed to incorporate a multi-disciplinary approach utilising MLOE. It was designed to broaden the fundamental scientific knowledge surrounding the critical stages associated with mixed-species biofilms and the mechanisms that lead to MIC.

The laboratory studies discussed in research chapters 3, 4, 5 and 6 serve as case studies to demonstrate how the novel standard protocol described, for a dual anaerobic reactor model to

study biofilm and MIC interactions on UNS G10180 CS and biocide efficacy, can be used as a standard best practice for MIC management within industry. These case studies investigate the effects that different test media has on biofilm characteristics, and the associated threat of MIC of CS, of an environmental marine consortium. It is essential to identify various microorganisms within a system and develop a reproducible biofilm model that accurately reflects operating conditions. This model supports the cultivation of mixed-species consortia and employs the most suitable analytical methods to comprehensively understand different MIC mechanisms. Moreover, the efficacy of different biocides at mitigating the effects of MIC can be assessed. Chapter 6 investigates the efficacy of glutaraldehyde at mitigating the effects of MIC. Through the data collected, we can start to understand the mechanism of corrosion under environmental conditions, providing novel insights and potentially highlighting new approaches to biocide development. The development of such a model will facilitate evidence-based biocide dosing, enabling asset owners to mitigate the impact of MIC. This will lead to reduced costs, enhanced sustainability, and extended asset lifetimes.

In research chapter 3, the primary aim was to gain new scientific insight and mechanistic MIC understanding whilst also making progress towards validating the proposed standard protocol. In this study, the dual bioreactor explored the development of MIC on CS in anaerobic ASW using a marine sediment microbial consortium. Notably, electrochemical analysis provided insights into the redox processes at the interface of the metal/electrolyte and the influence of the biofilm. The results demonstrated that the biofilm was acting as a physical barrier which affected the primary corrosion mechanisms. Importantly, respiratory electrogens, namely *Desulfomicrobium*, *Shewanella* and *Desulfuromonas*, were identified within the mixed-species biofilm. In isolation, SRB and IRB have both been researched extensively. However, knowledge of how these microorganisms behave within mixed biofilm communities is limited. Though, it is known that electroactive microorganisms, capable of exchanging electrons with their extracellular environment, play a key role in MIC. Thus, I can start to rationalise an idealised representation of the mixed-species biofilm based on the findings. For this study, there was a shift in the prevailing metabolic mechanisms over time. Initially, SO_4^{2-} reduction by SRB appeared to be the primary corrosion mechanism. However, over time it is hypothesised that there was a shift towards Fe^0 reduction by IRB. Ultimately, the presence of the biofilm caused diffusion limitations. Overall, it was demonstrated that EMIC was the predominant biotic corrosion mechanism with the formation of both $GR(CO_3^{2-})$ and $GR(S^{2-})$ corrosion products. Together, the combined action of the mixed-species biofilm, and the corrosion products, appeared to have a significant influence on the nature and extent of corrosion. As whilst uniform corrosion was reduced compared to the abiotic

condition, localised pitting corrosion was increased, as demonstrated by electrochemical analysis and surface profilometry. The biotic condition had a significantly greater *PD* ($P < 0.05$), with a greater pit depth and size when compared to the sterile abiotic ASW media.

The research so far demonstrated the applicability of the proposed standard protocol for a novel dual anaerobic reactor model to study mixed-species biofilm and MIC interactions on CS. This study provided the first insights regarding the effects of a mixed-species biofilm on corrosion mechanisms. At the biofilm/steel interface, knowledge of the pitting incidence is critical for industry. A deeper understanding of the MIC initiation and growth processes in an ecologically relevant environment is essential. In turn, this can inform the design of more sustainable prevention and mitigation strategies.

Research chapter 4 further aimed to demonstrate the applicability and reproducibility of the novel dual bioreactor protocol. However, this study also aimed to investigate the influence of a mixed-species biofilm on CS corrosion, with a key focus on enumerating SRM using selective MB media. Critically, the environmental conditions supported continuous biofilm growth. Biofilm characterisation through sequencing indicated a significant increase in SRB, particularly the electroactive and corrosive *Desulfovibrio* spp. In sulphate-containing anoxic environments, CMIC and EMIC are hypothesised to be the primary processes that drive Fe^0 corrosion. However, there is limited knowledge determining the relative contributions of EMIC and CMIC in different anoxic environments. Thus, these findings contribute to a deeper understanding of the relative contributions of EMIC and CMIC within a mixed-species biofilm. Initially, CMIC may have been the dominant corrosion mechanism when $\mathrm{H_2S}$ concentrations were high and organic substrates were more readily available. However, over time, it was hypothesised that EMIC, via the direct uptake of electrons from the metal surface, was the primary corrosion mechanism for this study. EMIC by SRB is characterised by the formation of large amounts of inorganic corrosion products. The results demonstrated there was an inorganic corrosion product on the metal surface, but there were also distinct dark green/black granular deposits present within a thick slimy biofilm. Whilst CMIC may have also been a contributing factor, the biofilm is a diffusion barrier which would have limited the availability of organic substrates at the interface of the metal/electrolyte. Moreover, *Desulfovibrio* spp. are well characterised electroactive corrosive bacteria capable of extracting electrons from the metallic Fe^0, thereby contributing to the granular deposits. Electroactivity within mixed-species biofilm communities is an important process, as electroactivity between fermentative electroactive bacteria and respiratory electroactive bacteria, enables food chains to be established.

The research acknowledges the importance of biofilm phenotype for influencing MIC. In industry, heterogeneous biofilms are characterised by species diversity, leading to challenges in

identifying corrosion mechanisms and informing mitigation strategies. Identifying the microbial mechanisms that drive the corrosion of CS under anoxic conditions at the metal/electrolyte interface is essential. By employing MLOE, we can develop a comprehensive understanding of the role that mixed-species biofilms play in MIC. Moreover, we can begin to identify and characterise key species present.

Research chapter 5 aimed to investigate the impact of ecologically relevant environmental conditions on natural mixed-species biofilm communities. For this study, PW was used to simulate environmental conditions. Case studies from offshore oilfield systems have consistently demonstrated that the composition of PW plays a crucial role in the development of biofilms and the severity of MIC on CS surfaces. However, there are limitations and challenges when testing *in situ*. As such, knowledge is limited. Thus, the objective was to provide deeper insights into the development and community dynamics of mixed-species biofilms, whilst also investigating the threat of MIC. Interestingly, the electrochemical response under biotic conditions was not too dissimilar to the abiotic condition. Furthermore, the results determined that mackinawite and iron oxide compounds were the primary corrosion products. However, surface analysis revealed that the biotic condition did display pits with a larger average area, indicative of MIC. Critically, biofilm characterisation demonstrated that the mixed-species biofilm contained *Marinobacterium*, *Malaciobacter*, *Pseudomonas*, and *Halomonas* which all contribute to biofilm formation in high salinity marine environments. It was hypothesised that within the mixed-species biofilm electroactive corrosive bacteria and fermentative electroactive bacteria were working synergistically, thereby altering the microenvironment. Through the production of organics and other metabolites by the fermentative electroactive bacteria, the growth of electroactive corrosive bacteria was supported. The results demonstrated that the biofilm was acting as a diffusion barrier, providing some passivation of the metal surface. However, it is hypothesised that with continuous long-term monitoring the threat of MIC is increased.

The research further acknowledges the need for studies which are ecologically relevant to industry. Moreover, long-term studies are recognised as critical to identify and characterise the full range of microorganisms involved in MIC, as well as understand their interactions. This research begins to bridge the gap between experimental and real-world scenarios involving mixed-species biofilms. By aligning laboratory conditions with those encountered *in situ*, further understanding of the dynamics of biofilm development and MIC in offshore systems can be gained.

Finally, research chapter 6 builds on preceding objectives and further proposes a targeted approach to MIC mitigation by utilising the novel dual bioreactor protocol to evaluate and optimise

biocidal treatment strategies. As, there is limited research evaluating approaches to enhance biocidal efficacy in a sustainable way. This study aimed to explore the biocidal efficacy of glutaraldehyde and was conducted in the context of ASW conditions. Critically, after each application of the biocide an electronegative shift alongside a decrease in H_2S concentration was observed. However, biofilm characterisation revealed that *Exiguobacterium*, *Vibrio*, and *Serpentinicella* were playing a critical role to enhance chemical tolerance. *Vibrio* are known for their ability to form biofilms on various surfaces, including metals. Whilst *Exiguobacterium* and *Serpentinicella* are known for their ability to survive under extreme environmental stress. Together, these species enabled the mixed-species biofilm to be more recalcitrant. The results demonstrated that whilst the biocide was influencing the biofilm, the cyclic treatment protocol employed failed to completely eradicate the mixed-species biofilm community. It was hypothesised that the structure of the mixed-species biofilm community in this present study acted as a diffusion barrier which limited the efficacy of the biocide. Moreover, *Exiguobacterium* and *Serpentinicella* may have been employing diverse strategies to enhance resilience and adaptability of the mixed-species biofilm.

This primary aim of this thesis was to develop and validate a representative model system in which inoculate relevant to industry, can be cultured to enhance the fundamental understanding of the role that biofilms play within MIC. To address this, a multi-disciplinary approach combining standard microbiological assays, molecular tools, electrochemical methods, and chemical and metallurgical assays was employed. Changes in the prevalence and activity of biofilm species were evaluated using NGS to characterize the microbial community dynamics and functional potential over time. The *CR* of the underlying metal was assessed through methods widely used in academia and industry, including EIS, LPR, and weight-loss analysis, providing a comprehensive understanding of metal degradation at the metal/electrolyte interface. The impact of biocides on biofilm viability was investigated using a MLOE framework, integrating viability assays such as fluorescence microscopy (LIVE/DEAD staining), and ATP quantification with metabolic activity measurements. The relationships between biofilm characteristics, corrosion processes, and biocide efficacy were elucidated through correlative analyses, revealing novel insights into how biocides affect biofilm structure, microbial activity, and subsequent corrosion mechanisms. Key questions were addressed by examining the metabolic and physical roles of the biofilm through oxygen and redox profiling, identifying the influence of corrosion products via SEM-EDS and Raman spectroscopy. Anaerobic conditions were maintained to determine key cathodic electron acceptors, and biofilm pit morphology was investigated to link patchy growth to localized pitting corrosion, uncovering mechanistic insights into MIC. Together, the research demonstrates applicability of the proposed standard protocol for a novel dual anaerobic reactor model to study mixed-species biofilm and MIC

interactions on UNS G10180 CS. Knowledge gaps pertaining to the development, structure and composition of mixed-species biofilms remain. Thus, advancing the fundamental understanding of natural biofilms, as well as biofilm treatment options is critical for an economical and more sustainable approach moving into the future.

7.2 Study Limitations

The complexity of MIC caused by mixed-species biofilms presents a significant challenge for research in this field. Whilst existing standards can be helpful, ultimately, they do not address the problem at the source, biofilms. Simplified laboratory simulations of natural MIC phenomena can underestimate the potential of microbial communities. As data based on planktonic microorganisms are of limited value, since planktonic microorganisms are not directly representative of sessile microorganisms which form biofilms and cause MIC. On the other hand, incorporating natural communities into these simulations often results in limited reproducibility. These limitations underscore the need for more robust and innovative approaches to studying MIC using more realistic laboratory simulations of industrial environments. Furthermore, there is a critical need for long-term studies on the influence of mixed-species biofilms on MIC. However, deciphering the mechanisms behind outcomes, such as MIC driven by natural communities, is highly complex. Therefore, using complex natural biofilms is not always practical when seeking to advance the scientific understanding of biofilm development.

In chapter 2, the standard protocol for a novel dual anaerobic reactor model to study mixed-species biofilm and MIC interactions on UNS G10180 CS is outlined. For the subsequent research chapters, a marine sediment was used to evaluate MIC. The coastal/estuarine marine sediment was selected to sample microorganisms living under low O_2 conditions and to broadly represent an ecological niche relevant to marine environments and to the energy sector. However, this was only intended to be used during early laboratory studies. Through the industrial collaborator (DNV), the intention was to source a biofilm sample from an offshore platform. This consortium would have been more directly relevant to the ecological niche of interest. As such, early in the project, a greater emphasis was placed on marine environments and more renewable energy infrastructure, such as offshore wind monopiles that are driven into the seabed.

Moreover, for this project three different types of media were used, ASW supplemented with yeast extract, MB media for the enumeration of SRB, and PW taken from an offshore platform. There were challenges in the cultivation of the mixed-species consortia used, specifically for the study using PW. For this study, the pre-culture was supplemented with additional organic sources.

However, during the 28 day experiment, the bulk media had no such supplementation. While this research attempts to understand mixed-species biofilms and MIC in marine environments broadly, it is critical to study an environmental biofilm sample from an ecologically relevant niche, such as from an offshore oilfield system. Cultivation of an ecologically relevant mixed-species biofilm is key. Moreover, it is critical to perform longer-term studies to gain a fundamental understanding of mixed-species biofilms on MIC.

Additionally, throughout the project there were challenges associated with maintaining anaerobic and/or low O_2 conditions. Due to the nature of the experiments, large quantities of media were required. As such, ensuring sterile conditions are maintained, whilst also limiting O_2 ingress after sterilisation was challenging. Sparging of the media was performed but may have been insufficient. Any ingress of O_2 could have influenced the observed *CR* and corrosion mechanisms. Overall, this may have been a contributing factor for the abiotic conditions of early studies. However, in subsequent studies, continual sparging over the 28 day experiment was employed to minimise this effect.

Chapter 2 also outlines a range of different analytical methods and information to collect. An overview of the research design is then given, with a detailed account of the materials and methods used. Generally, the scope of the research design may be too broad for one person. In practice, an extra pair of hands from a technician would be valuable. As it was challenging to manage my time when preparing samples for all the different analytical methods. For example, with CLSM, performing the imaging without fixing the samples could provide further insight and allow for greater analysis of the spatial distribution of the biofilm.

Interpretation of laboratory results to real-world efficacy is a challenge. The research described in this thesis attempted to overcome limitations associated with simplified laboratory simulations for the evaluation of single-species biofilms. While using natural microbial communities can make laboratory simulations more realistic, it also introduces variability that can limit the reproducibility of experiments. Future investigations should perform biological repeats using the same experimental parameters across each biological repeat to validate the protocol further and ensure a more robust research design.

7.3 Future Work

Some recommendations for future work are listed as follows:

- Further study of bacterial attachment and adhesion depending on the type of media used and the conditioning film present at the interface of the CS.

- Deeper understanding of the spatial community dynamics within a mature biofilm and the influence of EPS and extracellular DNA on biofilm development. Maybe using AFM and/or MALDI methods.
- It is essential to understand biofilm phenotype further. Future investigations should perform metabolomic and genetic analysis to understand molecular mechanisms of key species and to identify potential biochemical pathways and biomarkers.
- Further study on the biochemistry of mixed-species biofilms to identify critical electron donor/acceptors and to understand key metabolic pathways that may provide insight into the predominant MIC mechanisms.
- Further evaluation of commonly used as well as novel biocidal compound efficacy.
- Future work should sample and cultivate mixed-species biofilms from various field locations under conditions reflecting the original sampling location, with biological repeats.
- Future investigations should perform biological repeats using the same mixed-species biofilm composition and experimental parameters to validate the protocol. The importance of biological replicates lies in their role in capturing biological variability, which is essential for drawing meaningful and generalizable conclusions in experiments, particularly in MIC studies. Biological replicates are crucial for understanding how microbial communities or biofilm behaviours vary naturally and how this may influence corrosion under different conditions. Technical replicates ensure that observed differences are not due to experimental artifacts but do not provide insight into biological diversity or variability. Both types of replication are essential, but biological replicates are more critical for studying system-wide phenomena such as MIC, where biological complexity plays a central role.

Appendix A

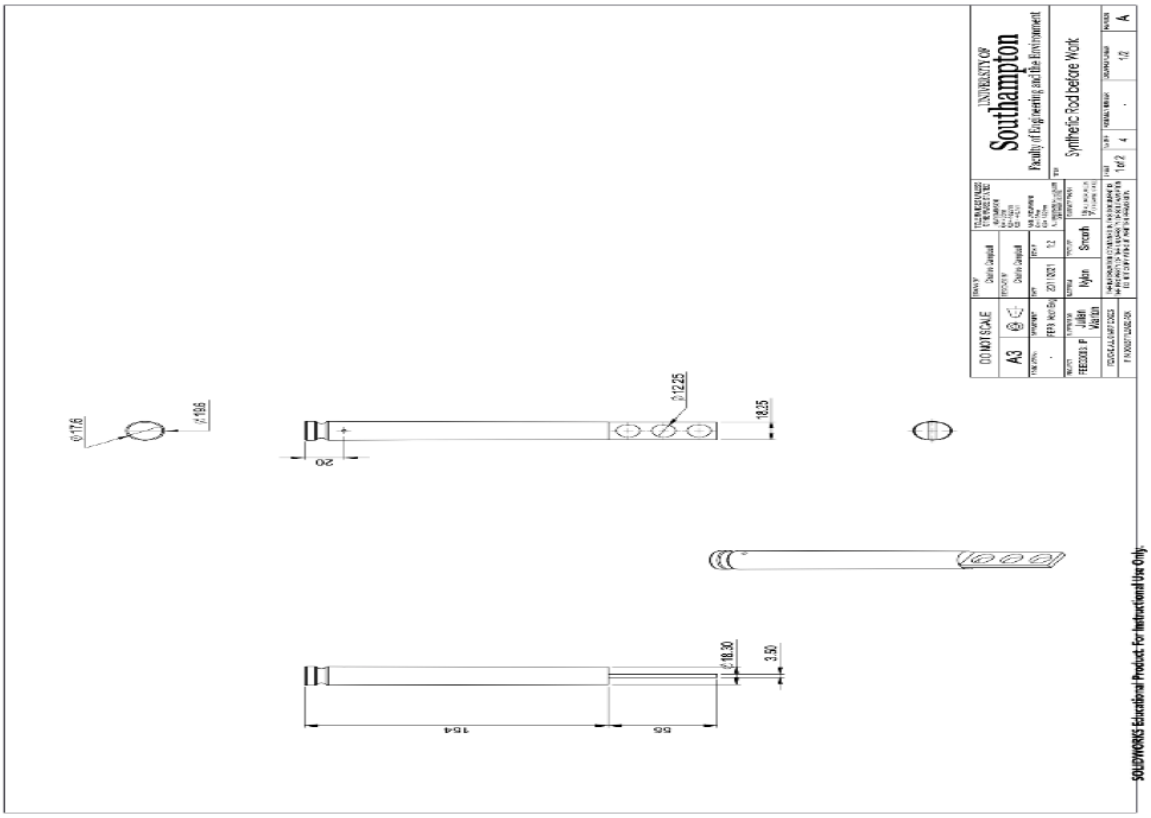

Figure A1. Engineering Drawing of a Bioreactor Rod before modifications.

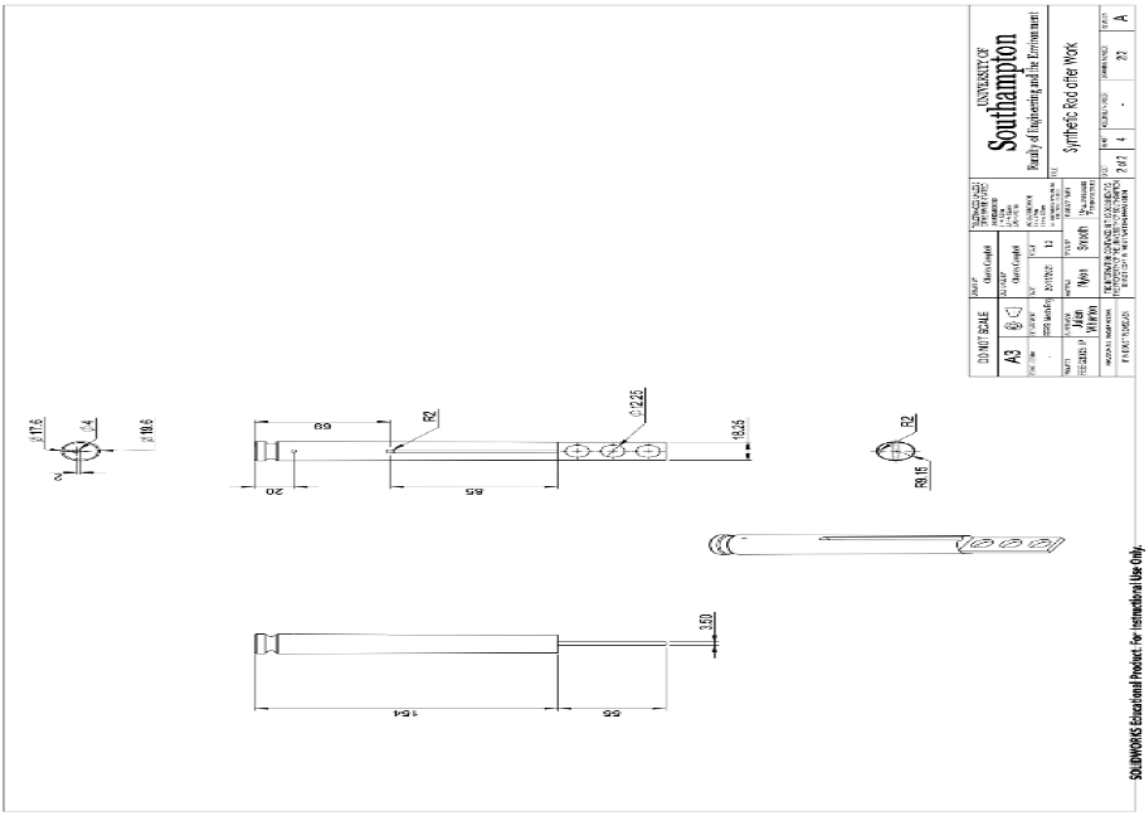

Figure A2. Engineering Drawing of Modified Bioreactor Rod after modifications.

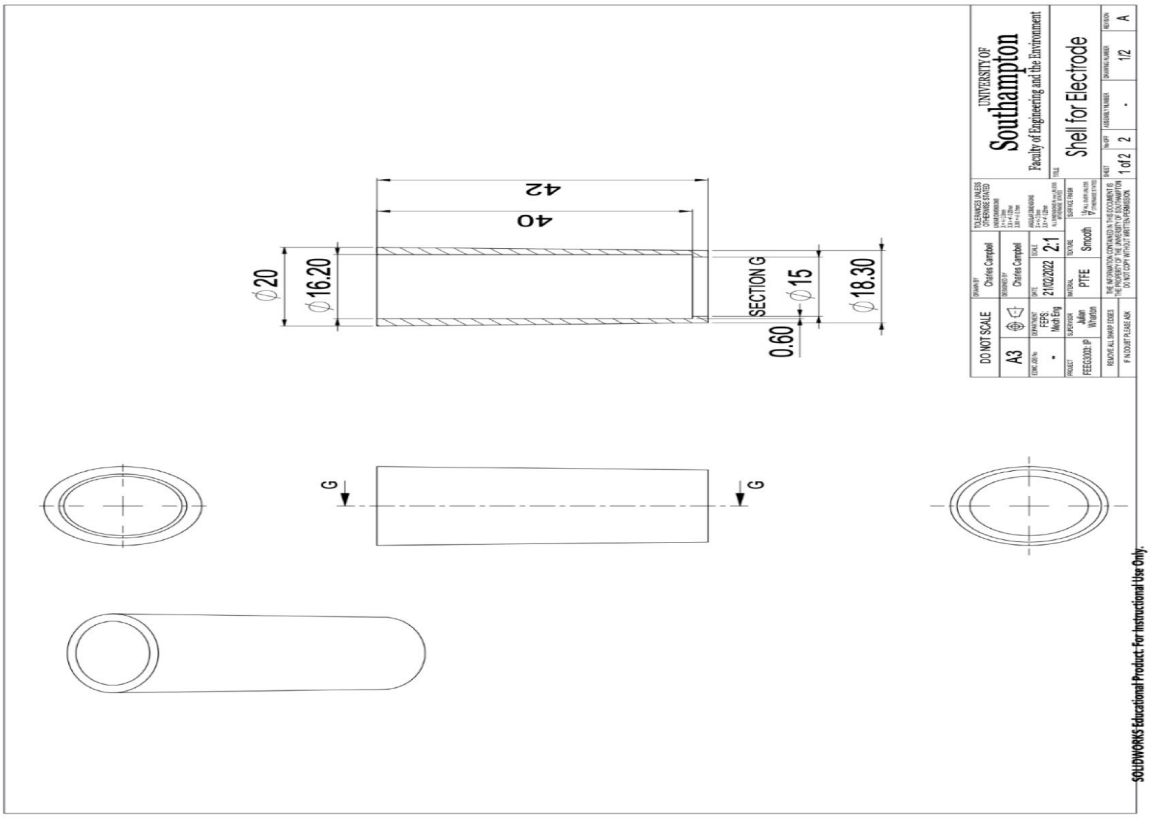

Figure A3. Engineering Drawing of Shell for Reference Electrode.

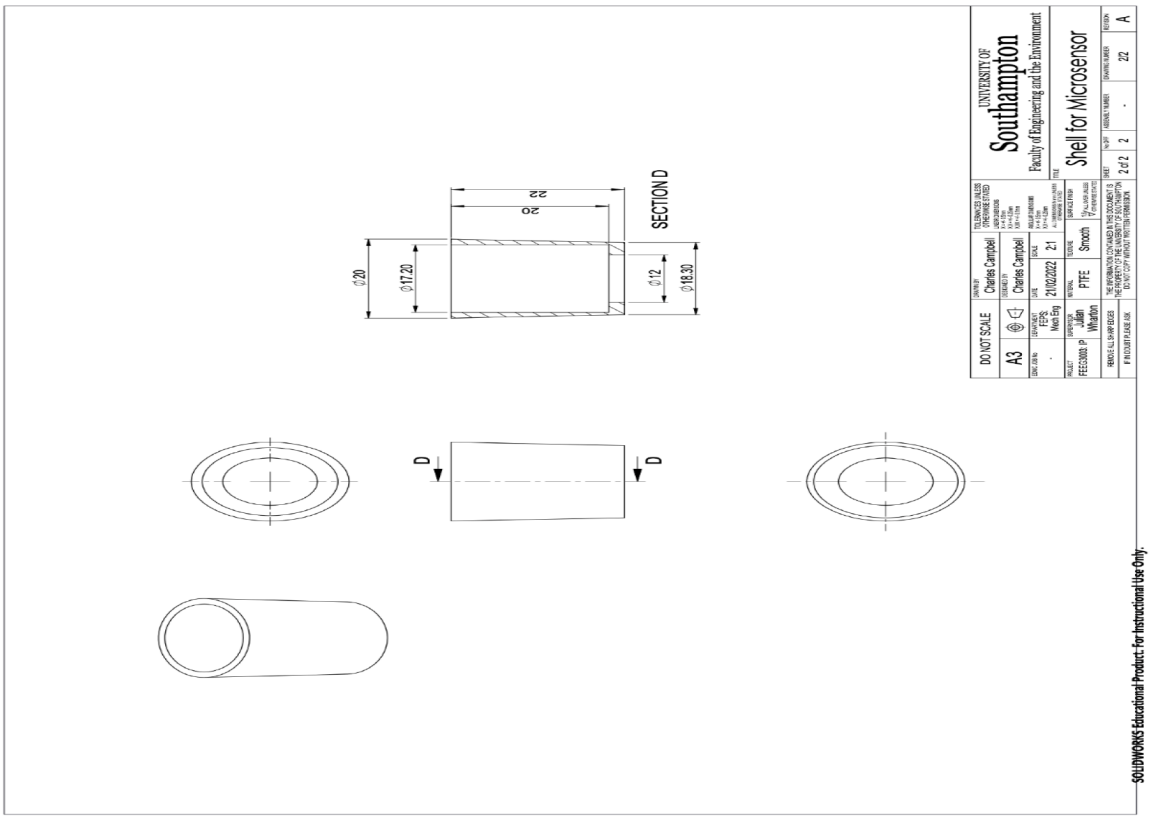

Figure A4. Engineering Drawing of Shell for Microsensor.

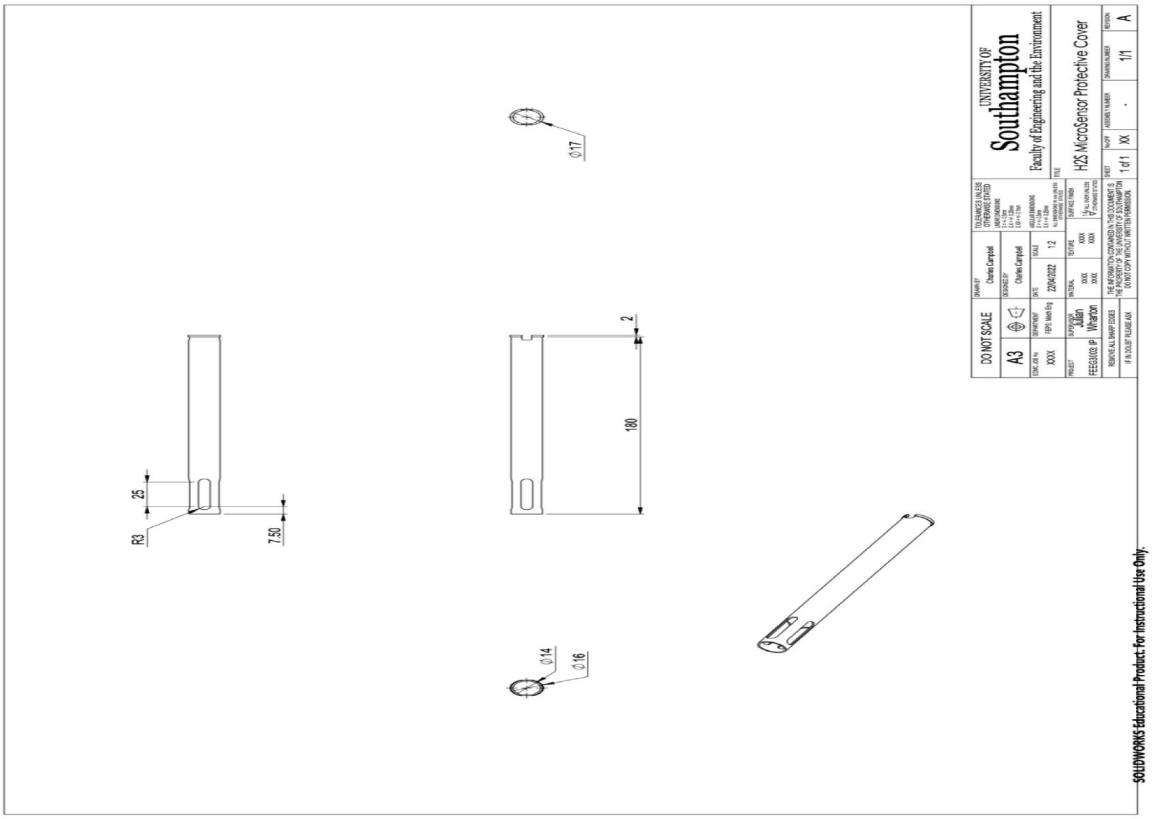

Figure A5. Engineering Drawing for New Microsensor Guard.

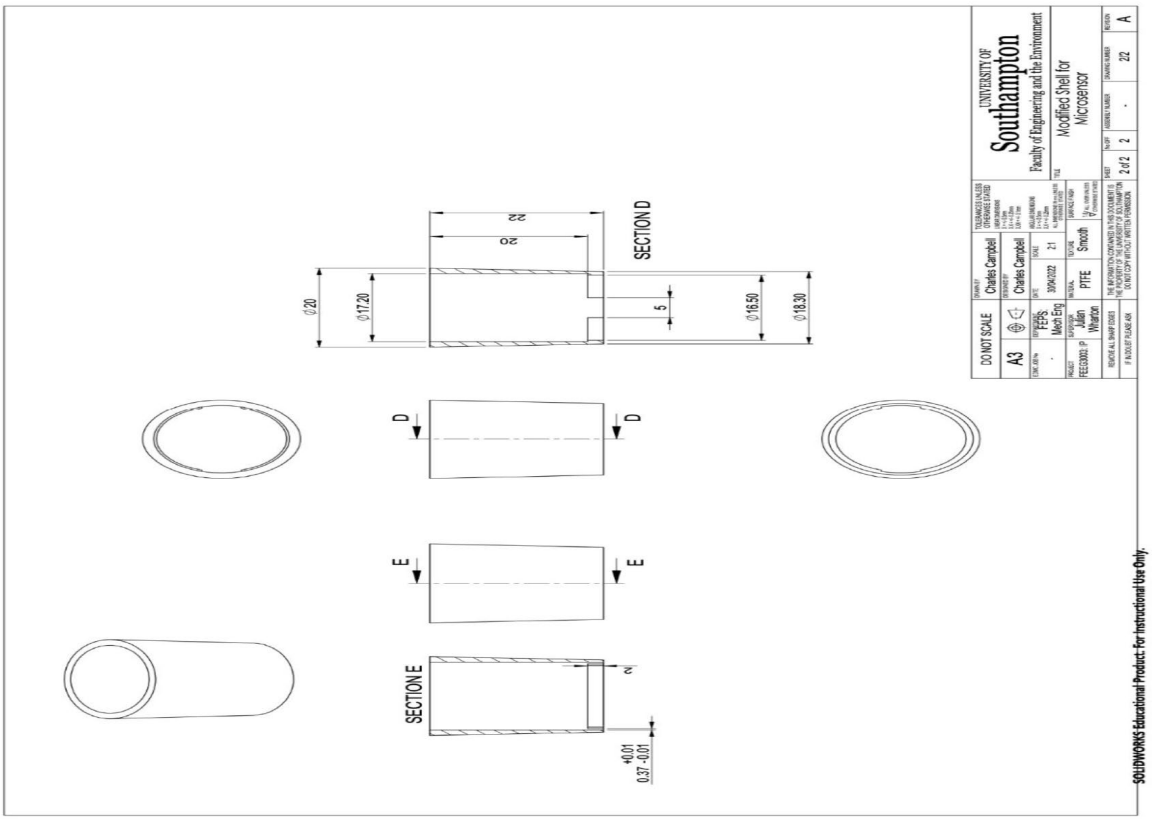

Figure A6. Engineering Drawing for Modified Microsensor Shell.

Appendix B

Table B1a. Artificial seawater test solution/media composition supplemented with 1000 mg L^{-1} of yeast extract. Yeast extract has a protein content of about 50%, of which about 20% is glutathione, 6% is nucleic acid. It is rich in 18 kinds of amino acids, functional peptides glutathione, dextran, mannan, trehalose, flavouring nucleotide, B vitamins, biotin, trace elements and volatile aromatic compounds and other components. Calcium, phosphorus, and trace element contents (µg g^{-1}) in yeast extract: Calcium 1120, Phosphorus 18020, Zinc 190, Iron 162, Chromium 5, Potassium 9300, Cobalt 1.2, Manganese 15, Strontium 3.5, Magnesium 2150.

Major Ion	% Total Weight	Concentration (mg L^{-1})
Chloride, Cl^-	47.47	18.74
Sodium, Na^+	26.28	10.454
Sulphate, SO_4^{2-}	6.6	2631
Magnesium, Mg^{2+}	3.23	1256
Calcium, Ca^{2+}	1.013	400
Potassium, K^+	1.015	401
Bicarbonate, HCO_3^-	0.491	194
Boron, B^{3+}	0.015	6
Strontium, Sr^{2+}	0.001	7.5
Solids Total	86.11%	34.09
Water	13.88	-
Total	99.99%	-

Table B2. Environmental conditions on the day the marine sediment was collected on September 14, 2022.

Date & Time	14/09/2022 07:32	14/09/2022 07:47	14/09/2022 08:02	14/09/2022 08:17	14/09/2022 08:32	14/09/2022 08:47	14/09/2022 09:02	14/09/2022 09:17	14/09/2022 09:32
pH units (pH/ORP)	7.99	7.99	7.99	7.98	7.98	8	8.01	8	8.01
Specific Conductivity mS/cm (Conductivity)	40.982	39.918	39.798	40.598	40.859	39.9	39.561	39.803	38.604
Turbidity NTU (Turbidity/Brush)	265.1	233	663	170.8	205.9	244.6	317.4	610	586
Barometric Pressure mmHg (Necessary Input)	766.7	766.7	766.7	766.7	766.7	766.7	766.7	766.7	766.7
DO mg/L (Hach LDO)	7.41	7.34	7.43	7.25	7.37	7.41	7.45	7.4	7.43
Depth meters (Depth 25 m)	0.197	0.203	0.199	0.194	0.196	0.194	0.192	0.202	0.194
Turbidity mV (Turbidity/Brush)	256.553	228.405	605.772	173.86	204.651	238.627	302.424	558.721	538.339
DO %SAT (Hach LDO)	91.7	90.5	91.5	89.6	91.3	91.5	91.9	91.4	91.2
ORPAgCl mV (pH/ORP)	220	222	220	216	219	216	220	220	218
Temperature °C (Temperature)	18.5	18.53	18.51	18.55	18.57	18.61	18.63	18.62	18.55
Total Dissolved Solids g/L (Conductivity)	26.228	25.548	25.471	25.983	26.149	25.536	25.319	25.474	24.706
Specific Gravity (Depth 25 meter)	1.019	1.018	1.018	1.018	1.018	1.018	1.018	1.018	1.017
Density kg/m³ (Depth 25 m)	1018.52	1017.94	1017.88	1018.3	1018.44	1017.91	1017.72	1017.85	1017.23
Salinity psu (Conductivity)	26.32	25.56	25.48	26.05	26.23	25.55	25.31	25.48	24.63
Chlorophyll a µg/L (Chlorophyll a)	5.99	6.2	2.41	2.26	9.23	2.25	2.4	2.47	2.14

Abiotic Coupons

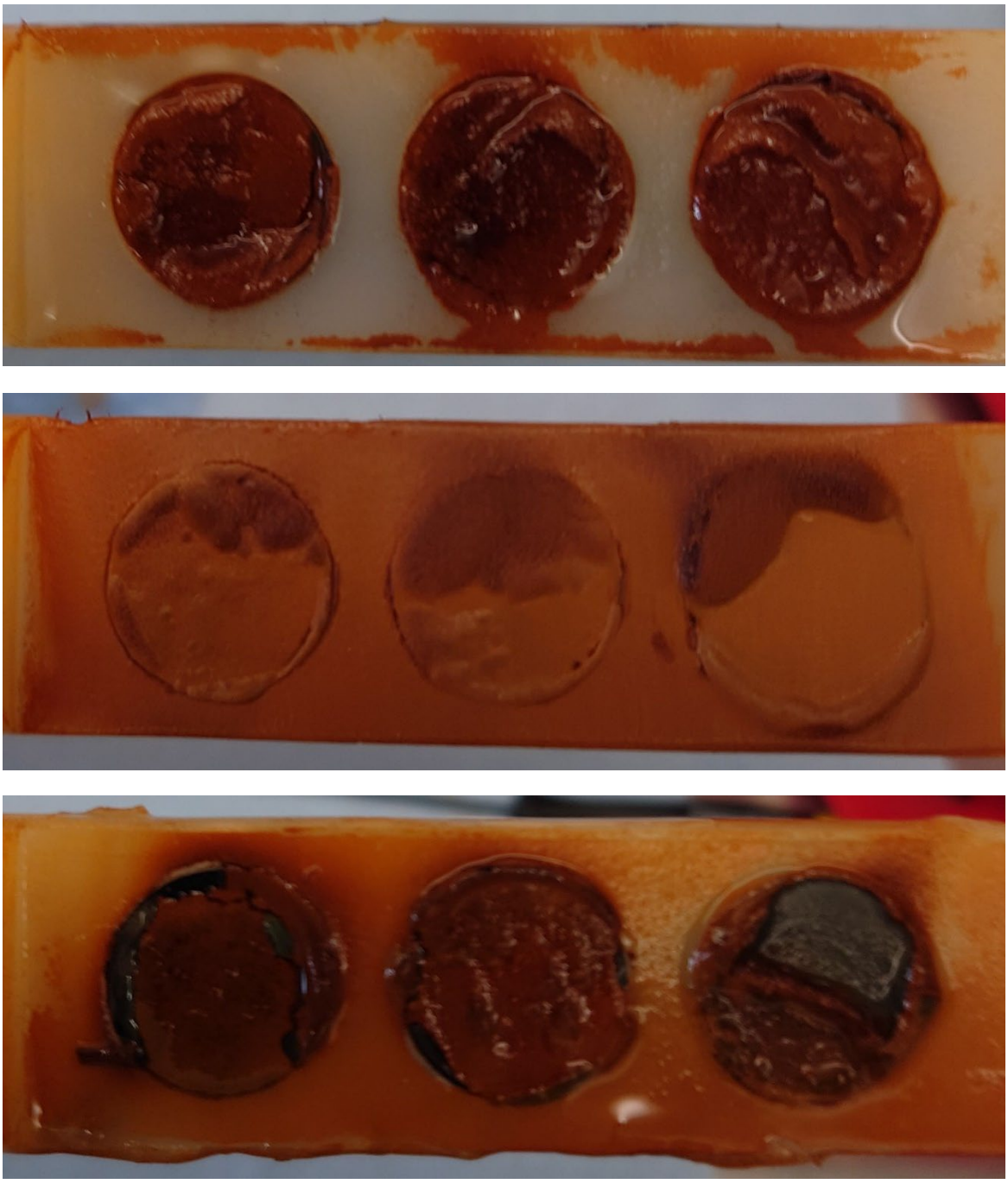

Figure B3a. Photographs taken of the coupon rods taken from the abiotic condition on Day 28, on dismantling the reactor, after exposure to anaerobic nutrient-enriched artificial seawater media for 28 days.

Biotic Coupons

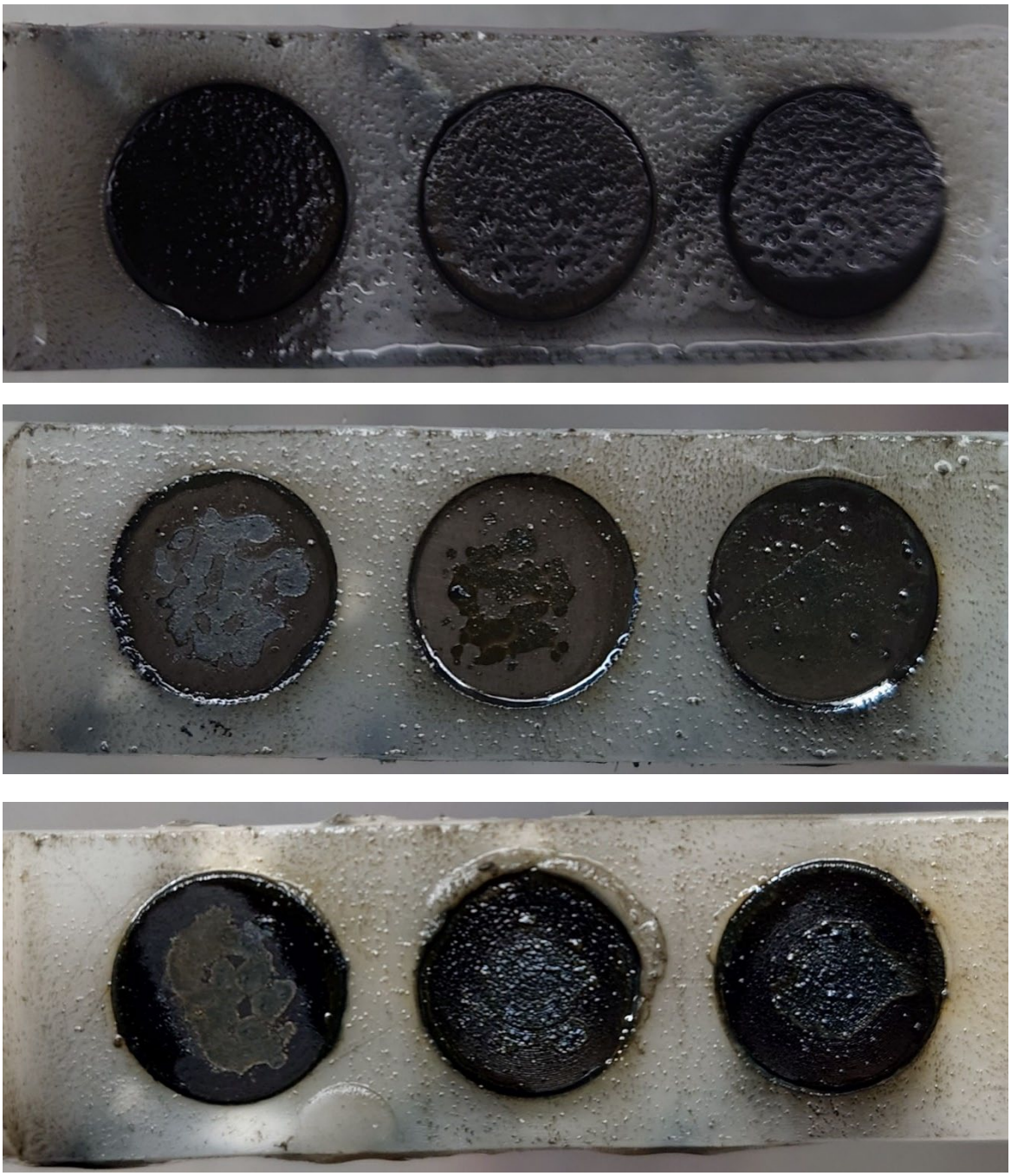

Figure B3b. Photographs taken of the coupon rods taken from the biotic condition on Day 28, on dismantling the reactor, after exposure to anaerobic nutrient-enriched artificial seawater media for 28 days.

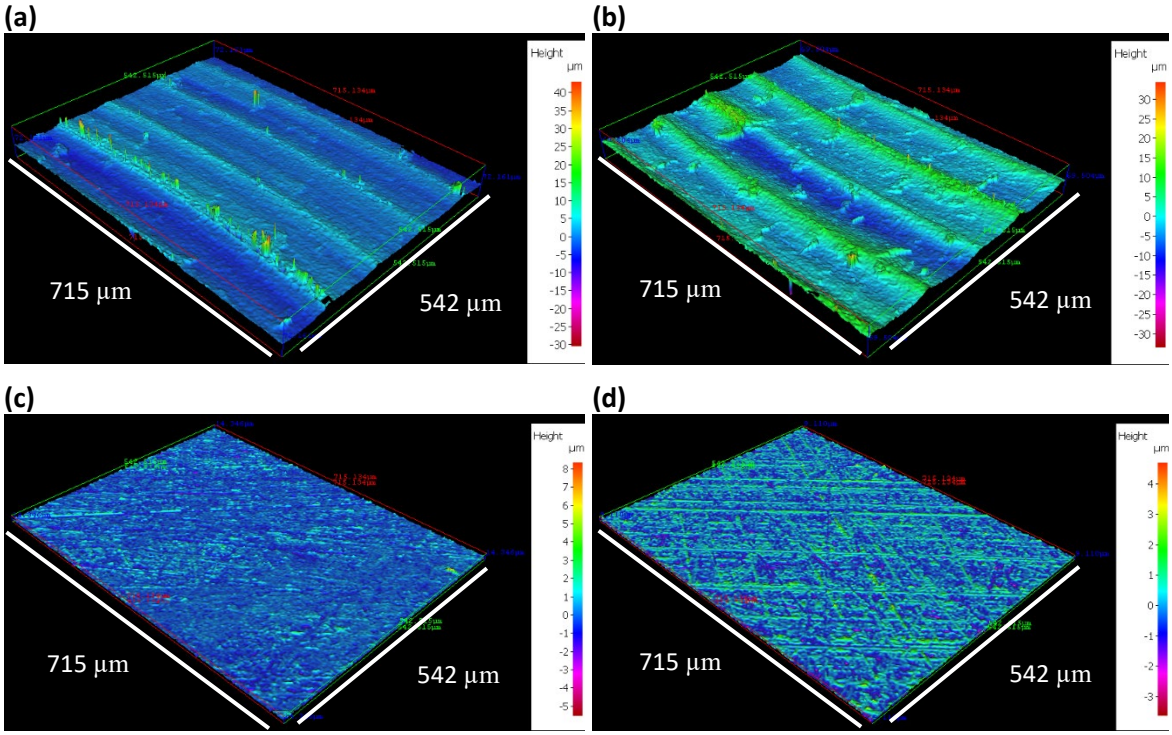

Figure B4. Three-dimensional optical surface profilometry of UNS G10180 surfaces at day 0. AR coupons for: **(a)** abiotic and **(b)** biotic conditions; and P coupons for: **(c)** abiotic and **(d)** biotic conditions, prior to exposure to anaerobic nutrient-enriched artificial seawater media for 28 days.

Table B5a. Quantitative surface roughness profiles for AR coupon samples on day 0 and day 28. R_a average roughness of profile, R_t maximum peak to valley height of roughness, R_z mean peak to valley height, R_p maximum peak height, R_v maximum valley height, R_c mean height of profile irregularities, R_{sm} mean spacing of profile irregularities, R_t/R_z extreme scratch/peak value of roughness profile (higher values (>=1) represent larger scratches/peaks).

Day	Reactor	R_a (µm)	R_t (µm)	R_z (µm)	R_{peak} (µm)	R_v (µm)	R_c (µm)	R_{sm} (µm)	R_t/R_z (µm)
0	Abiotic	1.3±0.7	19.5±11.5	10.3±4.8	12.1±7.3	7.4±7.9	9.1±7.6	193±202	1.8±0.6
	Biotic	1.4±0.8	12.4±6.9	8.3±3.6	8.1±5.2	4.3±2.5	6.5±3.8	156±128	1.5±0.4
28	Abiotic	2.2±0.7	33.6±16.0	17.2±6.8	10.7±5.2	22.9±12.0	18.4±12.5	248±167	1.9±0.5
	Biotic	3.5±1.2	48.3±19.0	26.0±8.7	15.4±5.1	32.9±15.1	27.6±11.7	328±235	1.9±0.4

Table B5b. Quantitative surface roughness profiles for P coupon samples on day 0 and day 28.

Day	Reactor	R_a (μm)	R_t (μm)	R_z (μm)	R_{peak} (μm)	R_v (μm)	R_c (μm)	R_{sm} (μm)	R_t/R_z (μm)
0	Abiotic	0.4±0.03	4.6±0.8	3.5±0.3	2.5±0.5	2.1±0.5	1.9±0.2	38±5	1.3±0.1
	Biotic	0.4±0.03	4.2±0.5	3.4±0.2	2.3±0.3	1.9±0.4	1.9±0.2	36±5	1.3±0.1
28	Abiotic	2.1±0.8	40.6±18.7	18.6±7.0	9.2±3.6	31.4±15.2	24.8±18.8	304±180	2.1±0.5
	Biotic	2.9±0.9	51.8±11.7	26.1±7.0	14.1±3.2	37.8±11.6	34.5±11.1	350±239	2.1±0.4

Table B6a. EIS parameters of the carbon steel coupons immersed in anaerobic nutrient-enriched artificial seawater media for the abiotic condition on days 1, 7, 14, 21 and 28. **Equivalent circuit:** ① – R_s+(Q_1/Q_2+R_{ct}); ② – R_s+(Q_1/R_{ct}); ③ – R_s+Q_1/(R_{film}+Q_2/R_{ct}).

Day	Coupon	R_s / Ω cm²	Q_1 / mΩ^{-1} cm^{-2} s^n	n_1	R_{film} / Ω cm²	Q_2 / mΩ^{-1} cm^{-2} s^n	n_2	R_{ct} / Ω cm²	$\chi^2 \times 10^{-4}$
1	AR ①	3.9±0.5	0.2±0.03	0.85±0.01	–	0.8±0.9	0.45±0.03	304±52	14
	P ①	4.0±0.2	0.1±0.01	0.87±0.01	–	0.6±0.3	0.45±0.07	612±179	18
7	AR ②	6.7±0.1	2.2±0.1	0.78±0.04	–	–	–	417±24	8.5
	P ②	6.6±0.1	1.2±0.1	0.81±0.01	–	–	–	374±14	3.4
14	AR ①	13.0±1.7	5.3±0.9	0.40±0.03	–	4.0±0.1	0.58±0.03	23±374	2.9
	P ③	13.0±0.6	3.6±2.1	0.42±0.08	28±11	3.4±0.9	0.60±0.04	903±409	2.9
21	AR ③	13.0±8.5	4.3±4.0	0.51±0.21	46±43	4.6±1.3	0.56±0.05	1454±485	3.2
	P ③	18.0±1.5	3.6±1.7	0.42±0.06	39±0.1	8.0±2.1	0.52±0.09	775±287	4.8
28	AR ①	13.6±5.8	3.2±5.6	0.59±0.22	–	4.2±6.7	0.59±0.28	84±124	3.7
	P ③	19.9±1.4	11.0±6.6	0.48±0.10	243±178	9.3±3.7	0.42±0.16	123±162	4.8

Table B6b. EIS parameters of the carbon steel coupons immersed in anaerobic nutrient-enriched artificial seawater media for the biotic condition on days 1, 7, 14, 21 and 28. **Equivalent circuit:** ④– R_s+Q_1+(Q_2/R_{ct}).

Day	Coupon	R_s / Ω cm^2	Q_1 / mΩ^{-1} cm^{-2} s^n	n_1	Q_2 / mΩ^{-1} cm^{-2} s^n	n_2	R_{ct} / Ω cm^2	$\chi^2 \times 10^{-4}$
1	AR ④	4.0±0.1	0.6±0.2	0.85±0.02	1.4±0.6	0.77±0.01	2509±1497	41
	P ④	3.7±0.9	0.4±0.3	0.93±0.06	0.9±0.1	0.69±0.20	1342±1251	41
7	AR ④	5.0±0.4	1.7±0.8	0.86±0.02	2.3±0.4	1.02±0.06	616±79	21
	P ④	5.3±0.2	1.5±0.3	0.94±0.07	2.0±1.0	0.92±0.09	939±465	21
14	AR ④	7.7±0.6	3.0±0.6	0.84±0.02	5.4±1.8	0.98±0.04	164±109	13
	P ④	8.2±0.2	3.3±0.6	0.88±0.03	3.7±0.5	0.85±0.02	206±66	15
21	AR ④	9.3±0.7	6.5±6.7	0.80±0.03	7.1±6.1	1.01±0.06	1506±2474	4.8
	P ④	10.0±0.3	2.5±0.4	0.87±0.04	8.1±3.8	0.91±0.09	97±105	5.0
28	AR ④	10.0±0.3	2.9±0.4	0.84±0.01	8.5±4.4	1.02±0.06	156±106	3.5
	P ④	10.8±0.3	3.1±1.2	0.87±0.04	6.6±4.3	0.91±0.13	163±161	4.2

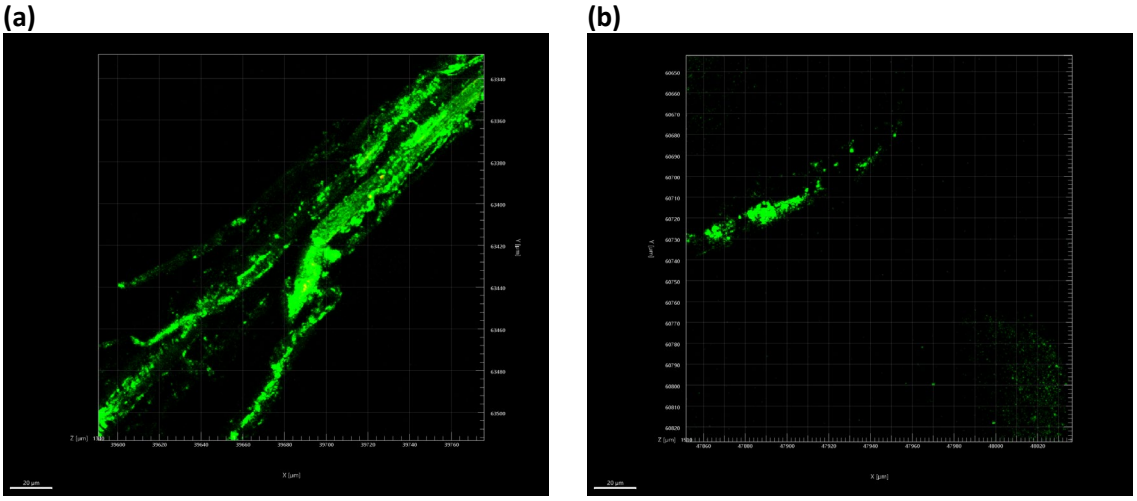

Figure B7. Confocal images of biofilms formed over UNS G10180 carbon steel surfaces for **(a)** AR and **(b)** P biofilms, after exposure to anaerobic nutrient-enriched artificial seawater media for 28 days.

Table B8. List of top 25 microbial genera identified through 16S rRNA amplicon sequencing with two target region, V3-4 for bacteria and archaea, after exposure to anaerobic nutrient-enriched artificial seawater media for 28 days.

Name	Sediment	Day0	Day28	AR	25M
Malaciobacter	0.002629	0.000723	51.51	30.96	31.06
Vibrio	0.1229	44.44	18.57	3.456	5.58
Oceanicoccus	0.02797	13.6	0.2062	0.3402	0.1696
Draconibacterium	0.0827	0.4161	12.77	3.469	3.492
Crassaminicella	0.006454	0.8045	6.202	10.68	10.35
Maridesulfovibrio	0.02844	2.335	3.183	10.64	6.391
Serpentinicella	0.004303	10.18	0.2291	1.389	3.472
Sulfurovum	8.113	0.002169	NA	0.000522	0.000689
Desulfomicrobium	0.06956	0.06236	0.5023	7.878	5.54
Halarcobacter	0.001434	NA	0.2581	3.965	7.52
Methanococcoides	0.08151	7.294	NA	NA	NA
Shewanella	0.01864	0.0103	1.287	5.786	6.979
Candidatus Prometheoarchaeum	6.812	0.015	NA	NA	NA
Candidatus Methanoplasma	6.768	0.03362	NA	NA	NA
Desulfosarcina	6.685	0.003615	NA	0.008087	0.003102
Desulfuromonas	5.615	0.001446	0.3122	5.735	5.274
Fusobacterium	0.001195	4.787	0.001397	0.00287	0.008271
Thiohalobacter	3.865	0.001084	NA	NA	NA
Sedimentibacter	NA	0.06091	1.74	3.18	2.776
Anaerotignum	0.001195	2.691	0.01886	0.1283	0.3395
Kineobactrum	2.52	0.000904	NA	NA	NA
Pseudodesulfovibrio	2.237	0.188	0.03544	0.4844	0.3563
Methanomassiliicoccus	2.058	0.003976	NA	NA	NA
Desulforapulum	0.2462	0.003796	0.000524	1.978	1.161
Woeseia	1.962	0.000362	NA	NA	0.000345

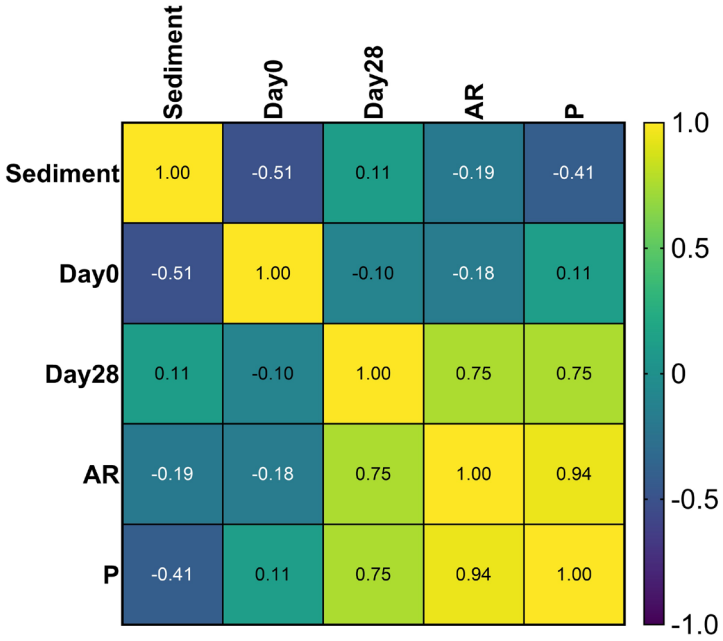

Figure B9. Spearman correlation coefficients for environmental marine sediment, Day 0, and Day 28 planktonic samples, AR and P biofilms, after exposure to anaerobic nutrient-enriched artificial seawater media for 28 days.

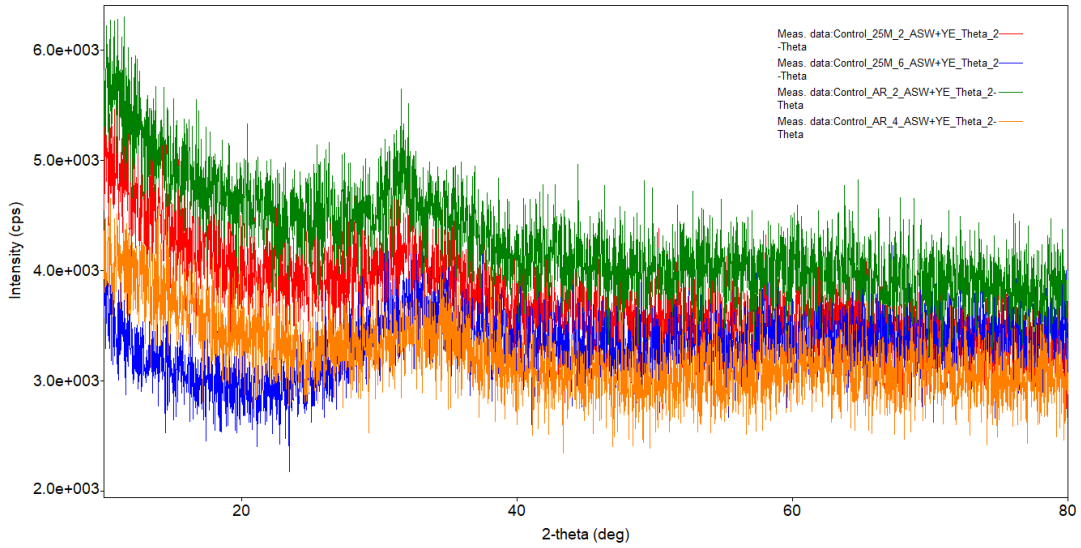

(a)

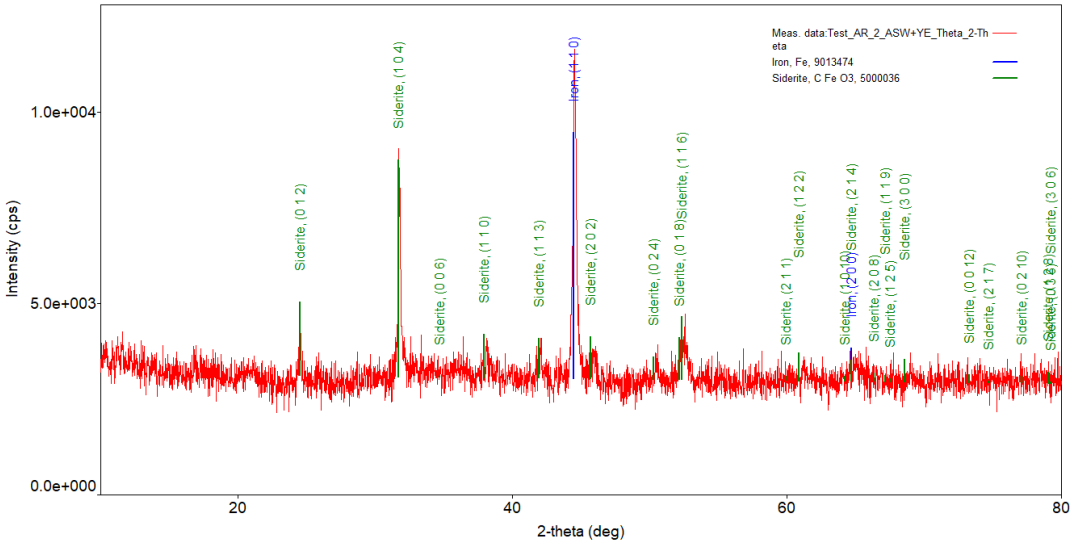

(b)

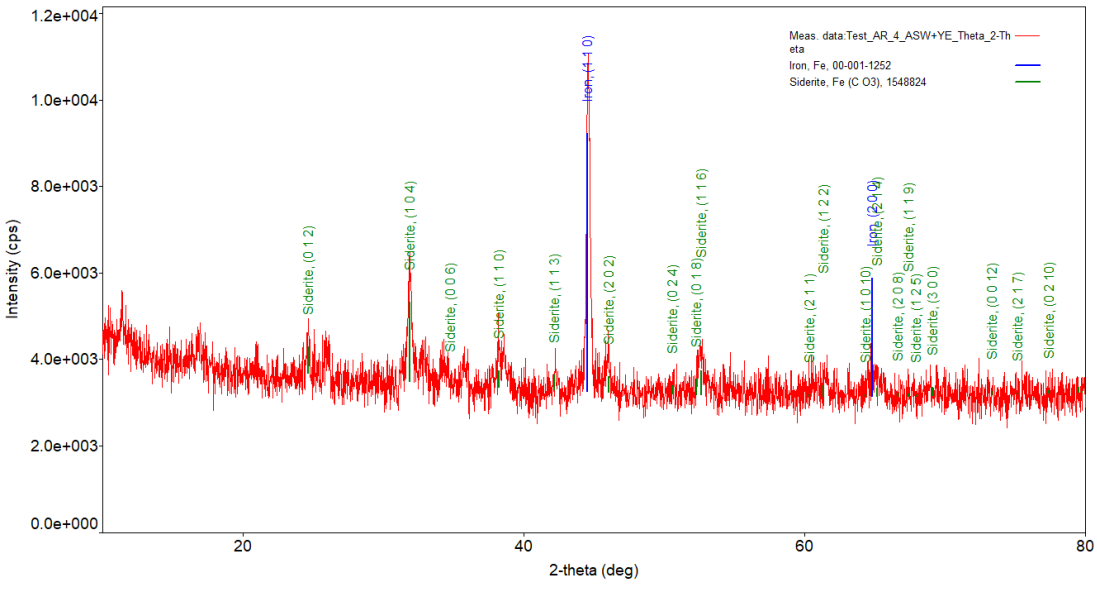

(c)

Figure B10. XRD patterns for corrosion products formed on carbon steel for abiotic **(a)**, and biotic coupons **(b, c)**, after exposure to anaerobic nutrient-enriched artificial seawater media for 28 days.

Appendix C

Table C1a. ATCC 1249 Modified Baar's media composition. Each component is adjusted to pH 7.5 and autoclaved at 121°C. The three components are mixed aseptically and stored under anaerobic conditions. The anaerobic chamber gas mixture consisted of 85% N_2, 10% CO_2 and 5% H_2.

Component 1	
$MgSO_4$	2.0 g
Sodium Citrate	5.0 g
$CaSO_4 \times 2H_2O$	1.0 g
NH_4Cl	1.0 g
DI Water	400.0 ml
Component 2	
K_2HPO_4	0.5 g
DI Water	200.0 ml
Component 3	
Sodium Lactate	3.5 g
Yeast Extract	1.0 g
DI Water	400.0 ml

Table C2. Environmental conditions on the day the marine sediment was collected on November 19, 2022.

Date & Time	14/09/2022 07:32	14/09/2022 07:47	14/09/2022 08:02	14/09/2022 08:17	14/09/2022 08:32	14/09/2022 08:47	14/09/2022 09:02	14/09/2022 09:17	14/09/2022 09:32
pH units (pH/ORP)	8.04	8.03	8.03	8.04	8.02	8.03	8.03	8.04	8.04
Specific Conductivity mS/cm (Conductivity)	46.726	46.782	46.798	46.762	46.158	46.046	46.063	46.207	46.374
Turbidity NTU (Turbidity/Brush)	3.3	1.8	2.9	1.8	1.4	2	1.7	1.7	1.9
Barometric Pressure mmHg (Necessary Input)	765.4	765.4	765.4	765.4	765.4	765.4	765.4	765.4	765.4
DO mg/L (Hach LDO)	8.84	8.83	8.96	8.73	8.9	8.75	8.97	8.82	8.79
Depth meters (Depth 25 m)	0.127	0.124	0.125	0.117	0.125	0.116	0.112	0.116	0.112
Turbidity mV (Turbidity/Brush)	30.198	26.851	29.206	26.79	25.966	27.288	26.568	26.641	27.012
DO %SAT (Hach LDO)	97.5	97.4	99	96.4	97.4	95.7	98.1	96.7	96.6
ORPAgCl mV (pH/ORP)	205	202	206	208	206	208	210	206	211
Temperature °C (Temperature)	11.43	11.42	11.5	11.5	11.19	11.21	11.19	11.25	11.35
Total Dissolved Solids g/L (Conductivity)	29.904	29.941	29.951	29.927	29.541	29.469	29.48	29.573	29.679
Specific Gravity (Depth 25 meter)	0.03113	0.03034	0.03009	0.02988	0.03002	0.03006	0.03341	0.03005	0.02979
Density kg/m^3 (Depth 25 m)	1.023	1.023	1.023	1.023	1.023	1.023	1.023	1.023	1.023
Salinity psu (Conductivity)	1023.22	1023.25	1023.25	1023.23	1022.94	1022.88	1022.89	1022.96	1023.04
Chlorophyll a µg/L (Chlorophyll a)	30.53	30.57	30.58	30.55	30.12	30.03	30.05	30.15	30.27

Abiotic Coupons

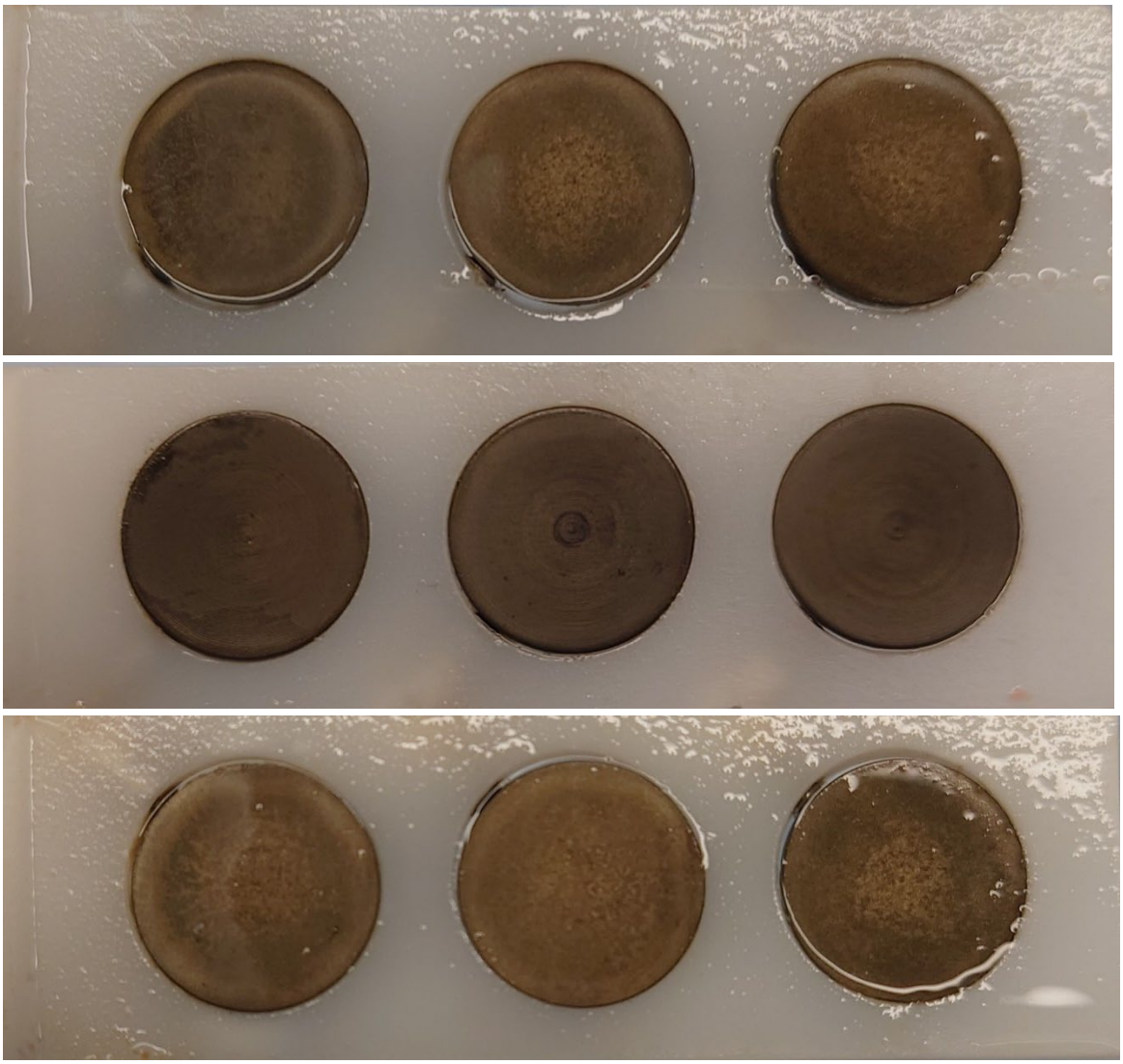

Figure C3a. Photographs taken of the coupon rods taken from the abiotic condition on Day 28, on dismantling the reactor, after exposure to anaerobic MB media for 28 days.

Biotic Coupons

Figure C3b. Photographs taken of the coupon rods taken from the biotic condition on Day 28, on dismantling the reactor, after exposure to anaerobic MB media for 28 days.

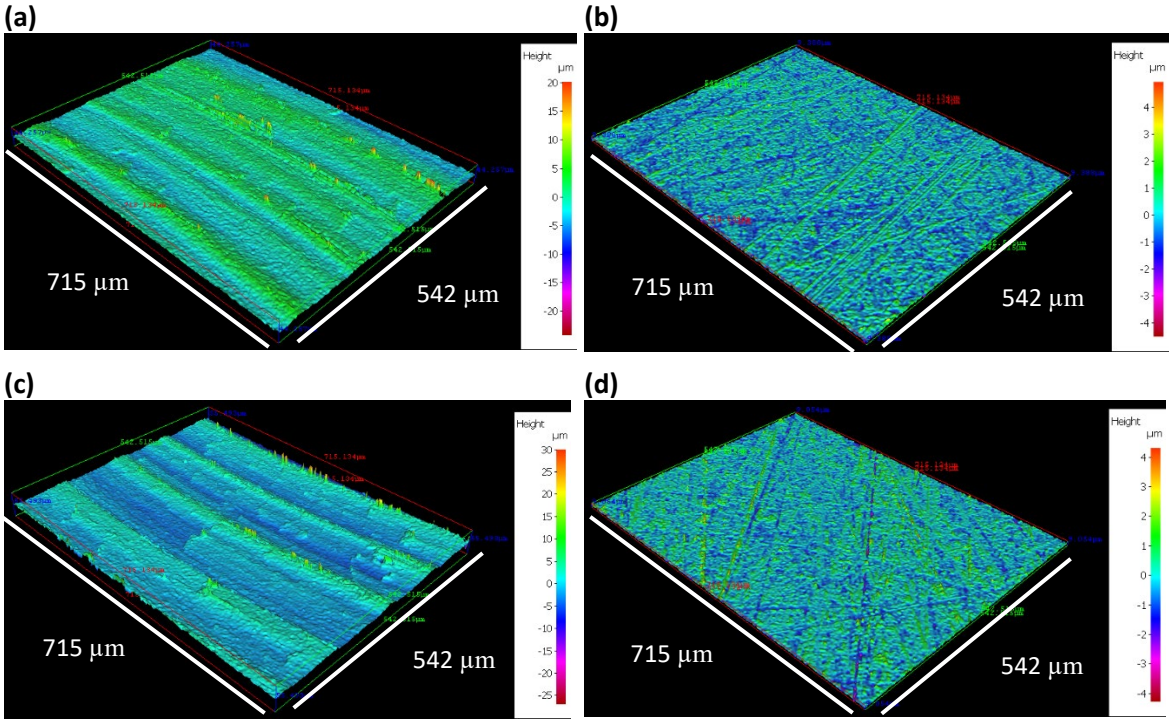

Figure C4. Three-dimensional optical surface profilometry of UNS G10180 surfaces at day 0. AR coupons for: **(a)** abiotic and **(b)** biotic conditions; and P coupons for: **(c)** abiotic and **(d)** biotic conditions, prior to exposure to anaerobic MB media for 28 days.

Table C5a. Quantitative surface roughness profiles for AR coupon samples on day 0 and day 28. R_a average roughness of profile, R_t maximum peak to valley height of roughness, R_z mean peak to valley height, R_p maximum peak height, R_v maximum valley height, R_c mean height of profile irregularities, R_{sm} mean spacing of profile irregularities, R_t/R_z extreme scratch/peak value of roughness profile (higher values (>=1) represent larger scratches/peaks).

Day	Reactor	R_a (µm)	R_t (µm)	R_z (µm)	R_{peak} (µm)	R_v (µm)	R_c (µm)	R_{sm} (µm)	R_t/R_z (µm)
0	Abiotic	1.2±0.6	16.0±10.9	9.4±4.8	10.6±7.0	5.4±5.2	8.5±7.7	216±190	1.6±0.4
	Biotic	1.1±0.4	13.3±6.4	8.2±3.3	9.2±5.6	4.1±1.8	6.3±3.5	171±106	1.6±0.3
28	Abiotic	1.7±0.8	16.7±9.3	10.3±3.4	7.2±1.9	9.5±8.1	9.1±6.2	163±122	1.6±0.5
	Biotic	2.0±1.3	23.1±13.4	14.4±8.1	8.6±3.9	14.5±10.6	10.6±5.6	182±80	1.6±0.3

Table C5b. Quantitative surface roughness profiles for P coupon samples on day 0 and day 28.

Day	Reactor	R_a (μm)	R_t (μm)	R_z (μm)	R_{peak} (μm)	R_v (μm)	R_c (μm)	R_{sm} (μm)	R_t/R_z (μm)
0	Abiotic	0.4±0.05	4.0±0.5	3.2±0.3	2.3±0.4	1.7±0.3	1.8±0.2	34±3	1.2±0.1
	Biotic	0.4±0.05	4.3±0.7	3.4±0.4	2.5±0.5	1.8±0.3	1.9±0.2	35±5	1.3±0.1
28	Abiotic	1.1±0.9	21.6±14.4	9.5±5.2	6.8±4.8	14.7±10.4	11.1±9.2	271±278	2.1±0.5
	Biotic	2.5±0.6	34.6±5.4	19.7±3.0	10.2±3.2	24.4±4.7	17.4±2.8	251±93	1.8±0.3

Table C6a. EIS parameters of the carbon steel coupons immersed in anaerobic MB media for the abiotic condition on days 1, 7, 14, 21 and 28. **Equivalent circuit:** ① – R_s+(Q_1/Q_2+R_{ct}); ③ – R_s+Q_1/(R_{film}+Q_2/R_{ct}).

Day	Coupon	R_s / Ω cm^2	Q_1 / mΩ^{-1} cm^{-2} s^n	n_1	R_{film} / Ω cm^2	Q_2 / mΩ^{-1} cm^{-2} s^n	n_2	R_{ct} / Ω cm^2	$\chi^2 \times 10^{-4}$
1	AR ①	38.8±3.3	0.56±0.07	0.78±0.00	–	442.3±745.6	0.01±0.02	415±746	15
	P ①	38.9±2.3	0.62±0.02	0.79±0.01	–	97.9±83.3	0.00±0.00	617±86	21
7	AR ①	17.9±15.6	0.61±0.33	0.33±0.07	–	0.44±0.49	0.79±0.29	121±82	18
	P ①	35.8±1.9	0.40±0.09	0.51±0.02	–	1.33±1.04	0.69±0.27	184±104	25
14	AR ③	33.6±7.7	0.27±0.26	0.76±0.28	5310±6067	0.55±0.34	0.89±0.07	1007±1680	14
	P ③	24.2±8.0	0.39±0.22	0.40±0.12	7.12E+07±6.18E+07	0.94±0.94	0.74±0.16	46±18	9.9
21	AR ①	30.6±4.8	0.31±0.03	0.43±0.06	–	0.25±0.01	0.93±0.03	117±45	18
	P ①	34.0±2.7	0.45±0.04	0.44±0.03	–	1.82±1.45	0.73±0.24	203±44	20
28	AR ③	14.6±25.3	0.29±0.46	0.61±0.23	1605±1345	2.17±2.43	0.89±0.09	366±561	13
	P ③	13.4±14.9	0.15±0.26	0.57±0.21	1935±619	0.80±0.16	0.83±0.03	26±16	2.6

Table C6b. EIS parameters of the carbon steel coupons immersed in anaerobic MB media for the biotic condition on days 1, 7, 14, 21 and 28. **Equivalent circuit:** ④– R_s+Q_1+(Q_2/R_{ct}).

Day	Coupon	R_s / Ω cm^2	Q_1 / mΩ^{-1} cm^{-2} s^n	n_1	Q_2 / mΩ^{-1} cm^{-2} s^n	n_2	R_{ct} / Ω cm^2	$\chi^2 \times 10^{-4}$
1	AR ④	41.9±4.7	2.56±0.24	0.77±0.07	0.19±0.02	0.90±0.02	3565±327	28
	P ④	42.4±2.2	2.41±0.45	0.78±0.08	0.19±0.03	0.90±0.01	2870±844	36
7	AR ④	33.6±3.6	1.67±0.48	0.88±0.11	2.29±0.80	0.93±0.08	551±429	43
	P ④	34.1±2.0	1.75±0.42	0.88±0.11	1.66±0.54	0.95±0.07	993±915	51
14	AR ④	23.5±20.4	2.95±1.18	0.90±0.09	1.58±2.05	0.81±0.18	225±353	36
	P ④	33.4±1.2	2.28±0.19	0.88±0.02	5.61±9.13	0.67±0.58	41±69	21
21	AR ④	26.3±23.1	2.00±0.16	0.84±0.02	7.91±6.85	1.00±0.00	59±29	29
	P ④	12.0±20.7	1.86±0.08	0.88±0.01	3.76±6.51	0.62±0.34	61±44	10
28	AR ④	37.0±3.2	1.93±0.17	0.84±0.02	6.51±5.53	1.00±0.00	59±60	44
	P ④	32.6±1.2	2.26±0.87	0.93±0.07	1.16±1.41	0.94±0.10	457±788	26

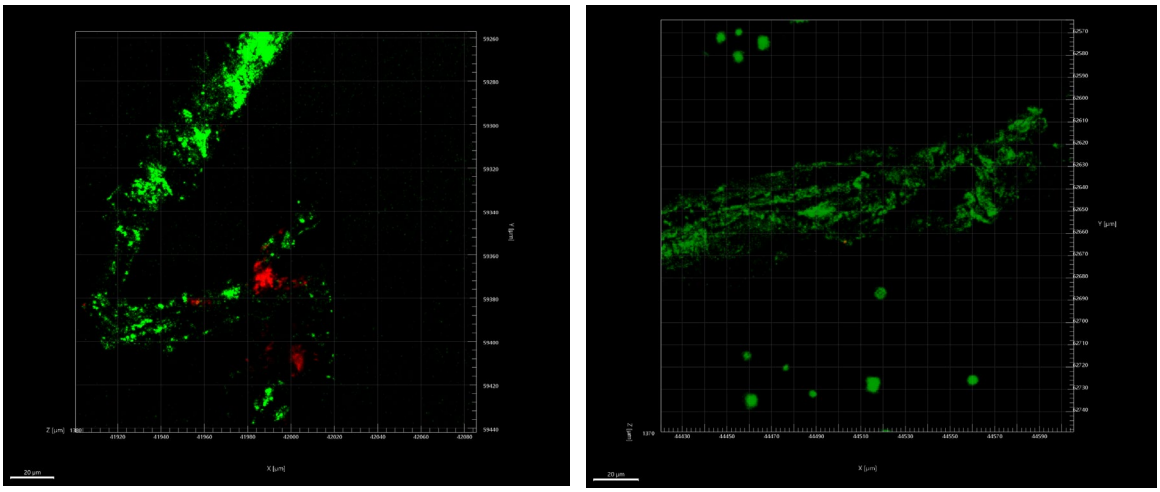

Figure C7. Confocal images of biofilms formed over UNS G10180 carbon steel surfaces for **(a)** AR and **(b)** P biofilms, after exposure to anaerobic MB media for 28 days.

Table C8. List of top 25 microbial genera identified through 16S rRNA amplicon sequencing with two target region, V3-4 for bacteria and archaea, after exposure to anaerobic MB media for 28 days.

Name	Sediment	Day0	Day28	AR	25M
Desulfovibrio	0.08945	0.09537	32.02	54.73	52.49
Clostridium	0.1979	13.26	0.7714	3.671	3.613
Klebsiella	0.09221	11.14	3.758	2.412	2.002
Sulfurovum	9.308	0.05396	0.001624	0.000427	0.000813
Escherichia	0.3072	8.908	4.851	3.425	3.041
Parabacteroides	0.004009	7.908	6.417	3.84	4.74
Veillonella	0.000251	7.777	0.04258	0.1269	0.2159
Anaerotignum	0.000752	7.061	3.891	1.256	1.512
Bacteroides	0.004009	6.807	4.553	2.663	2.405
Sulfurospirillum	0.01879	0.000267	6.502	0.4396	0.5303
Salmonella	0.1947	5.843	5.63	2.26	2.059
Desulfuromonas	5.616	0.02698	NA	NA	NA
Enterobacter	0.01077	2.699	5.362	1.23	1.121
Candidatus Prometheoarchaeum	5.229	0.02351	NA	NA	NA
Anaerotruncus	0.01077	0.276	5.202	1.447	1.483
Terrisporobacter	0.003508	5.164	0.007398	0.349	0.3042
Desulfosarcina	4.827	0.02244	NA	NA	NA
Thiohalobacter	3.976	0.01924	NA	0.000854	0.000407
Candidatus Methanoplasma	3.699	NA	NA	NA	NA
Kineobactrum	3.526	0.01229	NA	NA	NA
Fusobacterium	0.002004	1.875	1.166	2.857	3.313
Providencia	0.000251	0.05183	3.259	0.5887	0.501
Ruthenibacterium	0.006515	2.806	2.349	1.753	2.235
Aliarcobacter	0.01278	0.000802	2.759	0.9953	0.9821
Wenzhouxiangella	2.629	0.01015	NA	NA	NA

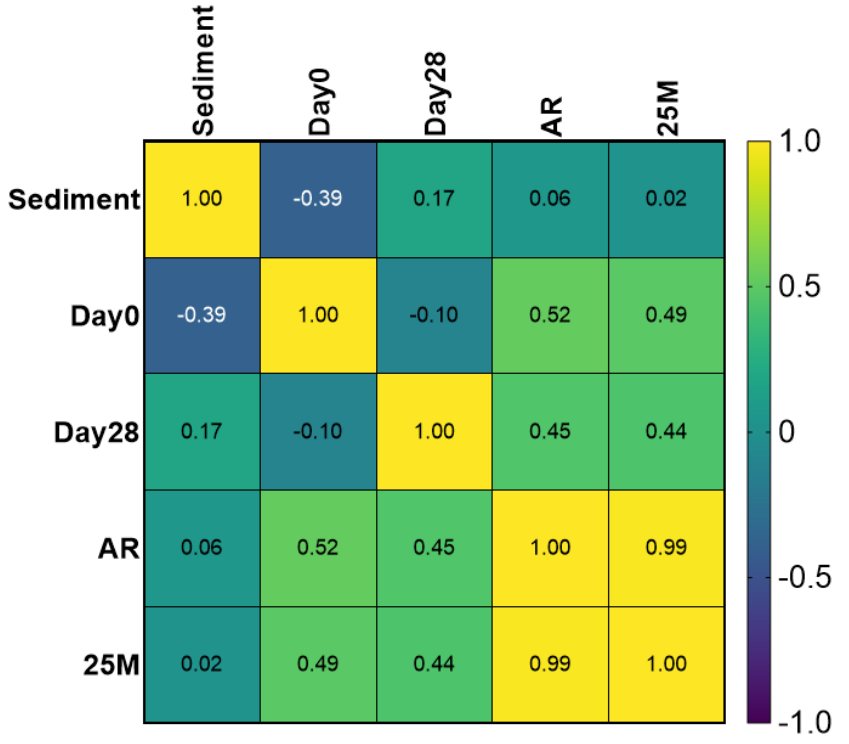

Figure C9. Spearman correlation coefficients for environmental marine sediment, Day 0, and Day 28 planktonic samples, AR and P biofilms, after exposure to anaerobic MB media for 28 days.

Appendix D

Table D1a. Produced water test solution/media composition. The produced water was filter sterilized using a 0.2 µm Vivaflow® TFF Cassette, PES (Sartorius).

Major Ion	Concentration (mg L^{-1})	Anions	Concentration (mg L^{-1})
Barium, Ba	141	Ammonium in water	54
Boron, B	73.4	Bicarbonate, HCO_3^-	642
Calcium, Ca	982	Bromide, Br^-	226
Chloride, Cl^-	31300	Chloride, Cl^-	31600
Iron, Fe	4.2	Fluoride	4
Magnesium, Mg	518	H2S dissolved in water	0.67
Potassium, K	259	Iodine, I^-	113
Sodium, Na	19100	Nitrate, NO_3^-	2
Strontium, Sr	96.5	pH at 20°C	6.7
Sulphate, SO_4^{2-}	750	Resistivity	0.136
Sulphur, S	523	Resistivity at temperature	22.4
Suspended solids	16	Specific gravity at 15°C	1.03868
Total dissolved salt	53300	Sulphate, SO_4^{2-}	550
Ionbalance (cation/anion)	1.9	Total alkalinity	19.5

Table D1b. Produced water test solution/media composition.

Organic Acids	**Concentration (mg L^{-1})**
Acetic acid	820
butanoic acid	15
Formic acid	12
Hexonic acid	<2
Pentoic acid	4
Propanoic acid	74

Abiotic Coupons

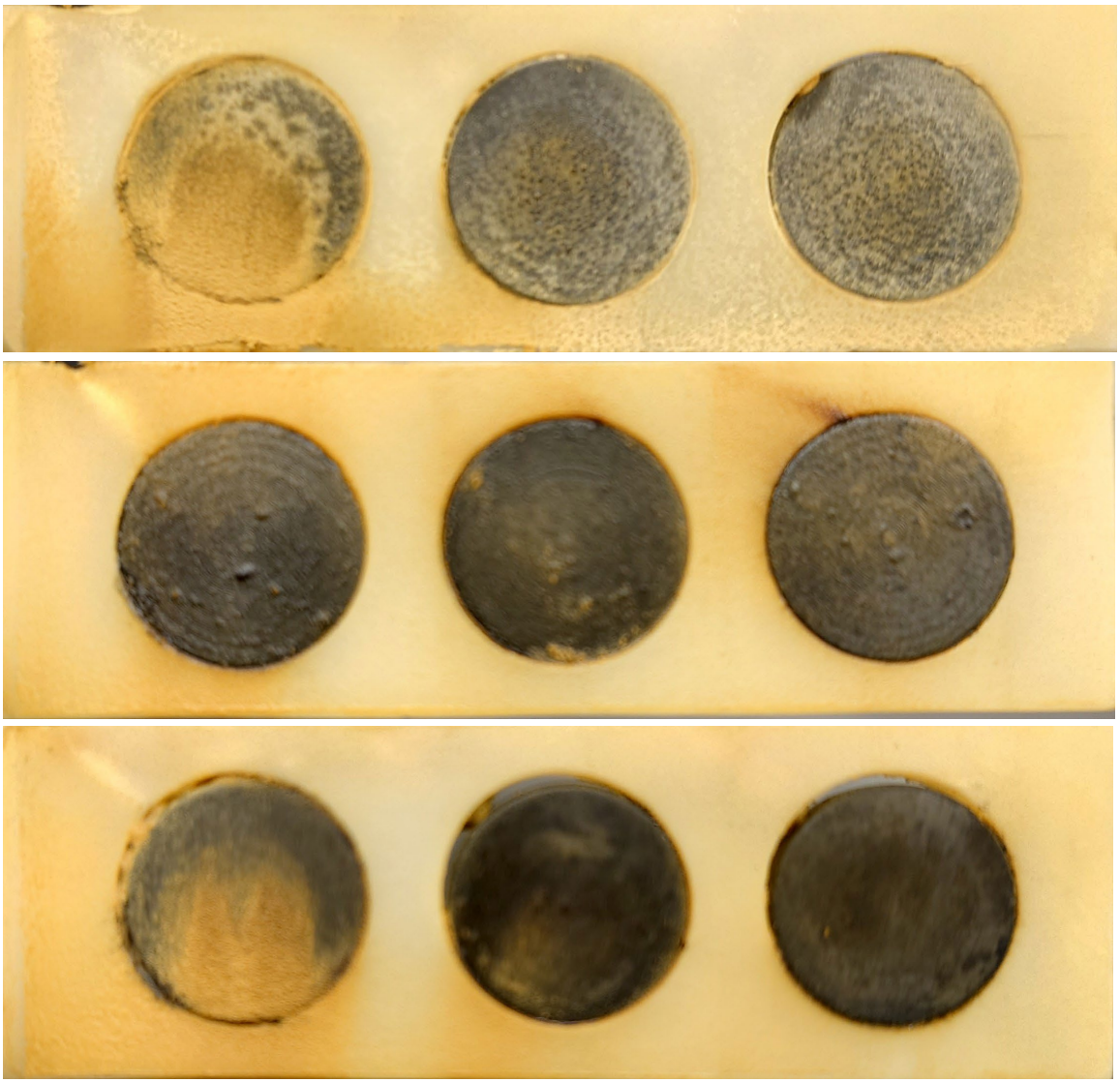

Figure D2a. Photographs taken of the coupon rods taken from the abiotic condition on Day 28, on dismantling the reactor, after exposure to anaerobic produced water media for 28 days.

Biotic Coupons

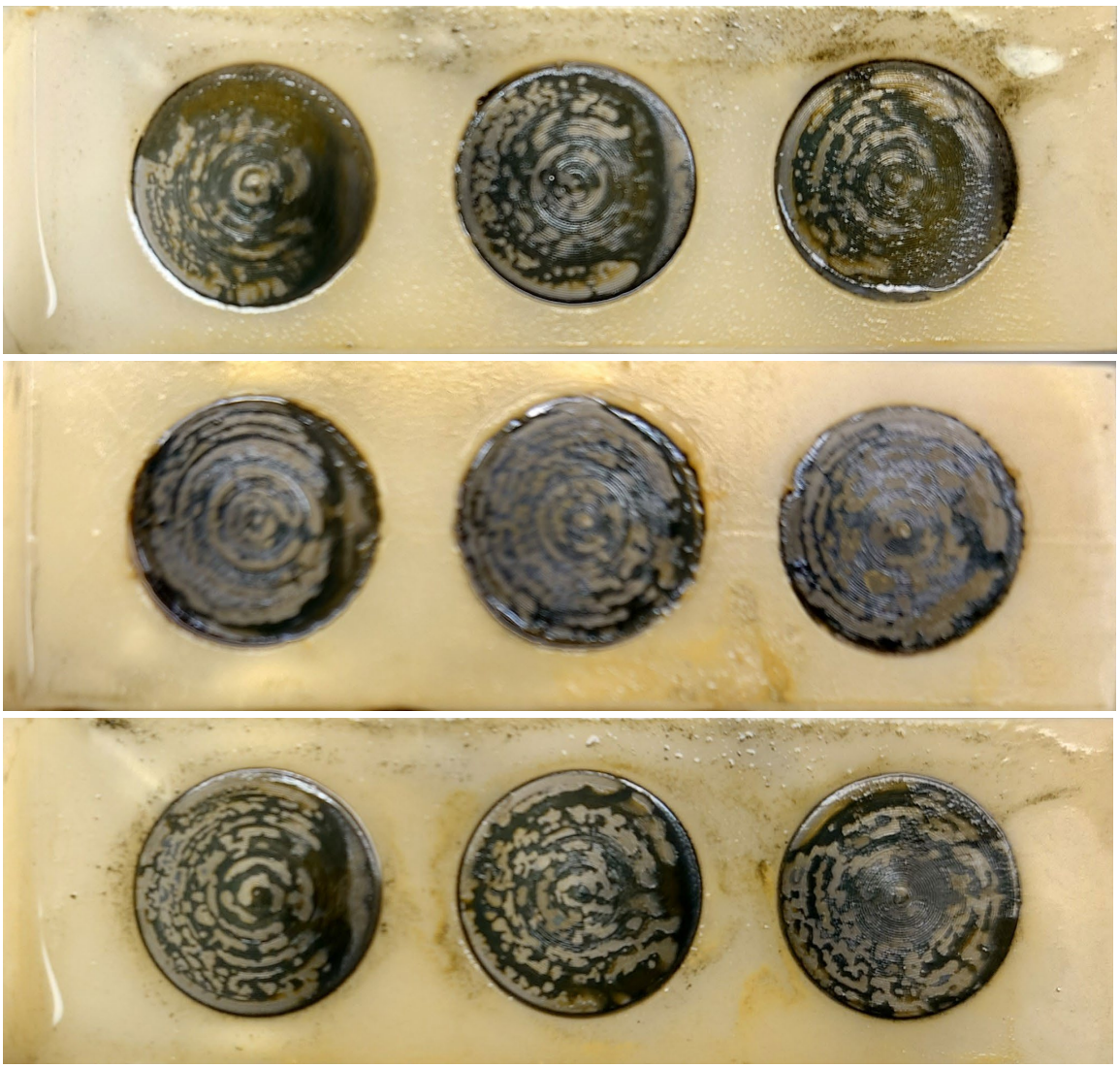

Figure D2b. Photographs taken of the coupon rods taken from the biotic condition on Day 28, on dismantling the reactor, after exposure to anaerobic produced water media for 28 days.

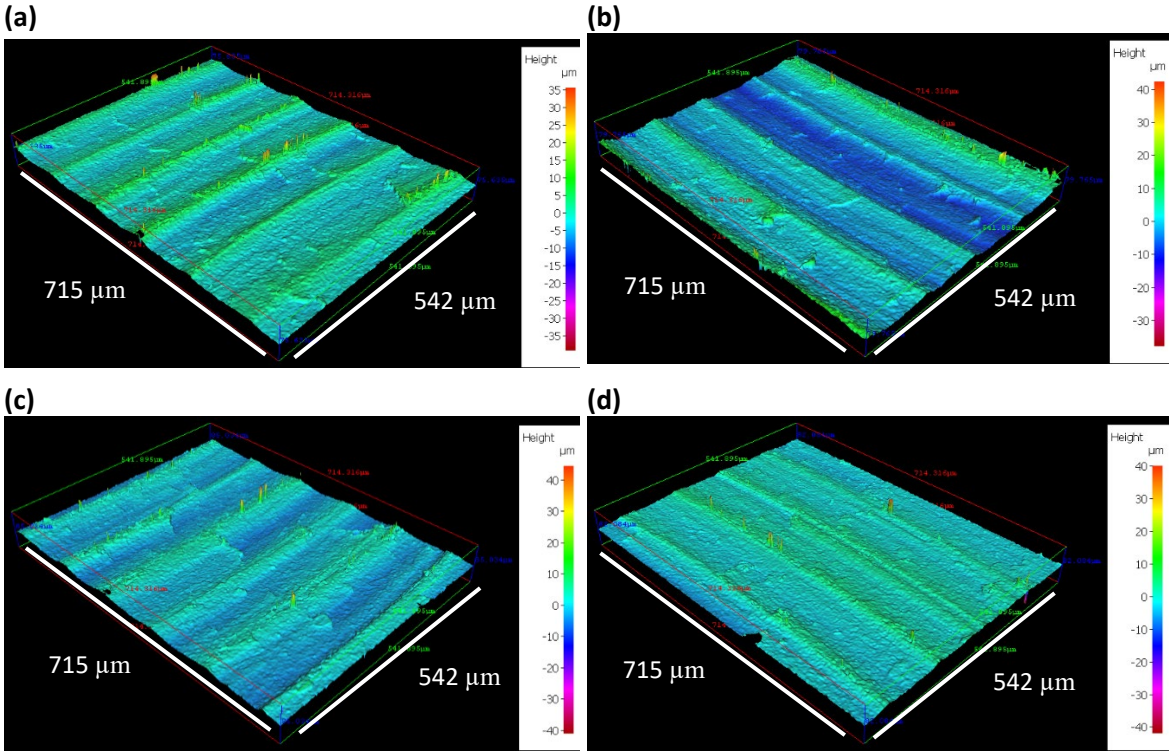

Figure D3. Three-dimensional optical surface profilometry of the cleaned UNS G10180 surfaces at day 28. AR coupons for: **(a,b)** abiotic and **(c,d)** biotic conditions, prior to exposure to anaerobic produced water media for 28 days.

Table D4. Quantitative surface roughness profiles for AR coupon samples on day 0 and day 28. R_a average roughness of profile, R_t maximum peak to valley height of roughness, R_z mean peak to valley height, R_p maximum peak height, R_v maximum valley height, R_c mean height of profile irregularities, R_{sm} mean spacing of profile irregularities, R_t/R_z extreme scratch/peak value of roughness profile (higher values (>=1) represent larger scratches/peaks).

Day	Reactor	R_a (µm)	R_t (µm)	R_z (µm)	R_p (µm)	R_v (µm)	R_c (µm)	R_{sm} (µm)	R_t/R_z (µm)
0	Abiotic	1.2±0.6	9.5±2.7	7.1±2.3	5.9±1.6	3.6±1.3	5.4±2.1	136±38	1.3±0.2
	Biotic	1.1±0.5	8.2±2.6	6.3±2.1	5.0±1.6	3.3±1.2	4.6±2.0	115±23	1.3±0.2
28	Abiotic	1.3±0.6	10.3±3.6	7.6±2.5	5.8±2.3	4.5±1.7	5.4±2.1	104±26	1.3±0.2
	Biotic	1.3±0.6	10.0±3.5	7.3±2.6	6.0±1.8	4.0±2.0	5.3±2.2	112±36	1.4±0.2

Table D5a. Quantitative SEM-EDS data collected from elemental mapping of the abiotic UNS G10180 carbon steel surfaces, after exposure to anaerobic produced water media for 28 days.

Statistic	O	F	Na	Mg	Al	Si	P	S	Cl	K	Ca	Mn	Fe	Ni	Cu	Mo	Rh	Sn	Ba	W
Max	37.35	8.94	22.92	1.30	0.00	4.49	1.43	2.33	23.16	0.82	9.63	0.00	46.00	0.00	0.00	0.00	2.33	0.00	7.65	1.74
Min	20.93	8.94	3.84	0.26	0.00	1.09	0.41	0.44	0.85	0.28	1.82	0.00	22.74	0.00	0.00	0.00	1.29	0.00	1.45	1.74
Average	29.88	8.94	11.29	0.80	-	3.38	0.70	1.42	8.03	0.50	5.69	-	33.89	-	-	-	1.74	-	3.87	1.74
StDev (σ)	3.56	-	4.66	0.20	-	0.82	0.22	0.48	6.13	0.18	1.76	-	7.03	-	-	-	0.39	-	1.26	-

Table D.5a. Quantitative SEM-EDS data collected from elemental mapping of the biotic UNS G10180 carbon steel surfaces, after exposure to anaerobic produced water media for 28 days.

Statistic	O	F	Na	Mg	Al	Si	P	S	Cl	K	Ca	Mn	Fe	Ni	Cu	Mo	Rh	Sn	Ba	W
Max	50.17	0.00	40.61	0.64	0.27	2.99	0.00	1.01	13.63	0.24	1.85	4.72	82.72	0.96	1.23	0.57	0.00	0.93	0.00	0.00
Min	12.10	0.00	1.34	0.27	0.27	0.19	0.00	0.22	0.23	0.24	0.25	0.53	9.22	0.34	0.26	0.57	0.00	0.93	0.00	0.00
Average	25.12	-	6.51	0.43	0.27	0.59	-	0.57	2.58	0.24	0.55	1.24	65.24	0.65	0.79	0.57	-	0.93	-	-
StDev (σ)	6.53	-	7.12	0.12	-	0.64	-	0.26	3.22	-	0.38	0.86	11.06	0.44	0.35	-	-	-	-	-

Table D6a. EIS parameters of the carbon steel coupons immersed in anaerobic produced water media for the abiotic condition on days 1, 7, 14, 21 and 28. **Equivalent circuit:** ① – $R_s+(Q_1/Q_2+R_{ct})$; ③ – $R_s+Q_1/(R_{film}+Q_2/R_{ct})$.

Day	Coupon	R_s / Ω cm^2	Q_1 / mΩ^{-1} cm^{-2} s^n	n_1	R_{film} / Ω cm^2	Q_2 / mΩ^{-1} cm^{-2} s^n	n_2	R_{ct} / Ω cm^2	$\chi^2 \times 10^{-4}$
1	AR ①	5.39±0.36	0.29±0.06	0.82±0.02	–	0.50±0.42	0.44±0.06	2921±2317	49
7	AR ①	4.90±0.40	0.72±0.06	0.84±0.03	–	0.43±0.19	0.68±0.17	1234±828	52
14	AR ①	4.32±2.16	2.01±1.09	0.75±0.09	–	1.34±1.06	0.72±0.14	382±559	42
21	AR ①	6.09±1.48	1.39±1.16	0.66±0.19	–	2.25±1.61	0.66±0.15	237±358	11
28	AR ③	5.37±3.41	0.55±0.58	0.64±0.22	2422±1385	0.81±0.51	0.63±0.23	176±304	29

Table D6b. EIS parameters of the carbon steel coupons immersed in anaerobic produced water media for the biotic condition on days 1, 7, 14, 21 and 28. **Equivalent circuit:** ① $-R_s+(Q_1/Q_2+R_{ct})$; ④$-R_s+Q_1+(Q_2/R_{ct})$.

Day	Coupon	R_s / Ω cm^2	Q_1 / mΩ^{-1} cm^{-2} s^n	n_1	Q_2 / mΩ^{-1} cm^{-2} s^n	n_2	R_{ct} / Ω cm^2	$\chi^2 \times 10^{-4}$
1	AR ①	5.22±0.38	0.38±0.15	0.86±0.02	1.42±0.72	0.38±0.11	419±322	34
7	AR ①	4.04±2.05	0.93±0.44	0.76±0.21	1.13±0.58	0.66±0.13	348±273	54
14	AR ④	4.74±0.59	3.20±1.33	0.79±0.02	2.52±1.31	0.89±0.06	42±20	50
21	AR ④	4.68±0.59	5.21±2.63	0.77±0.01	2.68±0.84	0.84±0.06	46±16	51
28	AR ④	4.74±0.36	6.97±2.97	0.81±0.08	4.73±0.76	0.82±0.03	85±107	30

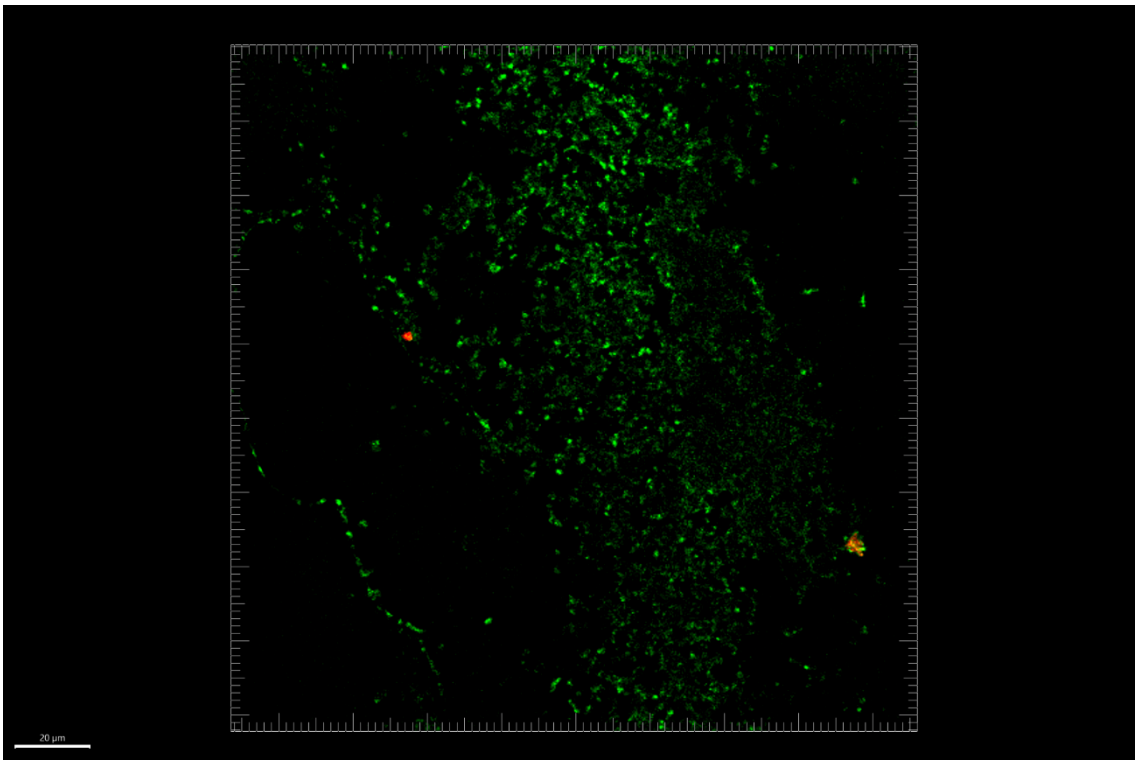

Figure D7. Confocal image of biofilm formed over UNS G10180 carbon steel surfaces for AR biofilms, after exposure to anaerobic produced water media for 28 days.

Table D8. List of top 25 microbial genera identified through 16S rRNA amplicon sequencing with two target region, V3-4 for bacteria and archaea, after exposure to anaerobic produced water media for 28 days.

Name	Sediment	Day0	Day28	AR
Marinobacterium	0.006341	0.001318	9.109	42.43
Vibrio	0.09423	32.41	0.1822	1.277
Marinobacter	0.003875	0.001538	30.26	2.837
Pseudomonas	0.273	0.005711	25.73	19.9
Halomonas	0.01233	0.000659	22.91	5.648
Sulfurovum	13.84	0.0246	0.0005165	0.0008302
Methanococcoides	0.03188	12.47	0.002238	NA
Malaciobacter	0.001585	0.0008786	1.755	9.184
Desulfosarcina	6.477	0.009885	NA	NA
Apibacter	0.02501	6.249	0.08867	0.2828
Methanococcus	0.1828	5.618	NA	NA
Desulfuromonas	5.464	0.01098	0.0001722	NA
Pseudodesulfovibrio	4.922	0.01955	0.002583	0.1962
Thiohalobacter	4.505	0.007029	NA	0.0002767
Idiomarina	0.0347	0.0004393	4.063	1.072
Geosporobacter	0.004051	3.942	0.02462	0.2779
Anaerotignum	0.001585	3.91	0.002755	0.01743
Fusobacterium	0.001761	3.861	0.002583	0.0005535
Flavobacterium	0.1402	3.579	0.1104	1.631
Kineobactrum	3.376	0.004174	0.0001722	NA
Hungatella	0.0001761	3.152	0.005165	0.03321
Wenzhouxiangella	3.111	0.003515	NA	0.0005535
Shewanella	0.02255	1.266	0.4752	3.07
Candidatus Prometheoarchaeum	2.843	0.03624	0.0003444	NA
Carnobacterium	0.0001761	NA	0.2726	2.626

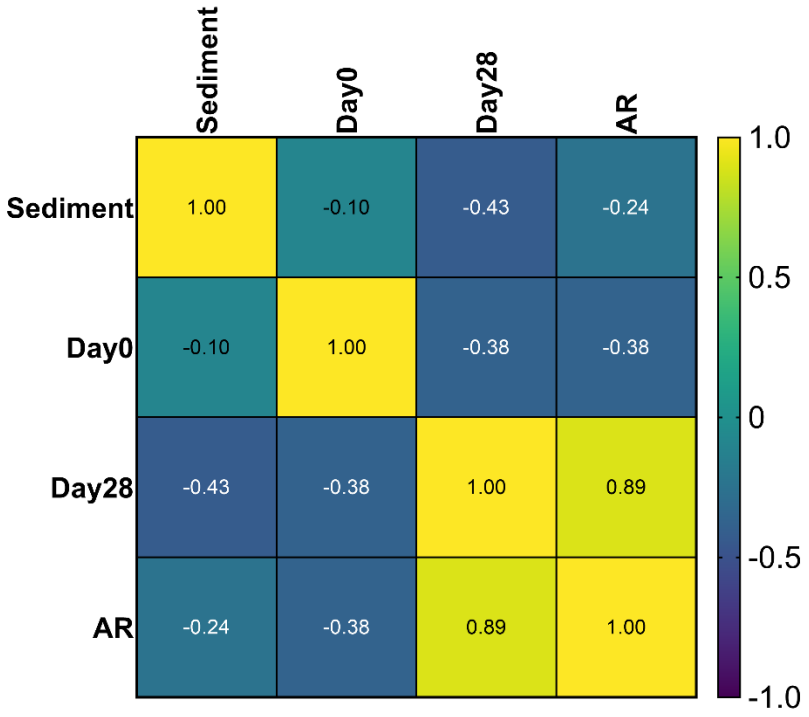

Figure D9. Spearman correlation coefficients for environmental marine sediment, Day 0, and Day 28 planktonic samples, and AR biofilms, after exposure to anaerobic produced water media for 28 days.

Appendix E

Abiotic Coupons

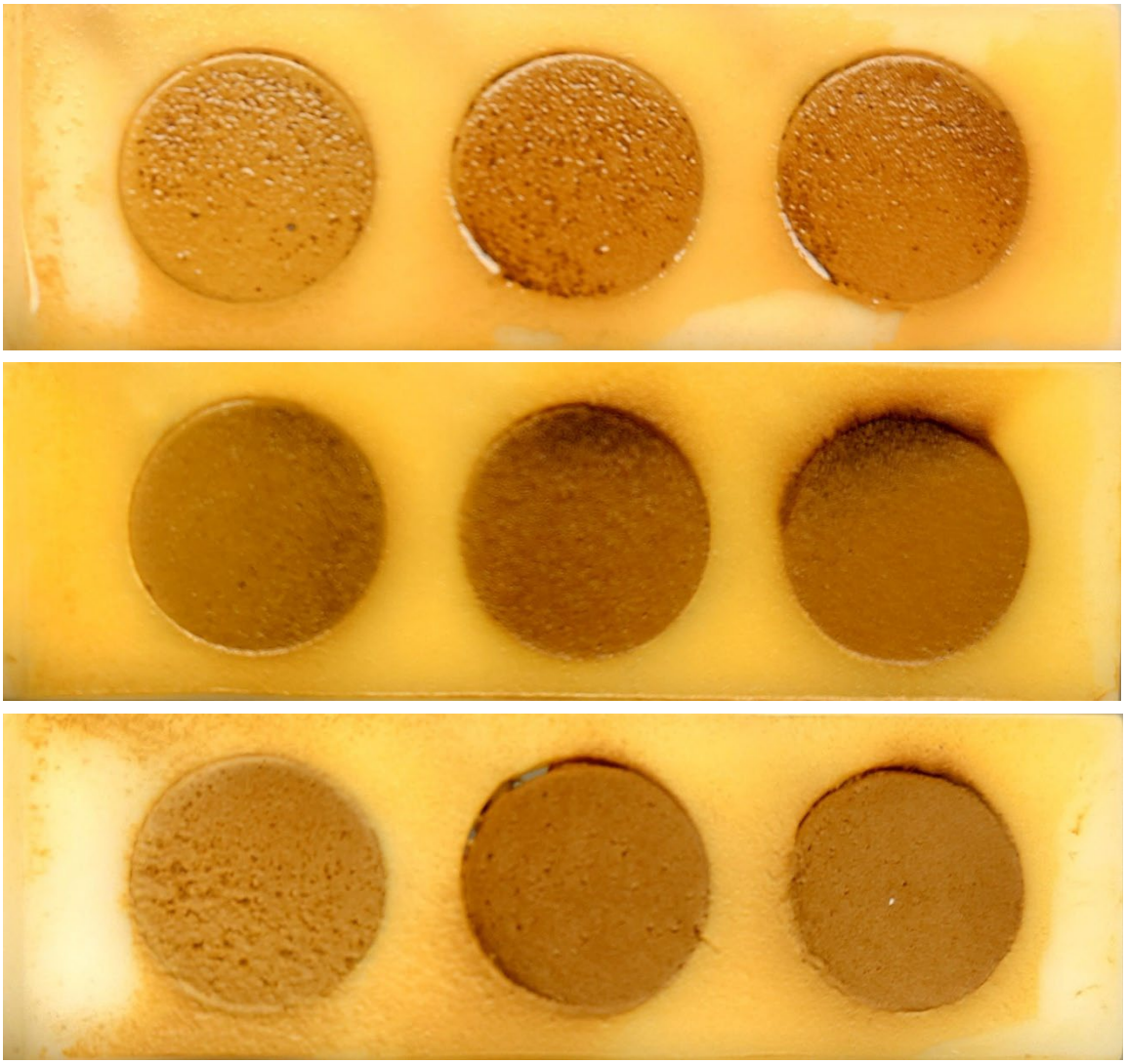

Figure E1a. Photographs taken of the coupon rods taken from the abiotic condition on Day 28, on dismantling the reactor, after exposure to anaerobic nutrient-enriched artificial seawater media dosed bi-weekly with glutaraldehyde for 28 days.

Biotic Coupons

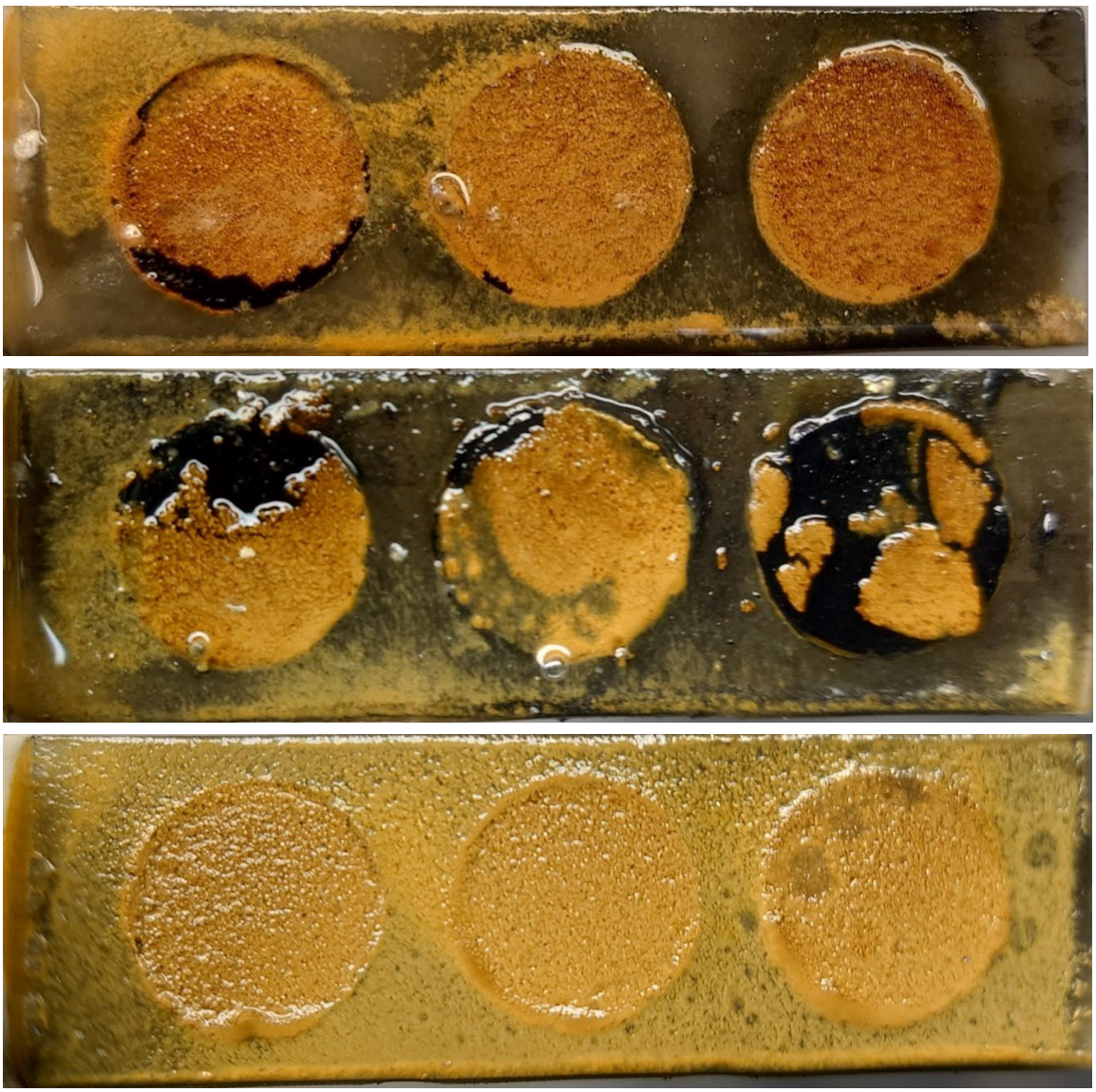

Figure E1b. Photographs taken of the coupon rods taken from the biotic condition on Day 28, on dismantling the reactor, after exposure to anaerobic nutrient-enriched artificial seawater media dosed bi-weekly with glutaraldehyde for 28 days.

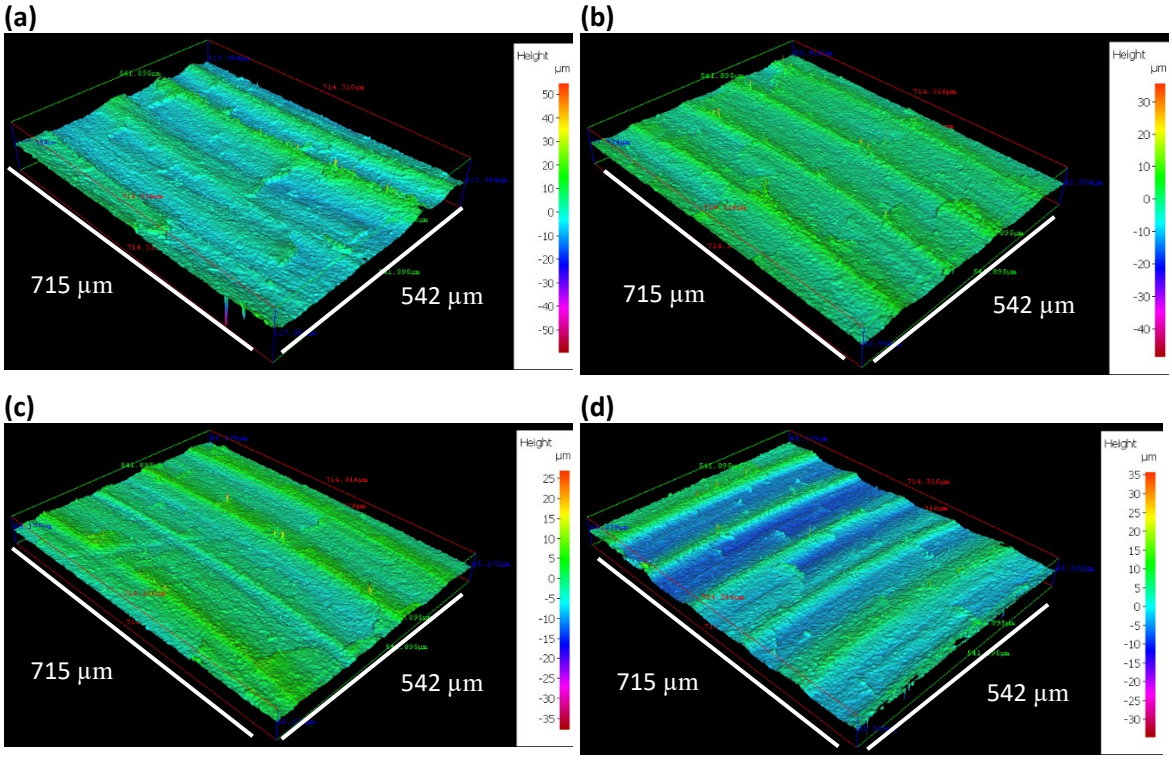

Figure E2. Three-dimensional optical surface profilometry of the cleaned UNS G10180 surfaces at day 28. AR coupons for: **(a,b)** abiotic and **(c,d)** biotic conditions, prior to exposure to anaerobic nutrient-enriched artificial seawater media dosed bi-weekly with glutaraldehyde for 28 days.

Table E3. Quantitative surface roughness profiles for AR coupon samples on day 0 and day 28. R_a average roughness of profile, R_t maximum peak to valley height of roughness, R_z mean peak to valley height, R_p maximum peak height, R_v maximum valley height, R_c mean height of profile irregularities, R_{sm} mean spacing of profile irregularities, R_t/R_z extreme scratch/peak value of roughness profile (higher values (>=1) represent larger scratches/peaks).

Day	Reactor	R_a (µm)	R_t (µm)	R_z (µm)	R_p (µm)	R_v (µm)	R_c (µm)	R_{sm} (µm)	R_t/R_z (µm)
0	Abiotic	1.2±0.7	9.6±3.7	7.1±2.9	5.7±2.4	3.9±1.7	5.3±2.3	126±34	1.4±0.2
	Biotic	1.3±0.6	10.0±3.2	7.4±2.3	6.3±2.4	3.8±1.1	5.6±2.2	139±38	1.4±0.2
28	Abiotic	1.2±0.6	8.4±3.6	6.6±2.8	4.8±2.2	3.6±1.5	4.7±2.6	104±30	1.3±0.1
	Biotic	1.1±0.5	8.3±2.1	3.4±1.8	4.3±1.2	3.9±1.4	4.4±1.6	104±20	1.3±0.1

Table E4a. Quantitative SEM-EDS data collected from elemental mapping of the abiotic UNS G10180 carbon steel surfaces, after exposure to anaerobic nutrient-enriched artificial seawater media dosed bi-weekly with glutaraldehyde for 28 days.

Statistic	O	F	Na	Mg	Si	P	S	Cl	K	Ca	Mn	Fe	Mo	Sn
Max	33.07	0.00	2.49	0.40	0.36	2.86	2.07	3.89	0.00	0.36	1.15	75.49	1.28	1.27
Min	22.56	0.00	0.54	0.40	0.22	0.29	0.32	0.23	0.00	0.27	0.60	61.14	1.28	1.05
Average	25.55	-	1.35	0.40	0.28	1.19	0.72	1.04	-	0.32	0.81	71.08	1.28	1.12
StDev (σ)	2.51	-	0.58	-	0.05	0.64	0.45	1.21	-	0.04	0.22	3.07	-	0.13

Table E4b. Quantitative SEM-EDS data collected from elemental mapping of the biotic UNS G10180 carbon steel surfaces, after exposure to anaerobic nutrient-enriched artificial seawater media dosed bi-weekly with glutaraldehyde for 28 days.

Statistic	O	F	Na	Mg	Si	P	S	Cl	K	Ca	Mn	Fe	Mo	Sn
Max	31.62	3.03	5.47	3.20	0.60	2.62	1.92	2.34	0.89	4.25	0.89	73.41	0.00	0.00
Min	21.81	3.03	0.54	0.39	0.20	1.00	0.20	0.19	0.28	0.23	0.51	55.60	0.00	0.00
Average	26.93	3.03	1.89	1.71	0.36	1.61	0.77	0.78	0.52	2.13	0.65	65.05	-	-
StDev (σ)	2.37	-	1.56	0.79	0.13	0.48	0.49	0.64	0.26	1.18	0.13	5.20	-	-

Table E5a. EIS parameters of the carbon steel coupons immersed in anaerobic nutrient-enriched artificial seawater media dosed bi-weekly with glutaraldehyde for the abiotic condition on days 1, 7, 14, 21 and 28. **Equivalent circuit:** ① – $R_s+(Q_1/Q_2+R_{ct})$; ② – $R_s+(Q_1/R_{ct})$; ③ – $R_s+Q_1/(R_{film}+Q_2/R_{ct})$.

Day	Coupon	R_s / Ω cm²	Q_1 / mΩ^{-1} cm^{-2} s^n	n_1	R_{film} / Ω cm²	Q_2 / mΩ^{-1} cm^{-2} s^n	n_2	R_{ct} / Ω cm²	$\chi^2 \times 10^{-4}$
1	AR ①	8.95±1.22	0.27±0.03	0.81±0.01	–	1.19±1.32	0.52±0.12	3960±1752	9.2
7	AR ②	8.51±0.87	0.67±0.13	0.90±0.01	–	–	–	5030±1547	6.2
14	AR ②	8.70±0.87	0.95±0.18	0.89±0.01	–	–	–	4859±1276	4.1
21	AR ②	8.60±0.85	1.02±0.20	0.90±0.01	–	–	–	4597±1038	4.5
28	AR ③	9.61±0.96	4.52±3.19	0.48±0.14	33920864±5062319	6.78±3.98	0.69±0.17	55±111	2.5

Table E5b. EIS parameters of the carbon steel coupons immersed in anaerobic nutrient-enriched artificial seawater media dosed bi-weekly with glutaraldehyde for the biotic condition on days 1, 7, 14, 21 and 28. **Equivalent circuit:** ① – $R_s+(Q_1/Q_2+R_{ct})$; ④– $R_s+Q_1+(Q_2/R_{ct})$.

Day	Coupon	R_s / Ω cm²	Q_1 / mΩ^{-1} cm^{-2} s^n	n_1	Q_2 / mΩ^{-1} cm^{-2} s^n	n_2	R_{ct} / Ω cm²	$\chi^2 \times 10^{-4}$
1	AR ①	7.68±1.43	167±176	0.30±0.19	3.51±1.02	0.83±0.05	265±57	1.1
7	AR ④	4.94±3.42	106±57	0.58±0.46	21.08±11.01	0.87±0.07	82±67	9.0
14	AR ④	6.55±1.10	104±111	0.67±0.32	65.55±81.51	0.79±0.38	106±98	8.7
21	AR ④	5.92±1.28	464±431	0.28±0.35	124.81±217.40	0.78±0.36	199±130	1.4
28	AR ④	6.65±1.26	40±16	0.84±0.02	543±219	0.12±0.13	273±357	1.1

Table E6. List of top 25 microbial genera identified through 16S rRNA amplicon sequencing with two target region, V3-4 for bacteria and archaea, after exposure to anaerobic nutrient-enriched artificial seawater media dosed bi-weekly with glutaraldehyde for 28 days.

Name	Sediment	Day0	Day28	AR
Exiguobacterium	0.003808	0.02348	54.96	70.16
Fusobacterium	0.001632	32.53	0.00535	0.006864
Vibrio	0.08542	6.611	14.94	8.264
Sulfurovum	10.8	0.008712	0.000502	NA
Oceanicoccus	0.02367	10	1.881	2.013
Shewanella	0.02911	0.005631	9.076	2.013
Methanococcoides	0.1387	7.771	0.00117	0.006374
Desulfuromonas	6.802	0.004462	0.000167	NA
Serpentinicella	0.005985	0.6435	2.17	6.596
Desulfosarcina	5.944	0.00425	0.000334	7.00E-05
Thiohalobacter	5.268	0.002762	NA	NA
Photobacterium	0.00272	4.897	0.04163	0.007285
Candidatus Methanoplasma	4.885	0.05716	NA	NA
Blautia	0.006529	4.732	0.0107	0.03754
Candidatus Prometheoarchaeum	4.104	0.02433	NA	7.00E-05
Marinobacterium	0.01387	0.001594	4.001	0.03159
Leptotrichia	0.001904	3.931	0.000836	0.001191
Halarcobacter	0.001088	0.0017	3.578	3.316
Maridesulfovibrio	0.01768	3.475	1.68	0.5737
Pseudodesulfovibrio	3.017	0.1271	0.2426	0.2431
Anaerotignum	0.000816	2.844	0.1206	0.4397
Clostridium	0.2535	2.544	0.03645	0.1919
Urechidicola	2.416	0.000531	NA	NA
Kineobactrum	2.337	0.0017	0.000167	NA
Woeseia	2.26	0.001169	0.000167	NA

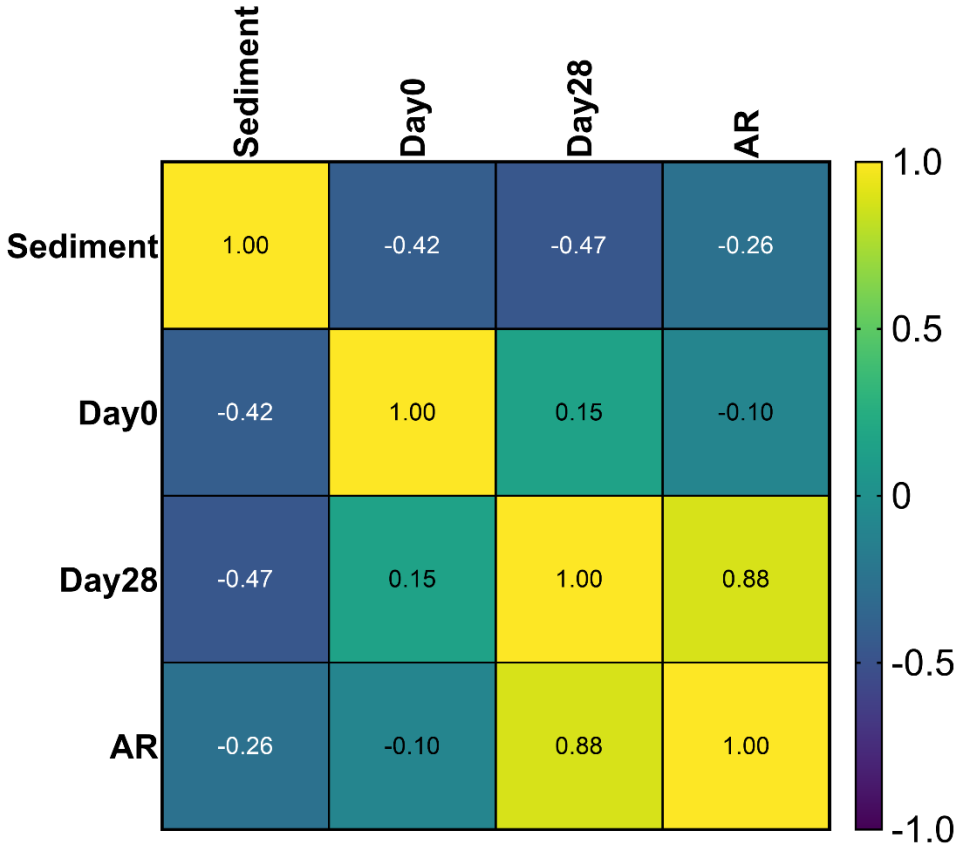

Figure E7. Spearman correlation coefficients for environmental marine sediment, Day 0, and Day 28 planktonic samples, and AR biofilms, after exposure to anaerobic nutrient-enriched artificial seawater media dosed bi-weekly with glutaraldehyde for 28 days.

Glossary of Terms

Anaerobic.....the absence of gaseous oxygen.

Abiotic.....the absence of living organisms.

Bacterial attachment .....the initial, reversible stage of contact between a bacterial cell and a substrate.

Bacterial adhesion.....the irreversible stage following attachment by which bacterial cells become permanently associated with a substrate or surface.

Biocide.....a chemical compound that aims to reduce bacterial viability.

Biofilm.....a sessile population of microorganisms living at an interface, usually associated with an aqueous phase.

Biotic .....conditions that contain living organisms.

Carbon steel (CS).....steel produced using carbon as the primary alloying element.

Conditioning film.....a layer of adsorbed organic and inorganic material in an interface.

Corrosion.....the process converting refined materials to more chemically stable forms.

Extracellular electron transport (EET) electron transfer between microbial cells and extracellular solid materials, including naturally-occurring metal compounds.

Electroactive microorganism are microorganisms that can exchange electrons with their extracellular environment.

Electrogens.....microorganisms that generate or donate electrons to natural extracellular electron acceptors.

Electromicrobiomes.....are environments in which microorganisms electrically interact with each other and/or their extracellular environment.

Electrotrophs.....microorganisms that consume or accept electrons to natural extracellular electron acceptors.

Extracellular polymeric substances (EPS) self-produced polymers that form the biofilm matrix, including proteins, eDNA and polysaccharides.

Microbiologically influenced corrosion (MIC)the corrosion initiated, mediated, or exacerbated by the presence and activity of microorganisms.

Microorganism.....a microscopic organism such as bacteria or fungi.

Bibliography/References

[1] G. Koch, J. Varney, N. Thompson, O. Moghissi, M. Gould and J. Payer, “International Measures of Prevention, Application, and Economics of Corrosion Technologies Study,” NACE International, 15835 Park Ten Place, Houston, TX 77084, 2016.

[2] K. M. Usher, A. H. Kaksonen, I. Cole and D. Marney, “Critical review: Microbially influenced corrosion of buried carbon steel pipes,” *International Biodeterioration & Biodegradation,* pp. 93, 84-106., 2014.

[3] H.-.. Flemming and J. Wingender, “The biofilm matrix,” *Nature Reviews Microbiology,* vol. 8, p. 623–633, 2010.

[4] R. M. Donlan, “Biofilms: Microbial Life on Surfaces,” *Emerging Infectious Diseases,* vol. 8, pp. 881-890, 2002.

[5] A. Vigneron, I. M. Head and N. Tsesmetzis, “Damage to offshore production facilities by corrosive microbial biofilms,” *Applied Microbiology and Biotechnology,* vol. 102, pp. 2525-2533, 2018.

[6] S. Wu, S. Altenreid, A. Zogg, F. Zuber, K. Maniura-Weber and Q. Ren, “Role of the Surface Nanoscale Roughness of Stainless Steel on Bacterial Adhesion and Microcolony Formation,” *ACS Omega,* vol. 3, pp. 6456-6464, 2018.

[7] R. Jia, T. Unsal, D. Xu, Y. Lekback and T. Gu, “Microbiologically influenced corrosion and current mitigation strategies: A state of the art review.,” *International Biodeterioration & Biodegradation,* pp. 137, 42-58, 2019.

[8] W. J. Costerton, The Biofilm Primer, Berlin, Heidelberg: Springer , 2007.

[9] M. Stipanicev, F. Turcu, L. Esnault, O. Rosas, R. Basseguy, M. Sztyler and I. B. Beech, “Corrosion of carbon steel by bacteria from North Sea offshore seawater injection systems: Laboratory investigation,” *Bioelectrochemistry,* vol. 97, pp. 76-88, 2014.

[10] L. L. Machuca, S. I. Bailey, R. Gubner, E. L. J. Watkin, M. P. Ginige and A. H. Kaksonen, “Crevice corrosion of duplex stainless steels in the presence of natural marine biofilms,” in *CORROSION 2012*, Salt Lake City, Utah, 2012.

[11] A. Rajasekar and Y.-P. Ting, “Microbial Corrosion of Aluminum 2024 Aeronautical Alloy by Hydrocarbon Degrading Bacteria Bacillus cereus ACE4 and Serratia marcescens ACE2,” *Industrial & Engineering Chemistry Research,* vol. 49, no. 13, p. 6054–6061, 2010.

[12] X. L. Li, J. Narenkumar, A. Rajasekar and Y.-P. Ting, “Biocorrosion of mild steel and copper used in cooling tower water and its control,” *3 Biotech,* vol. 8, no. 178, 2018.

[13] D. Ahmadkhaniha, A. Järvenpää, M. Jaskari, M. H. Sohi, A. Zarei-Hanzaki, M. Fedel, F. Deflorian and L. P. Karjalainen, “Microstructural modification of pure Mg for improving mechanical and biocorrosion properties,” *Journal of the Mechanical Behaviour of Biomedical Materials,* vol. 61, pp. 360-370, 2016.

[14] E. Ilhan-Sungur, T. Unsal-Istek and N. Cansever, “Microbiologically influenced corrosion of galvanized steel by Desulfovibrio sp. and Desulfosporosinus sp. in the presence of Ag–Cu ions,” *Materials Chemistry and Physics,* vol. 162, pp. 839-851, 2015.

[15] M. A. Javed, P. R. Stoddart, E. A. Palombo, S. L. McArthur and S. A. Wade, “Inhibition or acceleration: Bacterial test media can determine the course of microbiologically influenced corrosion,” *Corrosion Science,* vol. 86, pp. 149-158, 2014.

[16] M. Moura, E. Pontual, P. Paiva and L. Coelho, “An outline to corrosive bacteria,” in *Microbial pathogens and strategies for combating them: Science technology and education*, Badajoz, Spain, Formatex Research Center, 2013, pp. 11-22.

[17] S. J. Salgar-Chaparro, K. Lepkova, T. Pojtanabuntoeng, A. Darwin and L. L. Machuca, “Nutrient Level Determines Biofilm Characteristics and Subsequent Impact on Microbial Corrosion and Biocide Effectiveness.,” *Appl Environ Microbiol,* pp. Volume 86, Issue 7, e02885-19, 2020.

[18] H. A. Videla and L. K. Herrera, “Microbiologically influenced corrosion: looking to the future,” *Int Microbiol,* pp. 8(3):169-180, 2005.

[19] W. J. Rhoads, A. Pruden and M. A. Edwards, “Interactive Effects of Corrosion, Copper, and Chloramines on Legionella and Mycobacteria in Hot Water Plumbing,” *Environ Sci Technol,* vol. 51, pp. 7065-7075, 2017.

[20] D. F. Aktas, K. R. Sorrell, K. E. Duncan, B. Wawrik, A. V. Callaghan and J. M. Suflita, “Anaerobic hydrocarbon biodegradation and biocorrosion of carbon steel in marine

environments: The impact of different ultra low sulfur diesels and bioaugmentation," *International Biodeterioration & Biodegradation,* vol. 118, pp. 45-56, 2017.

[21] A. F. Forte Giacobone, S. A. Rodriguez, A. L. Burkart and R. A. Pizarro, "Microbiological induced corrosion of AA 6061 nuclear alloy in highly diluted media by Bacillus cereus RE 10," *International Biodeterioration & Biodegradation,* vol. 65, pp. 1161-1168, 2011.

[22] X. Dai, H. Wang, L.-K. Ju, G. Cheng, H. Cong and B.-M. Z. Newby, "Corrosion of aluminum alloy 2024 caused by Aspergillus niger," *International Biodeterioration & Biodegradation,* vol. 115, pp. 1-10, 2016.

[23] A. Widmer, "New Developments in Diagnosis and Treatment of Infection in Orthopedic Implants," *Clinical Infectious Diseases,* vol. 33, pp. S94-S106, 2001.

[24] S. K. Kotu and R. B. Eckert, "A Framework for Conducting Analysis of Microbiologically Influenced Corrosion Failures," *Inspectioneering,* pp. Volume 26, Issue 4, Pages 1-8, 2019.

[25] R. Eckert and K. Buckingham, "Investigating pipeline corrosion failures," *Inspectioneering,* pp. Volume 23, Issue 4, Pages 1-9, 2017.

[26] D. Enning and J. Garrelfs, "Corrosion of Iron by Sulfate-Reducing Bacteria: New Views of an Old Problem," *ASM Journal,* pp. Volume 80, 1226–1236, 2014.

[27] NACE TM0212-2018-SG, "Detection, Testing, and Evaluation of Microbiologically Influenced Corrosion on Internal Surfaces of Pipelines," NACE Standards, Houston, 2018.

[28] NACE TM0194-2014-SG, "Field Monitoring of Bacterial Growth," NACE Standards, Houston, 2014.

[29] A. Abilio, T. Skovhus, J. Wolodko and R. Eckert, "Development of an expert system for assessing failures in oil and gas pipelines due to microbiologically influenced corrosion (MIC)," *Engineering Failure Analysis,* vol. 163, p. 108426, 2024.

[30] D. R. Lovely and D. E. Holmes, "Electromicrobiology: The ecophysiology of phylogenetically diverse electroactive microorganisms," *Nat Rev Microbiol,* pp. 20, 5-19, 2022.

[31] G. Muyzer and A. J. Stams, "The ecology and biotechnology of sulphate-reducing bacteria," *Nature Reviews Microbiology,* vol. 6, pp. 441-454, 2008.

[32] S. Dannenberg, M. Kroder, W. Dilling and H. Cypionka, “Oxidation of H2, organic compounds and inorganic sulfur compounds coupled to reduction of O2 or nitrate by sulfate-reducing bacteria,” *Archives of Microbiology,* vol. 158, pp. 93-99, 1992.

[33] R. Thauer, E. Stackerbrandt and W. Hamilton, “Energy metabolism phylogenetic diversity of sulphate-reducing bacteria,” *Cambridge University Press,* pp. 1-37, 2007.

[34] L. Barton and F. Tomei, “Characteristics and activities of sulfate-reducing bacteria,” in *Sulfate-Reducing Bacteria*, Boston, MA, Springer, 1995, pp. 1-32.

[35] T. Gu and D. Xu, “Why are some microbes corrosive and some not?,” 2013.

[36] R. Jia, J. Tan, P. Jin, D. Blackwood, D. Xu and T. Gu, “Effects of biogenic H2S on the microbiologically influenced corrosion of C1018 carbon steel by sulfate reducing Desulfovibrio vulgaris biofilm,” *Corrosion Science,* vol. 130, pp. 1-11, 2018.

[37] D. Gupta, “Corrosion behaviour of 1040 carbon steel,” *Corrosion,* vol. 37, no. 11, pp. 611-616, 1981.

[38] T. Gu, S. Nesic and K. Zhao, “A Practical Mechanistic Model for MIC Based on a Biocatalytic Cathodic Sulfate Reducation Theory,” in *NACE - International Corrosion Conference*, Atlanta, Georgia, 2009.

[39] D. Xu, Y. Li and T. Gu, “Mechanistic modeling of biocorrosion caused by biofilms of sulfate reducing bacteria and acid producing bacteria,” *Bioelectrochemistry,* vol. 110, pp. 52-8, 2016.

[40] Y. Li, D. Xu, C. Chen, X. Li, R. Jia, D. Zhang, W. Sand, F. Wang and T. Gu, “Anaerobic microbiologically influenced corrosion mechanisms interpreted using bioenergetics and bioelectrochemistry: A review,” *Journal of Materials Science & Technology,* vol. 34, pp. 1713-1718, 2018.

[41] P. Liu, H. Zhang, Y. Fan and D. Xu, “Microbially Influenced Corrosion of Steel in Marine Environments: A Review from Mechanisms to Prevention,” *Microorganisms,* vol. 11, p. 2299, 2023.

[42] H. Jannasch, C. Wirsen, D. Nelson and L. Robertson, “Thiomicrospira crunogena sp. nov., a colorless, sulfur-oxidizing bacterium from a deep-sea hydrothermal vent,” *Int. J. Syst. Evol. Microbiol,* vol. 35, p. 422–424, 1985.

[43] Y. Kodama and K. Watanabe, “Sulfuricurvum kujiense gen. nov., sp. nov., a facultatively anaerobic, chemolithoautotrophic, sulfur-sulfuroxidizing,” *Int. J. Syst. Evol. Microbiol,* vol. 54, pp. 2297-2300, 2004.

[44] R. Jia, D. Yang, J. Xu, D. Xu and T. Gu, “Microbiologically influenced corrosion of C1018 carbon steel by nitrate reducing Pseudomonas aeruginosa biofilm under organic carbon starvation,” *Corrosion Science,* vol. 127, pp. 1-9, 2017.

[45] A. F. Mitchell, I. Skjevrak and M. Iding, “An Evaluation of Cessation of Nitrate Treatment of High-Volume Seawater Injection Systems,” in *CORROSION*, USA, 2021.

[46] A. Telang, S. Ebert, J. Foght, D. Westlake, G. Jenneman, D. Gevretz and G. Voordouw, “Effect of nitrate injection on the microbial community in an oil field as monitored by reverse sample genome probing.,” *Appl. Environ. Microbiol,* vol. 63, pp. 1785-1793, 1997.

[47] A. Gittel, K. Sorensen, T. Skovhus, K. Ingvorsen and A. Schramm, “Prokaryotic community structure and sulfate reducer activity in water from high-temperature oil reservoirs with and without nitrate treatment,” *Appl Environ Microbiol,* vol. 75, pp. 7086-96, 2009.

[48] J. Dolfing and C. Hubert, “Using Thermodynamics to Predict the Outcomes of Nitrate-Based Oil Reservoir Souring Control Interventions,” *Front Microbiol,* vol. 8, p. 2575, 2017.

[49] L. Gieg, T. Jack and J. Foght, “Biological souring and mitigation in oil reservoirs,” *Applied Microbiology and Biotechnology,* vol. 92, pp. 263-282, 2011.

[50] T. Fida, C. Chen, G. Okpala and G. Voordouw, “Implications of Limited Thermophilicity of Nitrite Reduction for Control of Sulfide Production in Oil Reservoirs,” *Applied and Environmental Microbiology,* vol. 82, pp. 4190-4199, 2016.

[51] C. Hubert, G. Voordouw and B. Mayer, “Elucidating microbial process in nitrate- and sulfate-reducing systems using sulfur and oxygen isotope ratios: The example of oil reservoir souring control,” *Geochimica et Cosmochimica Acta,* vol. 73, pp. 3864-3879, 2009.

[52] C. Hubert, “Microbial ecology of oil reservoir souring control by nitrate injection,” in *Handbook of hydrocarbon and lipid microbiology*, Berlin, Springer, 2010, pp. 2753-2766.

[53] D. Xu, Y. Li, F. Song and T. Gu, “Laboratory investigation of microbiologically influenced corrosion of C1018 carbon steel by nitrate reducing bacterium Bacillus licheniformis,” *Corrosion Science,* vol. 77, pp. 385-390, 2013.

[54] R. 2. Miller, K. Lawson, A. Sadek, C. Monty and J. Senko, “Uniform and Pitting Corrosion of Carbon Steel by Shewanella oneidensis MR-1 under Nitrate-Reducing Conditions,” *Appl Environ Microbiol,* vol. 84(12), pp. e00790-18, 2018.

[55] H. Wan, D. Song, D. Zhang, C. Du, D. Xu, Z. Liu, D. Ding and X. Li, “Corrosion effect of Bacillus cereus on X80 pipeline steel in a Beijing soil environment,” *Bioelectrochemistry,* vol. 121, pp. 18-26, 2018.

[56] P. Raspor and D. Goranovič, “Biotechnological Applications of Acetic Acid Bacteria,” *Critical Reviews in Biotechnology,* vol. 28, pp. 101-124, 2008.

[57] M. Saez-Lara, C. Gomez-Llorente, J. Plaza-Diaz and A. Gil, “The Role of Probiotic Lactic Acid Bacteria and Bifidobacteria in the Prevention and Treatment of Inflammatory Bowel Disease and Other Related Diseases: A Systematic Review of Randomized Human Clinical Trials,” *BioMed Research International,* p. 505878, 2015.

[58] M. Shuler and F. Kargi, Bioprocess engineering: Basic concepts, 2 ed., London: Pearson, 2002.

[59] T. Gu, “Theoretical Modeling of the Possibility of Acid Producing Bacteria Causing Fast Pitting Biocorrosion,” *Journal of Microbial & Biochemical Technology,* vol. 6, pp. 68-74, 2014.

[60] C. Olsson and D. Landolt, “Passive films on stainless steels—chemistry, structure and growth,” *Electrochimica Acta,* vol. 48, pp. 1093-1104, 2003.

[61] H. Wang, L.-K. Ju, H. Castaneda, G. Cheng and B.-M. Zhang Newby, “Corrosion of carbon steel C1010 in the presence of iron oxidizing bacteria Acidithiobacillus ferrooxidans,” *Corrosion Science,* vol. 89, pp. 250-257, 2014.

[62] J. Lee, J. McBeth, R. Ray, B. Little and D. Emerson, “Iron cycling at corroding carbon steel surfaces,” *Biofouling,* vol. 29, pp. 1243-52, 2013.

[63] C. Myers and K. Nealson, “Bacterial Manganese Reduction and Growth with Manganese Oxide as the Sole Electron Acceptor,” *Science,* vol. 240, no. 4857, pp. 1319-1321, 1988.

[64] B. Little, P. Wagner, K. Hart, R. Ray, D. Lavoie, K. Nealson and C. Aguilar, “The role of biomineralization in microbiologically influenced corrosion,” *Biodegradation,* vol. 9, pp. 1-10, 1998.

[65] A. Pedersen, K. Bilkova, E. Gulbrandsen and R. Nyborg, “Testing of CO2 corrosion inhibitor performance under sand deposits,” 2007.

[66] R. Barker, B. Pickles and A. Neville, “General corrosion of X65 steel under silica sand deposits in CO2 saturated environments in the presence of corrosion inhibitor components,” 2014.

[67] A. Pederson, K. Bilkova, E. Gulbrandsen and J. Kvarekval, “CO2 corrosion inhibitor performance in the presence of solids: Test method development,” 2008.

[68] G. Hinds and A. Turnbull, “Novel multi-electrode test method for evaluating inhibition of under deposit corrosion Part 1: Sweet conditions,” 2010.

[69] Y. Tan, Y. Fwu and K. Bhardwaj, “Electrochemical evaluation of under-deposit corrosion and its inhibition using the wire beam electrode method,” *Corrosion Science,* vol. 53, pp. 1254-1261, 2011.

[70] B. Brown and J. Moloney, “Under Deposit Corrosion,” in *Trends in Oil and Gas Corrosion Research and Technologies*, Amsterdam, Netherlands, Elsevier, 2017, pp. 363-383.

[71] R. Gupta, “Protein Phylogenies and Signature Sequences: A reappraisal of evolutionary relationships among archaebacteria, eubacteria, and eukaryotes,” *Microbiology and Molecular Biology Reviews,* vol. 62, pp. 1435-1491, 1998.

[72] K. Stetter, G. Lauerer, M. Thomm and A. Neuner, “Isolation of Extremely Thermophilic Sulfate Reducers: Evidence for a Novel Branch of Archaebacteria,” *Science,* vol. 236, pp. 822-824, 1987.

[73] L. Daniels, N. Belay, B. Rajagopal and P. Weimer, “Bacterial Methanogenesis and Growth from CO2 with Elemental Iron as the Sole Source of Electrons,” *Science,* vol. 237, no. 4814, pp. 509-511, 1987.

[74] J. Larsen, K. Rasmussen, H. Pedersen, K. Sorensen, T. Lundgaard and T. Skovhus, “Consortia of MIC Bacteria and Archaea Causing Pitting Corrosion in Top Side Oil Production Facilities,” San Antonio, Texas, 2010.

[75] H. Park, I. Chatterjee, X. Dong, S.-H. Wang, C. Sensen, S. Caffrey, T. Jack, J. Boivin and G. Voordouw, “Effect of Sodium Bisulfite Injection on the Microbial Community Composition

in a Brackish-Water-Transporting Pipeline," *Applied and Envieonmental Microbiology,* vol. 77, pp. 6908-6917, 2011.

[76] R. Boopathy and L. Daniels, "Effect of pH on anaerobic mild steel corrosion by methanogenic bacteria," *Applied and Environmental Microbiology,* vol. 57, pp. 2104-2108, 1991.

[77] K. Schuchmann and V. Müller, "Energetics and Application of Heterotrophy in Acetogenic Bacteria," *Applied and Environmental Microbiology,* vol. 82, pp. 4056-4069, 2016.

[78] I. Berg, D. Kockelkorn, W. Ramos-Vera, R. Say, J. Zarzycki, M. Hugler, B. Alber and G. Fuchs, "Autotrophic carbon fixation in archaea," *Nature review microbiology,* vol. 8, no. 6, pp. 447-460, 2010.

[79] J. Philips, E. Monballyu, S. Georg, K. De Paepe, A. Prévoteau, K. Rabaey and J. Arends, "An Acetobacteriumstrain isolated with metallic iron as electron donor enhances iron corrosion by a similar mechanism asSporomusa sphaeroides," *FEMS Microbiology Ecology,* vol. 95, no. 2, 2019.

[80] S. Wang, D. Liu, N. Du, Q. Zhao, S. Liu and J. Xiao, "Relationship between Dissolved Oxygen and Corrosion," *International Journal of Electrochemical Science,* vol. 10, pp. 4393-4404, 2015.

[81] J. Philips, "Extracellular Electron Uptake by Acetogenic Bacteria: Does H2 Consumption Favor the H2 Evolution Reaction on a Cathode or Metallic Iron?," *Frontiers in Microbiology,* vol. 10, p. 2997, 2020.

[82] B. Little, R. Staehle and R. Davis, "Fungal influced corrosion on post-tension structures," *Int. Biodeterior. Biodegrad,* vol. 47, pp. 71-77, 2001.

[83] R. Edyvean and H. Videla, "Biological corrosion," *Interdiscip. Sci. Rev,* vol. 16, pp. 267-282, 1991.

[84] B. Little and R. Ray, "The role of fungi in microbioligically influenced corrosion," in *Naval Research Lab Stennis Space Center*, St. Louis, Mississippi, 2002.

[85] A. Cojocaru, P. Prioteasa, I. Szatmari, E. Radu, O. Udrea and T. Visan, "EIS study on biocorrosion of some steels and copper in Czapek Dox medium containing Aspergillus niger fungus," *Revista de Chimie,* vol. 67, pp. 1264-1270, 2016.

[86] A. Lugauskas, G. Bikulčius, D. Bučinskienė, A. Selskienė, V. Pakštas and E. Binkauskienė, "Long-Time corrosion of metals (steel and aluminium) and profiles of fungi on their surface in outdoor environments in Lithuania," *Chemija,* vol. 27, pp. 135-142, 2016.

[87] J. He, Y. Tan, H. Liu, Z. Jin, Y. Zhang, F. He, Z. Yan, H. Liu, G. Meng and H. Liu, "Extracellular polymeric substances secreted by marine fungus Aspergillus terreus: Full characterization and detailed effects on aluminum alloy corrosion," *Corros. Sci.,* vol. 209, p. 110703, 2022.

[88] J. Landoulsi, K. Kirat, C. Richard, D. Feron and S. Pulvin, "Enzymatic approach in microbial-influenced corrosion: A review based on stainless steels in natural waters," *Environ. Sci. Technol.,* vol. 42, pp. 2233-2242, 2008.

[89] B. Little, R. Pope, T. Daulton and R. Ray, "Application of Environmental Cell Transmission Electron Microscopy to Microbiologically Influenced Corrosion," in *Corrosion*, Houston, Texas, 2001.

[90] B. Iannuzzi, "https://curtin-corrosion-centre.com/expertise/acid-gas-corrosion/," 2020. [Online]. Available: https://curtin-corrosion-centre.com/expertise/acid-gas-corrosion/. [Accessed June 2021].

[91] M. Rodríguez, "Anticipated Degradation Modes of Metallic Engineered Barriers for High-Level Nuclear Waste Repositories," *JOM,* vol. 66, pp. 503-525, 2014.

[92] Z. Foroulis, "Electrochemical behavior and corrosion of iron in aqueous sulfidic solution," *Materials and Corrosion,* vol. 31, no. 6, pp. 463-470, 1980.

[93] M. Yamamoto, Y. Takamura, Y. Kokubo, M. Urushihara, N. Horiuchi, W. Dai, Y. Hayasaka, E. Kita and K. Takao, "Solid-State Schikorr Reaction from Ferrous Chloride to Magnetite with Hydrogen Evolution as the Kinetic Bottleneck," *Inorganic Chemistry,* vol. 62, no. 36, p. 14580–14589, 2023.

[94] Y. Zheng, B. Brown and Nešić., "Electrochemical Study and Modeling of H2S Corrosion of Mild Steel," *Corrosion,* vol. 10, no. 4, pp. 351-365, 2014.

[95] T. Skovhus, D. Enning and J. Lee, Microbiologically Influenced Corrosion in the Upstream Oil and Gas Industry, Florida: CRC Press, 2017.

[96] R. Ayers, V. Patel, E. Burger, C. Cain, D. Ou-Yang, N. Wessel and C. Kleck, “Corrosion of Titanium Spinal Explants Is Similar to That Observed in Oil Field Line Pipe Steel: Evidence of Microbial-Influenced Corrosion In Vivo,” *Orthopedics,* 2019.

[97] D.-Q. Ng, C.-Y. Chen and Y.-P. Lin, “A new scenario of lead contamination in potable water distribution systems: Galvanic corrosion between lead and stainless steel. Science of The Total Environment,,” *Science of The Total Environment,* Vols. 637-638, pp. 1423-1431, 2018.

[98] D.-Q. Ng, J.-K. Lin and Y.-P. Lin, “Lead release in drinking water resulting from galvanic corrosion in three-metal systems consisting of lead, copper and stainless steel,” *Journal of Hazardous Materials,* vol. 398, p. 122936, 2020.

[99] S. Wilhelm, “Galvanic Corrosion in Oil and Gas Production: Part 1 Laboratory Studies,” *Corrosion,* vol. 48, no. 08, 1992.

[100] R. Dooley and B. Chexal, “Flow-Accelerated Corrosion,” *Corrosion,* 1999.

[101] G. Hinds, P. Cooling, S. Zhou and A. Turnbull, “Under deposit test method for assessing performance of corrosion inhibitors,” 2008.

[102] A. Shamso, N. Laycock, A. Abdullah and M. Ryan, “Under-deposit Corrosion: Investigating Dissolution Kinetics Using Artificial Pits,” *Corrosion,* 2018.

[103] U. Schröder, “Anodic electron transfer mechanisms in microbial fuel cells and their energy efficiency,” *Physical chemistry chemical physics,* no. 21, 2007.

[104] T. Gu, “New Understandings of Biocorrosion Mechanisms and their Classifications. , 04.,” *Journal of Microbial & Biochemical Technology,* vol. 4, p. 4, 2012.

[105] P. Zhang, D. Xu, Y. Li, K. Yang and T. Gu, “Electron mediators accelerate the microbiologically influenced corrosion of 304 stainless steel by the Desulfovibrio vulgaris biofilm,” *Bioelectrochemistry,* vol. 101, pp. 14-21, 2015.

[106] D. Xu and T. Gu, “Carbon source starvation triggered more aggressive corrosion against carbon steel by the Desulfovibrio vulgaris biofilm,” *Int Biodeterior Biodegradation,* p. 91:74–81, 2014.

[107] R. Jia, D. Yang, D. Xu and T. Gu, “Anaerobic Corrosion of 304 Stainless Steel Caused by the Pseudomonas aeruginosa Biofilm,” *Front Microbiol,* vol. 8, p. 2335, 2017.

[108] J.-D. Gu, “Microbiological deterioration and degradation of synthetic polymeric materials: Recent research advances,” *International Biodeterioration & Biodegradation,* vol. 52, no. 2, pp. 69-91, 2003.

[109] M. Finnegan, E. Linley, S. Denyer, G. McDonnell, C. Simons and J. Maillard, “Mode of action of hydrogen peroxide and other oxidizing agents: differences between liquid and gas forms,” *Journal of Antimicrobial Chemotherapy,* vol. 65, pp. 2108-2115, 2010.

[110] G. Kahrilas, J. Blotevogel, P. Stewart and T. Borch, “Biocides in hydraulic fracturing fluids: a critical review of their usage, mobility, degradation, and toxicity,” *Environ Sci Technol,* vol. 49, pp. 16-32, 2015.

[111] B. Downward, R. Talbot and T. Haack, “TetrakisHydroxymethylPhosphonium Sulfate (THPS), a new industrial biocide with low environmental toxicity,” New Orleans, Louisiana, 1997.

[112] D. Xu, Y. Li and T. Gu, “A synergistic d-tyrosine and tetrakis hydroxymethyl phosphonium sulfate biocide combination for the mitigation of an SRB biofilm,” *World Journal of Microbiology and Biotechnology,* vol. 28, pp. 3067-3074, 2012.

[113] S. Gorman, E. Scott and A. Russell, “Antimicrobial Activity, Uses and Mechanism of Action of Glutaraldehyde,” *Journal of Applied Bacteriology,* vol. 48, pp. 161-190, 1980.

[114] C. Ioannou, G. Hanlon and S. Denyer, “Action of Disinfectant Quaternary Ammonium Compounds against Staphylococcus aureus,” *Antimicrobial Agents and Chemotherapy,* vol. 51, pp. 296-306, 2007.

[115] C. Struchtemeyer, M. Morrison and M. Elshahed, “A critical assessment of the efficacy of biocides used during the hydraulic fracturing process in shale natural gas wells,” *International Biodeterioration & Biodegradation,* vol. 71, pp. 15-21, 2012.

[116] L. Bautista, C. Vargas, N. González, M. Molina, R. Simarro, A. Salmerón and Y. Murillo, “Assessment of biocides and ultrasound treatment to avoid bacterial growth in diesel fuel,” *Fuel Processing Technology,* vol. 152, pp. 56-63, 2016.

[117] P. Elumalai, P. Parthipan, J. Narenkumar, R. Sarankumar, O. Karthikeyan and A. Rajasekar, "Influence of Thermophilic Bacteria on Corrosion of Carbon Steel in Hyper Chloride Environment," *International Journal of Environmental Research,* vol. 11, pp. 339-347, 2017.

[118] I. Vance and D. Thrasher, "Reservoir Souring: Mechanisms and Prevention.," in *Petroleum Microbiology*, Washington D.C., Wiley, 2005, pp. 123-143.

[119] T. de Mello, d. S. R.L, L. Braga-Silva, L. Braquinha and M. dos Santos, "Fungal Biofilm – A Real Obstacle Against an Efficient Therapy: Lessons from Candida," *Curr. Top. Med. Chem,* vol. 17, pp. 1987-2004, 2017.

[120] D. Schowanek, T. Feijtel, C. Perkins, F. Hartman, T. Federle and R. Larson, "Biodegradation of [S,S], [R,R] and mixed stereoisomers of Ethylene Diamine Disuccinic Acid (EDDS), a transition metal chelator," *Chemosphere,* vol. 34, pp. 2375-2391, 1997.

[121] J. Wen, K. Zhao, T. Gu and I. Raad, "A green biocide enhancer for the treatment of sulfate-reducing bacteria (SRB) biofilms on carbon steel surfaces using glutaraldehyde," *International Biodeterioration & Biodegradation,* vol. 63, pp. 1102-1106, 2009.

[122] T. Jackson, Smith, D, J. Vargas and B. Andrews, "Corrosion Inhibitor Deliverability – A Corrosion Inhibitor Residual Success Story," 2020.

[123] A. Osnowski, S. Rankin, H. Grover, H. Grover and F. Carson, "On-Site Corrosion Inhibitor Detection for Improved Corrosion Management," 2021.

[124] T. Jackson, L. Huang and R. Morales, "Corrosivity of Oxygen Scavenger in a Sea Water Environment," Phoenix, Arizona, 2018.

[125] M. Lehmann, A. Lamm, H. Nguyen, C. Bowman, W. Mok, M. Salasi and R. Gubner, "Corrosion Inhibitor and Oxygen Scavenger for use as MEG Additives in the Inhibition of Wet Gas Pipelines," in *Offshore Technology Conference-Asia*, Kuala Lumpur, Malaysia, 2014. .

[126] A. Kerserovic and O. Biketveit, "Crevice Corrosion in Oxygen Scavenger Injection System," 2021.

[127] B. Morris and G. Van Der Kraan, "Application of Biocides and Chemical Treatments to Both Combat Microorganisms and Reduce (Bio)-Corrosion," in *Microbiologically Influenced Corrosion in the Upstream Oil and Gas Industry*, CRC Press, 2017, pp. 229-253.

[128] P. Williams, “Quorum sensing, communication and cross-kingdom signalling in the bacterial world,” *Microbiology,* vol. 153, pp. 3923-3938, 2007.

[129] J. Rocha-Estrada, A. Aceves-Dies, G. Guarneros and M. de la Torre, “The RNPP family of quorum-sensing proteins in Gram-positive bacteria,” *Appl Microbiol Biotechnol,* vol. 87, no. 3, pp. 913-923, 2010.

[130] C. Grandclément, M. Tannières, S. Moréra, Y. Dessaux and D. Faure, “Quorum quenching: role in nature and applied developments,” *FEMS Microbiology Reviews,* vol. 40, pp. 86-116, 2016. .

[131] C. Waters and B. Bassler, “Quorum sensing: cell-to-cell communication in bacteria,” *Annu Rev Cell Dev Biol,* vol. 21, pp. 319-46, 2005..

[132] N. Bhargava, P. Sharma and N. Capalash, “Quorum sensing inAcinetobacter: an emerging pathogen,” *Critical Reviews in Microbiology,* vol. 36, pp. 349-360, 2010.

[133] M. Hentzer, “Attenuation of Pseudomonas aeruginosa virulence by quorum sensing inhibitors,” *The EMBO Journal,* vol. 22, pp. 3803-3815, 2003.

[134] T. Rasmussen and M. Givskov, “Quorum sensing inhibitors: a bargain of effects,” *Microbiology,* vol. 152, pp. 895-904, 2006.

[135] H. Lade, D. Paul and J. Kweon, “Quorum Quenching Mediated Approaches for Control of Membrane Biofouling,” *International Journal of Biological Sciences,* vol. 10, pp. 550-565, 2014.

[136] J. Choo, Y. Rukayadi and J. Hwang, “Inhibition of bacterial quorum sensing by vanilla extract,” *Letters in Applied Microbiology,* vol. 42, no. 6, pp. 637-41, 2006.

[137] J. Paczkowski, S. Mukherjee, A. McCready, J.-P. Cong, C. Aquino, H. Kim, B. Henke, C. Smith and B. Bassler, “Flavonoids Suppress Pseudomonas aeruginosa Virulence through Allosteric Inhibition of Quorum-sensing Receptors,” *Journal of Biological Chemistry,* vol. 292, pp. 4064-4076, 2017.

[138] N. Feasey, M. Jordan, E. Mackay and I. Collins, “The Challenge that Completion Types Present to Scale inhibitor squeeze Chemical Placement: A Novel Solution using a Self-Diverting Scale Inhibitor Squeeze Process,” Lafayette, Louisiana, 2004.

[139] H. Guan, A. Lim, J. Hernandez and J.-T. Liang, “Increasing Treatment Lifetime through Sustained Release of Scale Inhibitor from Scale Inhibitor Nanoparticles,” 2021.

[140] R. Eckert, Field Guide to Internal Corrosion Mitigation and Monitoring for Pipelines, Houston, TX: AMPP, 2016.

[141] J. Thorogood and T. Crichton, “Operational Control and Managing Change: The Integration of Nontechnical Skills With Workplace Procedures,” in *SPE Drill & Completion*, SPE , 2013, pp. 203-211.

[142] R. B. Eckert and B. Amend, “MIC and Materials Selection,” in *Microbiologically Influenced Corrosion in the Upstream Oil and Gas Industry*, CRC Press , 2017, pp. 35-56.

[143] P. Wagner and B. Little, “Impact of Alloying on Microbiologically Influenced Corrosion. A Review,” 1993.

[144] S. Salgar-Chaparro and L. Machuca, “Complementary DNA/RNA-Based Profiling: Characterization of Corrosive Microbial Communities and Their Functional Profiles in an Oil Production Facility,” *Frontiers in Microbiology,* pp. 25-87, 2019.

[145] J. Knisz, R. Eckert, L. M. Gieg, A. Koerdt, J. S. Lee, E. R. Silva, T. L. Skovhus, B. A. A. Stepec and S. A. Wade., “Microbiologically influenced corrosion—more than just microorganisms,” *FEMS Microbiology Reviews,* vol. 47, no. 5, 2023.

[146] AMPP TM21465, “Molecular Microbiological Methods - Sample Handling and Laboratoey Processing,” AMPP standards, Houston, 2024.

[147] NACE TM0106-2016, “Detection, Testing, and Evaluation of Microbiologically Influenced Corrosion (MIC) on External Surfaces of Buried Pipelines,” NACE Standards, Houston, 2016.

[148] ASTM G161-00, “Standard Guide for Corrosion-Related Failure Analysis,” ASTM International, West Conshohocken, PA, USA, 2018.

[149] R. Eckert and T. Skovhus, “Pipeline Failure Investigation: Is it MIC?,” *Materials Performance,* vol. 58, no. 2, 2019.

[150] P. Scott, “Expert Consensus on MIC: Prevention and Monitoring – Part 1,” *American Public Health Association,* vol. 43, no. 3, p. 50, 2004.

[151] ASTM G1-03, “Standard Practice for preparing, cleaning, and evaluationg corrosion test specimens,” ASTM International, West Conshohocken, PA, USA, 2018.

[152] ASTM G46-21, “Standard Guide for Examination and Evaluation of Pitting Corrosion,” ASTM International, West Conshohocken, PA, USA, 2021.

[153] ASTM G48-11, “Standard Test Methods for Pitting and Crevice Corrosion Resistance of Stainless Steels and Related Alloys by Use of Ferric Chloride Solution,” ASTM International, West Conshohocken, PA, USA, 2020.

[154] ASTM D8412-21, “qPCR Quantification of microbial contamination in liquid fuels and fuel associated water by quantitative polymerase chain reaction (qPCR),” ASTM International, West Conshohocken, PA, USA, 2021.

[155] DNVGL-RP-F116, “Integrity management of submarine pipeline systems,” DNV, Høvik, 2021.

[156] DNVGL-RP-G101, “Risk-based inspection of offshore topsides static mechanical equipment,” DNV, Høvik, 2021.

[157] Energy Institute, “Guidance on the use of biocides in the oil industry,” Energy Institute, London, 2022.

[158] Energy Institute, “Guidelines on Managing Microbiologically Influenced Corrosion (MIC) in Water Injection Systems,” Energy Institute, London, 2022.

[159] Energy Institute, “Selection, applicability, and use of Molecular Microbiological Methods (MMM) in the oil and gas industry,” Energy Institute, London, 2023.

[160] Energy Institute, “Guidance for Corrosion Management in Oil and Gas Production and Processing,” Energy Institute, London, 2019.

[161] ISO 31000, “Risk Management, Principles and Guidelines,” International Standards, Geneva, 2018.

[162] ISO 55002, “Asset management - Management systems - Guidlines for the application of ISO 55001,” International Standards, Geneva, 2018.

[163] ISO 17776, “Petroleum and natural gas industries — Offshore production installations — Major accident hazard management during the design of new installations,” International Standards, Geneva, 2016.

[164] ISO 21457, “Petroleum, petrochemical and natural gas industries — Materials selection and corrosion control for oil and gas production systems,” International Standards, Geneva, 2010.

[165] ISO 9712, “Non-destructive testing — Qualification and certification of NDT personnel,” International Standard, Geneva, 2021.

[166] NACE 31205-2006-SG, “Selection, Application, and Evaluation of Biocides in the Oil and Gas Industry,” NACE Standards, Houston, 2006.

[167] NACE 3T199-2012, “Techniques for Monitoring Corrosion and Related Parameters in Field Applications,” NACE Standards, Houston, 2012.

[168] NACE SP0169-2013, “Control of External Corrosion on Underground or Submerged Metallic Piping Systems,” NACE Standards, Houston, 2013.

[169] NACE SP0499-2022, “Corrosion Control and Monitoring in Seawater Injection Systems,” NACE Standards, Houston, 2022.

[170] NACE SP0775-2023, “Preparation, Installation, Analysis, and Interpretation of Corrosion Coupons in Hydrocarbon Operations,” NACE Standards, Houston, 2023.

[171] NACE SP0106, “Control of Internal Corrosion in Steel Pipelines and Piping Systems,” NACE International, Houston, 2018.

[172] NACE TR 46107, “Control of Corrosion, Deposition, and Microbiological Growth in Recirculating Water Systems in Buildings,” NACE International, Houston, 2007.

[173] NACE TR 11206, “Biocide Monitoring and Control in Cooling Towers,” NACE International, Houston, 2006.

[174] NACE 1F192, “Use of Corrosion-Resistant Alloys in Oilfield Environments,” NACE International, Houston, 2013.

[175] NACE SP21430, “Standard Framework for Establishing Corrosion Management Systems,” NACE International, Houston, 2019.

[176] O. Ellabban, H. Abu-Rub and F. Blaabjerg, “Renewable energy resources: Current status, future prospects and their enabling technology,” *Renewable and Sustainable Energy Reviews,* vol. 39, pp. 748-764, 2014.

[177] G. Koch, M. Brongers and N. Thompson, “Corrosion costs and preventative straegies in the United States,” in *NACE International*, Houston, TX, 2002.

[178] K. Larsen, “A closer look at microbiologically influenced corrosion,” Materials Performance, Houston, TX, 2020.

[179] K. Larsen, “Corrosion risks and mitigation straegies for offshore wind turbine foundations,” Materials Performance, Houston, TX, 2020.

[180] C. Kagarise, “Microbiologically influenced corrosion threat assessment,” 2022. [Online]. Available: https://www.dnv.com/services/microbiologically-influenced-corrosion-threat-assessment-208330/.

[181] Biosurface Technologies Corporation, “CDC Biofilm Reactor®,” Biosurface Technologies Corporation, 1994. [Online]. Available: https://biofilms.biz/products/biofilm-reactors/cdc-biofilm-reactor/. [Accessed 21 June 2024].

[182] ASTM E2871-21, “Standard Test Method for Determining Disinfectant Efficacy Against Biofilm Grown in the CDC Biofilm Reactor Using the Single Tube Method,” ASTM International, West Conshohocken, PA, USA, 2021.

[183] T. Liu, Z. Guo, Z. Zeng, N. Guo, Y. Lei, T. Liu, S. Sun, X. Chang, Y. Yin and X. Wang, “Marine Bacteria Provide Lasting Anticorrosion Activity for Steel via Biofilm-Induced Mineralization,” *ACS Appl Mater Interfaces,* vol. 10, pp. 40317-40327, 2018.

[184] R. Jia, Y. Li, H. Al-Mahamedh and T. Gu, “Enhanced Biocide Treatments with D-amino Acid Mixtures against a Biofilm Consortium from a Water Cooling Tower,” *Frontiers in Microbiology,* vol. 8, 2017.

[185] R. Jia, D. Yang, Y. Li, D. Xu and T. Gu, “Mitigation of the Desulfovibrio vulgaris biofilm using alkyldimethylbenzylammonium chloride enhanced by D-amino acids,” *International Biodeterioration & Biodegradation,* vol. 117, pp. 97-104, 2017.

[186] T. Tidwell, R. de Paula, G. Nilsen and V. Keasler, “Visualization and Quantification of Biofilm Removal for the Mitigation of MIC,” Dallas, Texas, 2015.

[187] H. Liu, T. Gu, G. Zhang, Y. Cheng and H. L. H. Wang, “The effect of magneticfield on biomineralization and corrosion behavior of carbon steel induced by iron-oxidizing bacteria,” *Corrosion Science,* vol. 102, pp. 93-102, 2016.

[188] J. Xia, C. Yang, D. Xu, D. Sun, L. Nan, Z. Sun, Q. Li, T. Gu and K. Yang, “Laboratory investigation of the microbiologically influenced corrosion (MIC) resistance of a novel Cu-bearing 2205 duplex stainless steel in the presence of an aerobic marine Pseudomonas aeruginosa biofilm,” *Biofouling,* vol. 31, pp. 481-492, 2015.

[189] J. Narenkumar, P. Parthipan, J. Madhavan, K. Murugan, S. Marpu, A. Suresh and A. Rajasekar, “Bioengineered silver nanoparticles as potent anti-corrosive inhibitor for mild steel in cooling towers,” *Environ Sci Pollut Res Int,* vol. 25, pp. 5412-5420, 2018.

[190] J. Telegdi, Z. Keresztes, G. Pálinkás, E. Kálmán and W. Sand, “Microbially influenced corrosion visualized by atomic force microscopy,” in *Applid Physics A: Materials Science & Processing*, 1998, pp. 639-642.

[191] J. Chakraborty and S. Das, “Application of spectroscopic techniques for monitoring microbial diversity and bioremediation,” *Applied Spectroscopy Reviews,* vol. 52, pp. 1-38, 2017.

[192] W. Dou, R. Jia, P. Jin, J. Liu, S. Chen and T. Gu, “Investigation of the mechanism and characteristics of copper corrosion by sulfate reducing bacteria,” *Corrosion Science,* vol. 144, pp. 237-248, 2018.

[193] Y. Chen and L. Ju, “Method for fast quantification of pitting using 3D surface parameters generated with infinite focus microscope,” *Corrosion,* vol. 71, pp. 1184-1196, 2015.

[194] R. Jia, D. Yang, R. Abd, B. Hasrizal and T. Gu, “Laboratory testing of enhanced biocide mitigation of an oilfield biofilm and its microbiologically influenced corrosion of carbon steel in the presence of oilfield chemicals,” *International Biodeterioration & Biodegradation,* vol. 125, no. 19, pp. 116-124, 2017.

[195] E. McCafferty, Introduction to Corrosion Science, New York, NY: Springer, 2010.

[196] H. H. Uhlig, Uhlig'd Corrosion Handbook, Wiley, 1285 Pages, 2011.

[197] T. Tran, K. Kannoorpatti, A. Padovan, S. Thennadil and K. Nguyen, “Microbial corrosion of DSS 2205 in an acidic chloride environment under continuous flow,” *PLOS ONE,* p. 16(5): e0251524, 2021.

[198] H. Beyenal and J. T. Babauta, Biofilms in bioelectrochemical systemes: From laboratory practice to data interpretation, Hoboken, New Jersey: Wiley, 416 Pages, 2015.

[199] M. Sharma, H. Liu, S. Chen, F. Cheng, G. Voordouw and L. Gieg, “Effect of selected biocides on microbiologically influenced corrosion caused by Desulfovibrio ferrophilus IS5,” *Sci Rep,* vol. 8, p. 16620, 2018.

[200] B. Little, D. Blackwood, J. Hinks, F. Lauro, E. Marsili, A. Okamoto, S. Rice, S. Wade and H.-C. Flemming, “Microbially influenced corrosion—Any progress?,” *Corrosion Science,* vol. 170, 2020.

[201] B. W. P. Little, “Application of Electrochemical Techniques to the Study of Microbiologically Influenced Corrosion,” in *Modern Aspects of Electrochemistry*, vol. 34, Boston, MA, Springer, 2002, pp. 205-246.

[202] M. Eguchi, T. Nishikawa, K. Macdonald, R. Cavicchioli, J. Gottscahl and S. Kjelleberg, “Responses to Stress and Nutrient Availability by the Marine Ultramicrobacterium Sphingomonas sp. Strain RB2256,” *Appl Environ Microbiol,* vol. 62, no. 4, pp. 1287-84, 1996.

[203] N. Rabalais, R. Turner, D. Justic´, Q. Dortch and W. Wiseman, “Characterization of Hypoxia,” NOAA Coastal Ocean Program, Silver Spring, Maryland, 1999.

[204] J. S. Lee and B. Little, “Yeast extract, Technical Note: Electrochemical and Chemical Complications Resulting from Yeast Extract Addition to Stimulate Microbial Growth,” *Corrosion ,* pp. 1434-1440, 2015.

[205] K. R. Larsen, “Retrofitting wind turbine monopiles with cathodic protection,” in *AMPP Publications*, Houston, 2020.

[206] E. Puentes-Cala, V. Tapia-Perdomo, D. Espinosa-Valbuena, M. Reyes-Reyes, D. Quintero-Santander, S. Vasquez-Dallos, H. Salazar, P. Santamaría-Galvis, R. Silva-Rodríguez and G. Castillo-Villamizar, “Microbiologically influenced corrosion: The gap in the field,” *Front. Environ.,* p. 10:924842, 2022.

[207] H.-C. Flemming, P. Sriyutha Murthy, R. Venkatesan and K. Cooksey, Marine and Industrial Biofouling, Berlin, Germany: Springer. ISBN: 978-3-540-69794-7, 2009.

[208] H. Dang and C. R. Lovell, "Microbial Surface Colonization and Biofilm Development in Marine Environments.," *Microbiology and Molecular Biology Reviews,* pp. 80, 91-138., 2016.

[209] A. A. Biwen, E. Deland, O. Sobol, J. Yao, T. L. Skovhus and A. Koerdt, "The differences in the corrsion product compositions of Methanogen-induced microbiologically influenced corrosion (Mi-MIC) between static and dynamic growth conditions," *Corrosion Science,* pp. Volume 180, 109179, 2021.

[210] D. Xu, T. Gu and D. R. Lovley, "Microbially mediated metal corrosion," *Nature Reviews Microbiology,* vol. 21, p. 705–718, 2023.

[211] H. Venzlaff, D. Enning, J. Srinivasan, K. J. J. Mayrhofer, A. W. Hassel, F. Widdel and M. Stratmann, "Accelerated cathodic reaction in microbial corrosion of iron due to direct electron uptake by sulfate-reducing bacteria," *Corrosion Science,* pp. 88-96, 2013.

[212] A. Hernandez-Santana, H. N. Kokbudak and M. A. Nanny, "The influence of iron-binding ligands in the corrosion of carbon steel driven by iron-reducing bacteria.," *npj Materials Degradation,* vol. 12, p. 6, 2022.

[213] S. A. Wade, J. S. Webb, R. B. Eckert, G. E. Jenneman, A. A. Rice, T. L. Skovhus, P. Sturman, S. P. Kotu, M. Richardson and D. M. Goeres, "The role of standards in biofilm research and industry innovation," *International Biodeterioration & Biodegradation,* pp. 177, 105532, 2023.

[214] T. Skovhus, R. Eckert and E. Rodrigues, "Management and control of microbiologically influenced corrosion (MIC) in the oil and gas industry—Overview and a North Sea case study," *Journal of Biotechnology,* vol. 256, pp. 31-45, 2017.

[215] X. Muñoz-Berbel, C. García-Aljaro and F. Muñoz, "Impedimetric approach for monitoring the formation of biofilms on metallic surfaces and the subsequent application to the detection of bacteriophages," *Electrochimica Acta,* vol. 53, pp. 5739-5744, 2008.

[216] X. Muñoz-Berbel, N. Vigués, A. Jenkins, J. Mas and F. Muñoz, "Impedimetric approach for quantifying low bacteria concentrations based on the changes produced in the electrode–

solution interface during the pre-attachment stage," *Biosensors and Bioelectronics,* vol. 23, pp. 1540- 1546, 2008.

[217] F. Tian, X. He, X. Bai and C. Yuan, "Electrochemical corrosion behaviors and mechanism of carbon steel in the presence of acid-producing bacterium Citrobacter farmeri in artificial seawater," *International Biodeterioration & Biodegradation,* pp. Volume 147, 104872, 2020.

[218] T. Liu, Y. F. Cheng, M. Sharma and G. Voordouw, "Effect of fluid flow on biofilm formation and microbiologically influenced corrosion of pipelines in oilfield produced water," *J Pet Sci Eng,* p. 156:451–9, 2017.

[219] D. Enning, H. Venzlaff, J. Garrelfs, H. T. Dinh, V. Meyer, K. Mayrhofer, A. W. Hassel, M. Stratman and F. Widdel, "Marine sulfate-reducing bacteria cause serious corrosion of iron under electroconductive biogenic mineral crust," *Environ Microbiol,* vol. 14, no. 7, pp. 1772-87, 2012.

[220] T. R. Jack, "Biological Corrosion Failures," in *Failure analysis and prevention*, Materials Park, OH, ASM International, 2002, pp. 881-898.

[221] J. Duan, S. Wu, X. Zhang, G. Huang, M. Du and B. Hou, "Corrosion of carbon steel influenced by anaerobic biofilm in natural seawater," *Electrochimica Acta,* p. 22–28, 2008.

[222] M. Lv, M. Du and Z. Li, "Investigation of mixed species biofilm on corrosion of X65 steel in seawater environment," *Bioelectrochemistry,* pp. Volume 143, 107951, 2022.

[223] M. E. Orazem and B. Tribollet, Electrochemical Impedance Spectroscopy, Wiley, 737 Pages, 2017.

[224] A. Davydov, K. T. Chuang and A. R. Sanger, "Mechanism of H2S Oxidation by Ferric Oxide and Hydroxide Surfaces," *J. Phys. Chem. B,* vol. 102, pp. 4745-4752, 1998.

[225] R. Steudel, "Mechanism for the formation of elemental sulfur from aqueous sulfide in chemical and microbiological desulfurization processes," *Industrial and Engineering Chemistry Research ,* vol. 35, pp. 1417-1423, 1996.

[226] H. R. Krouse, C. A. Viau, L. S. Eliuk, A. Ueda and S. Halas, "Chemical and isotopic evidence of thermochemical sulphate reduction by light hydrocarbon gases in deep carbonate reservoirs," *Nature,* vol. 333, pp. 415-419, 1988.

[227] L. Qiu, G. R. Burton, S. Rousseu and J. Qian, “Kinetics and thermodynamics of sulfate adsorption on magnetite at elevated temperatures,” *J. Sol. Chem,* vol. 48, pp. 1448-1502, 2019.

[228] C. Mansour, C. Berger, M. Fédoroff, G. Lefèvre, A. Pages, E. M. Pavageau, H. Catalette and S. Zanna, “Influence of temperature and reducing conditions on the sorption of sulfate on magnetite,” *J. Colloid Interface Sci,* vol. 352, pp. 476-482, 2010.

[229] R. S. Juang and W. L. Wu, “Adsoprtion of sulphate and copper(II) on geothite in relation to the charges of zeta potentials,” *J. Colloid Interfaces Sci,* vol. 249, pp. 22-29, 2002.

[230] W. W. Wilson, M. M. Wade, S. C. Holman and F. R. Champlin, “Status of methods for assessing bacterial cell surface charge properties based on zeta potential measurements,” *Journal of Microbiological Methods,* pp. 153-164, 2001.

[231] S. J. Salgar-Chaparro, J. Tarazona and L. L. Machuca, “Corrosion of Carbon Steel by Shewanella chilikensis DC57 Under Thiosulphate and Nitrate Reducing Conditions,” *Front Bioeng Biotechnol,* p. 10:825776, 2022.

[232] J. Larsen, A. Andersen, F. Fontenay and L. Hilbert, “Investigation of Under Deposit Corrosion (UDC) in Halfdan Production Tubulars,” in *NACE CORROSION*, Vancouver, British Columbia, Canada, 2016.

[233] V. Eroini, M. C. Oehler, B. K. Graver, A. Mitchell, L. K. and T. L. Skovhus, “Investigation of Amorphous Deposits and Potential Corrosion Mechanisms in Offshore Water Injection Systems,” in *NACE CORROSION*, New Orleans, Louisiana, USA, 2017.

[234] V. Kapatral, I. Anderson, N. Ivanova, G. Reznik, T. Los, A. Lykidis, A. Bhattacharyya, A. Bartman, W. Gardner, G. Grechkin, L. Zhu, O. Vasieva, L. Chu, Y. Kogan, O. Chaga, E. Goltsman, A. Bernal, N. Larsen, M. D'Souza, T. Walunas, G. Pusch, R. Haselkorn and M. Fonstein, “Genome Sequence and Analysis of the Oral Bacterium Fusobacterium nucleatum Strain ATCC 25586,” *ASM Journals. Journal of Bacteriology,* pp. 184(7):2005-18, 2002.

[235] T. Skovhus, D. Søborg, F. Braga, B. Højris, K. Kristensen and K. Hansen, “Effects of early biofilm formation on water quality during commissioning of new polyethylene pipes,” *Environmental Science: Water Research & Technology,* pp. 1-14, 2022.

[236] C. C. Okoro, E. E. Nwezza and J. Lin, “Persistence of halophilic methanogens and oil-degrading bacteria in an offshore oil-producing facility,” *Geomicrobiol J ,* p. 35:323–333. , 2018.

[237] M. K. Schütz, M. L. Schlegel, M. Libert and O. Bildstein, “Impact of Iron-Reducing Bacteria on the Corrosion Rate of Carbon Steel under Simulated Geological Disposal Conditions,” *Environmental Science & Technology,* pp. 49 (12), 7483-7490, 2015.

[238] P. Refait, Grolleau, A-M, M. Jeannin, C. Remaxeilles and R. Sabot, “Corrosion of Carbon Steel in Marine Environments: Role of the Corrosion Product Layer,” *Corros. Mater. Degrad.,* pp. 1, 198–218, 2020.

[239] C. Y. Lin, A. V. Turchyn, A. Krylov and G. Antler, “The microbially driven formation of siderite in salt marsh sediments,” *Geobiology,* pp. 207-224, 2019.

[240] W. A. Hamilton, “Sulphate-reducing bacteria and anaerobic corrosion,” *Annu. Rev. Microbiol.,* vol. 39, pp. 195-217, 1985.

[241] W. Lee, Z. Lewandowski, P. Nielsen and W. Hamilton, “Role of sulfate-reducing bacteria in corrosion of mild steel: a review,” *Biofouling,* vol. 8, pp. 165-194, 1995.

[242] J. Costello, “Cathodic depolarization by sulphate-reducing bacteria,” *S. Afr. J. Sci.,* vol. 70, pp. 202-204, 1974.

[243] G. Booth and A. Tiller, “Polarization studies of mild steel in cultures of sulphate-reducing bacteria,” *Trans. Faraday Soc.,* vol. 56, pp. 1689-1696, 1960.

[244] J. Hardy, “Utilisation of cathodic hydrogen by sulphate-reducing bacteria,” *Br. Corros. J.,* vol. 18, pp. 190-193, 1983.

[245] Z. A. Iofa, V. V. Batrakov and Cho-Ngok-Ba., “Influence ofanion adsorption on the action ofinhibitors on the acid corrosion ofiron and cobalt,” *Electrochim. ,* p. Acta 9:1645–1653. , 1964.

[246] D. W. Shoesmith, P. Taylor, M. G. Bailey and O. D. G., “The formation of ferrous monosulfide polymorphs during the corrosion of iron by aqueous hydrogen sulfide at 21°C,” *J. Electrochem. Soc. ,* p. 127:1007–1015., 1980.

[247] R. Newman, B. Webster and R. Kelly, “The electrochemistry of SRB corrosion and related inorganic phenomena,” *ISIJ Int,* vol. 31, pp. 201-209, 1991.

[248] W. Sun and S. Nešic, “A mechanistic model of H2S corrosion of mild steel, paper 07655,” in *NACE International*, Houston, 2007.

[249] G. Booth and A. Tiller, “Polarization studies of mild steel in cultures of sulphate-reducing bacteria. Part 3: Halophilic organisms,” *Trans. Faraday Soc.,* vol. 58, pp. 2510-2516, 1962.

[250] H. Dinh, J. Kuever, M. Mußmann, A. Hassel, M. Stratmann and F. Widdel, “Iron corrosion by novel anaerobic microorganisms,” *Nature,* vol. 427, pp. 829-832, 2004.

[251] S. Ng and I. Hamilton, “Lactate Metabolism by Veillonella parvula,” *J Bacteriol,* vol. 105, 1971.

[252] S. Light, L. Su, R. Rivera-Lugo, J. Cornejo, A. Louie, A. Iavarone, C. Ajo-Franklin and D. Portnoy, “A flavin-based extracellular electron transfer mechanism in diverse Gram-positive bacteria,” *Nature,* vol. 562, pp. 140-144, 2018.

[253] M. Tahernia, E. Plotkin-Kaye, M. Mohammadifar, Y. Gao, M. Oefelein, L. Cook and S. Choi, “Characterization of Electrogenic Gut Bacteria,” *ACS Omega,* vol. 5, no. 45, pp. 29439-29446, 2020.

[254] Y. Lekbach, T. Liu, Y. Li, M. Moradi, W. Dou, D. Xu, J. Smith and D. Lovley, “Chapter Five - Microbial corrosion of metals: The corrosion microbiome,” *Advances in Microbial Physiology,* vol. 78, pp. 317-390, 2021.

[255] H. Tang, D. Holmes, T. Ueki, P. Palacios and L. D.R., “Iron Corrosion via Direct Metal-Microbe Electron Transfer,” *mBio,* vol. 10, no. 3, pp. e00303-19, 2019.

[256] H. Tang, C. Yang, T. Ueki, C. Pittman, D. Xu, T. Woodard, D. Holmes, T. Gu, F. Wang and D. Lovley, “Stainless steel corrosion via direct iron-to-microbe electron transfer by Geobacter species,” *ISME J,* vol. 10, pp. 3084-3093, 2021.

[257] J. Hardy and J. Brown, “The corrosion of mild steel by biogenic sulfide films exposed to air,” *Corrosion,* vol. 40, pp. 650-654, 1984.

[258] T. Jack, A. Wilmott, J. Stockdale, G. Van Bouven, R. Worthingham and R. Sutherby, "Corrosion consequences of secondary oxidation of microbial corrosion," *1998,* vol. 54, pp. 246-252, Corrosion.

[259] W. Lee, Z. Lewandowski, M. Morrison, C. W.G, R. Avici and P. Nielsen, "Corrosion ofmild steel underneath aerobic biofilms containing sulfate-reducing bacteria. Part I: at high dissolved oxygen concentrations.," *Biofouling,* vol. 7, pp. 217-239, 1993.

[260] D. MacDonald, B. Roberts and J. Hyne, "Corrosion of carbon steel during cyclical exposure to wet elemental sulfur and atmosphere.," *Corros. Sci.,* vol. 18, pp. 499-501, 1978.

[261] P. Nielsen, W. Lee, Z. Lewandowski, M. Morison and W. Characklis, "Corrosion ofmild steel in an alternating oxic and anoxic biofilm system," *Biofouling,* vol. 7, pp. 267-284, 1993.

[262] G. Booth, "Sulphur bacteria in relation to corrosion.," *J. Appl. Bacteriol.,* vol. 27, pp. 174-181, 1964.

[263] R. Cord-Ruwisch, "Microbially influenced corrosion ofsteel," in *Environmental microbe-metal interactions*, Washington, DC, ASM Press, 2000, pp. 159-173.

[264] I. Beech, C. Cheung, C. Chan, M. Hill, R. Franco and A. Lino, "tudy ofparameters implicated in the biodeterioration ofmild steel in the presence of different species of sulfate-reducing bacteria.," *Int. Biodeterior. Biodegradation,* vol. 34, pp. 289-303, 1994.

[265] C. Gaylarde, "Sulfate-reducing bacteria which do not induce accelerated corrosion.," *Int. Biodeterior. Biodegradation ,* vol. 30, pp. 331-338, 1992.

[266] R. Newman, K. Rumash and B. Webster, "The effect of pre-corrosion on the corrosion rate of steel in neutral solutions containing sulfide: relevance to microbially influenced corrosion.," *Corros. Sci.,* vol. 33, p. 1877– 1884, 1992.

[267] A. Tiller and G. Booth, "Polarization studies ofmild steel in cultures ofsulphate-reducing bacteria. Part 2. Thermophilic organisms.," *T. Faraday. Soc. ,* vol. 58, p. 110–115, 1962.

[268] A. Tiller, "Electrochemical aspects of corrosion: an overview," in *Microbial corrosion.* , Teddington, United Kingdom, The Metals Society, 1983, p. 54–65.

[269] W. Lee and W. Characklis, "Corrosion of mild steel under anaerobic biofilm," *Corrosion,* vol. 49, pp. 186-199, 1993.

[270] N. Rachel and L. Gieg, “Preserving Microbial Community Integrity in Oilfield Produced Water,” *Frontiers in Microbiology,* vol. 11, p. 581387, 2020.

[271] S. Lahme, J. Mand, J. Longwell, R. Smith and D. Enning, “Severe Corrosion of Carbon Steel in Oil Field Produced Water Can Be Linked to Methanogenic Archaea Containing a Special Type of [NiFe] Hydrogenase,” *Appl Environ Microbiol,* vol. 87, pp. e01819-20, 2021.

[272] A. Oldham, V. Sandifer and K. Duncan, “Effects of sample preservation on marine microbial diversity analysis,” *J. Microbiol. Methods,* vol. 158, pp. 6-13, 2019.

[273] P. Elumalai, M. Al Salhi, S. Mehariya, O. Karthikeyan, S. Devanesan, P. Parthipan and A. Rajasekar, “Bacterial community analysis of biofilm on API 5LX carbon steel in an oil reservoir environment,” *Bioprocess and Biosystems Engineering,* vol. 44, p. 355–368, 2021.

[274] T. Silva, L. Verde, E. Santos Neto and V. Oliveira, “Diversity analyses of microbial communities in petroleum samples from Brazilian oil fields,” *International Biodeterioration & Biodegradation,* vol. 81, pp. 57-70, 2013.

[275] L. Lv, L. Zhou, L.-Y. Wang, J.-F. Liu, J.-D. Gu, B.-Z. Mu and S.-Z. Yang, “Selective inhibition of methanogenesis by sulfate in enrichment culture with production water from low-temperature oil reservoir,” *International Biodeterioration & Biodegradation,* vol. 108, pp. 133-141, 2016.

[276] C. Struchtemeyer, J. Davis and M. Elshahed, “Influence of the Drilling Mud Formulation Process on the Bacterial Communities in Thermogenic Natural Gas Wells of the Barnett Shale,” *Appl Environ Microbiol,* vol. 77, p. 4744–4753, 2011.

[277] E. Santillan, W. Choi, P. Bennett and J. Diouma Leyris, “The effects of biocide use on the microbiology and geochemistry of produced water in the Eagle Ford formation, Texas, USA,” *Journal of Petroleum Science and Engineering,* vol. 135, pp. 1-9, 2015.

[278] C. Struchtemeyer and M. Elshahed, “Bacterial communities associated with hydraulic fracturing fluids in thermogenic natural gas wells in North Central Texas, USA,” *FEMS Microbiology Ecology,* vol. 81, no. 1, pp. 13-25, 2012.

[279] C. Wuchter, E. Banning, T. Mincer, N. Drenzek and M. Coolen, “Microbial diversity and methanogenic activity of Antrim Shale formation waters from recently fractured wells,” *Frontiers in Microbiology,* vol. 4, pp. 1-14, 2013.

[280] S. Nešić, “Key issues related to modelling of internal corrosion of oil and gas pipelines – A review,” *Corrosion Science,* vol. 49, no. 12, pp. 4308-4338, 2007.

[281] Y. Xiong, D. Fischer, F. Cai and J. Pacheco, “Impact of steel metallurgy on corrosion inhibitor performance: another gap in industry practice.,” in *NACE International*, Houston, Texas, 2019.

[282] H. Li, S.-Z. Yang, B.-Z. Mu, Z.-F. Rong and J. Zhang, “Molecular phylogenetic diversity of the microbial community associated with a high-temperature petroleum reservoir at an offshore oilfield,” *FEMS Microbiology Ecology,* vol. 60, pp. 74-84, 2007.

[283] D. Emerson, “The role of iron-oxidizing bacteria in biocorrosion: a review,” *Biofouling,* vol. 34, no. 9, pp. 989-1000, 2018.

[284] Y. Zhang, Y. Ma, J. Duan, X. Li, J. Wang and B. Hou, “Analysis of marine microbial communities colonizing various metallic materials and rust layers,” *Biofouling,* vol. 35, pp. 429-442, 2019.

[285] P. Elumalai, P. Parthipan, M. Al Salhi, M. Huang, S. Devanesan, O. Karthikeyan, W. Kim and A. Rajasekar, “Characterization of crude oil degrading bacterial communities and their impact on biofilm formation,” *Environmental Pollution,* vol. 286, p. 117556, 2021.

[286] S. Coetser and T. Cloete, “Biofouling and biocorrosion in industrial water systems,” *Crit. Rev. Microbiol,* vol. 31, pp. 213-232, 2005.

[287] C. Pillay and J. Lin, “Metal corrosion by aerobic bacteria isolated from stimulated corrosion systems: effects of additional nitrate sources,” *Int. Biodeterior. Biodegrad,* vol. 83, pp. 158-165, 2013.

[288] J. Lin, B. Hao, G. Cao, J. Wang, Y. Feng, X. Tan and W. Wang, “A study on the microbial community structure in oil reservoirs developed by water flooding,” *Journal of Petroleum Science and Engineering,* vol. 122, pp. 354-359, 2014.

[289] X. Zhang, K. Xiao, C. Dong, J. Wu, X. Li and Y. Huang, *Engineering Failure Analysis,* vol. 18, pp. 1981-1989, 2011.

[290] G. Genchev and A. Erbe, “Raman Spectroscopy of Mackinawite FeS in Anodic Iron Sulfide Corrosion Products,” *Journal of The Electrochemical Society,* vol. 163, no. 6, pp. 333-338, 2016.

[291] W. Zhang, D. Young, B. Brown, C. Shafer, F. Lu and E. Anyanwu, “An in-situ Raman study on the oxidation of mackinawite as a corrosion product layer formed on mild steel in marginally sour environments,” *Corrosion Science,* vol. 188, p. 109516, 2021.

[292] J. Neff, K. Lee and E. DeBlois, “Produced Water: Overview of Composition, Fates, and Effects,” in *Produced Water*, Springer, New York, NY, 2011, pp. 3-54.

[293] J. Kurth, H. Op den Camp and C. Welte, “Several ways one goal—methanogenesis from unconventional substrates,” *Appl Microbiol Biotechnol,* vol. 104, pp. 6839-6854, 2020.

[294] J. Li, T. Akinyemi, N. Shao, C. Chen, X. Dong, Y. Liu and W. Whitman, “Genetic and metabolic engineering of Methanococcus spp,” *Current Research in Biotechnology,* vol. 5, p. 100115, 2023.

[295] Y. Gao, D. Feng, M. Moradi, C. Yang, Y. Jin, D. Liu, D. Xu, X. Chen and F. Wang, “Inhibiting corrosion of aluminum alloy 5083 through Vibrio species biofilm,” *Corrosion Science,* vol. 180, p. 109188, 2021.

[296] R. Mugge, J. Salerno and L. Hamdan, “Microbial Functional Responses in Marine Biofilms Exposed to Deepwater Horizon Spill Contaminants,” *Front Microbiol,* vol. 12, p. 636054, 2021.

[297] L. Bird, R. Mickol, B. Eddie, M. Thakur, M. Yates and S. Glaven, “Marinobacter: A case study in bioelectrochemical chassis evaluation,” *Microb Biotechnol,* vol. 16, no. 3, pp. 494-506, 2023.

[298] P. Tedesco, S. Balzano, D. Coppola, F. Esposito, D. de Pascale and R. Denaro, “Bioremediation for the recovery of oil polluted marine environment, opportunities and challenges approaching the Blue Growth,” *Marine Pollution Bulletin,* vol. 200, p. 116157, 2024.

[299] K. Hobmeier, M. Cantone, Q. Nguyen, K. Pflüger-Grau, A. Kremling, H. Kunte, F. Pfeiffer and A. Marin-Sanguino, “Adaptation to Varying Salinity in Halomonas elongata: Much More Than Ectoine Accumulation,” *Front Microbiol,* vol. 13, p. 846677, 2022.

[300] J. Dutra, R. Gomes, G. Yupanqui García, D. Romero-Cale, M. Santos Cardoso, V. Waldow, C. Groposo, R. Akamine, M. Sousa, H. Figueiredo, V. Azevedo and A. Góes-Neto, “Corrosion-influencing microorganisms in petroliferous regions on a global scale: systematic review,

analysis, and scientific synthesis of 16S amplicon metagenomic studies," *PeerJ,* vol. 11, p. e14642, 2023.

[301] J. Mand and D. Enning, "Oil field microorganisms cause highly localized corrosion on chemically inhibited carbon steel," *Microb Biotechnol,* vol. 14, no. 1, pp. 171-185, 2021.

[302] S.-Y. Chang, S.-Y. Huang, Y.-R. Chu, S.-Y. Jian, K.-Y. Lo and Y.-L. Lee, "Antimicrobial and Anticorrosion Activity of a Novel Composite Biocide against Mixed Bacterial Strains in Taiwanese Marine Environments," *Materials,* vol. 14, p. 6156, 2021.

[303] F. Liu, X. Chang, F. Yang, Y. Wang, F. Wang, W. Dong and C. Zhao, "Effect of oxidizing and non-oxidizing biocides on biofilm at different substrate levels in the model recirculating cooling water system," *World J. Microbiol. Biotechnol.,* vol. 27, pp. 2989-2997, 2011.

[304] P. Kijkla, D. Wang, M. Mohamed, M. Saleh, S. Kumseranee, S. Punpruk and T. Gu, "Efficacy of glutaraldehyde enhancement by d-limonene in the mitigation of biocorrosion of carbon steel by an oilfield biofilm consortium," *World Journal of Microbiology and Biotechnology,* vol. 37, p. 174, 2021.

[305] K. Duncan, B. Perez-Ibarra, G. Jenneman, J. Harris, R. Webb and K. Sublette, "The effect of corrosion inhibitors on microbial communities associated with corrosion in a model flow cell system," *Appl. Microbiol. Biotechnol.,* vol. 98, pp. 907-918, 2014.

[306] R. Raman, P. Banerjee, D. Lobo, H. Gullapalli, M. Sumandasa, A. Kumar, L. Choudhary, R. Tkacz, P. Ajayan and M. Majumder, "Protecting copper from electrochemical degradation by graphene coating," *Carbon,* vol. 50, pp. 4040-4045, 2012.

[307] B. Pereira, M. Salim, N. Rai and I. Tagkopoulos, "Tolerance to Glutaraldehyde in Escherichia coli Mediated by Overexpression of the Aldehyde Reductase YqhD by YqhC," *Frontiers in Microbiology,* vol. 12, 2021.

[308] X. Shi, R. Zhang, W. Sand, K. Mathivanan, Y. Zhang, N. Wang, J. Duan and B. Hou, "Comprehensive Review on the Use of Biocides in Microbiologically Influenced Corrosion. Microorganisms," *Microorganisms,* vol. 11, no. 9, p. 2194, 2023.

[309] J. Stein, T. Chaturvedi, T. Skovhus and M. Thomsen, "Halophyte-based Biocides for Mitigation of Microbiologically Influenced Corrosion (MIC) in Industrial Water Systems," in *Petroleum Microbiology*, CRC Press, 2024, pp. 154-166.

[310] E. Gloag, A. Fabbri, D. Wozniak and P. Stoodley, “Biofilm mechanics: Implications in infection and survival,” *Biofilm,* vol. 2, p. 100017, 2020.

[311] H. Sun, B. Shi, Y. Bai and D. Wang, “Bacterial community of biofilms developed under different water supply conditions in a distribution system,” *Sci. Total Environ.,* vol. 472, p. 99–107, 2014.

[312] V. Gomez-Alvarez, R. Revetta and J. Santo Domingo, “Metagenome analyses of corroded concrete wastewater pipe biofilms reveal a complex microbial system,” *BMC Microbiol.,* vol. 12, p. 122, 2012.

[313] N. Høiby, T. Bjarnsholt, M. Givskov, S. Molin and O. Ciofu, “Antibiotic resistance of bacterial biofilms,” *Int J Antimicrob Agents,* vol. 35, pp. 322-332, 2010.

[314] S. Ramesh, S. Rajeswari and S. Maruthamuthu, “Effect of inhibitors and biocide on corrosion control of mild steel in natural aqueous environment,” *Mat. Lett.,* vol. 57, no. 29, pp. 4547-4554, 2003.

[315] H. Liu, T. Gu, Y. Lv, M. Asif, F. Xiong, G. Zhang and H. Liu, “Corrosion inhibition and anti-bacterial efficacy of benzalkonium chloride in artificial CO2-saturated oilfield produced water,” *Corrosion Sci.,* vol. 117, pp. 24-34, 2017.

[316] W. Lin, B. Niu, J. Yi, Z. Deng, J. Song and Q. Chen, “Toxicity and Metal Corrosion of Glutaraldehyde-Didecyldimethylammonium Bromide as a Disinfectant Agent,” *BioMed Research International,* pp. 1-7, 2018.

[317] S. Nawab, Q. Bao, L.-H. Ji, Q. L, X. Fu, S. Fan, Z. Deng and W. Ma, “The Pathogenicity of Fusobacterium nucleatum Modulated by Dietary Fibers—A Possible Missing Link between the Dietary Composition and the Risk of Colorectal Cancer,” *Microorganisms,* vol. 11, no. 8, 2023.

[318] S. Park, S. Yoshizawa, K. Kogure and A. Yokota, “Oceanicoccus sagamiensis gen. nov., sp. nov., a gammaproteobacterium isolated from sea water of Sagami Bay in Japan,” *J Microbiol,* vol. 49, no. 2, pp. 233-237, 2011.

[319] E. Kujawinski, K. Longnecker, K. Barott, R. Weber and M. Kido Soule, “Microbial Community Structure Affects Marine Dissolved Organic Matter Composition,” *Frontiers in Marine Science,* vol. 3, 2016.

[320] R. Logares, “Decoding populations in the ocean microbiome,” *Microbiome,* vol. 12, 2024.

[321] R. White, S. Soles, G. Gavelis, E. Gosselin, G. Slater, D. Lim, B. Leander and C. Suttle, “The Complete Genome and Physiological Analysis of the Eurythermal Firmicute Exiguobacterium chiriqhucha Strain RW2 Isolated From a Freshwater Microbialite, Widely Adaptable to Broad Thermal, pH, and Salinity Ranges,” *Frontiers in Microbiology,* vol. 9, 2019.

[322] A. Postec, M. Quéméneur, A. Lecoeuvre, N. Chabert, M. Joseph and G. Erauso, “Alkaliphilus serpentinus sp. nov. and Alkaliphilus pronyensis sp. nov., two novel anaerobic alkaliphilic species isolated from the serpentinite-hosted Prony Bay Hydrothermal Field (New Caledonia),” *Systematic and Applied Microbiology,* vol. 44, no. 2, p. 126175, 2021.

[323] A. Kahyarian, B. Brown and S. Nesic, “CO2 corrosion, H2S corrosion, Organic Acid Corrosion - a Unifying Perspective on Corrosion,” *Corrosion,* 2019.

[324] T. Tran, B. Brown, S. Nesic and B. Tribollet, “Investigation of the Electrochemical Mechanisms for Acetic Acid Corrosion of Mild Steel,” *Corrosion,* vol. 70, pp. 223-229, 2013.

[325] K. George and S. Nesic, “Investigation of Carbon Dioxide Corrosion of Mild Steel in the Presence of Acetic Acid—Part 1: Basic Mechanisms,” *Corrosion,* vol. 63, no. 2, pp. 178-186, 2007.

[326] Y. Guan, D. K. Ngugi, J. Blom, S. Ali, F. G. Ferry and U. Stingl, “Draft genome sequence of an obligately methylotrophic methanogen, Methanococcoides methylutens, isolated from marine sediment,” *Genome Announc,* pp. 2(6):e01184-14, 2014.